Cape Peninsula
University of Technology

Useful energy utilisation of integrated solar PV and thermal module with storage device

by

Anges Akim Aminou Moussavou

Thesis submitted in fulfilment of the requirements for the degree

Doctor of Engineering: Electrical Engineering
in the Faculty of Engineering
at the Cape Peninsula University of Technology

Supervisor: Dr. AK Raji
Co-supervisor: Dr. M Adonis

Bellville

June 2019

DECLARATION

I, Aminou Moussavou Anges Akim, declare that the content of this thesis represents my own work, and that the thesis has not previously been submitted for academic examination towards any qualification. Furthermore, it represents my own opinions and not necessarily those of the Cape Peninsula University of Technology.

Signed   Date

ABSTRACT

Lack of electrical energy has always been an issue for human society development. Several studies point out the expansion and integration of renewable energies into the society to solve the energy crisis. Renewable energies promote sustainable energy development, environmental, social, and economic sustainability throughout their life cycle. The integration of renewable energies, especially in the area of the photovoltaic technology becomes important, as it demotes the rates of consumption of non-renewable resources, therefore, decreasing the fossil fuels dependencies. A photovoltaic system has a low output conversion rate. Integrating photovoltaic and thermal (PV/T) system can improve the photovoltaic conversion efficiency. However, the overall efficiency of the PV/T is always compromised as one of the sub-system performance might overtake the other.

This research work is developed to enhance the knowledge of the thermal performance of photovoltaic models and also offered alternatives to improve and co-generate thermal and electrical energy. The purpose of the proposed PV/T model is to analyse the cooling method and the possibility of partially converting photovoltaic electrical energy into useful heat source (for hot water). The working fluid plays the role of cooling the PV cells, therefore, boosting the PV cell performance. The working fluid would collect the useful heat energy through the pipes in a closed loop attached at the back of the PV panel. The study also is aimed at proposing automated intelligent solutions for energy management to adjust the useful heat transfer capacity to working fluid based on energy demand and weather conditions to balance the thermal and electrical energy.

The overall research method was based on a theoretical analysis, the review of essential articles, the design of the most appropriate concepts, mathematical modelling and analysis of the proposed PV/T system. Also, an adequate control strategy based on the energy management algorithm to provide multi-functional energy performance was established to prioritise the energy balance according to demand. The simulation model of the PV/T system was developed with MATLAB/Simulink software to predict system performance with reasonable accuracy and to analyse the main phenomena related to thermal behaviour.

The simulation result of the proposed PV/T model under different operational conditions evaluated the cooling the PV cells and heating the working fluid. The outcomes turned out to be productive and cost-effective. Also, the PV modules can yield better electrical energy performance due to the cooling effect of the PV cells. The results revealed that the proposed system met cooling and heating based on the demands.

ACKNOWLEDGEMENTS

DEDICATION

This thesis is dedicated to the Almighty, the Entirely Merciful, and my source of inspiration.

TABLE OF CONTENTS

LIST OF FIGURES

LIST OF TABLES

ABBREVIATIONS & ACRONYMS	
ASHRAE	American Society of Heating, Refrigerating and Air Conditioning Engineers
AlGaAs	Aluminium gallium arsenide
AM	Air mass
AH	Ampere-hour rating
ASHP	Air-source heat pump
BIPVT	Building integrated photovoltaic thermal
CAES	Compressed air energy storage
c-PV/T	Concentrator-type PV/T
CFD	Computational fluid dynamics
COP	Coefficient of performance
CPC	Compound parabolic concentrator
C/R	Collector/regenerator
DHW	Domestic hot water
D_i	Inner diameter of heat exchanger tube (m)
D_o	Outer diameter of heat exchanger tube (m)
DX-SAHP	Direct expansion solar assisted heat pump
e	Per cent deviation
E_g	Bandgap energy (eV)
E_{ph}	Photon energy (eV)
EVA	Ethylene-vinyl acetate

EES	Engineering equation solver
ESS	Energy storage system
F	Fin efficiency
F'	Flat plate collector efficiency factor
FC	Fuel cell
FES	Flywheel energy storage
FGM	Functionally graded material
FBS	Flow batteries storage
I_{sc}	Short-circuit current (A)
g	Gravitational acceleration (m/s²)
G	Incident solar radiation (W/m²)
GaAs	Gallium arsenide
Gr	Grashoff number
h_f	Front convective heat transfer coefficient (W/m²·K)
HES	Hydrogen energy storage
IEA SHC	International energy agency solar heating cooling
k	Thermal conductivity (W/(m·K))
LCL	Lateral conducting layers
Li-ion	Lithium-ion
M	Mass (kg)
m	Variable defined to solve differential equations

NaS	Sodium-Sulphur
NASA	National aeronautics and space agency
Ni-Cd	Nickel-Cadmium
Ni–Zn	Nickel-Zinc
NPV	Net present value
NREL	National Renewable Energy Laboratory
Nu	Nusselt number
V_{oc}	Open-circuit voltage
PCM	Phase change material
P_d	Dissipated power (W)
PHES	Pumped hydro energy storage
PV	Photovoltaic
P_{PV}	PV power (W)
PHS	Pumped hydroelectric storage
PV/LHP	Photovoltaic /loop heat pipe
PV/T	Photovoltaic/thermal
PV-SAHP	Photovoltaic solar assisted heat pump
Q	Energy (W)
Q_{cond}	Thermal transfer coefficient by conduction (W)
Q_{conv}	Thermal transfer coefficient by convection (W)
RE	Renewable energy

R_{pi}	Internal parallel resistance (Ω)
R_{si}	Internal series resistance (Ω)
R_{se}	External series resistance (Ω)
SES	Supercapacitor energy storage
SHR	Shockley-hall-read
SMES	Superconducting magnetic energy storage
SOC	State of charge
SR	Spectral response
STC	Standard test conditions
T	Temperature (°C)
T_a	Ambient temperature (°C)
T_{a-b}	Ambient temperature at the back of the PV (°C)
T_{a-f}	Ambient temperature at the front of the PV (°C)
T_c	PV cell temperature (°C)
T_{env}	Environmental temperature (°C)
T_{env-f}	Environmental temperature at the front of the PV (°C)
T_{env-b}	Environmental temperature at the back of the PV (°C)
T_w	Water temperature (°C)
T_{wp}	Water temperatures within the pipes (°C)
T_{wt}	Water temperatures within the tank (°C)
TES	Thermal energy storage

TCL	Transparent conducting layers
U	Thermal transfer coefficient (W/m²·K)
V_{nom}	Nominal voltage (V)
$V1$	Specify the voltage
$\dot{W}$	Compressor power (kW)
W	Distance between tubes (m)
W_p	Peak power (W)
ZnBr	Zinc Bromine

Greek letters	
α	Absorption
βp	Temperature coefficient for PV efficiency
Δ	Thickness (m)
ε	Emissivity
η	Efficiency (%)
σ	Stefan-Boltzmann constant (K)
τ	Transmittance
v	Kinematic viscosity (m²/s)
ρ	Density (kg/m³)
ξ	Packing factor
λ	Thermal conductivity (W/m²·K)

Chapter 1

General introduction

1.1 Introduction

The energy used to heat and provide electricity to domestic and industrial sectors and to run cars is from a non-renewable resource. Fossil fuels such as coal, oil, and natural gas are non-renewable resource, and their uses are being limited due to energy savings and environmental protection (Chel & Kaushik, 2018; Owusu & Asumadu-Sarkodie, 2016). On the other hand, renewable energy (RE) offers a sustainable energy supply to domestic and industrial sectors and has demonstrated a promising energy economic development (Banks & Schäffler, 2006; Chel & Kaushik, 2018). Of all renewable energies, solar energy is considered the most sustainable energy source, especially photovoltaic and solar thermal technology (Owusu & Asumadu-Sarkodie, 2016). However, most of the solar energy captured by photovoltaic is converted to wasted heat, causing the degradation of the module and reduction in energy efficiency. The combination photovoltaic and solar thermal system can cool down and increase the energy efficiency of the photovoltaic module, while simultaneously generating electrical and thermal energy to the load (Ramos et al., 2017). Therefore, in this study, the focus was to determine the energy impact created from the combination of photovoltaic and thermal (PV/T) system. These systems provide analysis and modelling of the PV/T system, as well as the exchange of heat and electrical power generated. Also, the interaction between the systems and their energy efficiency were evaluated. Emphasis was placed on a system optimisation approach of the combined system design and simulations. Another aim of this study was to develop a methodology which explores the potential linkage and provides insight into the functioning and specificities of such interaction.

The efficiency improvement of various PV/T systems has been developed, providing unique advantages and disadvantages using air, water, refrigerants, heat pipes, nanofluid and phase change material. In this study, an absorber pipe attached to the PV cells, forming a water-based PV/T system is selected. In the processes, high-performance energy management between the interaction of the thermal and electrical energy is developed to regulate a PV/T system. Thus, it is necessary to conduct an in-depth study on the dynamic integration of the performance of energy

systems. The approach primarily focused on exploring the natural and forced convection using a water-based PV/T system. The first step was to present a basic model establishing the most effective modes of interaction of the system, while the second step provided data for selecting the most appropriate models to solve the problem investigated in the study.

1.2 Energy situation

Electrical energy, essential for human development, is used in three major areas: housing, transportation and industry. As such, the world's energy demand is increasing for several reasons:

- A rapid increase in population;
- Our industrial development;
- Improvement in people's standard of living (air conditioning, heating, household appliances, transportation, computer and lighting); and
- The rise of new, densely populated, industrialised countries.

For the reasons cited above, fossil energy resources are declining due to the growing global energy demand, especially in industrial sectors. Since the industrial revolutions of the 19th and 20th centuries, the use of fossil energies and electricity have been associated with numerous scientific discoveries, although there is a continuous increase in the consumption of energy and its elevating costs. In many countries, fossil energies are limited, representing 90% of the primary electrical energy consumption and cost. The unavailability of fossil fuels has resulted in its escalating price, leading to the depletion of crude oil and natural gas in the long run. Unfortunately, as a result of this limit of resources, many countries are at risk of facing inevitable energy challenges. To overcome these challenges, the use of fossil energy must be transferred to renewable energies, a necessary transition for fossil energy independence. This can be achieved through discoveries and designs of new energy sources.

Speirs *et al.* (2015) posited that the extensive use of fossil fuels causes severe global warming due to the massive emission of greenhouse gases, which has led to climate change and environment degradation. The greenhouse effect is undesirable for the survival not only for humans but all life as the accumulation of greenhouse gases (e.g. carbon dioxide) into the atmosphere, increases the annual average global air temperature. While a higher portion of carbon dioxide is released due to human activities, and this is exacerbated by industrials activities (Tkemaladze & Makhashvili, 2016). Several countries have attempted to confront their energy challenges to mitigate the impact of the oil crisis on the economy, they have accentuated the need

to find alternative solutions while addressing the greenhouse effect in particular (Kobek *et al.*, 2015).

The Institute of Statistics predicts the evolution of global energy consumption by energy sources from 1990 to 2040 (EIA, 2016). Figure 1.1 presents a graph of the past and future energy integration around the world (EIA, 2016). From this figure, it is observed that most of the energy sources making up the global energy mix will decrease or marginally increase over the years, from 2012 to 2040. Renewables, however, are expected to increase by about 42% over the same period.
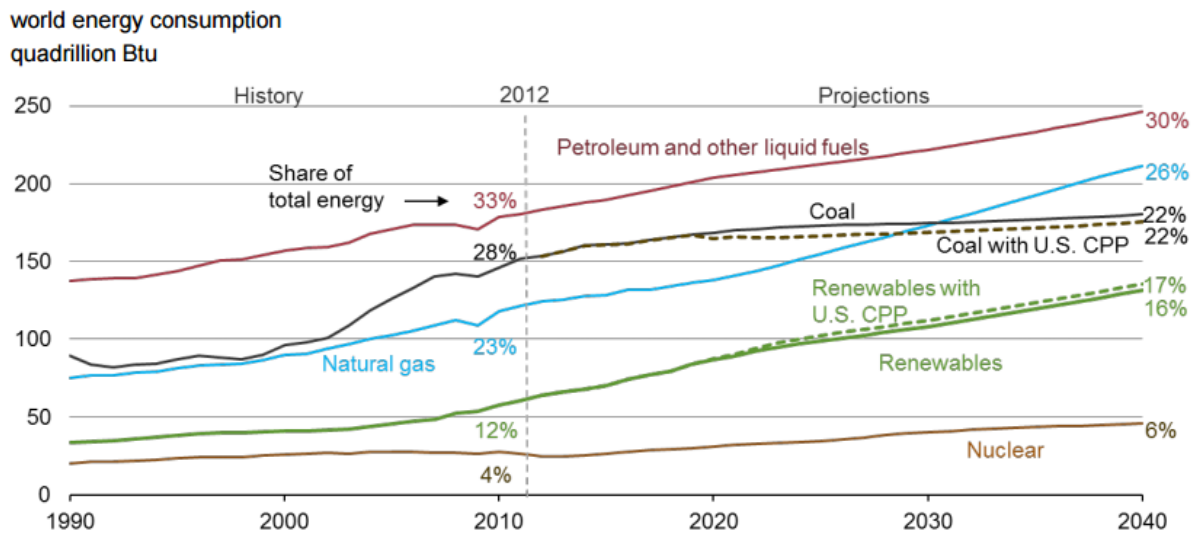
Figure 1.1: World energy consumption by energy source 1990-2040 (EIA, 2016)

1.2.1 Energy challenge

Since the European Union recommended the introduction of renewable energy (RE) in electricity production in all its countries in 2010, countries such as Sweden and Austria have integrated energy structures to accommodate RE (Nunes, 2018; Stocker *et al.*, 2011). RE is a necessary alternative to traditional power generation through the reduction of greenhouse gas emission and the simultaneous reduction of fossil fuel utilisation (Owusu & Asumadu-Sarkodie, 2016).

Several efforts have been made to promote renewable technologies through the following:

- Ensuring a global supply of clean energy (no carbon) and durable, sustainable energy through RE;
- Ensuring the preservation of natural heritage (resources, climate and environment);
- Introducing significant markets for RE; and
- Providing the co-training of renewable energies to promote their application and development continuity.

To solve the energy challenges, carbon dioxide could be captured and stored in equipment (under land reserves) while still using fossil fuels. This is, however, certainly not economically and technically viable at this time. In this energy challenge, based on the Kyoto Protocol, a reduction of 5.2% from the 2012 greenhouse gas emissions is required, as compared to 1990. Therefore, alternatives to fossil fuels must be sought. Furthermore, RE has been determined to be less harmful than fossil fuels.

Fossil fuels have been exploited since the early 20th century for economic reasons. Some countries introduced various support policies in some local areas for the development of solar energy. These decisions were taken to achieve the goal of reducing greenhouse gas emissions by 75% of the total emissions and also to support the improvement of energy efficiency research projects that integrate RE production systems. These actions are particularly relevant to RE sources such as biogas, biomass, micro and small cogeneration, micro-hydropower and cyclical adjustment of a PV system (Owusu & Asumadu-Sarkodie, 2016; Ahuja & Tatsutani, 2009).

RE is readily available, and it is not associated with fuel costs. However, RE is not free: it still has to be converted, and it has weak performance and intermittent supply, which affect its economic competitiveness and integration (such as electricity) in the distribution network. RE involves a long process that requires several scientific challenges and technological changes, requiring investment and high subsidies. Also, the instalment price is relatively high to recover. The South

African government has substantially increased photovoltaic generation development on the grid to promote the development of new buildings since the lifetime of solar cell power has been determined to be 30 years. It is imperative to take note of the current South African National Solar Water Heater Strategy activities. Solar water heaters (SWHs) have emerged as one of the most exciting projects in South Africa. SWHs can potentially decrease the electricity consumption of middle-income households by 25%, and provide 100 litres of hot water per day to low-income families (SEA, 2010; Covary & Kritzinger, 2016; Rycroft *et al.*, 2016).

In April 2006, the European Green Industry Association (EGIA) conducted studies generating specific data for a better understanding of a PV system. One study facilitated a limit to the assessment of carbon dioxide indicators across 26 countries. Likewise, the South African Renewable Energy Independent Power Producer Procurement Program (REIPPPPP) is a delicately focused procedure intended to encourage private sector investment associated with RE production (Eberhard & Naude, 2016).

Given the above, this present study focuses on solar energy. Emphasis is placed on solar energy conversion to heat storage. In the photoelectric conversion process, the solar energy is converted into electrical energy and most often stored in a battery.

1.2.2 Sources of renewable energies

RE is in different forms, with the rate of energy consumption at least equal to the continuous replenishment of energy. The various potential energy source is listed as follows (Owusu & Asumadu-Sarkodie, 2016):

- *Geothermal energy:* The interaction between different underground formations can produce energy, due to the relative movement of the latter. Heat in the form of vapour is then produced from the high-temperature fluid which is generated from the earth's crust.

- *Gravitational energy:* This occurs because of the combined effect of the moon and the sun 's gravity forces, tides (potential energy) and some ocean currents (kinetic energy) performance.

- *Solar energy:* This is produced from cosmic radiation that embodies the operation of the solar atmosphere. It is found under different components such as biomass, wave, water, heat, photoelectric and wind energy. As this energy has a higher potential than

the previous forms of RE, it has enormous potential for economic growth and development.

Figure 1.2 shows the composition making up the RE consumption in the USA; solar energy comprises 6% of the RE in 2017.
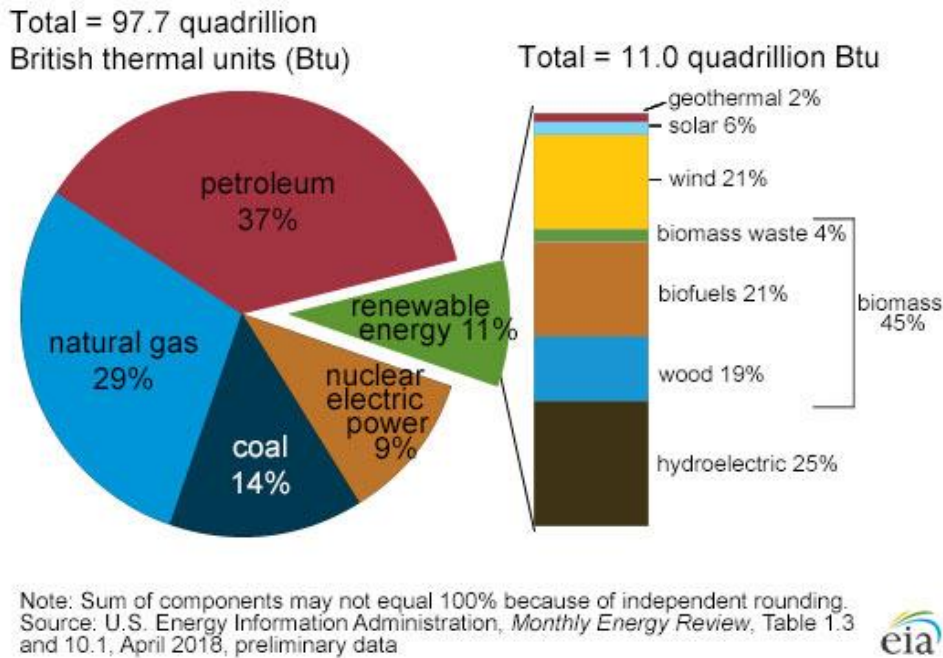
Figure 1.2: USA energy consumption by energy source (EIA, 2018)

1.2.3 Solar thermal collector

Water and space heating are the second-largest end-use energy demand. The heating is provided from different sources such as electrical heating system, propane, fuels and gas and they are often used in residences and commercial areas. Due to the increase in conventional electricity tariffs, solar energy conversion water heaters are economically preferred to traditional gas heating systems (EIA, 2019; Reyna & Chester, 2017). Flat-plate collectors, evacuated tubes or concentrating systems use solar heating to produce high temperature.

Figure 1.3 illustrates the constant increase in solar thermal (flat-plate and evacuated tube) capacity to supply heat through the years. Moreover, it shows the global contribution of solar heat in the application of glazed and evacuated tube capacity per 1000 inhabitants.
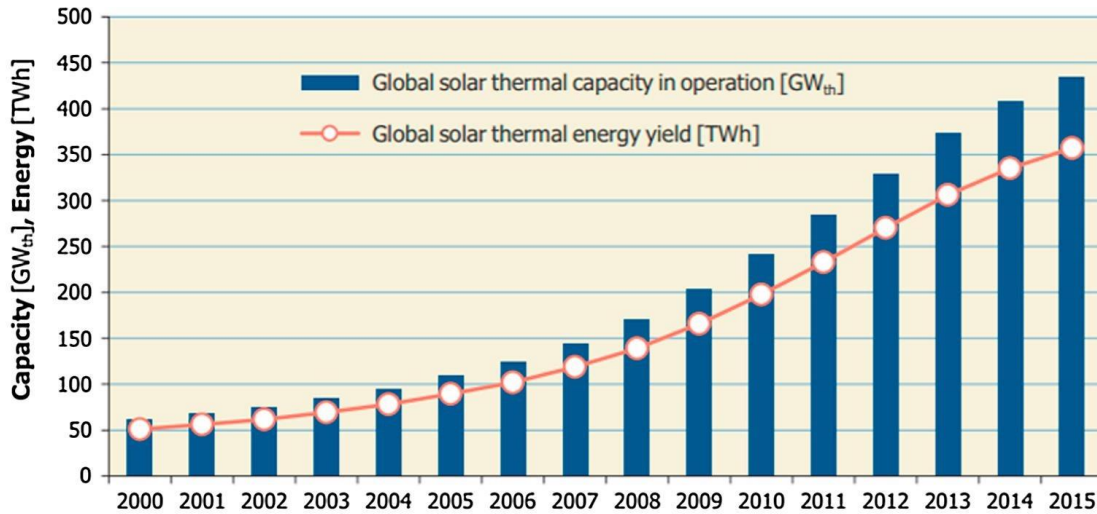
Figure 1.3: Global solar thermal capacity (Ramos *et al.*, 2017)

1.2.4 Solar photovoltaic technology

The conversion of solar radiation into electrical energy has been intensified with broad applications for human development. A continuous increase in the capacity of photovoltaic has been observed over the past decade. From an optical point of view, the PV modules are optimised by minimising reflection losses. Anti-reflective coatings are also added at the cell surface, usually in blue, from the rear to the front face.

The layers are as follows:

- *Glass:* thickness between 3 and 4 mm, depending on the manufacturer.
- *A thin layer of EVA (ethylene-vinyl acetate):* used as a glue (it is difficult to determine with precision its thickness after solidification); an optically thin layer is usually 75 μm of TiO_2); and
- *A thickness of photovoltaic silicon cell:* about 200 to 300 μm, again, depending on the manufacturer.

The optical behaviour of the encapsulation in the cell panels absorb a part of the radiation and convert it into electricity, depending on the gap (from 400 nm to 1010 nm) of the material used. For example, modules with crystalline silicon have a yield in the order of 10 to 15%, while the rest of this energy (85-90%) is converted as heat or it is evacuated from the cells through the encapsulation by thermal conduction and convection (Shamachurn & Betts, 2016). The

photovoltaic module dissipates this thermal energy through its surface in convective, irradiative and the infrared heat modes. However, this thermal energy is neglected in the literature.

Several semiconductor materials are used to build solar cells, each semiconductor material having advantages and disadvantages. The semiconductor materials are generally made of silicon and crystalline and thin-film type as described in Table 1.1.

Table 1.1: Crystalline (wafer-based) and thin-film photovoltaic cells

	Bulk type/wafer-based (crystalline)		
	• Mono-crystalline	• Poly-crystalline Si	• Poly-crystalline band
Pros	• High efficiency	• High efficiency concerning price	
Cons	• Increase manufacturing cost caused by the supply shortage		
	Thin-film type		
	Amorphous Si	CIGS	CdTe	Polymer organics
Pros	• Low price	• Low price • Able to automate all manufacturing process		• Low manufacturing • Can be more efficient
Cons	• Low efficiency	• Low efficiency		

1.3 Statement of research problem

The PN junction of the semiconductor material converts solar radiation intensity into electricity (Blaabjerg *et al.*, 2004; Md Kafiul Islam, 2011). The main problem is the low energy conversion efficiency of the semiconductor materials. Most of the absorbed radiation is discarded in the PV module as wasted heat, increasing the solar cell operating temperature (Han *et al.*, 2018; Moussavou *et al.*, 2016; Koech *et al.*, 2012). The output characteristics of a solar PV module mostly depend on solar radiation, as well as its operating temperature. An increase in the solar cell temperature decreases the open-circuit voltage and slightly increases the short-circuit current. Example, the solar cell efficiency reduces by approximately 0.5%/°C and 0.48%/°C rise in temperature respectively for silicon and multi-crystalline module. Thus, the solar cell is less efficient at high operating temperature (Matsukawa & Kurokawa, 2005; Rupnik & Westbrook, 2014; Sun & Chen, 2014).

On the other hand, the combination of the photovoltaic and solar thermal system is used to increase the energy efficiency of the system, while simultaneously generating electrical and thermal energy to the load (Ramos et al., 2017; Singh et al., 2013; Delucchi, 2011) (Delucchi, 2011) (Singh *et al.*, 2013). However, the overall efficiency of the combined PV and thermal energy is always compromised as one of the sub-systems performances might undesirably overtake the other. For example, the glass cover creates additional reflections, which substantially decrease the electricity efficiency in PV/T system. The top of the glass layer decreases the direct sun radiation transmission while the evaporation at higher temperature remains the central problem of the design that reduces the thermal efficiency since the water evaporation pressure is significant. Also, this glass is fragile, especially at the backside (Lan *et al.*, 2012; Tian & Zhao, 2013). Other PV/T system designs are based on air, water, refrigerants, heat pipes, nanofluid and phase change material present some shortcomings on the material properties used, the high component cost, chemical reaction and corrosion. Hence, more research and development need to be carried out to improve the efficiency of a PV/T system.

1.4 Investigative questions

This research project tends to develop a multifunctional performance of PV module so that the integration of photovoltaic and solar thermal (PV/T) system can vary the thermal (internal heat generation) and electrical energy production depending on the user energy need and weather conditions.

The investigative questions to guide this research are as follows:

- Are there any energy gains in coupling the photovoltaic and thermal system?
- What is the potential improvement of the proposed PV/T system?
- What are the optimal performances of the proposed PV/T system?
- What type of energy storage technology is suitable for the proposed PV/T system at the implementation level?
- What is the efficiency analysis of the proposed PV/T model?

The answers to these questions, far from being trivial, are intuitive and deepening. Several modelling simulations were able to provide elements of responses.

1.5 Objectives of the research

Several challenges which include inefficiency and inadequate energy supply according to the demand are still experienced in PV/T systems. This study aims to develop a multiple energy performance of the PV panel, so that the PV/T system can produce electrical energy, as well as thermal energy (internal heat generation of the PV cells into useful thermal energy for domestic hot water), depending on the user need and weather conditions.

To achieve this aim, the study has identified the following objectives:

- To conduct a comprehensive literature review over PV, solar thermal, energy storages and PV/T technology;

- To propose a simple PV/T system configured to balance the production of the electrical and the thermal energy according to the energy demand and weather conditions;

- To define the optimal performances of the multi-energy production of the proposed PV/T system;

- To implement and analyse the proposed PV/T system; and

- To validate the efficiency of the proposed PV/T system.

1.6 Research design and methodology

To realise this, the following stages were carried out:

- The investigation of PV/T technologies

  o Comprehensive literature review over Photovoltaic, solar thermal, storages and PV/T technology were consulted to discover potential problems and obstacles in these areas, as well as potential research to increase the effectiveness of PV/T technology;

  o Highlight the advantages and disadvantages of existing PV/T technology, as well as its fundamental operating mechanism; and

  o Identify potential problems and solutions for PV/T technology.

- Conceptual design of the proposed technology

  o The selection of the model: further review is carried out on the energy conversion and energy storage employed for the solar PV and thermal system;

  o Discussion of the model: the proposed PV/T model provides a cooling method for the PV cells and useful heat source (for hot water). Also, identifying the energy storage systems associated with a robust control algorithm that is used to balance the energy demand; and

  o Identification of a relevant platform for system implementation: computer software utilised to carry out the study of integrated solar PV and thermal module with storage system.

- Optimisation techniques of the PV/T system

  o Key features of the proposed PV/T system regarding its functionality, components, solar thermal collector design and technical barriers are identified;

  o A control strategy based on the energy management algorithm is developed to provide multi-functional performance and energy balance of the proposed PV/T system (thermal and electrical energy); and

  o Optimisation and prediction of operational performance of the proposed PV/T system are established, including prioritisation of the electrical and thermal energy according to demand and weather conditions.

- Computer modelling and simulation of the proposed PV/T system

  o The mathematical model adopted for Integrating absorber pipe, PV array, hydraulic pump, energy storage and control unit;

  o Assignment of appropriate operating parameters of the proposed PV/T system and the optimum size and capacity of the electrical, thermal energy are other components of the system are determined; and

  o The dynamic computer simulation model is developed in MATLAB/Simulink platform, and the multi-energy production by partially converting internal heat generation of the PV cells into useful thermal energy for domestic hot water is evaluated.

32

- Validation of computer simulation models

    o Performance analysis of the system on different test levels is carried out.

    o The performance of the dynamic simulation model of the PV/T system is verified;

    o The operational performance under different environments of the designed system is evaluated and verified against the conventional PV/T systems; and

    o The efficiency of the proposed PV/T system is analysed.

1.7 Research delineation

Emphasis is placed on optimising heat exchange between the PV module and the heat transfer fluid since the conventional conversion of solar radiation into electrical and thermal energy faces several challenges.

1.8 Significance of the research

This research will:

- Establish a reliable method of combining the PV cells with the absorber pipe to form the proposed PV/T system;

- Present a computation method of the PV array temperature based on heat transfer theory, thermoelectric theory, and an analogy between basic thermal (internal heat generation) and electrical processes;

- Predict the optimum operating points of the thermal and electrical power using linear regression analysis;

- PV/T system that varies the thermal and electrical energy production depending on the user demand weather conditions;

- Develop subsequent control decisions to improve energy conversion methods within the PV/T collector system; and

- Develop an energy efficiency conversion which will produce and maintain electrical and thermal energy to an optimum efficiency;

- Contribute to the body of knowledge on the usefulness of PV thermal energy.

1.9 Chapter outlines

It is essential to describe this research approach and to understand the organisation of the chapters in the thesis. This thesis is partitioned into six chapters, following this introductory chapter, the research work is presented as follows:

Chapter 2 provides insights into the progress of the simulation and experimental results obtained from other researchers. A thorough review is carried out on solar PV and Solar thermal systems in order to understand state-of-the-art, as well as different energy storage system and technology.

Chapter 3 presents a comprehensive literature on PV/T technology and describes the overall functionality of each physical component of PV/T system performance. Also, this chapter identifies the shortcomings of the existing PV/T types systems that restrict optimum performance and propose a PV/T system model.

Chapter 4 provides a developed model for each component with a specific configuration for the simulation. A thermodynamic model is developed considering the physical properties of the materials used in the manufacturing of solar panels, under different weather conditions such as wind speed, ambient temperature, solar radiation. A comparative study is carried out to evaluate the efficiency of the PV array system while highlighting the most impacting parameters.

Chapter 5 completes the work from the previous section and also explores the improvement of the energy balance as compared to the previous chapter. A modelling of the storage tank, the electrical storage and the hydraulic pump are also carried out. It also evaluates the system dynamics of PV/T systems by integrating photovoltaic and solar thermal as a single unit. From the selected configuration, an optimisation study is conducted to obtain the optimal values of the parameters. The energy performances of the simulated systems are presented, and conclusions drawn as to their effectiveness and potential for improvement.

Chapter 6 outlines the answer to the research questions developed in the thesis, the conclusions and also recommendations for future work.

1.10 Research publications: research output

Peer-reviewed publications list

C1.   Anges Akim Aminou Moussavou, Marco Adonis and Atanda Raji "Enhanced PV module system for improved electricity conversion" 17th International Conference on Sustainable Energy Technologies (SET 2018), August 21st to 23rd, 2018, Wuhan, China.

C2.   Anges Akim Aminou Moussavou, Marco Adonis and Atanda Raji "Mitigation of the Impact of solar PV module exposed to partial shading condition" 17th International Conference on Sustainable Energy Technologies (SET 2018), August 21st to 23rd, 2018, Wuhan, China.

C3.   Anges Akim Aminou Moussavou, Marco Adonis and Atanda Raji "Impact study of partial shading phenomenon on solar PV module performance" International Conference on Industrial and Commercial Use of Energy (ICUE 2018), 16th- 17th August, 2016, Cape Town, South Africa.

C4.   Anges Akim Aminou Moussavou, Marco Adonis and Atanda Raji "Design and Simulation of Solar Cell System under Different Environmental Conditions" International Conference on Industrial and Commercial Use of Energy (ICUE 2016), 16th- 17th August 2016, Cape Town, South Africa, pp. 270-277.

C5.   Anges Akim Aminou Moussavou, Marco Adonis and Atanda Raji, "Microgrid Energy Management System and its Control Strategy", International Conference on Industrial and Commercial Use of Energy (ICUE 2015), 17th- 19th August 2015, Cape Town, South Africa ISBN 978-0-620-65912-3, pp. 147-154.

C6.   A, A. Aminou Moussavou, M. Adonis, AK. Raji, "Energy Management System in Autonomous Microgrid", South Africa University Power Engineering Conference (SAUPEC), University of Johannesburg, 28-30 January 2015, pp. 93-97, ISBN: 978- 0- 86970-786-9.

Book Chapter Publication

BC1.   A. A. Aminou Moussavou, AK. Raji and M. Adonis, 2017. "Chapter 8: Intelligent Load Shedding for Stability Enhancement in an Autonomous Microgrid System". Book

Distributed Generation: Systems, Performance and Emerging Technologies, City: Wuhan, Novas, pp. 240-262.

Journal Publications

J1.   Moussavou, A.A., Raji, A. & Adonis, M. 2019. Controllable and flexible energy production in a water-based photovoltaic/thermal system. International Journal of Engineering & Technology, 8(4): 473–477

Pending Journal Publications

J1.   Anges Akim Aminou Moussavou, Marco Adonis and Atanda Raji "Performance evaluation of coolant fluids in a solar photovoltaic-thermal (PV/T) system" Renewable Energy Focus, submitted on 15/04/2019

Chapter 2

Literature review

2.1 Introduction

The sun produces a considerable amount of energy that is released through space in the form of radiation. As the distance between the earth and the sun is far (149.6×10^6 km), only a small fraction of solar radiation reaches the atmosphere of the earth at a constant equal to 1367 W/m^2. When the solar radiation reaches the earth's atmosphere, the moisture and particles in the atmosphere diffuse the radiation by absorption, while the rest of the radiation is spread directly onto the surface. The total amount of solar radiation that reaches the horizontal surface corresponds to a combination of direct, diffuse radiation and the angle of incidence. The solar radiation reaches the earth at different wavelengths and the radiation power per unit area is designated under the spectral emission received. The effects of atmospheric spectral energetic illumination depend on the path length and the transmission characteristics (Markvart *et al.*, 2003).

The spectral irradiance attenuates the radiation propagation exponential in the function of the distance, and the air mass (AM) defines the ratio of the actual travel distance and the shortest path or the inverse cosine of the angle between the vertical and its solar zenith. The AM represents the extra-terrestrial spectrum where the sun is defined at its zenith by AM1. Additionally, the AM value referring to the photovoltaic international standards testing is AM1.5, where the mean annual latitude spectrum is 41.8° solar elevation (clear sky) (Riordan & Hulstron, 1990). The irradiation value of PV systems is one of the most common long-term assessments or analysis values, which can be used as the total annual amount of irradiation [$kWh/m^2/year$].

Both the solar thermal and solar PV generates energy from solar radiation. Solar thermal collectors transform direct solar radiation into heat and then use this medium to transfer the heat to liquid form (water with or without antifreeze), gaseous (usually air). The photovoltaic systems convert solar radiation into electrical energy.
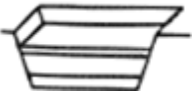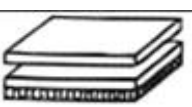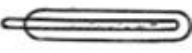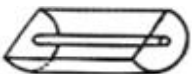
In this chapter, a review of the development of integrated solar collectors, as well as the performance characteristics of PV modules with an emphasis on temperature effects are conducted.

2.2 Collector components

The absorber is the main element of a solar thermal system and its function is to absorb solar radiation and then transform it into heat. The absorber surface is placed on a particular incline and orientation, to absorb as much heat as possible from the solar radiation. This surface should have higher absorption, around 0.95, with a dark colour which is ideal as it adds a high value of absorption. Thus, the colour selection has a significant effect, and an important replenishment could result in thermal collector losses. Material selection and construction methods have a considerable impact on the performance of the collector. The absorber also possesses an emissivity property as low as possible, less than 0.15, to limit radiation emission losses. Thermal insulation limits heat losses due to reduce heat exchange with the external temperature. Many insulating products are suitable for the rear and side insulation of a collector such as rock, wool, glass wool, polyurethane foams and melamine resin. Insulation should be preserved against corrosion and high temperature inside the collector.

The thermal energy is transferred to an energy storage tank or used directly through a natural liquid flow or forced flow. The ratio of the aperture area to the receiver area determines the concentration ratio of the solar collector in the individual categories. Solar thermal collector technology is divided into two categories: low-temperature generation and concentration temperature generation. Table 2.1 presents some of the typical solar collectors, categorised by low, medium and high temperatures.

Table 2.1: Types of solar energy collectors (Norton, 2006)

Motion	Collector type	Absorber type	Concentration ratio	Indicative temperature range T(K)
Stationary				
Stationary	Flat plate collector (FPC)	Flat	C ≤ 1	300 < T < 360
	Evacuated tube collector (ETC)	Flat	C ≤ 1	300 < T < 350
	Evacuated Envelop	Tubular	C ≤ 1	300 < T < 460
Single-axis tracking	Compound parabolic collector (CPC)	Tubular	1 ≤ C ≤ 5	340 < T < 510
			5 ≤ C ≤15	340 < T < 560
	Parabolic trough collector (PTC)	Tubular	15 < C < 40	340 < T < 560
	Fresnel lens collector (FLC)	Tubular	10 < C < 40	340 < T < 540
	Cylindrical trough collector (CTC)	Tubular	10 < C < 50	340 < T < 540

	Parabolic dish reflector (PDR)	Point absorber	100 < C < 1000	340 < T < 1200
Two-axes tracking	Heliostat field collector (HFC)	Point absorber	100 < C < 1500	400 < T < 3000

2.2.1 Non-concentrated solar thermal collectors

The non-concentrated solar thermal collector is the most simplistic form of solar thermal technology. This type of solar thermal technology consists of a receiving surface (absorber) that directly absorbs solar radiation and diffuses it into liquid. This liquid circulates in an array of tubes which are in direct contact with the absorber surface. Non-concentrated solar thermal collector, usually in the form of black carpet tubes, are made of a synthetic material which is resistant to ultraviolet radiation and is easy to put in the square. They also can be used to heat swimming pools at a low-temperature level of about 30°C at a lower cost. These types of solar thermals are limited to low temperatures due to high thermal losses.

2.2.1.1 Flat-plate collectors (air and water)

A flat plate solar collector is a heat exchanger that transfers heat energy to a fluid when it is exposed to solar radiation. Flat glass collectors are the most prevalent thermal collectors due to their high performance, insulation, absorber, low absorption of the visible light and low emissivity of the infrared (Alta *et al.*, 2010). The glazing is designed to limit the convective and irradiative heat losses, creates a virtually opaque glass property in the infrared, thereby reducing the exchange with the external environment. There is also an insulating layer on the rear module to avoid conduction losses. Flat plate solar collectors warm working liquids to a temperature scope of 10–50°C above surrounding temperatures relying upon the structure. Moreover, double glazing can achieve water temperatures of about 100°C. Their applications are used mainly for providing domestic hot water, heating of buildings and solar drying systems for agricultural products (Bakari *et al.*, 2014).

2.2.1.2 Vacuum tube collector

A vacuum tube is represented in the form of small diameter into which the absorber is placed. The tube is coated with a thin film whose optical property allows high absorbance of the solar radiation, and the reduction of heat loss. Air is evacuated from the tube to eliminate the losses due to the connection between the absorber and the wall of the tube. The surface of the absorber is covered with a selective layer and a glass to avoid infrared emissions. It is advantageous to use a vacuum collector compared to the flat plate solar collector discussed in Section 2.2.1.1. Vacuum tube solar collectors have a better performance compared to flat collectors, achieving a higher temperature performance ranging from 77 to 170°C. Vacuum isolation is an advanced technology in terms of production, which is superior to a flat collector (Azmi *et al.*, 2005).

Budihardjo and Morrison (2009) studied the properties of glass cooling tubes for solar water heaters such as optical and thermal losses, comparing the effects of flat solar collectors to solar panels. Their research reported that the evacuated tube collector array generally have lower thermal performance than the two flat plate array in the domestic water heating, in Sydney, Australia. Solar water heaters with vacuum tubes in the glass are the largest and the most widely used form of vacuum tube collector due to the high thermal efficiency.

Ma *et al.* (2010) studied the thermal performance of a glass tube solar collector using a U-tube that provides balanced energy. They concluded that if the conductivity increased from 5 to 40W/mK, the efficiency increased by 10% and the water temperature by 16%. Also, due to the heat resistance of the air, the temperature of the coating increased by 30°C. In evaluating the thermal performance of a vacuum safety valve, it is necessary to consider only the heat efficiency and the surface temperature of the heat-absorbing material.

Vacuum tubes are categorised into two systems: the conventional direct-flow absorber system, and the heat pipe system (Bloss & Pfisterer, 2013). The heat transfer fluid receives direct solar energy captured by circulating within the vacuum bulb. The cold fluid within the collector flows in the inner tube and then into the absorber surface of the vacuum, going up to the outer tube. However, it is complicated to manufacture this type of thermal collector because of the connections between the glass parts and the metallic material parts. To overcome this problem and reduce manufacturing costs, an innovative structure comprised of a heat pipe to transfer the energy captured into the fluid is used (Kumar *et al.*, 2013).

A heat pipe is an enclosed hermetic fluid containing liquid vapour equilibrium. Through evaporation and condensation of its internal fluid, this system allows the exchange of heat with

only minimal temperature deviation. The created steam is directed upward to the heat pipe, to condense in contact with the heat transfer medium. The condensed steam then returns into the evaporator through the capillary tube (Bellos & Tzivanidis, 2018).

The next section discussed the concentrator type PV/T (c-PV/T) collector used for intensifying solar radiation onto a small surface material to achieve a high-efficiency.

2.2.2 Concentrated solar thermal collectors

A large surface received and redirected solar flux to a smaller absorber surface through reflections (on mirrors, lenses) to achieve a high temperature (above 120°C); the ratio between these two surfaces defines the concentration ratio. These collectors increase in temperatures due to the reduction in the thermal losses proportional to the surface area of the receiver. However, their optical efficiency is reduced because of the concentration techniques used. Maintenance is necessitated to achieve a state of cleanliness for proper functioning. A primary constraint, besides the high cost of these devices to the plane collectors, is the tracking system intended to follow the sun along its course.

These types of collectors come with different designs such as linear geometry and densely packed modules.

2.2.2.1 Cylinder-parabolic collector (1 axis)

The cylinder-parabolic collector, consisting of a parabolic reflector (mirror), metal structure, receiver tube and a solar tracker, is the largest solar power plant (thermodynamics) ever developed for electricity generation. The parabolic section mirrors concentrate the solar radiation to a focal line with only one direction of curvature. The receiver is a tube placed on a narrow focus, in which a heat transfer fluid circulates. The heat transfer fluid (water or oil) circulates through the system and can heat up to 450°C. The advantage of these parabolic mirrors is that the tracking of the sun takes place on a single axis instead of the two axes like the heliostats. The concentrators are generally oriented to the north-south and pivot from the east toward the west to follow the course of the sun (Heinloth, 2006). High power is achieved by interconnecting several collectors together. However, it is limited to the drops in pressure and thermal losses which increases with the size of the installation (Bellos & Tzivanidis, 2018).

Based on a small parabolic dish, Kribus *et al.* (2006) designed a small and straightforward concentrator PV system for rooftop application. This design was capable of intensifying solar radiation 500 times.

Some high latitude countries are more attracted to concentrators and reflectors because sunlight varies throughout the year, and clouds cover the sky during the rainy season. Two types of parabolic reflector materials have been used and compared are anodised aluminium, and stainless steel, the record from experimental measurement data revealed that the two materials have similar output energy (Nilsson *et al.*, 2007).

Kostic *et al.* (2010) also studied the reflection efficiency of a flat plate composed of an aluminium sheet and aluminium foil collectors. Both materials have the same total reflectance, but the specular reflector was dominated by the aluminium foil concentrator, resulting in an increase of the solar radiation intensity. The energy produced by a c-PV/T collector using aluminium foil is higher than the energy produced using an aluminium sheet.

2.2.2.2 Fresnel lens collectors (1 axis)

Fresnel mirror collectors provide an alternative solution to cylinder parabolic collectors which require high cost and a parabolic shape to the glass. Several research groups worked on the Fresnel collector prototypes, focusing on the idea of approximating the parabolic shape of the collector by a succession arranging plate mirrors in parallel form. The radiation is reflected at the focal point by a set of mirrors and reflectors, which redirect the radiation to the receiving absorber (Nayak *et al.*, 2015). The heat transfer fluid (water, oil, steam) circulating in the absorber and can be heated up to 400ºC (Saxena *et al.*, 2016). The result is a simple and less expensive system with low efficiency as regards to concentration. The first reflector stage is installed on the floor while the second stage reflector redirects the radiation toward the receiver tube. The Fresnel mirror acts as an insulator of the receiver tube, covering an essential layer of insulation in the upper part (Bellos & Tzivanidis, 2018). The main advantages of this technology over traditional concentrators are as follows:

- Lower cost of the mirror;
- Lack of vacuum in the receiving tube, beneficial to its design and sustainability; and
- The disposition scope mirror is reduced due to wind pressure and mechanical stress.

The system combination of a low concentrator PV/T system prototype with the flat plate below the PV collector and linear Fresnel concentrator has been developed to provide more than 60%

efficiency. In 2005, Rosell *et al.* reconfirmed the theoretical analysis of the importance of thermal conduction. An energy flux ratio range from $10 < C < 40$ was used for an experiment on a c-PV/T collector (Li *et al.*, 2011). The results obtained were improved while the distribution light intensity was uniform on the collector plate. A low tracking system was developed for a compound parabolic concentrator associated with PV systems which improved the output voltage (Guiqiang *et al.*, 2012).

2.2.2.3 Parabola of revolution (2 axes)

Parabola axes follow the direction of the sun so that the rays could reflect the focus location (zone of maximum concentration). Mobilising the parabola on two axes of rotation ensures the continuation of sunshine and limits the unit size of this type of installation. The surface areas of the parabolas are typically from 50 to 100 m^2, with the largest one being 500 m^2. Furthermore, the average concentration factor obtained in focus can reach an exceedingly high temperature (over 800°C) (Bellos & Tzivanidis, 2018).

2.2.2.4 Parabolic and spherical collectors

The solar radiation reflected by the parabolic reflector converges towards a single point called the parabolic focus. The system must be oriented towards the sun at any time, depending on the two axes, which means that a precise control drive is required. The average concentration factor is more than a thousand, allowing high-temperature fluid to exceed 700°C. The maximum concentration of the collector is 46165; the maximum yield is 25%. The models of these plates, ranging from 50 to 100 m^2, are well suited to generate moderate power (5 to 25 kW) (Senthil & Sundaram, 2018). Parabolic or spherical concentrators are also known as plates.

2.2.2.5 Solar power tower station

Central solar collector is a popular system and operates at a higher temperature, with high electrically conductive materials. It is desirable to use a steel solar heating system due to its high temperatures. The solar power tower is suitable for selective damping coatings at temperatures above 200°C. This system is promising but often affected by a shorter experience of parabolic techniques (cylinder-parabolic mirrors). The solar tower requires fewer hoses on the ground but suffers from a large number of heliostats equipped with sophisticated two-axis trackers (AlZahrani & Dincer, 2018). Photovoltaic energy conversion is discussed in the section below.

2.3 Photovoltaic modules

Photovoltaic modules are made to convert solar radiation into electrical energy. They are characterised by their peak power under certain conditions in the laboratory. Besides this, the performance of the PV module is related to the operating temperature of the PV modules. Generally, the generated electricity decreases when the temperature increases above the threshold value (Maghami *et al.*, 2016).

The solar module converts photons of different wavelengths into electricity by its spectral response (SR). SR is determined by its band gap, cell thickness and transport properties of the carriers in the material. The amount of current generated by a module depends on the wavelength of the spectral response to the given input power in the form of light. The spectral response defines a short-circuit current that is obtained at the wavelength of the photovoltaic modules and it is measured in watts per square metre per nanometre ($W \cdot m^{-2} \cdot nm^{-1}$). The short-circuit current depends on the band gap of the PV module, which depends on the PV cell technology used. The short-circuit current (I_{sc}) of the photovoltaic module is calculated through the integral product of the external SR and the required spectrum (Tanabe, 2009; Hsu *et al.*, 2013).

2.3.1 Photovoltaic module performance parameters

A photovoltaic module is a semiconductor device that can be approached by a simple dark diode equation, derived from the current-voltage (*I-V*) characteristic curve. It allows the current to flow in the direction of forward-bias and blocks any reverse current flowing in the circuit, or so-called reverse bias, as shown in Equation 2.1.

$$I_D = I_0 \left(e^{\frac{q(V_j)}{nkT}} - 1 \right)$$

(2.1)

where:

I_0 is called the saturation current of the diode, (A);

n is the ideal factor of the diode;

q is equal to 1,602 x 10^{-19} C, absolute value of electron charge;

k is the Boltzmann constant, equal to 1.38×10^{-23} J/K;

T is the temperature of the device in Kelvin (*K*); and

V_j is the voltage across the diode junction, (V).

A diode equation has a significant influence on the circuit, as it affects the operation of the diode. A junction voltage is represented by the following equation:
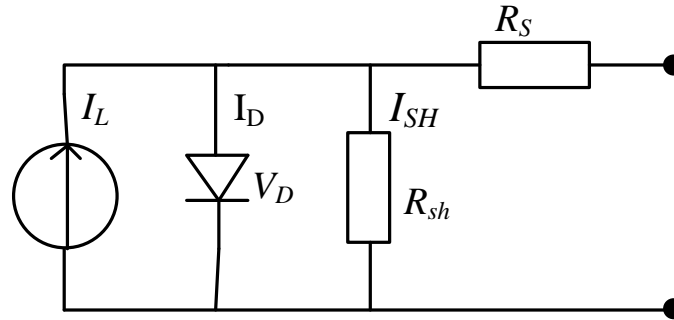
Figure 2.1: PV cell model

$$V_j = V + IR_s \tag{2.2}$$

The diode is a good correspondent of the photovoltaic cell. Figure 2.1 shows the photovoltaic cell model: the current source in the circuit shows the photon-current, I_L. However, when considering a practical device, it has some limitations. This modification entails expressions by adding parallel and series resistance and has high ohmic parasitic losses.

The series resistance (R_s) is relative to the contact resistance between the metal and the semiconductor, the semiconductor layer resistance and the resistance of the front side of the external conductive electrode. While Shunt resistance is comparative to the semiconductor material, including the PN-junction of the solar cell, the edge defects of the solar cell surface, the concentration of impurity, and the defections caused by the carrier compound or capture and so on (Wang *et al.,* 2017).

Analysis using a simple equation of net global extraction gives the following (Tian *et al.,* 2012):

$$I = I_L - I_0 \left(e^{\frac{q(V_j)}{nkT}} - 1 \right) - \frac{V_j}{R_{sh}} \tag{2.3}$$

The fill factor (FF) is the ratio between the maximum power of the module (P_{mp}) and the ideal power ($I_{sc} \cdot V_{oc}$). FF can provide information about efficiency and can be used as an indicator of the module quality. Also, it shows the effect of parasitic resistance on the PV module. Maximum power point (P_{mp}) is a state of voltage and current specific to the power of the solar cell and reaches a maximum when the derivative of the power is equal to zero. The equation is given as follows:

46

$$FF = \frac{V_m I_m}{V_{oc} I_{sc}}$$ **(2.4)**

where:

V_m is the voltage at the Maximum power point (V)

I_m is the current at the Maximum power point (A)

I_{sc} is the short-circuit current (A)

V_{oc} is the open voltage (V)

The conversion efficiency of the module is the ratio of maximum power transfer of the PV module and the incident of the solar radiation on the surface of the photovoltaic module given by Equation 2.5. It is determined under standard test conditions (STC): 1000 W/m^2 irradiance; air mass 1.5; the module temperature 25°C; and an incident angle 0°C. Under these conditions, the power of the module is referred to as peak power (W$_p$). The equation is given as follows:

$$n = \frac{V_{oc} I_{sc} FF}{AG}$$ **(2.5)**

where:

A is the surface of the module (m^2);

G is the irradiance falling on the surface of the module (W/m^2).

2.3.2 Influence of the operating temperature of the PV module

The performance of the PV module depends on the ambient temperature and solar radiation. The range of temperature depends heavily on the local wind speed, the material and structure of the photovoltaic module such as glazing-cover transmittance and absorbance. A photovoltaic module is directly affected by temperature as it reduces the V_{oc} and, consequently, the maximum power (P_{mp}). High temperatures reduce the effectiveness of the module band gap. When the temperature increases due to the formation of electron-holes which require less energy, the open-circuit voltage decreases, the band gap decreases and the dark current saturation increases (Löper *et al.*, 2012; Singh & Ravindra, 2012). Photovoltaic performance is characterised by the *I-V* characteristic curve shown in Figure 2.2.
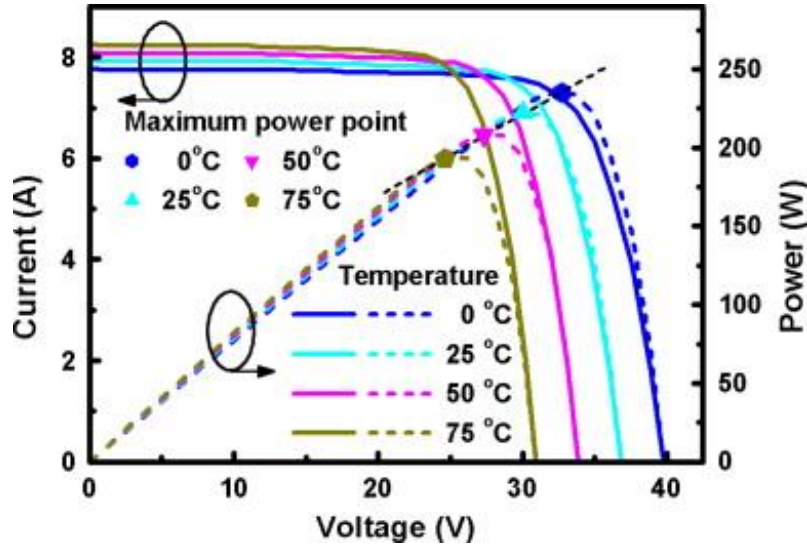
Figure 2.2: The PV array characteristic under various temperatures and an irradiation intensity of 1000 W/m^2 (Wang *et al.*, 2011)

The curve is used to obtain photovoltaic parameters, such as short-circuit current, open-circuit voltage, fill factor and efficiency. Figure 2.2 shows that when the temperature increases, the open-circuit voltage of the photovoltaic module decreases, with a slight increase in the short-circuit current. As temperature varies, the effect on the I_{sc} is marginal, while the impact on V_{oc} is substantial (Löper *et al.*, 2012; Singh & Ravindra, 2012). The equation is given as follows:

$$V_{oc} = \frac{nkT}{q} \ln\left(\frac{I_L}{I_o}\right)$$

(2.6)

2.3.3 Problems of heating of photovoltaic cells

The use of RE has been widely promoted in many countries around the world to significantly reduce greenhouse gases (Lu, 2017; Moussavou *et al.*, 2015). Additionally, solar photovoltaic technology is preferred because of its availability, sustainability and environmentally friendliness. The transformation of solar radiation into electrical energy has been intensified in recent decades. Several applications — such as solar electric propulsion and solar desalination — are also derived from solar energy. Photovoltaic systems are integrated into society to promote energy autonomy. However, the main problem of this type of conversion is its low energy output efficiency.

Solar modules are connected in parallel and/or in series in the array to provide the desired current and voltage. When the *I-V* characteristic curve of the photovoltaic module has a different value

due to cell damage, radiation change, temperature inequality, local shading and pollution, the power output of the PV generator decreases considerably (Teo *et al.*, 2018; Swart & Hertzog, 2016; Arjyadhara, 2013)

The electrical characteristics of a solar cell depend on the temperature of the junction. Furthermore, the short-circuit current increases with temperature while the open-circuit voltage decreases approximately linearly with the temperature. Consequently, the yield of a photovoltaic module decreases when its operating temperature increases (Chander *et al.*, 2015). The yield of the solar cell reduces by about 0.5% per degree unless the climate is considered (Dupré *et al.*, 2018).

The PV power significantly decreases when lower shunt resistance and higher series resistance (Zegaoui *et al.*, 2012). The local ohmic shunt of a solar cell heats up under local shading conditions, creating a hot spot, due to the reverse current through the shunt. Depending on the size of the hot spot and the reverse current, this can damage the solar module (Zaraket *et al.*, 2017; Warta *et al.*, 2011). When the module operates under partial shading, the energy conversion rate is amplified in the opposite direction. In this case, all photovoltaic cells connected in series will produce the same amount of current while the shading cells generate the smallest currents. For this reason, the shadow cell is reversely polarised, producing high temperatures because it is charged (Humada *et al.*, 2014; Lu *et al.*, 2013).

Previous studies have neglected the analysis of the origin of the problem. The performance of the photovoltaic module instantaneously decreases when the temperature increases and favours long-term degradation (Chander *et al.*, 2015; Royne *et al.*, 2005). It exists in various types of solar cell material, for instance, silicon, monocrystalline, polycrystalline and amorphous solar cells have efficiencies of 20%, 12% and 7%, respectively (Kosyachenko, 2011). The PV module overheating is proportional to the reverse current (Zaraket *et al.*, 2017). These phenomena become important when some cells operate under reverse bias mode and in turn, destroy the particular cells, thereby disrupting the entire photovoltaic system (Tiwari & Dubey, 2010).

Solar energy technologies are environmentally beneficial as compared to conventional energy sources. Besides, solar technologies are the most suitable for use in urban areas (Bose, 2010; Theocharis *et al.*, 2005).

According to Alharbi and Kais (2015) and Humada *et al.* (2014), the main factors of loss and physical limits of photon-electrons within a photovoltaic cell are in presented in Sections 2.3.4 and 2.3.5 below.

2.3.4 Losses due to extrinsic and intrinsic in a solar cell

The power losses in the solar cell been reported and classified according to extrinsic and intrinsic losses, and optical and electrical losses (Jha, 2009; Henry, 1980) as shown in Figure 2.3.
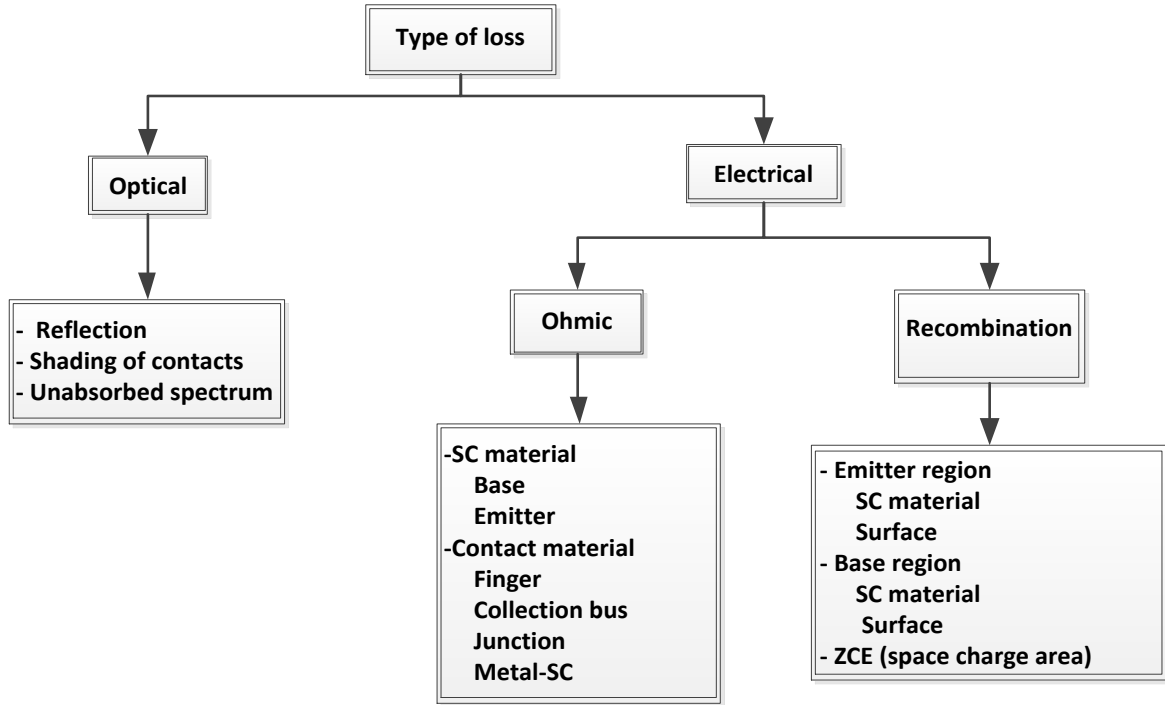
Figure 2.3: Different sources of losses (Jha, 2009)

Extrinsic loss: these losses can be eliminated and are due to external factors. They include losses due to reflection, shading, series resistance, incomplete collection of generated photocarriers, absorption in the window layer and non-radiative recombination.

Intrinsic losses: these types of losses are due to two factors:

- The inability of the single-junction solar cell to respond efficiently to all wavelengths of the solar spectrum. The solar cell becomes transparent for photons whose energy is less than the energy of the forbidden band of the semiconductor when $E_{ph} < E_g$. On the other hand, provided that the photons have an energy higher than the forbidden band when $E_{ph} > E_g$, the extra energy is dissipated in the form of heat.

- The second type is as a result of radiative recombination in the solar cell.

2.3.5 The recombination loss

Recombination is defined as the reverse mechanism of generation. It engages a loss of energy; excess carriers disappear by restoring their thermodynamic equilibrium. A disturbed semiconductor restores its thermodynamic equilibrium through several possible mechanisms:

- *Radiative recombination:* direct band gap materials are often restricted by radiative recombination;

- *Indirect or assisted recombination:* SHR constrains solar cell with low material quality;

- *Auger recombination:* solar cells with high V_{oc} are regularly restricted by Auger recombination; and

- *Surface recombination.*
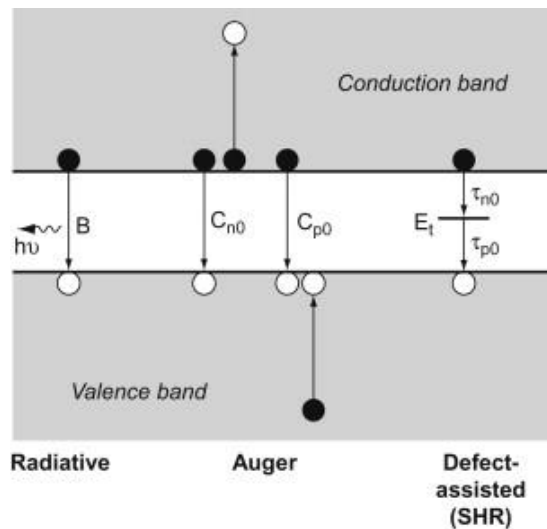
**Figure 2.4: Diagram of the main recombination processes
in a semiconductor (Jha, 2009)**

The radiative and the Auger recombination are intrinsic processes, while SRH and surface recombination are extrinsic processes assisted by a defect level in the band gap and thus are at the origin of heating during their realisation. Figure 2.4 presents the primary recombination process in a semiconductor.

2.3.5.1 Radiative recombination

This mechanism is dominant in pure semiconductors, with a direct gap structure such as GaAs. Radiative recombination is described as the reverse mechanism of optical absorption; an electron

from the conduction band combines with a hole in the valence band. The energy of the emitted photon will correspond to the gap energy of the forbidden band of the material. This phenomenon is characterised by the short life of the minority carriers. The spontaneous radiative recombination is shown in Figure 2.5.
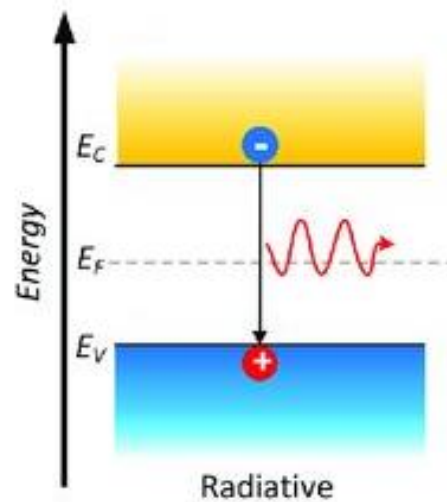
Figure 2.5: Radiation recombination

The rate of total recombination is proportional to the concentration in the material. In the absence of a generation phenomenon, the overall recombination rate is calculated by the following formula (Vázquez & Rey-Stolle, 2008):

$$U_{rad} = B(np - n_i^2) \tag{2.7}$$

where:

B is a constant that depends on the semiconductor used;

n_i the intrinsic concentration; and

n and p represent the concentrations of electrons and holes at equilibrium.

2.3.5.2 Indirect or assisted recombination (SHR)

The Shockley-Read-Hall (SRH) recombination process relies on the material quality and imperfections of the material. Assisted recombination occurs in indirect gap semiconductors. This mechanism introduces a step in the transition between the conduction and valence (the depletion zone) in the form of a trap located at a level in the forbidden band, as seen in Figure 2.6. The defect comes from impurities or the structure of the network.
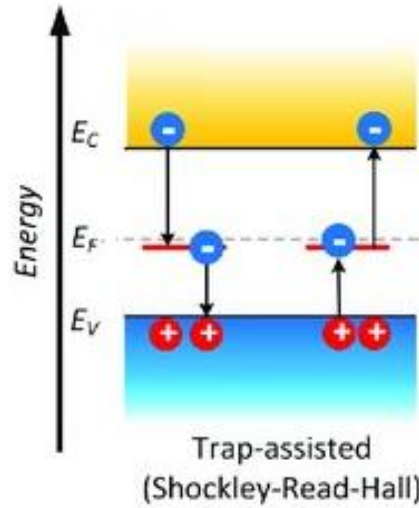
Figure 2.6: SRH recombination process

The indirect recombination rate for N_t defect concentration located at an energy level and in the forbidden band is represented by the Shockley-Read-Hall formula (Vázquez & Rey-Stolle, 2008):

$$U_{SHR} = \frac{\sigma_p \cdot \sigma_n \cdot V_{th} \cdot N_t \cdot (np - n_i^2)}{\sigma_n \cdot (n + n_1) + \sigma_p \cdot (p + p_1)}$$

(2.8)

It has been diminished using watchful creation strategies that reduce surrenders in the semiconductor precious stone. The equation is given as follows:

$$n_1 = n_i \cdot \exp(\frac{E_t - E_i}{kT})$$

(2.9)

$$p_1 = p_i \cdot \exp(\frac{E_t - E_i}{kT})$$

(2.10)

where:

N_t : concentration of defects;

σ_p , σ_n sections of effective capture by the hole and the electron;

V_{th} : thermal speed;

E_i : intrinsic Fermi level; and

U_{SHR} >> is given in free carriers, cm^{-3}. s$^{-1.}$

2.3.5.3 Surface recombination

The surface of the semiconductor has many defections after being treated during polishing and etching. The local oxide increases in a matter of minutes over several tens of angstroms in the environment interfering with the crystalline structure near the surface. When the material is uniformly illuminated, the recombination of the surface results in an excess carrier concentration on the surface rather than in the volume. Figure 2.7 shows the surface recombination through one gap state within defect density.
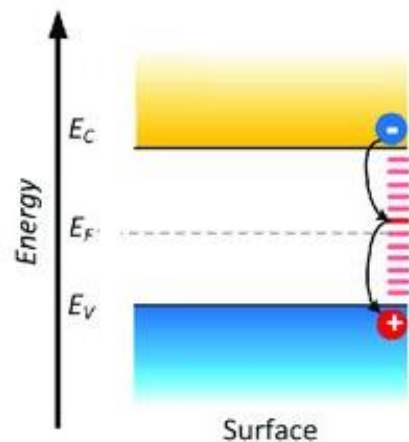
Figure 2.7: Surface recombination

The equation is given as the following (Sze & Lee, 2012):

For the material of type P:

$$J_{surface} = q \cdot S_p \cdot (p_n - p_{n0)}$$

(2.11)

For the material of type *N*:

$$J_{surface} = q \cdot S_p \cdot (n_p - n_{n0})$$ (2.12)

where:

S is the surface recombination rate (cm/s).

The recombination of the surface is documented here as a significant parameter in solar cell research, influencing the saturation of the current and quantum efficiency of the cells. The velocity depends on the properties of the semiconductor material used. The velocity is high for the direct gap of semiconductors. Some semiconductor materials are stimulated to reduce their recombination rate. For instance, in the silicon cells, an oxide layer is added, and the GaAs cell increases the window layer using the AlGaAs layer, thereby reducing the surface recombination rate which represents the surface layer recombination rate.

2.3.5.4 Auger recombination

The Auger recombination is the mechanism that occurs during a high concentration of free carriers as in the indirect gap semiconductors (Haug, 1983). The energy released by recombination transfers an electron to a higher level of the conduction band or a hole at a deeper level of the valence band. The Auger recombination is illustrated in Figure 2.8.
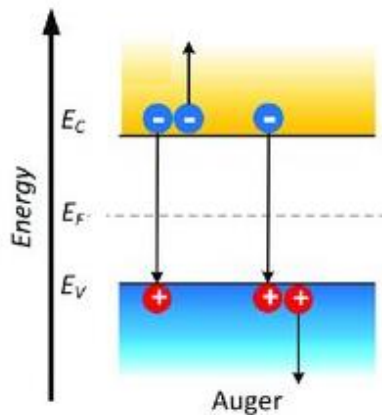
Figure 2.8: Auger recombination

The total recombination rate is calculated by the following formula (Jha, 2009):

$$U_{Auger} = (C_{p0} + C_{n0})(np - n_i^2)$$ **(2.13)**

where:

C_{p0}, C_{n0} are Auger capture coefficients of the hole and the electron.

2.3.5.5 Joule effect

Concerning the influence of Joule, it is reasonable to consider the heat dissipation due to the passage of the charge carriers in a resistivity material. It is used to determine the thermoelectric phenomenon found when charge carriers pass through an electric field. Joule heating losses associated with the internal series resistance of the module depends on the electrical properties of the metals used. Figure 2.9 illustrates the power lost through the cable due to Joule heating.
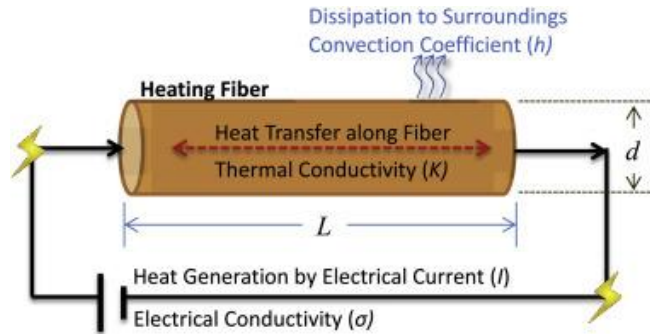
Figure 2.9: Combined loss due to Joule heating phenomenon

The combined loss in cable resistance, the contact resistance in the terminals, fuses, connectors, shunt resistance and the diode voltage drop in the array. The equation of the Joule effect leads to Equation 2.14 (Lindefelt, 1994):

$$Q(x) = \vec{I}_L(x) \cdot \vec{E}(x)$$ **(2.14)**

In n-type material, the charge distribution function of Fermi-Dirac statistic reveals that there are electrons in the conduction band in larger quantities than in the case of p-type material and that in thermal models all these electrons do not have the same energy.

In the case where the diode is in direct polarisation, the electrons of the n-doped zone move towards the p-doped zone under the effect of the electron concentration gradient between these two zones. This natural movement is due to the gradient as opposed to the potential barrier born

from the *PN*-junction. Among the electrons, only those with enough energy will be able to cross the potential barrier and conserve the electronic distribution of the doped material. These will repopulate the high energy levels and thus maintain the electronic balance of the doped material. In the case of a photovoltaic cell in direct polarisation, the photo-generated minority carriers are injected into the zone where they become the majority. During this transfer, they give up some of the energy they carry in thermal form by emitting photons. This process induces a release of energy, heating the cell.

2.3.5.6 Peltier effect

As the current flows through the metal-semiconductor interface, the difference in potential between the working output level of the metal and the valence or conduction band induces heating. It is essential to observe that despite the simplicity of the metal-semiconductor interface, the amount of energy loss in the model under the Peltier effect is the loss in a real contact in thermal form. Even with a more extensive interface, the Fermi level of the semiconductor at the surface is aligned with the output work of the metal. Thus, the charge carriers transiting between the semiconductor and the metal. This charge will always lose energy between the valence or conduction band and the output work of the metal in thermal form, either by Peltier effect or by Joule effect, provided that the surface of the semiconductor is highly doped, or by tunnel resistance, if the interface is a tunnel diode and no longer a metal-semiconductor interface without defect (Straube *et al.*, 2009).

2.3.5.7 Parasite resistances

Practically, photovoltaic modules are not ideal; they have additional parasitic resistance (series resistance, R_s and shunt resistance, R_{sh}). Both high series resistance value and low shunt resistance value influences the fill factor of the module. The efficiency of the solar cell is influenced by the parasitic resistance parameter, by dissipating the solar cell power, so their effect depends on the geometry of the solar cell and the manufacturing technology. Both resistors have a significant impact on the characteristics of the solar cell and the performance of the device (Dhass *et al.*, 2016).

(1) **Series resistance**

The series resistance (R_s) in a PV module represents the resistance in front, rear and terminal contacts and cell resistivity of the PV module interconnection; caused by the

impedance of the cathodes (gate metallization and the back face) and the deficient doping in the relatively neutral regions (emitter-base). The low estimation of the series resistance does not influence the short-circuit current and the open-circuit voltage, but slightly diminishes the value of the shape factor. On an excellent cell quality, R_s must be less than 1 Ω.
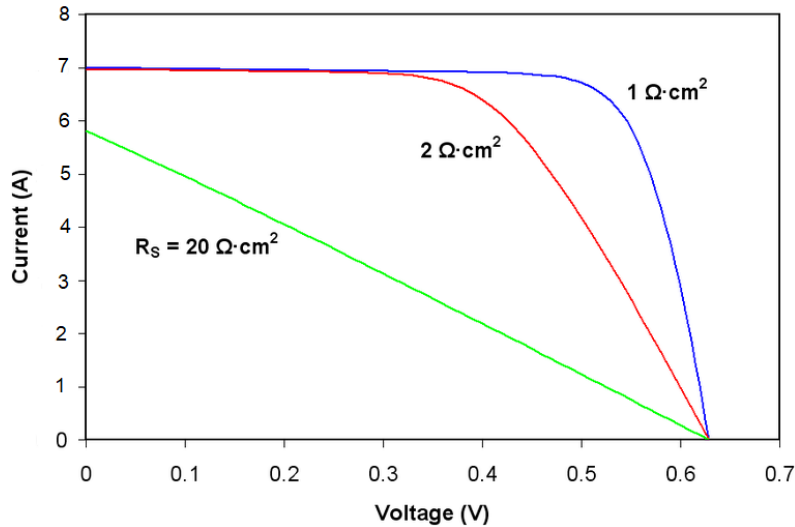
Figure 2.10: *I-V* characteristic curves under different series resistance values

The influence of the series resistance is noticeable in the *I-V* characteristic curve, with R$_s$ diminishing the short-circuit current without influencing the open-circuit voltage. The transmitter and the upper grid of the solar cell characterise the main factors of loss due to the series resistance. The optimisation is achieved by reducing the thickness of the emitter and the metal-semiconductor contact area which will reduce the resistivity of the material (Dhass *et al.*, 2016; Bensalem & Chegaar, 2013).

It is noted in Figure 2.10 that the open-circuit voltage (V_{oc}) and the short-circuit current (I_{cc}) are slightly shorter, and the characteristic curve is distorted quickly under the effect increasing in R_s value. Expansion of the series resistance impact on the operating point and the fill factor (FF) of the cell*: $P_{loss} = V \cdot R_s \cdot I = I^2 \cdot R_s$* and doubled by the current. Therefore, the loss of resistance in series is significant for the loss.

(2) Shunt resistance, R_{sh}

Manufacturing defects commonly cause losses due to shunt resistance (R_{sh}), occurring when the diffusion of high-temperature metal contacts that puncture the transmitter and

insufficient materials for photovoltaic modules, or the resistance between the terminals and the path of the PV unit not passing through the junction. This relates to the intersection resistance, which becomes significant when the PN junction is placed close to the surface. Likewise, it restricts the separation distance between grid lines in thin-film solar (Dhass *et al.*, 2016; Bensalem & Chegaar, 2013).

Figure 2.11 shows the effect of the parallel resistance R_{sh} on the *I-V* characteristic curve of the solar cell under illumination. Note that the open-circuit voltage (V_{oc}) and the short-circuit current (I_{sc}) are not modified. However, the characteristic deforms rapidly when R_{sh} increases. It is further moved from the origin point, resulting in a reduction of the photovoltaic modules FF, thereby leading to power loss. It reduces the impact on the R_{sh} photovoltaic module of the *I-V* curve.
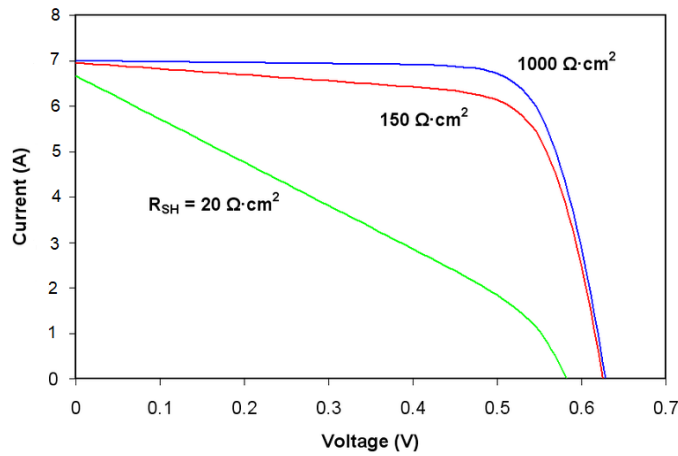
Figure 2.11: *I-V* **characteristic curve under different shunt resistance values**

Khan *et al.* (2010) have examined the behaviour of solar radiation intensity variation on silicon photovoltaic cell parameters. It has been noted that R_s diminishes consistently with solar radiation intensity. However, R_{sh} increments marginally with lower solar radiation intensity and is stable at high solar radiation intensity.

Bensalem and Chegaar (2013) examined the impact of temperature on the series resistance and shunt resistance of polycrystalline silicon solar cells, and to define a mathematical expression to fit R_s as functions of a rise in cell temperature. They reported the current-voltage attributes of polycrystalline silicon solar cell at various temperatures under consistent solar radiation (1000 W/m^2). The outcomes demonstrate that the series resistance, R_s, increasing with temperature, it is a positive temperature coefficient type, as seen in Figure 2.12; in any case, the shunt

opposition, R_{sh}, decreases with temperature and is a negative temperature coefficient type (Figure 2.13).
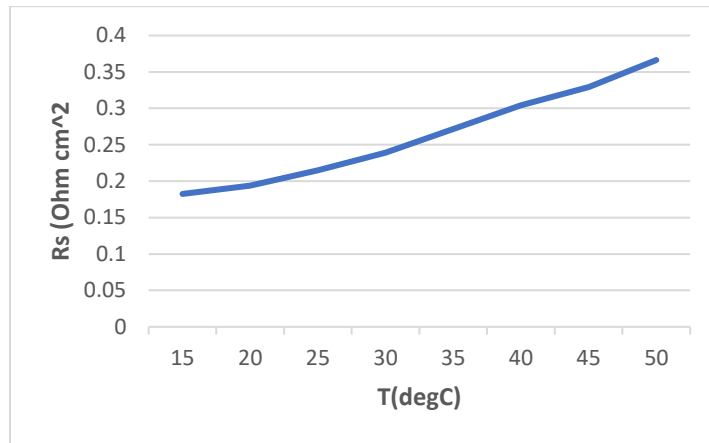
Figure 2.12: Evolution of R_s with temperature (Bensalem & Chegaar, 2013)
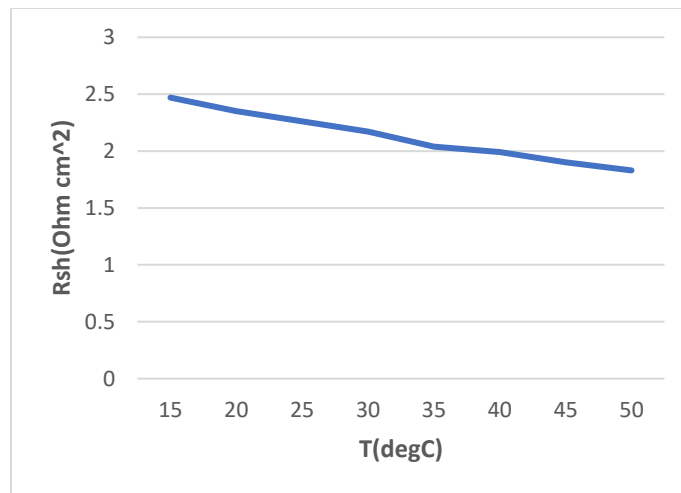
Figure 2.13: Evolution of R_{sh} with temperature (Bensalem & Chegaar, 2013)

2.3.6 Temperature and performance degradation of a PV module

Different types of photovoltaic material degradation occur through their useful lifetime. PV cells also lose output power over time, and ageing of cells can limit the power to as much as 80% of its original maximum power over 20 years. A series of factors cause module degradation of its lifetime performance and ultimate failure. Therefore, the photovoltaic material increases in R_s and

decreases in R_{sh}, encapsulating discolouration of the module or stratified packaging material and causing optical degradation.

The deterioration reflects the progress of degradation characteristics of the component or system that can affect the ability to perform operations within the acceptance criteria and the serviceability of the solar module. Whenever the module does not work correctly, it loses its primary function of generating electricity through solar radiation. However, the different degradation modes of most of the degradation of the PV module may be problematic, and it is difficult to determine the level of performance degradation through the module information, as this depends on operating conditions and manufacturing quality (Wohlgemuth *et al.*, 2006). The efficiency of solar cell modules may be reduced due to a number of factors such as temperature, humidity, radiation, dust and mechanical contact (Ndiaye *et al.*, 2013; Munoz *et al.*, 2011; Osterwald & McMahon, 2009; Wohlgemuth *et al.,* 2006; Wohlgemuth *et al.,* 2005). The photovoltaic module degradation factors can be evaluated by power loss (Dhoke & Mengede, 2017). The problem of deterioration may be due to change in colour, stratification, corrosion, cell ruptures and cracks. The foremost degradation mode of the photovoltaic module is reviewed below (Dhoke & Mengede, 2017; Luo *et al.*, 2017; Munoz *et al.*, 2011; Vázquez & Rey-Stolle, 2008).

2.3.6.1 Corrosion of PV module

Moisture appears in the PV module through the edges of the coating causing corrosion. Corrosion reacts with the metal connections of the PV module, subsequently increasing the leakage current and reducing the efficiency of the system. It also decreases the adhesion between the cell and the metal frame (Kapur *et al.*, 2009). The deterioration of the silicon PV module is triggered by oxygen, a significant factor in the corrosion and separation of silicon (Osterwald *et al.*, 2002). The weather also has a considerable impact on the degradation rate of PV modules, especially in excessively hot and humid weather. Water penetration into ethylene-vinyl acetate (EVA) is the most common source of the moisture entering solar panels during the lifetime of the module, even though the PV module is protected by the double glass to prevent moisture from penetrating the module. The method of avoiding moisture is adapted to seal the diffusion of large material (Luo *et al.*, 2017; Kempe, 2005).

2.3.6.2 Delamination of PV module

Delamination is the primary degradation mode of the solar module. Corrosion causes a loss of adhesion of the encapsulated polymer, between the solar cell and the front glass. This has two effects of concern: an increase in reflection, and water permeation into the module structure (Munoz *et al.*, 2011).

Delamination occurs mostly at the edge of the solar module, causing power dissipation and degradation of the PV module. It also creates an electrical hazard and damage to the module and all installations. This degradation of the PV module is typical in hot and humid weather. Also, it promotes moisture permeability in the module and leads to different chemical reactions in the PV module leading to decomposition, such as metal corrosion in the module structure (Han *et al.*, 2018; Skoczek *et al.*, 2008). Moreover, the penetration of salt and water into the solar panels acts as a factor for promoting delamination. It is also believed that joints can be etched with acid, hydrofluoric acid, and tin oxide available in the module (Han *et al.*, 2018; Jansen & Delahoy, 2003).

2.3.6.3 Colour change in the PV module

The colour change of photovoltaic modules occurs in the material used for encapsulation, typically in the ethylene-vinyl acetate (EVA), or glass-cell adhesion materials. This colour change may cause the cover material to turn yellow or brown. It also changes the transmission of the PV cell sealant, thereby reducing the energy generated from the PV module (Kapur *et al.*, 2009). Colour shifts may occur in various and non-adjacent areas of the same module. This may be due to the encapsulating polymers and the EVA. EVA yellow substances are used as sealants in photovoltaic modules (Wohlgemuth *et al.*, 2013). Experiments were conducted in a study based on silicon module testing from 1982 to 2003. Findings from the study indicated that there was a relationship between electricity and the discolouration of solar cell encapsulate. The discolouration of the PV module reduces the short-circuit current and may change from 6% to a nominal value of 8% (Realini, 2003).

2.3.6.4 Cracks and broken glass of PV module

Glass breakage and cracking are significant factors in the degradation of PV modules, primarily resulting from handling; for instance, during shipping, installation and maintenance. Besides, other types of degradation can result from cracked glass, corrosion and discolouration (Quintana

et al., 2002; Wohlgemuth & Kurtz, 2011). For years, to save silicon wafers and reduce the cost of producing solar cells, manufacturers have relied on decreasing the thickness of cover material as well as the thickness of the cells. Therefore, the thickness of silicon solar cells has reduced, rendering the solar cells susceptible to damage during transportation (Han *et al.*, 2018; Dallas *et al.*, 2007).

2.3.6.5 Partial shading operation

Due to the shadows of buildings, dust, trees and leaves, bird droppings, cloud cover, atmospheric fluctuations and daily changes in the angles of the sun, solar panels rarely have the same intensity of illumination (Kajihara & Harakawa, 2005). Shading also causes the total voltage drop of the photovoltaic module by absorbing energy as a load; as a result, it creates hot spots that dissipate power (Herrmann *et al.,* 1997). The effect of shade depends on many factors such as module type, fill factor, diode position and string configuration. Typically, solar panels have a bypass diode to prevent damage from reverse currents in partially shaded cells (Maghami *et al.*, 2016). Some shadow cells receive energy from shadow-free areas and force all the solar cells in series to operate at the same current. The shadow cells in the module are reverse biased, resulting in power dissipation and heating effect, creating hot spots and causing permanent damage to the PV array (Salem & Awadallah, 2016). Some authors demonstrate a substantial reduction in electrical power under the shading conditions, of the two highest points of the power-voltage characteristic curve (Samantaray & Sasmita, 2016; Meyer & Dyk, 2004). An additional discrete component (bypass diode) is introduced to the interconnected photovoltaic modules, to prevent compressed local heating due to partial shade. Variation of shunt resistance (R_{sh}) value also has an impact on the inverse *I-V* slope of PV cell, resulting in high power dissipation. This dissipated power introduces a sudden change in the local connection area, forming a hot spot which increases the overall temperature and degrades the modules (You *et al.*, 2015; Moore & Shi, 2014).

In the present study, the types of degradation of photovoltaic modules will be determined, with the factors and methods of degradation of these modules highlighted. Finally, the degradation patterns proposed in the literature will also be identified and discussed.

2.3.6.6 Hotspots and bypass diode

A solar module is a set of series/parallel solar cells whose overall appearance may vary depending on the solar radiation, the ageing of the solar cell, and the effects of shadows or discontinuous solar radiation. The shadowing or degradation of some sets of solar cells is enough to cause a significant reduction of the current flow from the photovoltaic module. The current output is higher than the current produced by a defected solar cell and the voltage becomes negative and acts as a receiver. Therefore, it was determined that at relatively high heat dissipation levels, the destruction of the solar cell might occur (Guerrero *et al.*, 2014; Hermann *et al.*, 1998). To solve this problem, the photovoltaic module is equipped with a bypass diode to protect the passive cell (defective or parasitic). The bypass diode prevents the reverse current from flowing through the defective module/cell. However, this efficient solution reduces the power and voltage at the module terminals.

This local power loss phenomenon is equivalent to the loss of any module when there is a damaged cell in the PV module (Dong *et al.*, 2016; Rabii *et al.*, 2003). Dust deposits, rain, snow and dead leaves are other factors supporting the presence of hot spots in photovoltaic modules.

2.3.6.7 Photovoltaic modules and mismatch factors

The photovoltaic modules are interconnected by a plurality of photovoltaic cells and the composition of the package encapsulated to provide cell protection during operation. The PV module is connected in series according to the Kirchhoff's law to increase the voltage, arranged in parallel to increase the current. The PV module connected in series is a relatively commonly used method. The disadvantage of this method is that the connected cells must match the current or voltage rating of the selected cell (Maghami *et al.*, 2016).

When one of the cells connected in the series produces little or no current due to manufacturing defects or shade, the other cells connected will start to dump current into the shaded cell. This results in power dissipation in the defective cell module and is equal to the current multiplied by the reverse voltage generated by the weaker solar cell. This could lead to a decrease in the photovoltaic power, while more dangerous circumstances may occur when a reverse voltage across the terminals of the defected solar cell is equal to the generated voltage at the other cell (when the module is short-circuited). This results in an even worse situation in which the solar cell is at its maximum reverse power, and the PV module is subjected to local overheating (hot spots) which can damage the PV module (Ramaprabha & Mathur, 2012; Wilson *et al.*, 2006). Therefore,

it requires quality controls in the manufacturing process to ensure that proper sequencing of photovoltaic cells is based on rated power. High shunt resistance cells limit the reverse current of the solar cell, which results in uniform solar cell heating and gradually reaches a point where it damages the solar cell (Großer *et al.*, 2012; Meyer & Dyk, 2004).

Heat may cause permanent damage to some photovoltaic modules, especially crystalline silicon technology modules. A bypass diode must be enabled to allow the current flow in the module to bypass shaded cells. Also, with this method, the PV power is reduced, which protects the module from permanent damage. When each solar cell of a module is connected to the bypass diode, the highest tolerance value is reached. However, due to manufacturing reasons, it is only connected to a cell pack. Thus, the number of bypass diodes depends on the number of unit modules. The bypass diodes are not limited to PV cells, as they are used for modules connected in arrays and mismatched when they are connected. The bypass diodes are connected across PV module terminals to allow protection of the whole PV system.

2.3.6.8 Synthesis

PV module degradations have been reviewed; many studies pointed out that delamination, corrosion and yellow discolouring are due primarily to environmental parameters such as temperature, humidity and ultraviolet radiation (Monitor & Kurtz, 2012). Silicon PV module degradation is dominated by delamination, breakage and corrosion by 42%, 19% and 19%, respectively, as shown in Figure 2.14.
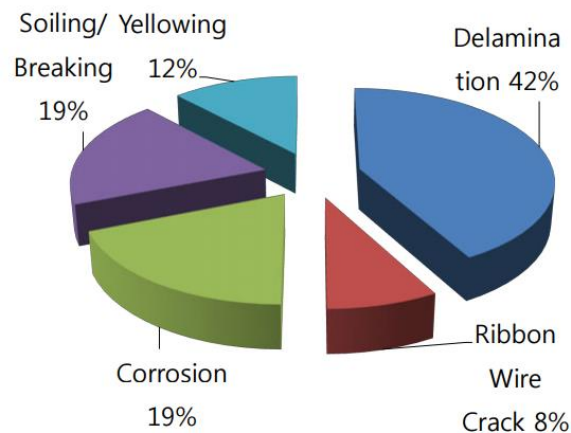
Figure 2.14: Silicon module failure (Monitor & Kurtz, 2012)

It is imperative to study reliable and efficient techniques for storing the generated thermal and electrical energy. The section below discussed the type of energy storage used in RE.

2.4 Energy storage technologies

In essence, renewable energies are intermittent; the case of solar energy illustrates the evident time lag between energy needs and the availability of the resource. One of the challenges encountered in the exploitation of solar energy is intermittency. It is impossible to store energy produced for later use. Several storage technologies are used in RE such as electrical and thermal energy. Figure 2.15 shows that the energy storage used is classified as mechanical, electrochemical, electrical and chemical.
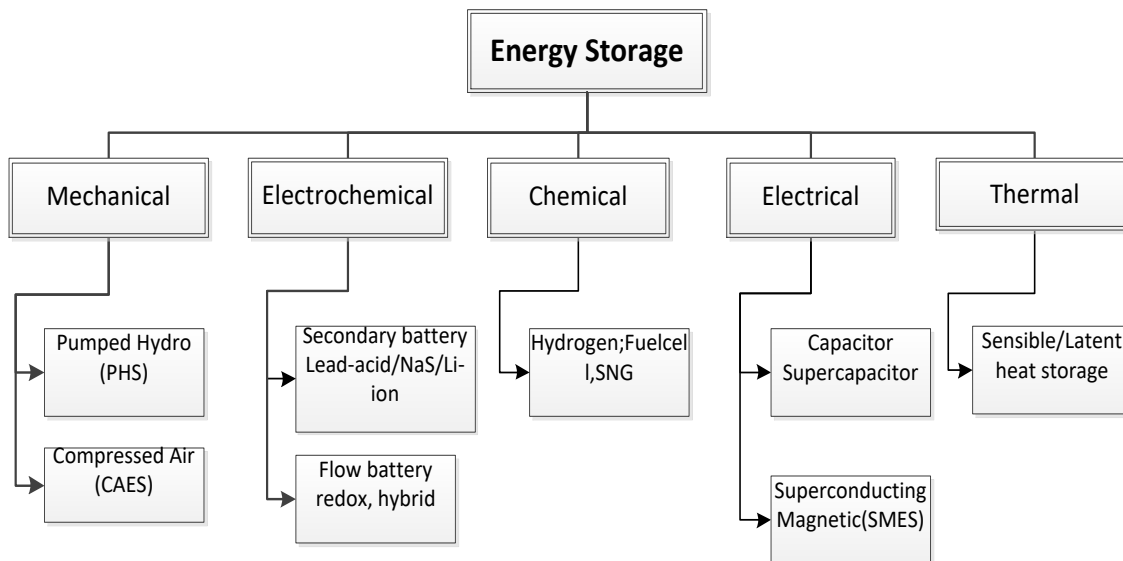
Figure 2.15: Classification of energy storage technologies (Luo et al., 2015)

2.4.1 Mechanical energy storage system

Mechanical energy storage systems (ESSs) are the most commonly used to store energy by the application of a force. The most widely recognised types of mechanical energy storage systems are pumped hydroelectric storage (PHS), flywheel energy storage (FES) and compressed air energy storage (CAES).

(1) Flywheel energy storage (FES)

The flywheel was used thousands of years ago to store energy in the form of the kinetic energy. It comprises of driving a mass (disc, ring or tube) at high speed and then

recovering stored energy during the recovery quality of braking motion (as seen in Figure 2.16). The energy capacity stored in flywheel energy storage (FES) depends on the linear speed of rotation and its inertia. In the field of transport, it is possible to store the energy in the braking system of vehicles so as to redistribute it at the start. Thus, it can store mechanical energy directly or store electrical energy by using a particular electric motor; this is used as a generator during destocking. The installed capacity of FES is estimated as slightly less than 25 MW for electrical storage. In general, the flywheel energy storage device can provide enough power in a short time at average capacity. However, it was not used as separate standby power, unless used in conjunction with other electrical energy storage or power generation systems such as a battery. The main disadvantage is that the inertia flywheel device is subjected to standby losses at idle FES in the steering wheel, resulting in a high self-discharge of up to 20% per hour (Nadeem *et al.*, 2019; Amiryar & Pullen, 2017; Ould Amrouche *et al.*, 2016; Luo *et al.*, 2015; Molina, 2012; Peña-Alzola *et al.*, 2011).
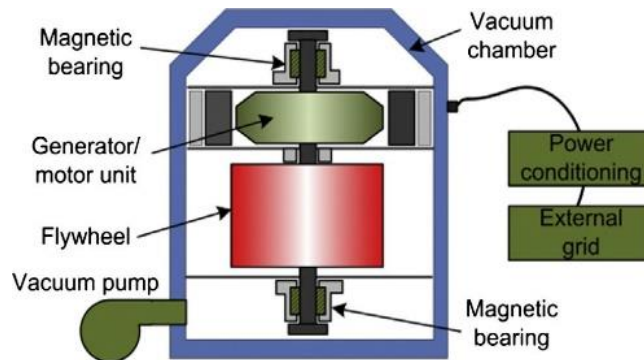
Figure 2.16: Structure of a conventional flywheel (Luo et al., 2015)

(2) Pumped hydroelectric storage

The pumping station stores electrical energy as the potential energy of water. This occurs when the stored water flow is pumped from the lower reservoir to upper storage, which increases its potential energy. Then it returns to its starting point through the turbine to generate electricity. Pumped hydroelectric storage (PHS) nominal power depends on the pressure of water through a turbine and a pump flow velocity and nominal power/turbine and a motor/generator unit (Figure 2.17). This type of storage is commonly used and makes up to 127 million kilowatts of the world's installed capacity; PHS accounts for about 3% of the total global storage capacity. PHS system operations for particular applications

are related to energy management in areas of time shift, frequency control, non-spinning reserves and supply reserves. However, with operational site constraints, PHS plant suffers high capital investment for a long time (Nadeem *et al.*, 2019; Ould Amrouche *et al.*, 2016).
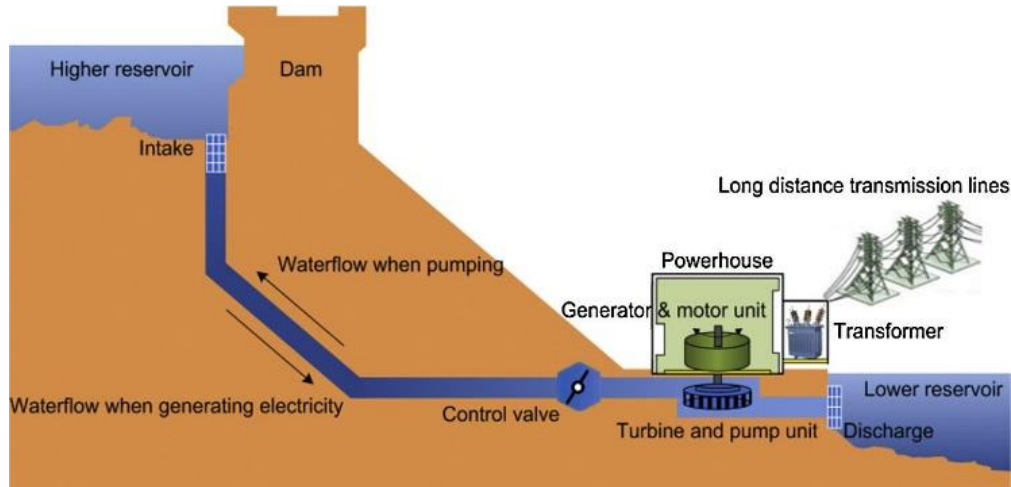
Figure 2.17: Pumped hydroelectric storage plant layout
(Molina, 2012; Luo *et al.,* 2015)

(3) Compressed air energy storage (CAES)

As an alternative to pumped hydroelectric storage, it is possible to store electricity as internal energy by compressing air, which is then stored in tanks or natural cavities (former salt mines or old natural gas reservoirs) and this is known as the compressed air energy storage system as seen in Figure 2.18.

The energy is later recovered using a decompression turbine. The global installed capacity of this type of storage device is approximately 440 MW that can deliver more than 100 megawatts of power output through a unit. Compressed air storage can work with intermittent RE applications like in wind power generation systems. As a result, CAES can perform sufficiently on a short time scale to mitigate naturally occurring fluctuations in the wind. The main barrier related to the implementation of large-scale CAES is to find an appropriate location and to fix a capital cost of the plant. The low efficiency is an additional weakness of CAES as compared to PHS and battery technologies (Nadeem *et al.*, 2019; Lutyński, 2017; Luo *et al.*, 2015).
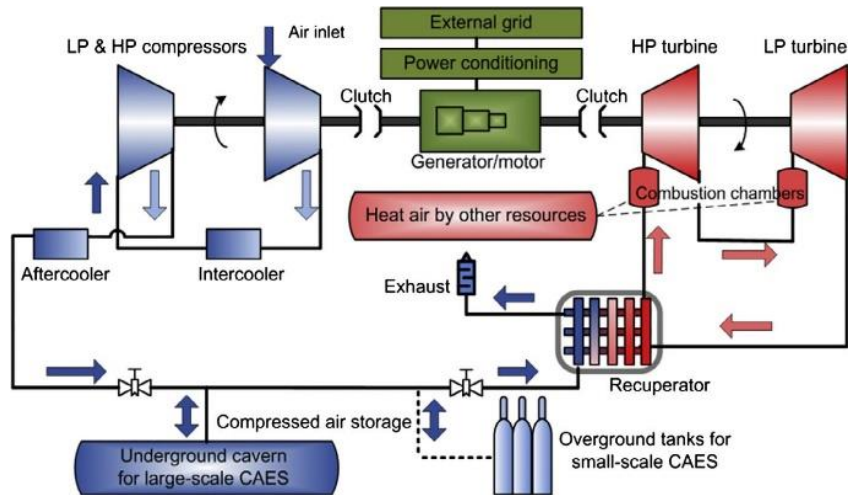
Figure 2.18: Schematic diagram of a CAES plant/facility (Luo et al., 2015)

2.4.2 Electrochemical energy storage system for the PV system

The battery is charged by an internal chemical reaction under a potential voltage applied to both electrodes. The reaction is reversible, which allows the battery to release the absorbed energy for discharging. A large portion of this type of battery storage is integrated into the photovoltaic systems. Batteries are connected in a network of series and parallel arrangements to achieve the desired charging voltage and power capacity. Every cell contains a fluid, paste or solid electrolyte together associated with anode and cathode. The most broadly perceived electrochemical energy storage is nickel-cadmium (Ni-Cd), nickel-hydrogen, nickel-metal hydride nickel-zinc (Ni-Zn) or lead-acid, sodium-sulfur (NaS), sodium nickel chloride, lithium-ion (Li-ion) and flow battery. These batteries have characteristics such as high charging/discharging efficiency, low self-discharge and long cycle life (Mohammedi *et al.*, 2016).

(1) Nickel-cadmium (Ni-Cd) batteries

The Ni-Cd battery is generally identified as inexpensive and of durable storage. The positive nickel cathode is nickel hydroxide/nickel and oxyhydroxide ($Ni(OH)_2$/NiOOH), and the negative cadmium anode is comprised of metallic cadmium (Cd) and cadmium hydroxide ($Cd(OH)_2$). The electrolyte is associated with potassium hydroxide (KOH). Ni-Cd batteries have a high energy density, reliable and require low maintenance and relatively short cycle life. This innovation, when evaluated financially, displays the most reduced cost per cycle. The Ni-Cd battery experiences downsides though, for example, the memory effect, the negative environmental impact of cadmium and a high starting

expense. Thus, it is not recommended to integrate Ni-Cd technology into RE systems (Zhao *et al.*, 2015).

(2) Nickel-hydrogen batteries

Nickel-hydrogen batteries introduce a few points of interest, for example, long cycle life and protection from overcharging. These are commonly deemed appropriate for spacecraft and satellite communications. However, the use of this type of battery for the installation of RE sources is limited by a high initial cost, especially combined with the high pressure of the battery (Oman, 1998).

(3) Nickel-metal hydride batteries

These hydride batteries are used in vehicles, medical applications and compact gadgets. This battery is like the Ni-Cd battery, excluding the fact that a hydrogen-absorbing alloy is used as the electrode instead of cadmium. Their integration into RE experienced a few disservices, for example, self-discharge, diminished life cycle and high pressure driving to failure. A larger capacity battery that can store wind and solar power are under development, especially since nickel-hydride metal batteries have fewer environmental issues and can replace nickel batteries (Ould Amrouche *et al.*, 2016).

(4) Nickel-zinc batteries

The cathode (positive terminal) of this battery is made of the nickel oxide while the anode (negative terminal) is made of zinc metal. This sort of battery has a high energy density (25% higher than nickel-cadmium), and it is environmentally friendly. The Ni-Zn battery is less expensive as compared to the Ni-Cd battery. Moreover, the Ni-Zn battery has higher energy to mass proportion and a higher capacity to mass ratio than the lead-acid battery. As a result, the Ni-Zn innovation is used in RE systems rather than both the Ni-Cd and lead batteries (Oman, 1998; Ould Amrouche *et al.*, 2016).

(5) Lead-acid batteries

The lead-acid battery system is based on electrochemical energy storage systems, a charging/discharging reaction between the positive electrode containing lead dioxide (PbO_2) and a negative electrode comprising sponge lead (Pb). The two electrodes are immersed in an aqueous solution of sulphuric acid electrolyte implicated in the charge/discharge reaction. Lead-acid batteries are commonly integrated with renewable energies such as in off-the-grid applications and UPS (uninterrupted power supply). The

lead-acid batteries are easy to carry and have a low cost compared to other types of batteries. However, conventional lead-acid batteries face a variety of technical problems, most of which are short life cycles (< 500), low depth of discharge (< 20%), limited life from three to four years, low-temperature performance slow, charging and maintenance requirements. A thermal management system is required to minimise these difficulties; also, the latest lead-acid batteries have been introduced whereby the positive electrode is less corrosive, leading to a longer lifetime and better performances than the conventional lead-acid technology (McKeon *et al.*, 2014).

(6) Sodium-sulfur (NaS) batteries

In sodium-sulphur batteries, sodium and sulphur in liquid form serve as electrodes, while sodium is the cathode and sulphur works as the anode. This enables just the positive sodium particles to travel through it and join with the sulphur to form sodium polysulfide. The battery has a high energy density, high charge and discharge efficiency (89% to 92%), long cycle life, low-cost materials, and requires smaller space for installation. Sodium-sulphur requires a high working temperature (350°C), rendering sulphur batteries difficult to use for special applications. The photovoltaic systems associated with NaS batteries can be used for peak-shaving in utilities to increase the reliability of their systems. Sodium-sulphur was the main market innovation; however, it needs to contend with the lithium-particle battery (Xu *et al.*, 2018; Ould Amrouche *et al.*, 2016).

(7) Sodium nickel chloride batteries

As sodium nickel chloride batteries work at high temperatures from around 270°C to 350°C, they are reasonably used to store large amounts of energy in RE plants because of their long release time, long cycle life and quick reaction. In any case, their utilisation is restricted by the way that heat is required to keep the liquid state temperature. Also, liquid sodium responds perilously with water and causes fires in announced episodes (G. Li et al., 2016).

(8) Lithium-ion (Li-ion) batteries

The Li-ion particle batteries depend on the exchange of lithium particles from the positive anode to the negative terminal amid charging and the other way around amid releasing. The positive electrode of the lithium-ion battery is composed of a quantity of a lithium metal oxide capable of storing lithium ions and a negative electrode electrolyte battery of a

lithium-ion battery as a carbon electrode. Lithium particle batteries require temperature control for a protected and proficient task.

Lithium-ion batteries have revolutionised electronics consumer, especially in mobile phones but shortly after that spreading to laptops, digital cameras and digital media players. The advantage is that its performance is much higher than other existing rechargeable batteries, improving energy efficiency and power density. Several positive and negative materials exist. Therefore, there are many lithium-ion chemical batteries with different output characteristics and specific energy. Although this type of battery has the most elevated value, in RE since it demonstrates the most expensive per cycle (Mahmood & Hou, 2014).

(9) Flow batteries

The flow battery stores energy at least in one kind of ion, which dissolved in the liquid electrolyte, this is the fastest-emerging storage technology. Flow batteries incorporate redox (the vanadium battery) and hybrid batteries (the zinc-bromine [Zn–Br] battery).

In a redox, flow battery is an advanced type of battery used in solar applications. Two fluids are stored in different external cartridges and pumped through the dried electrochemical cell when the battery is in use.

On account of hybrid flow batteries, just a single solution to store in an external tank; the other one is continuously maintained in the electrochemical unit. The battery capacity relies upon the size and structure of the electrochemical reactor (Leung *et al.*, 2012).

Table 2.2: Summarises the main electrical properties of two battery technologies

Lithium-ion Batteries	Lead-acid Batteries
• Becoming more common in domestic grid-connected solar PV storage systems	• Used for off-grid storage systems where additional storage is needed
• More expensive	• Less expensive
• Lighter and smaller	• Heavier and larger
• Requires integrated controller to manage the charging and the discharging	• Requires proper charging and discharging process to maintain battery health
• More efficient	• Less efficient
• Can discharge more energy stored	• Shorter expected lifetime
• Longer expected lifetime	

Several types of batteries are used in photovoltaic systems. However, the most widely recognised types of batteries are lead-acid batteries and lithium-ion batteries. Table 2.2 compares the two most popular types of batteries.

2.4.3 Hydrogen energy storage (HES)

Hydrogen energy storage is a critical innovation in RE (wind and photovoltaic system). Hydrogen is the fuel with the highest energy per mass when contrasted with other ones. The battery development requires low density at room temperature, to achieve higher energy densities. Diverse hydrogen storage modes can include compressed, liquefied and metal hydride.

In hydrogen and oxygen, a fuel cell reacts with water to generate electricity. The fuel cell is mainly composed of electrodes isolated by an electrolyte. Many fuel cells must be combined to obtain a fuel cell stack, to obtain an efficiently distributable output voltage.

2.4.4 Electrical energy storage system

(1) Supercapacitor energy storage (SES)

The supercapacitor is known as ultra-capacitor energy storage and it stores energy in the form electrolytic capacitors between the electrochemical storage components midway, allowing much higher energy density. They provide a high-power density of the battery and electrolyte tick between the conventional capacitors, with the ability to release energy more quickly than the storage battery. However, supercapacitors have limitations with low voltage and high power.
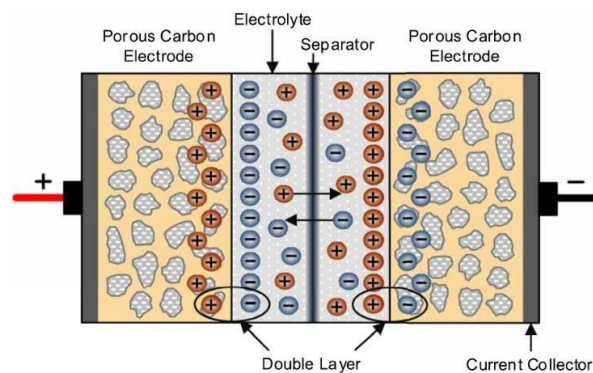
Figure 2.19: Graphical representation of symmetrical SCES (Molina, 2012)

These possible components store the amount of intermediate energy stored between two electrodes which are separated by a layer of an insulator and recover faster than the battery (Nadeem *et al.*, 2019; Mishra & Saxena, 2017; Molina, 2012). The electric charge will generate between the porous electrodes and liquid electrolytic solution, as shown in Figure 2.19.

SES is used to stifle quick wind control variances on a small-time scale. In this manner, they are viewed just as helpful for wind turbines systems and with a battery system in a hybrid storage system.

(2) Superconducting magnetic energy storage (SMES)

Superconducting magnetic energy storage is mainly comprised of a cryogenically cooling coil superconducting material, a power conditioning system and a refrigeration system (Figure 2.20). Energy is stored in the magnetic field created by the flow of direct current in the coil. SMES presents almost zero ohmic losses due to the negligible resistance of the superconducting coil. This vitality is put away as long as the refrigeration is operational. The main advantage of SMES is its effectiveness, as the system requires continuous activity and countless cycles to release the load. In wind vitality transformation framework, SMESs are not commonly used because of the coil, which is extremely sensitive to temperature changes (Nadeem *et al.*, 2019). However, SMES system requires a significant amount of power to keep the coil at low temperatures combined with the high overall cost of its employment. It is suitable for short cyclic periods only because of the memory effect and its quick full discharge time.
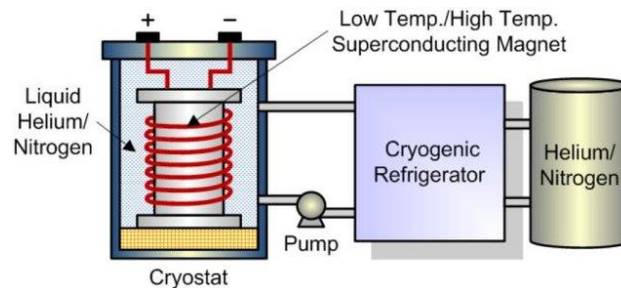
**Figure 2.20: Super magnetic energy storage (SMES)
system design (Molina, 2012)**

2.4.5 Thermal energy storage (TES)

Energy storage has emerged as a critical piece of RE technology systems. Thermal energy storage (TES) is a technology that stores thermal energy. It stores thermal energy in advance to anticipate future needs for heating and cooling applications. In a hot water tank, heat is generally provided during 'off-peak' hours.

TES technology is used worldwide and has an installed capacity of 3.3 GW, representing 1.9% of global energy storage in 2017, as described in Figure 1.3 (see Section 1.2.3). The demand for heating and cooling accounts for 45% of the total energy consumption in households and businesses globally. TES systems can significantly contribute to the heating and cooling applications, and power generation needs in both industrial and domestic sectors (Ramos *et al.*, 2017). Moreover, TES can address the mismatch between the supply and demand for energy, particularly relevant to RE. A typical TES system consists of three main components: a heat storage tank, a heat transfer mechanism (refrigeration system, hot runner and pump) and a control system unit. Initially, available heat is stored in a separate reservoir using unique techniques. Thus, the stored heat is transferred directly or indirectly for usage or generating electricity. Although the efficiency of the total cycle of the TES system is as low as 30 to 50%, its advantages are as follows: daily self-discharge almost equal to (~1%); the energy density is relatively high (specific energy 80–250 Wh/kg); and it takes environment and ecology into consideration. Low investment costs make the TES system the best choice for ample energy storage, with no significant risk in any applications (Nadeem *et al.*, 2019).
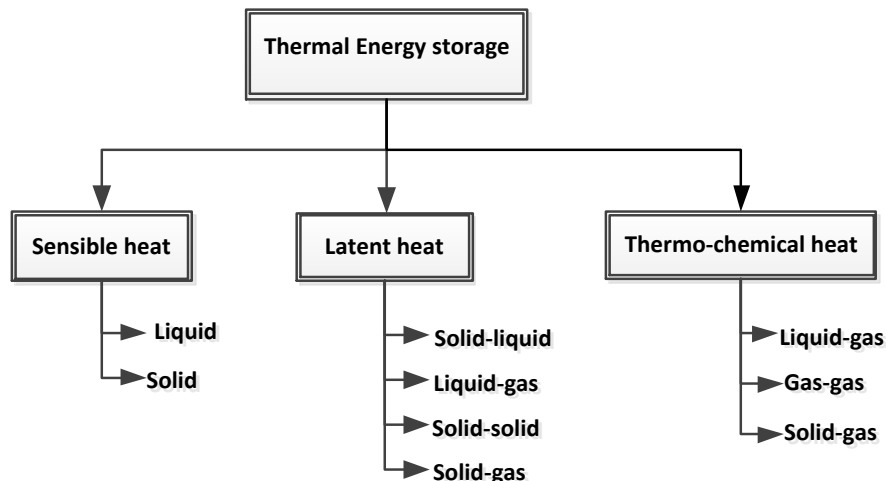
**Figure 2.21: Thermal energy storage technology-based
on the material (Pavlov & Olesen, 2012)**

Three types of thermal storage are distinguished: sensitive energy storage, latent heat storage and thermochemical storage, presented in Figure 2.21 and Table 2.3.

Table 2.3: Thermal energy storage systems comparison (Sarbu & Calin, 2018)

TES System	Capacity (kWh/t)	Power (MW)	Efficiency (%)	Storage Period	Cost ($/kWh)
Sensible (hot water)	10–50	0.001-10.0	50–90	days/months	0.1–10
Phase-change material (PCM)	50–150	0.001-1.0	75–90	hours/months	10-50
Chemical reactions	120–250	0.01-1.0	75–100	hours/days	8–100

(1) Sensible heat storage (SHS)

Sensible heat storage is the least complicated. The amount of heat stored in SHS depends on the specific heat transfer medium, the temperature change, and the amount of storage material. The most used medium is heated water, notable and cost-effective for thermal energy storage. Table 2.4 shows the main characteristics of the most commonly used solid-state thermal storage materials. Sensible heat storage can store large amounts of energy without significant risk. The loss of daily self-discharge is a small (~ 0.05–1%) tank that provides reasonable energy density, and the system is economically viable with a low cost of construction. However, the efficiency of the TES system cycle is generally low (~ 30–60%) (Sarbu & Calin, 2018; Mangold *et al.*, 2004).

Table 2.4: List of selected solid-liquid materials for sensible heat storage (Tian & Zhao, 2013)

Medium	Fluid Type	Temperature Range (°C)	Density (kg/m³)	Specific Heat (J/(kg·K))
Sand	-	20	1555	800
Rock	-	20	2560	879
Brick	-	20	1600	840
Concrete	-	20	2240	880
Granite	-	20	2640	820
Aluminium	-	20	2707	896
Cast iron	-	20	7900	837
Water	-	0–100	1000	4190
Calorie HT43	Oil	12–260	867	2200
Engine oil	Oil	≤160	888	1880
Ethanol	Organic liquid	≤78	790	2400

Propane	Organic liquid	≤97	800	2500
Butane	Organic liquid	≤118	809	2400
Isotunaol	Organic liquid	≤100	808	3000
Isopentanol	Organic liquid	≤148	831	2200
Octane	Organic liquid	≤126	704	2400

- **Water tank storage**

Water is the most commonly used material in a sensible heat storage system. The heat-resistant reinforced concrete water tanks and the heat loss due to the transfer of vapour through the wall and a glass fibre reinforced plastic composite wall. The storage tanks are low cost, rendering water a good storage media suitable for low-temperature solar cooling applications, easily improved by the stratification and insulation layers of the container. This innovation is likewise appropriated for solar thermal integrated into the building. The hot water storage systems serving as buffer storage for domestic hot water are generally in the range of several of cubic meters, with temperatures rising between 80 and 90°C.

- **Underground storage**

Underground thermal power storage (UTES) offers technology storage using the ground as a medium, such as dirt, sand, rocks and clay, to store heat. The hot water storage consists of a partially buried water tank, usually made of reinforced concrete (Sarbu & Calin, 2018).

- o *Aquifer storage* is carried out via two wells dug in a layer of rock permeable (gravel, sand and limestone) containing underground water and equipped with pumps and injection-pipes. In the charging phase, groundwater extracted from the cold well is heated by solar energy and then injected into the hot well (Mangold *et al.*, 2004; Sarbu & Calin, 2018).

- o *The gravel-water storage* usually is buried in the ground, waterproofed and insulated. In an attempt to reproduce the exchanges involved in a natural aquifer, the storage material is a mixture of stones and water. The heat is stored/extracted by direct heat exchange with water or via a network of plastic pipes inserted into different layers of the storage medium. Due to its lower thermal capacity, this type of storage requires on average 50% more volume

than a hot water tank storage system to achieve the same storage capacity (Mangold *et al.*, 2004; Sarbu & Calin, 2018).

o *Cavern thermal energy storage* is another form of thermal storage using artificial caverns such as abandoned mines and tunnels to store thermal energy. However, it does not have the accessibility of reasonable caves. It is made of rock with low thermal conductivity, high stability and inability to separate: during a work cycle under favourable conditions, the heat loss should be less than 10% (Sarbu & Calin, 2018).

(2) Latent heat

Latent heat is the energy associated with a change of state, such that material changes its phase from the solid to the liquid. The system has the property of releasing or absorbing energy with a change in physical state. The phase is reversible when the thermal energy stored is extracted by a load. The materials used, called phase change materials (PCM), are materials which change phase at a precise temperature range. PCM allows storing an average of 10 times more energy per unit volume than sensible heat storage systems (Mangold *et al.*, 2004; Sarbu & Calin, 2018).

A comprehensive solid-liquid PCMs of latent heat materials based on their physical change for heat-absorbing and release capacity is presented in Figure 2.22 by categories of organic, inorganic and eutectic materials. Further, Table 2.5 shows the advantages and disadvantages of these PCM materials.
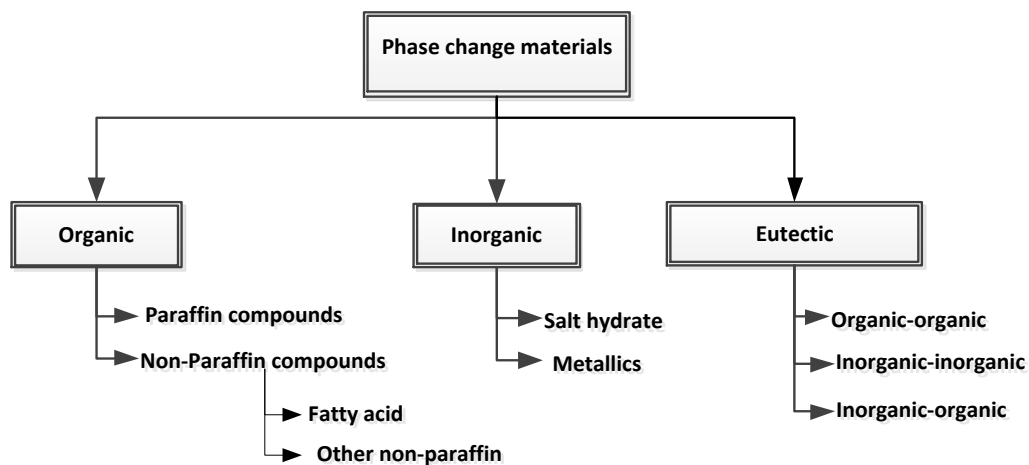
Figure 2.22: Classification of phase-change materials (PCMs)
(Pavlov & Olesen, 2012; Hassan *et al.,* 2016)

One of the weak points of PCM is its low thermal inertia, as this causes significant fluctuations in the internal temperature. In a hot water tank, both the absence of stratification and the presence of uniform temperature throughout the tank can pose a serious problem. The incorporation of capsules of different PCM creates and maintains layers of stratified water; the temperature of a segment corresponds to the melting temperature of the different materials used.

Table 2.5: Advantages and disadvantages of PCM material (Nadeem *et al.,* 2019)

Classification	Advantages	Disadvantages
Organic PCMs	• Availability in a large temperature range • The high heat of fusion • No super-cooling • Chemically stable and recyclable • Compatibility with other materials	• Low thermal conductivity • Relatively large volume change • Flammability
Inorganic PCMs	• High heat fusion • High thermal conductivity • Low volume change • Low cost	• Super-cooling • Corrosion
Eutectics	• High melting temperature • High thermal storage density	• Unavailability of current physical data of thermophysical properties

(3) Thermochemical storage

Thermochemical storage stores energy in the form of chemical bonds during reversible reactions, for example, solid-gas reactions. The energy thus stored can be released using the reverse, exothermic reaction, sometimes requiring the use of a catalyst (Kalaiselvam & Parameshwaran, 2014).

The latter, however, has the advantage, among other things, of separating the thermal power from the reactor and the storage capacity of the installation, which would make it possible to increase the storage density.

The advantage of solid-gas reactions is the high reaction rates, the possibility of using compact devices and the short reaction times in some cases. A thermochemical storage cycle uses the heat produced in a solar receiver, when it is active during the hours of sunshine, to activate an endothermic chemical reaction that must be completely reversible, thereby allowing total restitution of the thermal energy via the inverse exothermic reaction during non-sunny hours. Energy storage in the form of chemical bonds has the advantage of energy storage over long periods, without losses. This system is conducive to inter-seasonal storage. However, a disadvantage of thermochemical storage is the loss of sensible energy necessary to bridge the temperature difference between the storage (charge) and the release of energy (discharge). Thermochemical storage is the least advanced of the three existing solar energy thermal storage systems, still being at the laboratory scale of development (Pardo *et al.*, 2014; Kalaiselvam & Parameshwaran, 2014).

2.4.6 Summary and comparison of various energy storage system technologies

An in-depth analysis of the diversity of electrical storage system technologies has been addressed based on the appropriate and physical constraints from large, medium and small-scale applications.

Table 2.6 presents a comparison of different ESS technologies based on advantages and disadvantages of characteristics of the maximum storage capacity. Each ESS has its appropriate application, for example, PHS, CAES, FC, VRFB and TES have the ability to meet high energy capacity while FES and SCES/SMES are progressively appropriate for power quality. The maturity of the technology and the mass production of particular storage technology affect the capital cost necessary to develop the ESS, such as Na-S, Ni-Cd, Ni-MH, Pb-A, Lithium-Ion, FES, SCES which are at their mature stage of development and commercialise. In addition, the development of small and medium-scale commercial availability of Na-S, Ni-Cd, Ni-MH, Pb-A, Lithium-Ion, FES, SCES, FC, FES, SCES, SME, VRFB, HFB and TES in particular support various applications such as RE, standalone grid and electric vehicle (EV) applications (Table 2.7).

Table 2.6: Characteristics of electrical energy storage (Zhao *et al.*, 2015)

Storage Technology		Power rating (MW)	Lifetime		Efficiency (%)	Main Advantages (relative)	Disadvantages (relative)
			In (years)	In (cycles)			
Pumped Storage		00–5000	> 50	> 15,000	70–80	High Capacity, Low cost	Special site requirement
CAES		5–300	> 25	> 10,000	41–75	High Capacity, Low cost	Special site requirement, need gas fuel
Flow Batteries:	VRB	0.03–3	5–20	> 10,000	60–75	High Capacity, Independent power and Energy ratings	Low energy density
	ZnBr	0.05–2	5–10	1000–3650	65–75		
Metal-Air						Very High Energy Density	Electric charging is difficult
NaS		0.05–8	10–15	2500–4500	70–85	High Power and Energy Densities, High Efficiency	High cost, safety concerns (addressed in design), high operation temperature
Li-ion		0–0.1	5–100	600–1200	65–75	High Power and Energy Densities, High Efficiency	High production cost, requires a special charging circuit
Ni-Cd		0–40	5–20	1500–3000	60–80	High Power and Energy Densities, High Efficiency	Dependent on the cycle depth, suffer from the memory effect
Lead-Acid		0–20	3–15	250–1500	75–90	Low capital cost	Limited cycle life when deeply discharged

Flywheels	0–0.25	15–20	104–107	80–90	High power density, high efficiency, cycle stability, a long life, little maintenance cost,	Low energy density, short operation duration, high self-discharge losses
SMES, DSMES	0.1–10			75–80	High power, rapid response	Low energy density, high production cost, very sensitive to temperature changes
S Capacitors	0–0.3	4–12	104–105	85–98	Larger capacitance, energy density, rapid response	Low energy density

Table 2.7: Storage technology application

Storage technology	Storage service	Service applications
PHS CAES (underground) TES VRFB / HFB FC Pb-A Ni-Cd / Ni-MH Na-S	Long duration (frequent)	• Load levelling • Hot reserve • Arbitrage • Bulk energy storage • Peak Shaving • Frequency regulation • Intermittent seasonal balancing • Renewable penetration • Area control
CAES (above ground) Pb-A Na-MeCl2 (ZEBRA) Li-ion VRFB / HFB FC Ni-Cd / Ni-MH TES FES Metal-air (Zn-air)	Medium duration (fast response)	• Black start • Valley filling • Demand side management • Distributed storage • Loss reduction • Investment deferral • Contingency service • Area control

SMES		• Spinning reserve
		• Capacity credit
		• T&D support
FES	Short duration (highly frequent)	• Power quality
SCES		• Intermittency mitigation
		• Transient stability
		• End-user application
Pb-A		• Frequency regulation
Na-MeCl2 (ZEBRA)		• Renewable integration
Li-ion		• Fluctuations smoothing
Ni-Cd / Ni-MH		• Emergence power bridging
SMES		

Also, the integration TES development is used to mitigate the intermittency of RE sources, and for heating applications such as RE area, buildings and electric vehicle (EV). Figure 2.23 shows the standards of some energy storage strategies and their capacity limit.
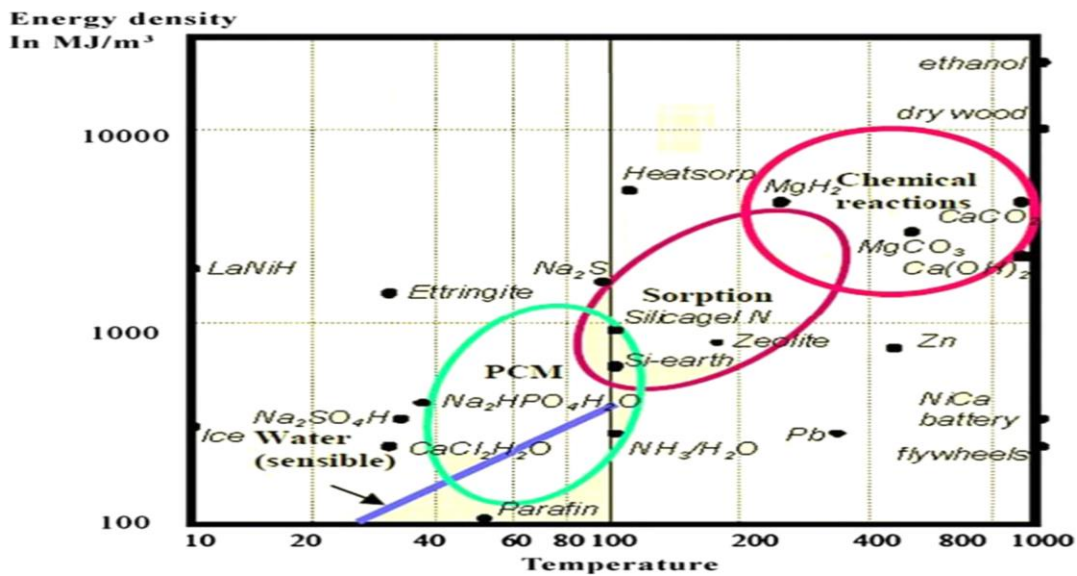
Figure 2.23: TES energy densities as a function of temperature comparison (Aydin et al., 2015)

A brief review of sensitive heat storage (SHS) technologies, as well as strategies for water storage, underground storage system integration and store size temperature levels, have been evaluated. Idle latent heat storage systems (LHS), especially PCM for heating and cooling of

buildings, renewable, solar water heating systems, heat, as well as thermochemical reactions such as adsorption, can be used to accumulate and dissipate heat and cooling. Also, the uses of different chemical reagents to control moisture in various applications were discussed.

2.5 Conclusion

In this chapter, the performance characteristics of various solar thermal with an emphasis on thermal loss and efficiency are reviewed in-depth to understand state-of-the-art, followed by the mechanism of photovoltaic conversion and as the study of the influence of the various parameters (illumination, temperature, series and parallel parasitic resistances and the ideal factor) of solar cells.

Energy storage technologies are accelerating in popularity, emerging in the field of RE to address the issue of intermittency. The integration of these storage options offers stability and efficiency in renewable energies technology. Various energy storage options have been discussed based on their characteristics, efficiencies, limitations, capacity applications and other factors.

The next chapter will present a state of the art that provides knowledge on the advancement of the simulation/experimental of combined photovoltaic/thermal (PV/T) energy.

Chapter 3

Evaluation of the existing PV/T system and the proposed PV/T model

3.1 Introduction

Solar modules convert only 4 to 17% of solar radiation depending on the type of solar cell and the operating conditions (Bai et al., 2016). Most of the solar energy captured by the photovoltaic cell is converted to wasted heat, causing the degradation of the module and reduction in energy efficiency. Cooling the solar module using air or water can significantly increase the energy yield by reducing its temperature (Ramos et al., 2017). A combination of photovoltaic module and solar thermal (PV/T) components can generate electrical and thermal energy simultaneously. This double function of PV/T system allows for more efficient use of the solar energy and results in higher solar energy conversion, depending on the fluid used and the shape of the pipe, such as air-based PV/T and water-based PV/T collectors (Zondag *et al.*, 2003).

This chapter presents a review of comprehensive literature regarding research and development concepts and the practical applications of PV/T technologies.

3.2 PV/T system design analysis

3.2.1 Hybrid photovoltaic- solar thermal system description

Photovoltaic/thermal (PV/T) collectors are presently accessible and available in the market and have been in existence since the 1970s (Kern & Russell, 1978). Figure 3.1 illustrates the PV/T system composed mainly of PV/T panel, thermal tank, control unit, auxiliary heater, and power supply. The PV/T system creates both heating and cooling. The mostly used coolants are air, water or a mixture of antifreeze and water. Also, similar to thermal collectors, there are glazed or unglazed panels.

Many countries have concentrated their efforts on developing PV/T systems to efficiently produce electricity and useful heat (Ahuja & Tatsutani, 2009). Moreover, the PV/T system demand has increased in the field of RE application in both domestic and industrial sectors such as agriculture, building and processing plants (Ahuja & Tatsutani, 2009; Oyedepo, 2012).
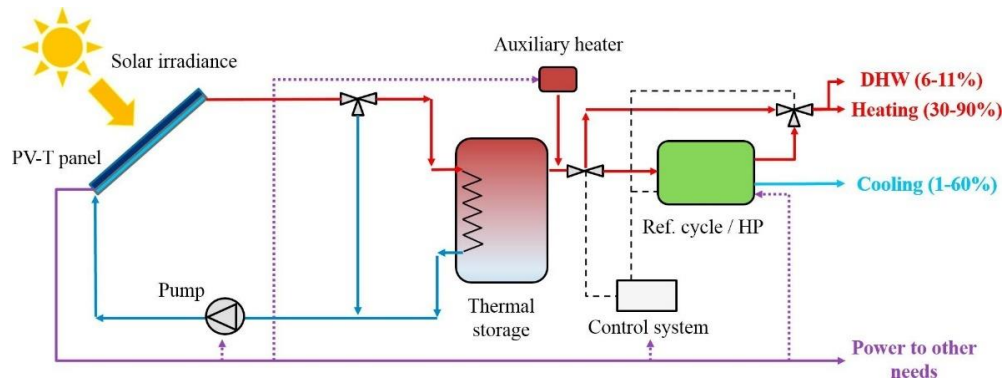
Figure 3.1: PV/T collector system (Ramos *et al.*, 2017)

Some PV/T systems are also used as a solar cooling system. Figure 3.2 shows the continuous increase in the number of global installations capacity of solar cooling between the year 2004 and 2014.

**Figure 3.2: PV/T system market growth worldwide between
the year 2004-2014 (Ramos *et al.*, 2017)**

PV/T collectors have better electrical effectiveness than a single PV module. Various examinations have been directed on strategies to design a *combined* solar thermal and PV system (Ramos *et al.*, 2017). The innovative ideas reside in the integration of coexisting technologies for robust design and reliable system operation. The combination of these systems offer multi-power generation in buildings (Richarz & Schulz, 2013). Figure 3.3 presents different types of PV/T systems.
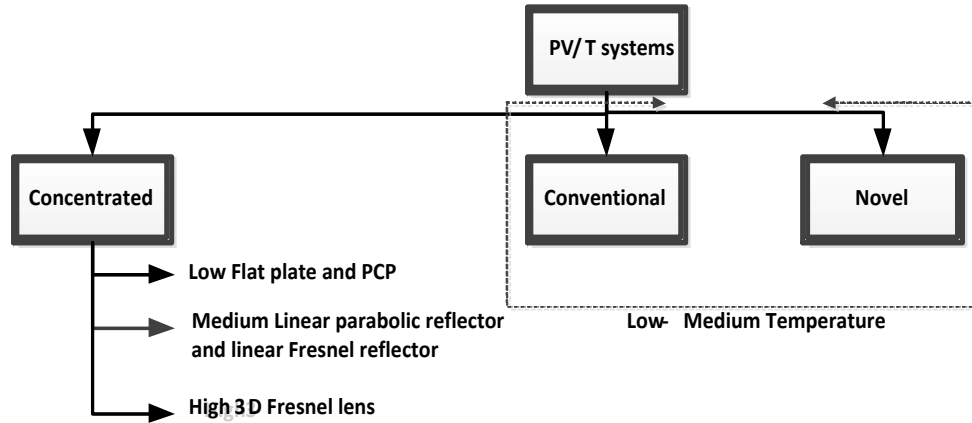
Figure 3.3: Various types of PV/T systems

3.2.2 PV/T system technologies

The PV/T system development focused on the thermal and the electrical efficiency and to ensure the economic feasibility of the system (Brittman *et al.*, 2015; Tiwari *et al.*, 2006). This process includes the integration of solar photovoltaic and thermal systems for the co-generation of electricity and thermal energy (Brett & Rick, 2012; K. Li et al., 2016).

Figure 3.4 shows the classification of PV/T technology based on their characteristics and configurations with air, water, refrigerants, heat pipes, nanofluid and PCM (Elbreki et al., 2016; Mohammed et al., 2013; Yinghao & Peter, 2011).

The advantages and disadvantages of several PV/T system configurations are reviewed below.
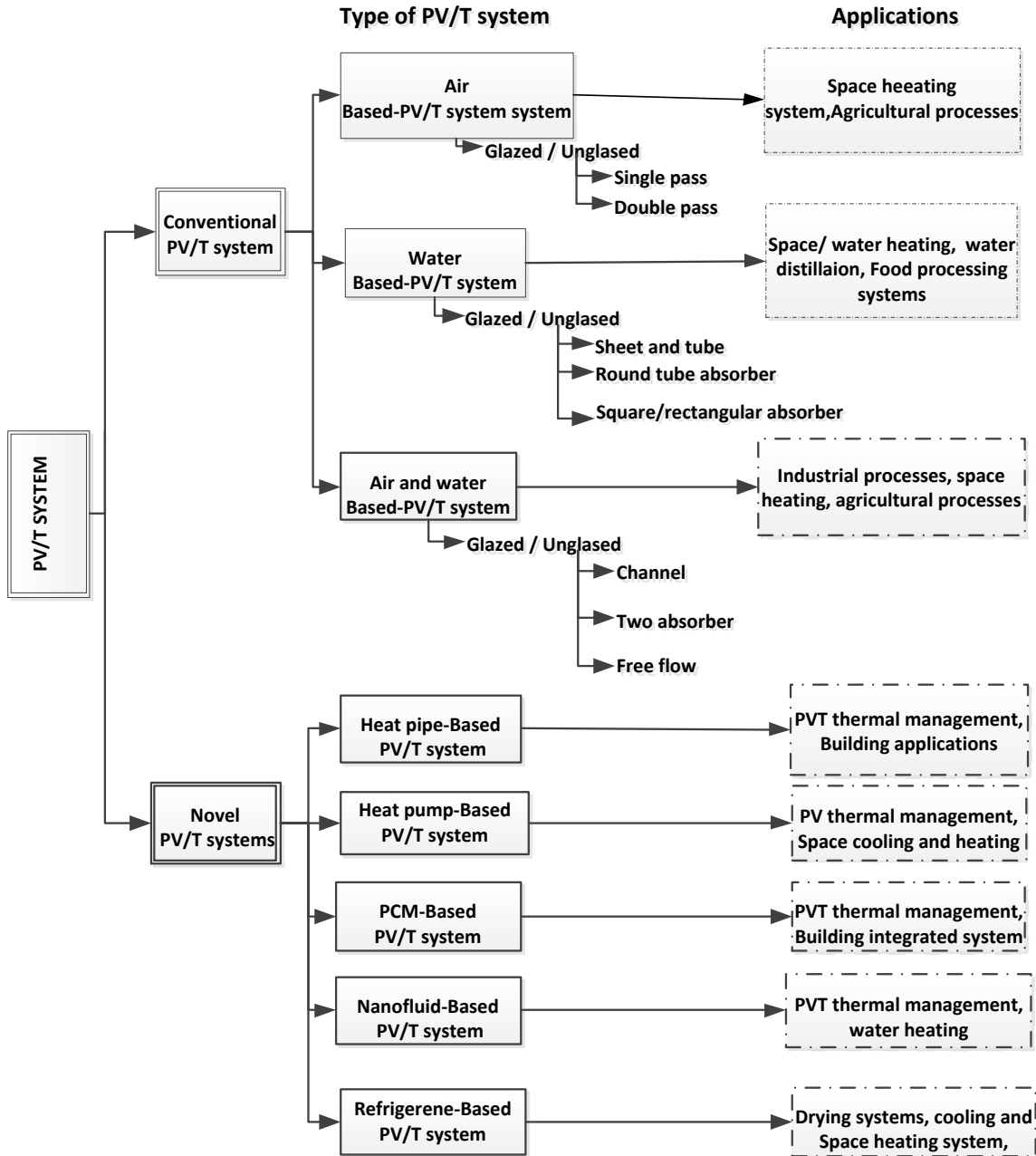
Figure 3.4: Classification of PV/T systems based
(Moradi et al., 2013; Elbreki et al., 2016)

3.2.2.1 Air-based PV/T system (glazed and unglazed)

Air-based PV/T collector is a simple and economical system that is used in the thermal application. It can be developed as either glazed or unglazed configuration. Also, it is a simple and cost-

effective solution for cooling of the PV cells. Air-based PV/T collector efficiency is primarily dependent on air speed, flow path and temperature. The air flow in the air-based PV/T collector can be forced or natural. The forced air flow is better than natural air flow due to better circulation, even if the power consumption of the fan limits the net power. However, air-based PV/T collector presents low output efficiency. The issue with the air-based system lies in its insignificant heat exchange capability attributed to the thermodynamic properties of air, for example, density, specific heat and thermal conductivity. Some important research works conducted on air-based PV/T systems are detailed below:

Figure 3.5 presents various air-based PV/T collector configurations. The air flow path may be situated over the absorber (configuration I), underneath the absorber (configuration II) or on either side of the absorber, single-pass (configuration III) or double-pass (configuration IV) (Kamel *et al.*, 2015). The investigations into some output research on air-based PV/T collectors are as follows:
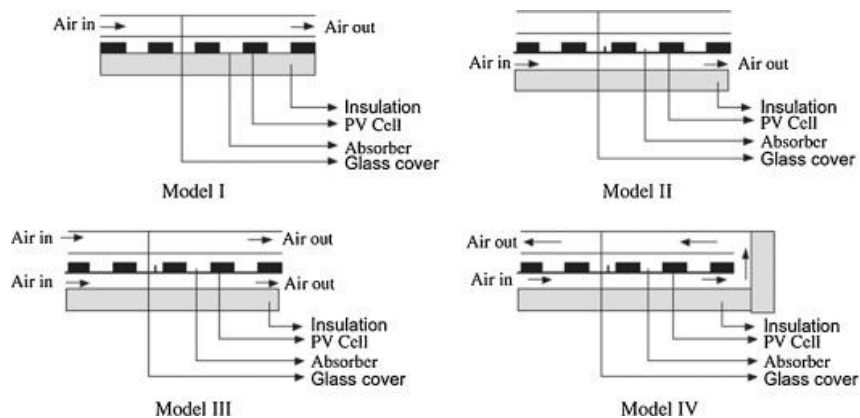
Figure 3.5: Cross-sectional view of air-based PV/T collector models (Kamel *et al.*, 2015)

Concerning the thermal efficiency of air-based PV/T design, a single glaze is higher than the unglazed. In 2000, Hegazy compared the thermal and electrical properties of the four air solar PV/T hybrids. This type of solar PV/T system design is used for cooling the photovoltaic modules and for both sides of the absorber and through the double air circulation. Hegazy also indicated that the performance of the solar air-based PV/T hybrid collector depends on the maximum air outlet temperature, the thermal and electrical efficiency and net power available as required energy for the operating fan and other electrical installations. The simulation results show that increasing the flow rate of ventilation improves thermal efficiency.

Theoretical and experimental evaluation studies of natural and mechanical ventilation of solar air-based PV/T collector at steady-state have been proposed (Tiwari *et al.*, 2006). The PV/T collector is composed of solar collectors of each area of the two PV modules, connected in series and mounted on the Tedlar non-corrosive insulation. The PV module is bonded together by an EVA layer, protecting the solar cell through a glass layer. The assembly PV module has been integrated into a test bench with reclined steel and installed in New Delhi. The inlet fan of the air gap between the wood insulator layers allows the PV module to be ventilated at the rear. The generated electrical energy is stored in a battery. The evaluation shows that the additional recovery of thermal energy allows about 18% improvement in the overall performance of air-based PV/T collector (Tiwari *et al.*, 2006).

Theoretical performance of solar air-based PV/T collector for domestic heating and cooling has been analysed by Vokas et al. (2006). The solar collector is a solar thermal collector attached to a PV panel. The thermal efficiency of the PV/T collector is compared to standard solar thermal with a selective absorber. When the air inlet temperature in the solar collector is equal to the ambient air temperature, the results show that the solar PV/T hybrid air collector has an efficiency 9% lower than the standard solar thermal collector. The solar collector with selective absorber has the highest thermal efficiency (about 75%). However, the advantage of the hybrid solar collector is that it can produce a further significant amount of thermal energy and electrical energy on an area equivalent to that of the standard solar collector on a lower surface than that of the solar collector with a selective absorber (Vokas *et al.*, 2006).

Othman *et al.* (2007) have conducted theoretical and experimental studies on the thermal and electrical productivity of the air-based PV/T hybrid double-cycle collectors. In their work, they revealed that the parts of an air-based PV/T hybrid double-cycle collector consist of two slides of air circulations: the first air gap is between a front glass layer before the PV module; the second air gap is on the underside of the PV module. The rear surface of the module has a vertical blade, not in contact with the rear module of the solar collector. These blades allow for increased convection heat transfer between the air and the PV module. The total efficiency is improved by achieving a double-pass collector system and fins compared to hybrid photovoltaic thermal system design for practical applications. Relatively, a steady-state single-directional thermal model of this hybrid component has been developed. Using the results of the experimental study, compared with the simulated data show that fins improve both the thermal and the electrical efficiency of the hybrid component.

Tripanagnostopoulos (2007) has improved the PV/T solar collector study: heat-transfer fluid (air or water) has been conducted to reduce the operating temperature of the V modules and increase the production of preheated air through the system. The parameters of the air-based PV/T system show that the small air layer thickness improves the heat transfer but reduces the mass flow rate of the blade ventilation, thereby reducing the thermal efficiency of the system. The solution to the problem remains with the optimisation of thermal convection and radiation transfer mitigation by increasing the exchange surface between air and PV modules. Some configurations that incorporate ribbed or plane plates, tubes welded to the absorber, or fins within the airspace have been predicted.

Dubey *et al.* (2009) studied the performance of the accumulation of the PV/T collectors, cadmium glass and tellurium at the Indian Institute of Technology (place). The expression of the analysis was developed based on the parameters of climate conditions and design for electrical efficiency developed by Solanki *et al.* (2009). Furthermore, different configuration designs of glass-to-glass and glass-to-Tedlar PV modules have been studied. Dubey *et al.* (2009) concluded that a glass-to-glass design has more electrical efficiency than glass-to-Tedlar.

Kumar and Rosen (2011) introduced an extract vertical fin area to the lower air channel of a double-pass air-based PV/T collector to significantly reduce the solar cell temperature. Building an integrated air-based PV/T system usually provides an air gap for cooling the PV arrays cells.

Karim and Hawlader (2006) also conducted a theoretical analysis and experiments of the v-corrugated air heater in fins and a flat plate, to improve the conventional air heater performance according to ASHRAE standards. The test kits were implemented in the Singaporean climate to understand the characteristics. After careful consideration of the performance of all three collectors, it was resolved that the v-corrugated was the most efficient and the flat plate collector the least efficient. Test results show that v-corrugated collectors are 10–15% and 5–11% efficient compared to single and double-pass modes, respectively.

Lin *et al.* (2006) studied the thermal performance of cross-corrugated solar collectors which consist of a similarly absorbent sheet and a similar bottom plate with a transverse position to create a flow of air. The purpose of using the cross-corrugated absorber plate and the bottom plate is to improve the turbulence and heat transfer rate of the air flow path, vital for enhancing the efficiency of the solar air collector. It was essential to construct a solar collector with a longitudinal structure in the direction of airflow to achieve substantial efficiency in the solar air collector, with a small gap between the absorber and the bottom plate.

El-Sebaii *et al.* (2011) conducted a theoretical and experimental study on the performance of the double pass-finned plate solar thermal air collectors in Titan's hot weather conditions. The comparative result analysis shows that the influence of air mass flow rate on pressure decreases the heat and efficiency. The thermohydraulic performance of v-corrugated double plate solar air heater was 9.3–11.9% more efficient as compared to double pass-finned plate solar air heater.

Furthermore, the unglazed PV/T/air collector has been studied intensely throughout five different climatic zones to determine the optimum operation of the single, double design and the annual thermal energy efficiency. From the performance views, the double design is better than the single design type (Hegazy, 2000; Raman & Tiwari, 2009; Sopian *et al.*, 1996; Tiwari *et al.*, 2006). However, the efficiency is reduced when the design is under intense radiation (Dubey, Solanki, *et al.*, 2009; Solanki *et al.*, 2009).

Solar air collector is widely used commercially for commercial warehouses, agricultural warehouses, and other heating applications usually at a low cost without problems of freezing and high pressure. However, one significant disadvantage of solar hot-air collectors is the efficiency of low heat transfer coefficients due to their low density, heat conduction and thermal conductivity. The air must be packed into large storage spaces to reduce this gap, resulting in a high cost and size of the roof (Ucar *et al.*, 2006).

3.2.2.2 Water-based PV/T collectors

A great deal of energy research and development is focused on improving the PV/T system. Water-based PV/T collector has proven to be technically feasible, with economic opportunities that have not been discovered with air PV/T systems. For example, a method of circulating water in the PV/T collector to extract the heat and to increase the performance of the photovoltaic module has been developed. These water-based PV/T collectors are like conventional collectors with liquid; an absorber with a serpentine tube or series of parallel vertical piping is applied. The effectiveness of water-based PV/T technology is generally determined by electrical and thermal efficiency. They can also be influenced by water temperature, flow rate, shape and size, as well as water flow channel configurations and environmental conditions. However, the heat exchanger viability of the system is inadequate in practice because the water temperature rises continuously throughout its use, and the efficiency of the solar cell cannot be increased when used at high water temperatures. Also, freezing can be problematic when the system is operating in cold

climatic condition. Some important research developments carried out on water-based PV/T collectors are detailed below:

A comparative study of the performance of a water-based PV/T collector and solar collector water has also been previously conducted by Chow *et al.* (2007). The results obtained showed that the second prototype (glazed solar collector composed of crystalline silicon PV panel bonded to a metal absorber) was more effective than the first prototype. The water circulation within the tube is attached to the back of the absorber and coupled to a water storage tank. Simulation results show that water-based PV/T collector has an annual thermal efficiency of 38.1% while the solar collector water is 43.2%. Also, the comparison of the hybrid solar collector to a PV solar collector shows that by choosing water as a coolant, the operating temperature of the PV module can be reduced. The annual power output of the hybrid solar collector is 2.2% higher than that of the PV solar collector (Chow *et al.*, 2007).

Kostić *et al.* (2010) studied the effect of additional reflector materials made of aluminium sheet on PV/T/water collector. Both numerical computation and experimental measurements determined the optimal angle position of the reflector. Besides, an energy gain can range between 20.5-35.7% during summer. The literature on combined PV/T collector design has increased in recent years. The research in this field was initially more focused on the investigation of the optimisation of the overall design of a PV/T collector, especially for sheet and tube designs. Due to the water PV/T problems cited above, water and air-based PV/T system have been developed.

3.2.2.3 Water and air-based PV/T system

Numerous studies have focused on working with two working fluids in a single PV/T system, identified as a bi-fluid PV/T system. Air and water-based PV/T systems have a more significant heat dissipation which serves to improve the thermal and electrical efficiency and also to overcome the limitations of the separate system (air-based PV/T and water-based PV/T system). However, the system is faced with the issues of ionisation of water and corrosion. Some of the research development carried on water and air-based PV/T collectors are detailed below.

Figure 3.6 presents a different pattern of air and water-based PV/T systems; it tends to be dependent on the flow configuration of the medium used. For example, water and air or a mix of both can be placed above, beneath or on both sides of the absorber and can be either single or double pass.
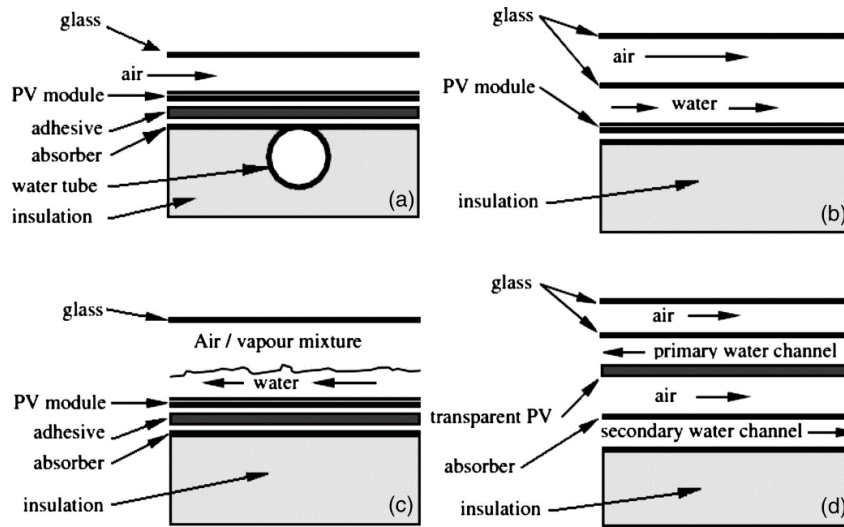
Figure 3.6: Sheet and tube (a), channel (b), free flow (c) and two absorber types (d) (Zondag *et al.*, 2003; Ibrahim *et al.*, 2011)

The sheet-and-tube PV/T collector shown in Figure 3.6a, is a simple configuration from previous technologies. It integrates a conventional PV panel into the thermal collector. In this technology, the thermal insulation and some top glass covers are added. However, each glass cover creates additional reflections, decreasing substantial electricity efficiency in the PV/T collector (Khelifa *et al.*, 2014; Musallam *et al.*, 2014). The advantages and vulnerabilities of this system are addressed in this study. The water-based PV/T module consists of an absorber plate, along with several solar cells arranged in parallel or serial configuration. These modules are fixed to a lower part of the series of parallel tubes underneath where water flows. If the water temperature remains low, the PV cells are cooled, and the efficiency of electrical conversion is improved. The water temperature increases when extracting heat from the solar cell layer. This hot water can be used in various applications. When air-based PV/T system is compared to water-based PV/T systems, the water-based systems will be able to boost production efficiency because of the higher heat capacity of water (due to the high thermal conductivity of water) and thereby improving thermal and electrical efficiency (Zhang *et al.*, 2012). Furthermore, Saitoh *et al.* (2003) studied a single-glazed sheet-and-tube PV/T collector using propylene glycol solution as the coolant.

The channel PV/T collector is shown in Figure 3.6b, configured with the absorption spectrum and allows the PV cell to receive incoming solar radiation. This design, primarily used with water, usually produces a small overlap. However, the disadvantage of this design is that it is fragile, especially at the backside. Two configuration options are explained here:

94

- The channel below a conventional opaque PV panel, which withstands the water pressure when strengthened with a metal back unlike a transparent PV panel.

- The channel below a transparent PV panel with a separate black thermal absorber underneath the channel. This method has a higher thermal efficiency but it is more expensive. The backside of the PV laminate is also fragile.

The design configuration presents a layer in which water flows through the heat absorber of the PV cells. Another part of the design transfers heat from the water layer to the glass plate on top of the water channel (Xu *et al.*, 2012; Musallam *et al.*, 2014).

Cristofari *et al.* (2009) simulated a suitable wall integrated water-based PV/T collector channel model comprising of copolymer material functioning in low-flow. Similarly, Chow *et al.* (2009) also developed a water-based PV/T simulation model for building-integrated PV (BIPV/T) and heating systems, analysing the annual energy performance of the water-based PV/T system operating in natural and forced circulation modes. Both operation modes present a thermal transmission efficiency reduction of 72 and 71%, respectively.

The free flow PV/T collector is illustrated in Figure 3.6c. In this method, a free fluid flows over the absorber, and the solar spectrum must be in contact (transparent) with the fluid flowing over the PV panel. This method can be compared to the channel PV/T collector where it is seen that the design of free flow PV/T collector has lesser glass layer, lesser reflection, fewer materials and thus a lower cost of constructions. However, the condensation which formed on top of the glass layer decreases the direct solar radiation transmission, while evaporation at higher temperature remains the main problems of the design. Higher evaporation also reduces thermal efficiency since the water evaporation pressure is significant. The equations of the free flow PV/T collector are similar in similarity to the channel PV/T collector. In the absence of some variants on the top glass 1, thermal radiation and convection can take place directly between the two water layers and the top glass 2 (Zondag *et al.*, 2003; Kim *et al.*, 2012; Zondag, 2008).

The two absorbers PV/T collector contains two absorbers as illustrated in Figure 3.6d. The primary absorber is a PV laminate, and the back plate is the second absorber. This system includes two water channels in which water flows through the upper channel and returns through the lower channel (Kim *et al.*, 2012; Zondag, 2008). The system also has high thermal efficiency. However, the geometric complexity makes it difficult to manufacture. Air-based PV/T and Water-based PV/T collectors in different configurations were compared in outdoor tests and placed to receive a significant amount of radiation at collector surfaces. A range of thermal efficiency has

been recorded from 38% to 75% for PV/T/air collectors and 55% to 80% for PV/T/water designs (Tripanagnostopoulos *et al.*, 2002; Tonui & Tripanagnostopoulos, 2007; Tripanagnostopoulos, 2007). According to Garg and Adhikari (1999), a sheet of metal was introduced in the middle of the air channel to reduce cost. However, this method is relevant to the small collector length. An air-based PV/T system enabling the prediction of the thermal and electrical energy productivity modelling procedures has been proposed. A linearly decreasing function calculates the yield of PV cells. This solar collector consists of a transparent cover, painted black absorber and well-isolated back support. The PV cells were bonded to the absorber by selecting an excellent thermal conductivity and electrically insulating material.

Table 3.1: Thermal and electrical efficiency on nine different PV/T collectors (Zondag *et al.*, 2003)

Panel type	Thermal efficiency (%)	Electrical efficiency (%)	Annual thermal efficiency (%)	Annual electrical efficiency (%)
PV laminate	-	9.7	-	7.2
Sheet and tube PV/T collector 0 cover	52	9.7	24	7.6
Sheet and tube PV/T collector 1 cover	58	8.9	35	6.6
Sheet and tube PV/T collector 2 cover	58	8.1	38	5.8
PV/T collector with channel above PV	65	8.4	38	6.1
PV/T collector with channel below opaque PV	60	9	35	6.7
PV/T collector with channel below transparent PV	63	9	37	6.5
Free flow PV/T collector	64	8.6	34	6.3
Two-absorber PV/T collector (insulated type)	66	8.5	39	6.1
Two-absorber PV/T collector (non-insulated type)	65	8.4	37	6.1
Thermal collector	83	-	51	-

Table 3.1 summarises the electrical and thermal energy efficiency evaluation of water-air PV/T system configurations. Zondag *et al.* (2003) discussed the review of nine different PV/T collector designs, observing that the uncovered sheet-and-tube performs poorly due to convection radiation losses. When adding covers to the sheet-and-tube, efficiency appears to increase while

their electrical efficiency drops accordingly. The thermal and electrical energy performances are highly dependent on the configuration of PV/T collector (channel above PV, channel below opaque PV, channel below transparent PV). Adding insulation does not influence the two-absorber PV/T collector performances or that of the free flow PV/T collector.

Given the limitation of the water and air-based PV/T collectors, the refrigerant PV/T system is an alternative solution to improve both the electrical and thermal energy.

3.2.2.4 Refrigerant-based PV/T collectors

The power conversion efficiency of solar cells decreases as its operating temperature increases. A PV/T refrigerant system made of PV module and thermal collector is used to overcome the barrier of air and water-based PV/T system. Refrigerant -based PV//T system improves the energy efficiency conversion of both electrical and thermal energy compared to combined water-air-base PV/T system. Also, its efficiency depends on the thermal properties of the refrigerant as well as the configuration structure of the refrigerant flow channels. Nevertheless, the PV/T refrigerant system still faces numerous difficulties; for instance, the refrigerant pipe cycle requires an ideal seal to keep up various pressures in different sections. Due to a large number of welded joints, it is difficult to protect the air from being stuck in various places. Likewise, there are also high risks of refrigerant leakage, and the issue of accomplishing balanced refrigerant circulation over the multiple coils introduced in a considerable PV module area is practically strenuous. In addition, the efficiency is mainly reliant on the thermal properties of the refrigerant as well as the configuration structure of the refrigerant flow channels.

The PV/T refrigerant system performance was conducted by Chen *et al.* (2011) using a refrigerant as an evaporator for heat pump applications. The R134a refrigerant can be used to cool the photovoltaic modules. The results show that the electrical properties of solar panels are 3.9% higher and 1.9% higher than the reference PV compared without cooling.

3.2.2.5 Heat pipe-based PV/T system

The heat pipe is a transfer mechanism that integrates the thermal conduction and phase change, it has the ability to overcome the difficulties encountered in refrigerant-based PV/T system, cooling PV cells and heat. The heat pipe-based PV/T, consisting of three parts (an evaporator, an adiabatic and a condenser) is a viable solution for removing and transferring heat. In this method, the hot steam is converted into a liquid by capillarity in a PV/T system using the heat

pipe and then returned to the evaporator. Heat pipes are used to extract the heat from the back of the PV (Tang *et al.*, 2010). One of the difficulties of high-temperature heat pipes is the corrosion from the incompatibility between the working fluid and the shell material. This incompatibility leads to a chemical reaction, producing non-condensable gases which considerably affect the thermal performance of the heat pipe (Jouhara et al., 2017). This type of PV/T system also has drawbacks that require additional modifications, such as the unexpected expense of the heat pipe and the control of the heat pipe's reliable performance. Performance of heat pipe-based PV/T is reliant on the configuration and material of the heat pipe and vacuum, difficulties in high-temperature heat pipes, chemical reaction, continuous flow limit, capillary limit, viscous limit, boiling limit. The working fluid thermal property, the fluid inlet temperature and the flow rate of the secondary fluid. Some of the research development associated with heat pipe PV/T systems are detailed below.

Gang *et al.* (2011) built a copper heat pipe-based PV/T system which uses a working fluid. The dynamic model of the design was simulated using various methods. The thermal and electrical efficiency of the heat-pipe PV/T thermal system was 41.9% and 9.4%, respectively.

Zhang *et al.* (2013) adopted the idea of using photovoltaic/loop-heat-pipe (PV/LHP) for the operation of heat pumps. Under test conditions, the results showed that the electrical, thermal and overall efficiency of the PV/LHP module were approximately 10%, 40% and 50%, respectively.

Jianfeng *et al.* (2010) also proposed a new concept of integrating PV/T systems using an oscillating heat pipe, an idea of designing an external wall assembly component that transmits heat from a concealed solar cell. The system consists of a rectangular heat exchanger and a fin header, a metal conductor, a PV frame, a PV module, a laminate and a subwoofer. The running water is a metal heat pipe that absorbs heat from the solar cell and evaporates to steam. Liquid steam enters the fin tube, which emits heat into the liquid by condensation and returns to the adsorbent by gravity and friction.

3.2.2.6 Building integrated photovoltaic-thermal (BIPV/T) systems

Combining the solar systems in a building is useful to the integration process of RE in buildings to save energy and to accomplish global green power. The construction sector has become increasingly interested in integrating photovoltaic and thermal into buildings (Ahmed-Dahmane et al., 2018). Moreover, the BIPV/T system can be categorised to semi-transparent or the opaque.
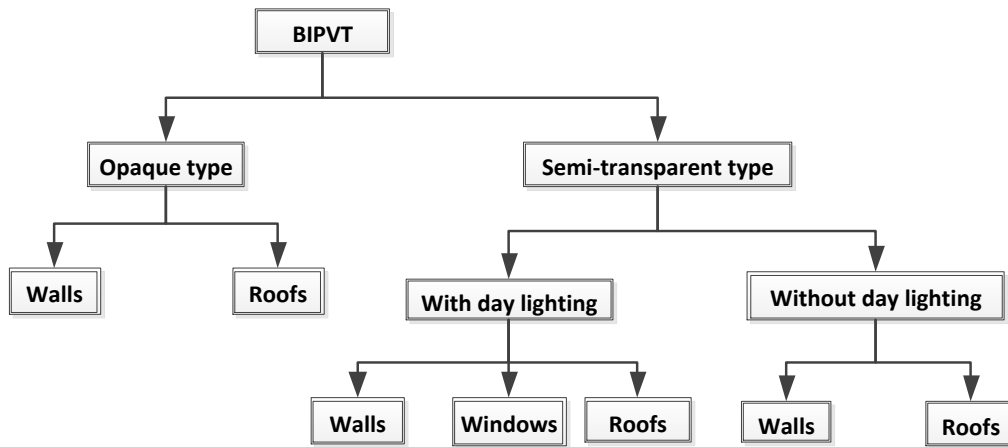
Figure 3.7: Classification of BIPV/T systems (Dash et al., 2018)

The semi-transparent daylight system can be integrated into the walls, roofs and windows of buildings while an opaque system is integrated only into the walls and roof of a building, as described in Figure 3.7. Some important research works carried out on BIPV/T systems are detailed below:

Simulations of the thermal behaviour of two different platforms (ESP-r and TRNSYS) have been used to determine the operation and control modes of a roof-mounted air-based PV/T system. The data collected from energy is used in a TRNSYS model to validate the experimental data from a pc-Si PV façade and also to investigate the dynamic performance of air-based BIPV/T collector system (Mei *et al.*, 2003). The simulation predicts that the heating energy could be saved in winter when using preheating ventilation inside the building. Different methodologies have been applied to the BIPV/T/air facades to determine the thermal performance under heat loss and radiation gain factors (Infield *et al.*, 2004). This method is complicated for estimating the convective heat transfer coefficient due to some parameters such as forced and natural flow convection, laminar and turbulent flow with the developing flow at the air entrance and the external wind load on the plates. Sandberg and Moshfegh (2002) also developed a mathematical expression to predict the experimental results; however, this method was found to be inaccurate for ducts with open ends.

A dynamic model of air-based PV/T collector integrated in the front of the building based on the previous European project has been proposed by Mei *et al.* (2003). As a framework, the photovoltaic system is designed by Teulades Multi-Functional (TFM) in considering the natural ventilation of both sides of the photovoltaic panels into the public library facade. The solar air

collector and PV module are connected in series through a 14 cm air gap, separated by a double inner plate and brick wall. The PV module consists of two layers of glass encapsulated between the polycrystalline units. Other facades are made of porous concrete and metal cladding. The air is stretched on the substrate of the air layer on the back of the PV module (Mei *et al.*, 2003).

Anderson *et al.* (2009) analysed the water-based BIPV/T system designed in Australia. The BIPV/T system includes the standing seam or the roof of the circular saw blade in the crevice channel. The hot water with heat exchanger stability test demonstrates the efficiency of the Hottel-Whillier model, with results showing that the primary design factors — consumption, stratification, thermal conductivity and efficiency—affect electrical and thermal performances. It is recommended to replace the absorbent material with copper or aluminium for maintenance efficiency.

Corbin and Zhai (2010) examined the dynamic model of computer liquid (CFD) for the new integrated solar collector and an experimental model was designed to determine the cell efficiency of the heat recovery system used and efficiency in the solar water heater. The results showed that the effectiveness of the cell increased by 5.3%. The thermal and electrical efficiency reached 34.9% and 19.0%, respectively. A new relationship to calculate the cell efficiency involving the electrical efficiency to the collector inlet temperature, air temperature and solar radiation was developed.

Yin *et al.* (2013) designed and monitored the overall system performance of a building integrated multifunctional roofing system. The PV silicon layer is embedded between the transparent protective layer and the functionally graded material (FGM), which consists of a mixture of insulated aluminium, high-density plastic insulation and a water channel in FGM. Besides, when solar radiation is converted into electrical and thermal energy by the PV cells, heat is transferred to FGM due to its high thermal conductivity. This heat is also absorbed by the water that flows through the built-in hose so that the temperature can be controlled and also improve the efficiency of photovoltaic cells. During testing, the maximum temperatures of PV cells were recorded at 50°C and 55°C, for irradiation of 850 W/m^2 and 1100 W/m^2, respectively. At these temperatures, the photovoltaic efficiency was estimated to be 13.1% and 9.9% when the irradiation was 850 W/m^2 and 1100 W/m^2, respectively, without water flow. Besides, when the water flow is activated, the PV cells temperature is reduced to 32°C and 38°C for corresponding radiation. For a given solar radiation and PV cells temperatures and the total energy efficiency of the panels, hybrids were 58.8% and 65.3%, respectively. Also, Kim *et al.* (2014) surveyed a building's heating system

associated with water-based PV/T collector roof. The results obtained showed that the proposed method has 30% thermal efficiency and 17% electrical efficiency. Also, the water temperature can achieve a maximum temperature of 40℃, which can be used as a heat source.

3.2.2.7 Phase change material-based PV/T system

The phase change material (PCM) is capable of absorbing/releasing a considerable amount of thermal energy toward a stable temperature (Cao *et al.*, 2018). PCM has been used to control the temperature of electronic equipment (Yuan *et al.*, 2017). It has improved the performance of photovoltaic by taking the heat and improving the electrical efficiency systems. PCM-based PV/T system applications involve temperature, heat transfer, melting, thermal conductivity, chemical inertness, and safety for health and the environment, all of which are critical. Some of the research development associated with PCM-based PV/T systems are detailed below.

Hendricks and van Sark (2013) discussed the use of PCMs in PV modules. With their studies, they acknowledged the improvements in the performance of photovoltaic and which PCM-based PV/T system took the heat away and enhancing the PV cell electrical system efficiency. Compared to conventional or air-cooled thermal ventilation, PCM has a distinct advantage of achieving higher thermal efficiency without the need for mobile equipment, thereby reducing power and maintenance costs. It was also determined that the PCM system only benefits in hot and stable weather conditions (Hasan *et al.*, 2015).

PCM-based PV/T system has been developed to improve PV array efficiency. The PV/T-PCM system performance is compared to the conventional water-based PV/T systems based on the evaluation of output power, thermal, fluid temperature and tank temperature, including its ability to save energy. Moreover, the integrated PCM layer into the PV/T module was observed as exceptional in improving thermal and electrical power. The average efficiencies of water-based PV/T and PCM-based PV/T systems were resolved to be 63.93% and 76.87%, although their essential energy-saving efficiencies were 73% and 87.5%, respectively (Yang *et al.*, 2018).

3.2.2.8 Nanofluids-based PV/T system

Over the last two decades, the use of nanofluids has spread in all areas. Nanofluids generally carry nanoparticles of less than 100 nanometers in a coolant such as ethylene glycol and oil and water. The properties of nanofluids can be improved in some specific applications. Nanofluids typically dissipate heat through a heat transfer and can be applied productively in various

applications such as solar energy conversion systems. A fair amount of research work is being done as regards to nanofluids associated with solar system heat transfer fluids or optical filters (Verma & Tiwari, 2015; Sathe & Dhoble, 2017).

Xu and Kleinstreuer (2014) adopted a nanofluid method to heat and cool a concentrated PV/T system. The electrical and thermal performance in different climatic conditions were determined. Also, it was noted that at a temperature of about 62°C, the controlled flow rate of the nanofluid yielded a total efficiency of 70%, while the electrical and the thermal efficiency were 11% and 59%, respectively. This method is costly, however, and it faces problems such as a drop-in pressure. It is also troublesome to keep hold of nanoparticles suspended in the base liquid (Al-Waeli *et al.*, 2018; Nagarajan *et al.*, 2014).

3.2.2.9 Solar-assisted heat pumps (SAHP) based PV/T system combined

The solar-assisted heat pump system (SAHP) is a new technology that considerably diminishes energy sources such as coal and natural gas while maximising the RE sources. It collects thermal energy from solar radiation through heat transfer medium or absorber in the form of low temperature to a high-temperature source. The SAHP system consists of commonly used components: solar collectors, heat pumps, function and storage systems (thermal tank storage and or electric storage), and the interaction between these components. Also, the efficiency of such a system relies on the ratio of the size of the components and the adaptive controls. Commitment surveys show that most systems are used to combine domestic hot water and heat generation for space heating circuits through processes such as evaporation and condensation and to the thermal storage (Chu & Cruickshank, 2014). Various types of SAHP configuration are described below.

(1) Parallel system

A conventional solar system is installed parallel to the heat pump, as seen in Figure 3.8. This type of system installation provides thermal energy either by solar radiation or by a heat pump. It uses solar radiation when there is enough solar radiation on the collector surface to meet the heat demand. If there is no solar radiation, for example, on a night or in cloudy weather, the heat pump works to meet the demand (Kamel *et al.*, 2015).
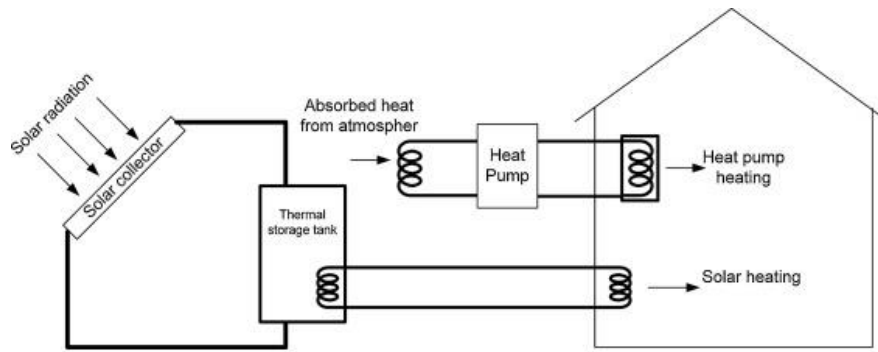
Figure 3.8: Parallel SAHP configuration
(Kamel *et al.*, 2015)

(2) Series system

In the series system configuration, as seen in Figure 3.9, the heat pump is limited by the energy of the collector, which means the heat pump is highly dependent on the energy drawn from the solar collector. If solar radiation does not provide alternative energy, direct solar heating is used.
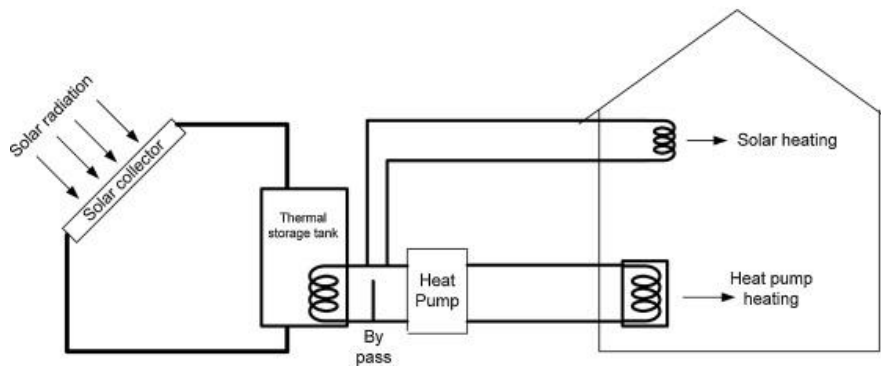
Figure 3.9: Series SAHP configuration
(Kamel *et al.*, 2015)

(3) Dual-source system

This dual solar heat pump design uses two different evaporator configurations, as shown in Figure 3.10. The solar evaporator is installed in the solar storage tank loop while the air evaporator is located inside a fan coil of the heat pump. The solar collector or the external air source is used heat source by the heat pump.
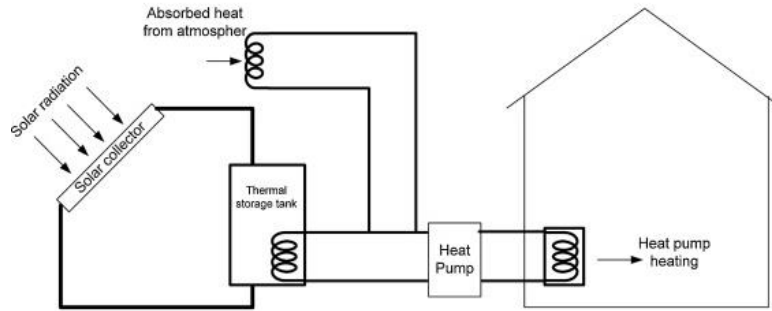
Figure 3.10: Dual-source SAHP configuration
(Kamel *et al.*, 2015)

3.2.3 Advantages and disadvantages of some PV/T systems

Table 3.2 presents a summary of the advantages and disadvantages of diverse PV/T technologies. This table indicates the maximum efficiency achieved by various PV/T systems, according to the works in literature.

Table 3.2: A comparison of various PV/T systems
(Wu *et al.*, 2017; Chandel & Agarwal, 2017)

PV/T model	Maximum efficiency	Advantages	Disadvantages	Reference
Air- based PV/T system	24%	• Low cost • Simple structure • Less concern corrosion • No high-pressure protection needed	• Low heat capacity thermal conductivity results in a low heat transfer rate • Low thermal mass • Large air volume • Water cooling achieves great efficiency in hot climatic conditions compared to air cooling • Poor thermal removal effectiveness • High heat loss	(Kamel *et al.*, 2015)
Water-based PV/T system	59%	• Low cost • Direct contribution • High thermal mass • Low flow volume	• Still high PV temperature • Unstable heat removal effectiveness • Complex structure • Possible pipe freezing • Cannot achieve optimal efficiency because of the constant flow rate	(Wu *et al.*, 2017)

System	Efficiency	Advantages	Disadvantages	Reference
Refrigerant-based PV/T system	74%	• Low PV temperature • Stable performance • High efficiency • Effective heat removal	• Risk of leakage • Unbalanced liquid distribution • High cost • Difficult to operate	(Wu *et al.*, 2017)
Heat-pipe- based PV/T system	68%	• Low PV temperature • Stable performance • High solar efficiency • Effective heat removal • Reduced power input • Enhanced heat transfer coefficient due to the larger heat transfer area of the heat pipe • Increased number of thin liquid films in the evaporator and condenser sections by the microgrooves	• High cost • Risk of damage • Design complexity increased with structure • Rise of the thermal resistance and reduction of the contact area between the tubes and the solar panel, lead to the development of non-uniform temperatures along with the panel and reduction of the system efficiency	(Wu *et al.*, 2017; Jouhara *et al.*, 2017)
PCM -based PV/T system	69%	• The advantages of MCP systems, such as specific heat or temperature adjustments due to phase change • Higher heat absorbing efficiency with no mobile equipment and electrical consumption and low maintenance cost • Ability to store a large amount of heat with small temperature change	• PCM is limited with thermal storage • Absorptive capacities of the material degrade over time • Regarding economic feasibility and material life cycle • Effective only in hot and stable climatic conditions	(Yang *et al.*, 2018)
Nanofluids-based PV/T system	70%	• Improved heat transfer	• Caused higher pressure • Difficult to maintain nanoparticles suspended in the base liquid • Very expensive	(Al-Waeli *et al.*, 2018; Nagarajan *et al.*, 2014)

3.2.4 PV/T system for industrial process heat applications

PV/T system fits a wide range of industrial process applications, in low to medium temperature range below 50°C (Kalogirou & Tripanagnostopoulos, 2007). Industrial applications requiring a temperature above 100°C, are not unsuitable for PV/T systems. However, a high proportion of low-temperature process applications, for examples food, wine, beer and general beverage industries, paper and textiles industries can be applied in the PV/T system; Table 3.3 lists (in bold) related process applications which can be applicable in PV/T system, and their temperature range requirements.

Table 3.3: Temperature ranges for different industrial processes (Kalogirou, 2003)

Industry	Process	Temperature (°C)
Dairy	**Pasteurisation**	**60–80**
	Sterilisation	100–120
	Drying	120–180
	Concentrates	**60–80**
	Boiler feedwater	**60–90**
Tinned food	Sterilisation	110–120
	Pasteurisation	**60–80**
	Cooking	**60–90**
	Bleaching	**60–90**
Textile	**Bleaching, dying**	**60–90**
	Drying, decreasing	100–130
	Dyeing	**70–90**
	Fixing	160–180
	Pressing	**80–100**
Paper	**Cooking, drying**	**60–80**
	Boiler feedwater	**60–90**
	Bleaching	130–150
Chemical	Soaps	200–260
	Synthetic rubber	150–200
	Processing heat	120–180
	Pre-heating water	**60–90**

Meat	Washing, sterilisation	60–90
	Cooking	**90–100**
Beverages	**Washing, sterilisation**	**60–80**
	Pasteurisation	**60–70**
Flours and by-products	**Sterilisation**	**60–80**
Timber by-products	**Thermodiffusion beams**	**80–100**
	Drying	**60–100**
	Pre-heating water	**60–90**
	Preparation pulp	120–170
Bricks and blocks	Curing	60–140
Plastics	Preparation	120–140
	Distillation	140–150
	Separation	200–220
	Extension	140–160
	Drying	180–200
	Blending	120–140

3.2.5 PV/T system thermal losses

Most of the thermal losses in the solar collectors are from the front glass cover because the sides and the back of the collectors are often fully insulated. Thus, the thermal performance of the solar collector depends on the climatic conditions, designs and glass cover material. Figure 3.11 depicted the factors affecting the PV/T collector based on the research reports on the thermal losses (Elbreki et al., 2016; Ion & Martins, 2006; Khoukhi & Maruyama, 2005).

Factor affecting the PV/T collector performance

Climate parameters
- Solar irradiance
- Relative humidity
- Wind speed
- Ambient temperature
- Accumulation dust

Design parameters
- Duct channel collector lengh
- Duct channel collector depth
- Number of collectors
- Sun tracking systems
- Boost diffuse reflector
- Collector tilt angle
- PV module type
- No. of gazing and glass thickness
- Anti-reflection
- Absorber plate design parameter
  - Tube diameter
  - Tube spacing
  - Fin thickness
- Riser configuration
- Riser location
- Thermal insulation
- Effect of absorber
- Effect of fins

Operational parameters
- Mass flow rate
- Thermalresistance
- Inlet and outlet fluid temperature
- Heat loss coefficient
- Packing factor
- Effect of fans/pump
- Effect of metal bars
- Effect of other coolants

Figure 3.11: Losses from a PV/T system (Elbreki *et al.,* 2016)

3.2.6 Summary of software supporting hybrid photovoltaic thermal energy

Several simulation software tools have been developed to determine the potential energy production from RE. Simulation is the most widely used method and accepted tool for system analysis, research and development. It can provide a comparative study on the power generation performance and costs of different system configurations.

This section presents some simulation software features used for the system performance analysis, including redefined sizes and economic feasibility of the system and the architecture-based design of RE. A summary of software features based on the hybrid photovoltaic/thermal energy system design is listed in Table 3.4.

Table 3.4: Software tool features for hybrid photovoltaic thermal systems (Sinha & Chandel, 2014)

Software/ Developed by	Research papers in which the model was implemented	Type of analysis	Advantages	Disadvantages
National Renewable Energy Laboratory Solar Advisor Model (NREL SAM) National Renewable Energy Laboratory (NREL), USA, In 2007	(Lalwani & Singh, 2010; Sharma *et al.*, 2014)	• Predicting performance and excepted financial of renewable energy projects • Returning the level cost of electricity to reflect the cost of a generation with respect to the capital investments	• User-friendly; easy to understand; graphical representation of results • Manually add custom modules and inverters • To facilitate decision making for alternating on renewable energy • Provides financial computation for other renewable systems platform	• 3D shade modelling is not supported; • No available weather data for other locations of the world • No deep analysis of PV/T system
Photovoltaic systems (PVsyst) Institute of Environmental Sciences (ISE), University of Geneva, Switzerland, in 1971.	(Lalwani & Singh, 2010; Sharma *et al.*, 2014; Odeh, 2018)	• Performance and Financial analysis for both grid-connected and stand-alone • Analysis based on meteorological and PV-components database provided from PVsys	• Not identify the weaknesses of the system design through Loss Diagram • Results include several dozens of simulation variables • Modelling result in tabular form, graphs and metrics that show the level cost of electricity, operating, capital and maintenance rather than cost it also shows the peak and annual system efficiency, system energy output and hourly system production	• Can change the font see parameters if using a small monitor; • Inability to handle shadow analysis; No single line diagram priced

Hybrid Optimization Model for Electric Renewables (HOMER) National Renewable EnergyLaboratory (NREL), USA, in 2006.	(Lalwani & Singh, 2010; Sharma *et al.*, 2014)	• Energy modelling software: optimisation and sensitivity analysis • Technical analysis and financial analysis • Technical analysis; economic analysis; emission analysis	• Determines the possible combinations of a list of different technologies (hybrid power systems) and its size • Very detailed results for analysis and evaluation • Has optimization algorithms used for feasibility and economic analysis • Provides meteorological and PV-components database	• Inability to guest missing values or size • Does not have a solar collector • Need other software like Matlab to solve the complex mathematical model
Photovoltaic Solar Expert (PV*SOL Expert) Valentine Energy Software, Germany	(Lalwani & Singh, 2010; Sharma *et al.*, 2014)	• Performance analysis; economic analysis • Solar project analysis and planning tools	• Vast meteorological database with over 8000 climatic location worldwide • Strong module and inverter database with over 13000 modules and 3100 inverters; • Manually add custom modules and inverters • Calculate shading on the basis of 3D object • Can optimize the allocation of the module based on the shading position	• Sensitivity analysis is not supported; • Complexity Inability to guest missing values or size; Sophisticated and time-consuming; • Detailed input data is needed to be Supported in building and site modelling; • Error in the presentation of the circuit diagram; • Advanced scientific calculation is not supported
RETScreen The Canadian Institution, Natural Resources Canada, in 1998.	(Lalwani & Singh, 2010; Sharma *et al.*, 2014)	• Benchmark analysis; feasibility analysis; performance analysis; • Portfolio analysis valuates renewable-energy and energy-efficient technologies • Financial, environmental analysis	• Strong meteorological and product database; contains extensive integrated training material • High strength in financial analysis model a base case and an improved case at converting units • RETScreen is user-friendly and has the capability to model various renewable technology, like PV and solar thermal but excludes PV/T system.	• Data sharing problem • Does not support advanced calculations • Data source its monthly versus hourly and it is displayed in w/m^2/day. • The weather data points vary from point to point cannot be directly compared to that of another location
Solarius PV ACCA software, Italy		• Technical, economic and shading analysis	• Provide meteorological database • Numerical and graphical results can be easily exported	• Require a level of expertise • Advanced feasibility analysis is not supported

		Technical analysis	Advantages	Limitations
HelioScope Folsom Lab, San Francisco, USA, in 2011.		• Technical analysis; shading analysis	• User-friendly • Is a web-based tool, so there is no software to • Download • Provides a detailed wiring diagram; has 3d model design	• Does not support • Financial analysis; • Does not support feasibility analysis; • Does not support advanced • Scientific calculation
Solar Pro Laplace Systems Company, Japan, in 1990.	(Lalwani & Singh, 2010)	• Technical analysis; shading analysis; • Economic analysis; Performance modelling • Power curve, Power and Financial Analysis	• Strong meteorological database • Advanced 3D shading analyses • Provides system layouts • Provides detailed and customised reports which can be exported • Optimisation option setting before the installation of • Panel electricity generation under different conditions that are varied by each system	• Sophisticated software as compared to other software • An advanced feasibility study is not supported
SOLARGIS Slovakia, in 2010.	(Sharma *et al.*, 2014)	• Technical analysis; planning and optimisation	• User-friendly • Is a web-based tool, so there is no software to download • Provides a detailed output with graphs and tables	• Not suitable for • Financial analysis; • Less technical parameters; feasibility analysis is not supported • Internet is needed to run the simulation
CombiSun & F-Chart software developed by Klein and Beckman, in 1991.	(Lalwani & Singh, 2010; Sharma *et al.*, 2014)	• Technical analysis; financial analysis • This tool covers a number of collectors including flat plate, CPCs, evacuated tube and tracking systems • Combisystemscombisun was a tool meant to assist with the performance prediction of hybrid systems	User-friendly • Provide detailed graphical and numerical output; • Weather data can be added manually • It is based on the fractional Solar consumption method • Models included various storage systems, boilers and applications	• Not suitable for shading analysis • Not supporting advanced calculation • Graphs and tables can be generated but cannot be exported

Transient Systems Simulation (TRNSYS) Jeff Thornton and Alexander Fiksel, at University of Wisconsin Solar, in 1994.	(Jonas *et al.*, 2017; Lyu *et al.*, 2017; Sharma *et al.*, 2014; Aldubyan & Chiasson, 2017)	• Optimally design solar thermal systems • Simulate transient system behaviour	• Has PV, SHW, and PV/T collectors in its library of components • Other research has used TRNSYS to model their experiments • Popularly used in researcher and industrial professionals • For transient studies, the use of TRNSYS is a very good choice • Many o software use TRNSYS to calculate system performance	• It requires a level of expert in modelling
Environmental Systems Performancere newable (ESPr) University of Strathclyde, Scotland, in 1993.	(Lalwani & Singh, 2010; Sharma *et al.*, 2014)	• Combined heat and electrical power generation and photovoltaic exterior of the building • Computational fluid dynamics, multi-gridding in 2D/3D environment and control systems • Analysis thermal, visual and acoustic performance of buildings	• An integrated renewable energy modelling tool for simulation of the visual-acoustic and thermal performance of a building • The energy use and gaseous emissions along with associated environmental control system • It equipped to model heat, air, moisture and electrical power flows at a user-determined resolution • Analyses the intricate relationships between a building's form, fabric, air flow, plant and control, • It can simulate many innovative technologies including daylight utilization, natural ventilation, contaminant distribution	• Having problem being converted into a set of the conservation equation
MATLAB/ Simulink Jack Little and Cleve Moler, in 1984.	(da Silva & Fernandes, 2010; Hammami *et al.*, 2017)	• Discretise models, convert models to other types, simulate and predict the output • Mathematical modelling of each component • Design analysis • Linearize nonlinear models,	• A very rich and complete API (Application Programming Interface), allowing to create new blocks using a programming language, is provided • It provides design and simulation heat transfer in solids, fluids and solving convection-diffusion equations	• It requires a level of expert in modelling • It does provide an extensive meteorological and PV-components database

		• Computational fluid dynamic (CFD) analysis • Customized controller • For transient studies analysis • Thermal/ electrical analysis • The heat generated/lost by the PV cell	• Creating the PV/T system from scratch from in MATLAB/Simulink	
ANSYS FLUENT John Swanson, in 1970.	(Pauly *et al.*, 2016; Khelifa *et al.*, 2015)	• Geometric model and the domain of the fluid	• Perform all the simulations and used to develop the model geometry	--
Dymola/ Modelica European company Dassault Systèmes, in 1997.	Fraunhofer Institute for solar energy, Germany	• Modelling hybrid systems; financial evaluation	--	--
TRANSOL Aiguasol and the French research center CSTB, in 2004.	--	• Calculation and optimization of solar thermal systems.	• Transol does dynamic simulation easy • A user-friendly interface. • This tool comes from an ambitious project • Solar thermal energy	• Use TRNSYS engine

The comparative features of these software tools based on technical and economic analysis capabilities and RE generator options are shown in Table 3.5.

Table 3.5: Hybrid system software analyser tools (Sinha & Chandel, 2014)

Tools	Economic Analysis	Technical Analysis	PV System	Wind System	Generator set	Storage device	Bio-energy	Hydro energy	Thermal System
HOMER	✓	✓	✓	✓	✓	✓	✓	✓	-
HYBRID2	–	✓	✓	✓	✓	✓	–	–	✓
iHOGA	✓	✓	✓	✓	✓	✓	–	✓	–
RETScreen	✓	✓	✓	✓	–	✓	–	–	–
HYBRIDS	–	✓	✓	–	–	✓	–	–	–
SOMES	✓	✓	✓	✓	–	✓	–	–	–
RAPSIM	–	✓	✓	✓	✓	✓	–	–	–
SOLSIM	✓	✓	✓	✓	✓	✓	✓	–	–
ARES-I &II	–	✓	✓	✓	✓	✓	–	–	–
HYSYS	–	✓	✓	✓	✓	✓	–	–	–
INSEL	–	✓	✓	✓	✓	✓	–	–	✓
SOLSIM	✓	✓	✓	✓	✓	✓	✓	–	–
HybSim	✓	✓	✓	–	✓	✓	–	–	–
Dymola/Modelica	✓	–	✓	✓		✓			
SOLSTOR	✓	✓	✓	✓	✓	–	–	–	–
HySim	✓	✓	✓	–	✓	✓	–	–	–
IPSYS	–	✓	✓	✓	✓	✓	–	✓	–
Hybrid Designer	✓	–	✓	✓	✓	✓	–	–	–
TRNSYS	✓	✓	✓	✓	✓	✓	–	–	✓
iGRHYSO	✓	✓	✓	✓	–	✓	–	✓	–
HYSYS	–	✓	✓	✓	✓	✓	–	–	–
INSEL	–	✓	✓	✓	✓	✓	–	–	✓
MATLAB/Simulink	–	✓	✓	✓	✓	✓	✓	✓	✓

3.3 Proposed PV/T model

The unpredictable and fluctuating nature of solar flux leads to uncontrollable thermal and electrical energy production and increase the vulnerability of the conventional combined PV/T system. The PV/T system development may be limited by its real-time capacity to monitor the energy demand and the energy fluctuations produced (Sarkar *et al.*, 2018).

Existing PV/T system types have many shortcomings that restrict their optimum performance when they are practically applied. The primary issue with the air-based PV/T system lies in its insignificant heat exchangeability, this is credited to the low thermodynamic properties of air, for example, density, specific heat and thermal conductivity.

The challenges associated with water-based PV/T systems are that the heat exchanger is not efficient enough to prevent the water temperature in the collector from rising over time. The subsequent rise in the temperature of the PV module, if maintained, will reduce its efficiency. Moreover, corrosion and freezing can be another issue when the system is working in cold environments.

Refrigerant-based PV/T system is an alternative to water and air PV/T system with more substantial improvement. There is, however, a high risk of refrigerant leakage and difficulty of balancing the circulating refrigerant in the coils as used in PV module having a big area. It is also difficult to maintain pressure throughout the operation duration.

The heat-pipe-based PV/T systems also have drawbacks such as the continuous flow limit, capillary limit, difficulties in high-temperature heat pipes, chemical reaction, viscous limit and boiling limit and they require extra costs, for example, for individual heat pipes and the control of heat pipe operation.

In this present study, it is proposed to improve a simple water-based PV/T system efficiency. This is achieved by developing and analysing the cooling method and as well as, the possibility of partially converting the photovoltaic electrical output into a useful heat source (for domestic hot water) of the proposed model. The working fluid plays the role of cooling the PV cells to the average operating temperature and maintain the electrical energy to the optimum efficiency, therefore boosting the PV cells performance. The working fluid also would collect the useful heat energy through the pipes in a closed loop attached at the back of the PV panel. A control method can adjust the useful heat transfer capacity to the working fluid based on energy demand. This PV/T system will be designed to balance the thermal (internal heat generation of the PV cell) and

electrical energy based on weather condition and energy (thermal and electrical) need. Therefore, the PV/T system can be used as a multifunctional energy device. The PV/T model proposed is illustrated in Figure 3.12.
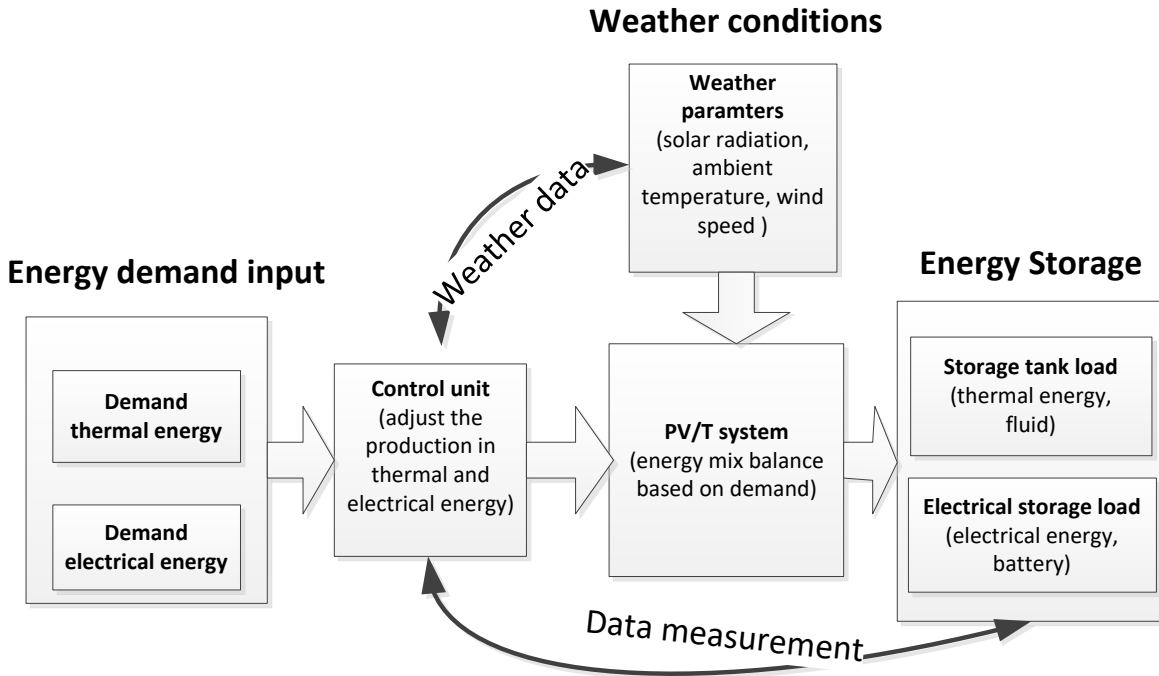
Figure 3.12: Proposed PV/T system

Advantages of the development of the proposed PV/T system are listed below:

- Space management and the total energy efficiency (electrical and thermal energy) are higher per square meter as compared to the use of two separate systems.

- PV/T system results in a lower cost of construction for the combined system instead of two separate systems (conventional solar PV and thermal collectors).

- The efficiency of PV cells increases by cooling them through the solar thermal system

- PV/T system is reliable and can work in a quiet environment.

- The energy management monitors of a PV/T system operating mode.

- PV/T system provides broad applications as compared to the independent system.

- This PV/T system is based on the interpretation of the thermal (internal heat generation of the PV cell), electrical energy demand and production to achieve the energy balance.

3.4 Conclusion

In this chapter, a comprehensive study of the PV/T technologies and their reasonable applications have been reviewed. The outcome of the study assists in better comprehending the present advancement of PV/T technology and also to discover potential problems, obstacles in this area, and as well as potential research to increase the effectiveness of PV/T technology.

PV/T systems are available in a variety of configurations, associated with air, water, refrigerant-based PV/T and heat pipe-based PV/T, nanofluids-based PV/T, BIPV/T and PCM-based PV/T system (for comparison see Table 3.2). The efficiency of a PV/T system is generally evaluated by electrical and thermal performance, while environmental and economic benefits are assessed in terms of cost reduction and carbon reduction over their lifespan.

An air-based PV/T system is commonly used for place heating application. However, the major problem with the air-based system is that the heat exchange capacity is not significant because of the low thermodynamic properties of air such as thermal density and thermal conductivity.

Water-based PV/T system is commonly used for electrical and thermal efficiency; however, the heat exchanger is not suitable in practice because water temperature continually rises during use and the effectiveness of the solar cell cannot be increased when used at high temperatures. Also, freezing can be a problem when the system is operating in cold weather. However, water-based PV/T and air-based PV/T system can be combined to improve output efficiency and to overcome the limitation of individual systems. Even so, the system continues to face issues of ionisation of water and corrosion.

Refrigerant-based PV/T system is an alternative system to water and air-based PV/T system with more substantial improvement; however, it presents a high risk of refrigerant leakage and the problem of balancing of refrigerant circulation in the different coils used in large areas of PV modules. There is also the problem of keeping the pressure constant during the operation.

A heat-pipe-based PV/T system is used for cooling the PV module and providing thermal energy. However, this type of PV/T system has difficulties in high-temperature heat pipes, chemical reaction, the problem of the high component cost, continuous flow limit, capillary limit, viscous limit and boiling limit.

The nanofluid-based PV/T system presents an effective heat transfer for cooling and heating in the PV cell applications, but it is difficult to maintain, and it is expensive.

Based on previous research output and potential opportunities for the future PV/T system development, this research work proposes to develop the following in Chapter 4 and Chapter 5:

- Influence the PV cell performance and to partially convert the internal heat generation of the PV cell into useful thermal energy for domestic hot water. Therefore, it is necessary to analyse the heat produced by the PV cell before integrating it with the absorber pipe to form the PV/T;

- Control the water mass flow rate of the working fluid within the absorber pipe, and to reduce PV cell temperature which increases the PV electrical output;

- Control the heat conduction capacity (useful heat) to increase heat (to heat water in the PV/T system and achieve medium range temperature applications as detailed in Table 3.3); and

- Develop a control strategy to balance thermal and electrical efficiency. These tasks are aimed at the development of PV/T systems, addressing prevalent gaps in previous studies. The results will add value to the PV/T system development. The subsequent two chapters will discuss the development of the proposed PV/T system.

Chapter 4

Performance evaluation and analysis of the PV array

4.1 Introduction

The evaluation and calculation of the solar cell temperatures are vital to the proper functionality of the photovoltaic model and to predict its characteristic. The main focus of this work is on the electrical performance and thermal output, as well as the operating temperatures of the PV modules. Heat transfer and temperature gradients at each layer will be discussed and, taking heat transfer into account in three ways: by conduction, convection and radiation.

In this chapter, a thermodynamic model of solar module, under different climatic conditions (wind speed, ambient temperature and solar radiation) is developed. Also, the optical properties of each layer of the solar module, the electrical properties are addressed to explain the distribution of the primary temperature in the photovoltaic module layers. The model presents a method of temperature calculation based on heat transfer theory, thermoelectric theory, and an analogy between basic thermal and electrical processes. The solutions of the equations give the distribution of temperature, using digital approaches by applying MATLAB software to accurately define the thermal behaviour of the photovoltaic module.

4.2 Operating principle and design parameter of the PV array

The development of the PV array model is as follows:

- To operate the photovoltaic module as a partial useful heat source, hypothetically by using simulation to evaluate the thermal and electrical performance of a PV module;

- To examine the operational performance of a PV cell against different variables; and

- To develop an analytical model of the PV cell for maximising the useful heat transfer capacity.

A further intention is to predict the optimum operating characteristics of the thermal and electrical power, and efficiency, using linear regression to determine the equation applicable to the PV cells.

4.2.1 Operating principle

The internal heat generation of the solar cell can be used for medium-range temperature application (see Table 3.3); since the electrical efficiency of a PV cell decreases with an increase in temperature. It is preferable to obtain a controllable self-heating (useful heat) of the PV cell using an external parameter. The focus of this work is to study the thermal behaviour of a photovoltaic cell, and the heat transfer via radiation, convection, and particularly conduction (useful heat), which is provided by a PV cell. The modelling is based on the calculation of the heat balance, heat transfer occurring in the PV cell, the temperature within the PV cell, thermal and electrical power, and other efficiencies which will be accessed using the following parameters:

- solar radiation;
- ambient temperature;
- convective heat transfer coefficient; and
- external series resistance.

Energy analysis is essential to evaluate the electro-thermal performance of a PV system and to assess the energies generated. It is viable to determine the magnitude of thermal losses and the energy principle in terms of the second law of thermodynamics (Akyuz *et al.*, 2012).

It should be noted that during the simulation time, non-cloudy periods occurred, preventing the PV cell from reaching a high air temperature at the exit of the absorber duct. For the simulation of a physical phenomenon like the problem of heat transfer in Simulink/Simscape, it is necessary to develop all the equations of the heat transfer phenomenon in this study.

Thermal energy produced on the surface of the PV module depends on the absorption and transmission coefficients. PV module heating rates are a significant factor influencing the efficiency of solar cells. The internal heat generated in the photovoltaic cell is ascertained dependent on a mathematical equation, as well as the sum of the $I^2 \cdot R$ losses for each of the resistance and the losses in each of the diodes.

4.2.2 Design parameters of the PV array

A PV module is generally made of solar cells connected in series (for example 36 or 72 cells connected in series). In this study, the PV modules parameters appear in Table 4.1 and Table 4.2.

Table 4.1: PV module parameters

Component	Parameter	Value
PV modules	Cell type	mono-crystalline
	Packing factor	0.91
	Conversion efficiency	16%
	Module peak power	3.25 kW
	Maximum voltage, V_m	255 V
	Maximum current, I_m	12.4 A
	Open circuit voltage, V_{oc}	310 V
	Short circuit current, I_{sc}	14.64 A
	Internal Series resistance R_{si} / cell	0.0042
	Parallel resistance R_{pi} /cell	10.1 Ω

Table 4.2: Optical parameters of PV cells

	Absorbance α	Emissivity ε	Thermal Conductivity	Thickness δ	Temperature Coefficient	Energy gap EG
PV module type	0.8	0.75	840	0.003	0.000905	1.11
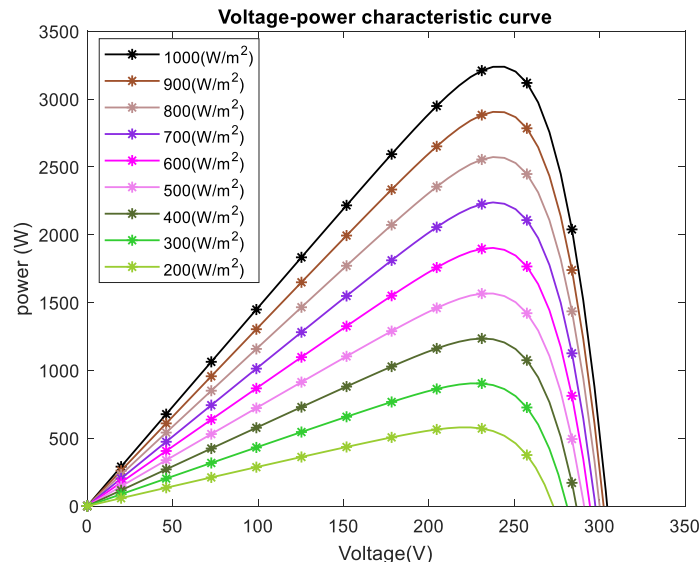
Figure 4.1: PV module voltage-power characteristic curve

The entire PV system consists of two PV arrays assumed to perform identically and in a parallel configuration; the system has a capacity of 3.24 kW$_p$ at 1000 W/m^2 (Figure 4.1).

4.2.3 Mathematical model and thermal performance of PV array

The numerical analysis of thermal and electrical energy from the PV array is presented in this section. The PV array is assumed to lay perfectly flat on the Earth's surface and receive full solar radiation. The transfer of thermal energy generated in the PV array has the following process: the solar radiation is converted to electrical/thermal energy by the PV array.

To simplify the physical structure of the proposed PV array, the following assumptions should be ensured when configuring the model:

- The overall efficiency of the system is in a quasi-steady-state condition.
- All surfaces of layers incorporate uniform temperature.
- The temperature of the gradient around the tube is considered insignificant.
- No air layer between the PV cell and the heat exchanger.
- Heat dissipation is as one-dimensional.
- Forced flow through heat exchanger tubes exists.
- Edge loss is considered insignificant because of insulation.
- Due to the high resistance to heat, the heat loss through the insulation is low.
- Heat loss through the insulation is considered insignificant due to the high thermal resistance features.
- The PV module is in a horizontal orientation upwards, with solar radiation perpendicular to the module.
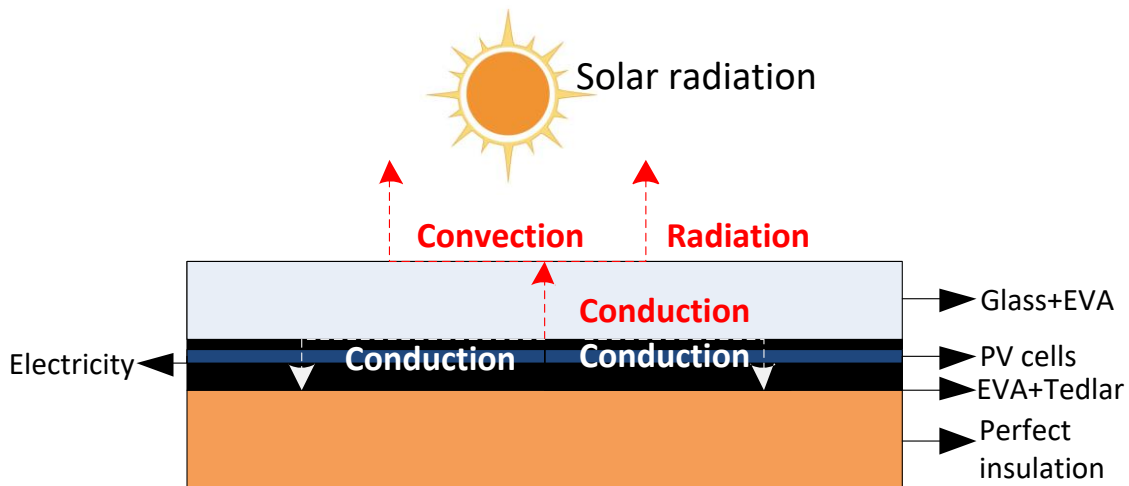
Figure 4.2: Heat transfer characteristic of the PV system

The design and mathematical equations given in this study are not necessarily the most well-defined due to the assumptions, but they are generally used in the literature and are straightforward to apply and acceptable for most design calculations. Figure 4.2 depicts the heat transfer characterisation of the PV system.

4.2.3.1 Thermal modelling

The equation of the energy balance is well defined in solar energy thermal processes by Duffie and Beckman (1991).

The useful energy Q_u is extracted under conditions of stability, proportional to the useful energy absorbed by the collector, minus the amount lost by the collector and it is expressed as follows equation (Duffie & Beckman, 1991):

$$Q_u = Q_{in} - Q_{loss} \qquad \textbf{(4.1)}$$

where:

Q_u is the useful energy

Q_{in} is the absorbed energy

Q_{loss} is the energy losses

The solar cell energy increases when the solar radiation reaches the absorber plate surface. Energy gained by the absorber is the active optical fraction of the solar radiation; the following equation expresses the amount of solar radiation received by the solar cell (Duffie & Beckman, 1991):

$$Q_{in} = (\alpha \tau) * G * A_c \qquad \textbf{(4.2)}$$

where:

G is the intensity of the solar radiation, (W/m^2)

A_c is the surface area of the Solar cell, (m^2)

τ is the transmission coefficient of the glazing is lower; and

α is energy absorbed in a fraction.

The amount of incoming radiation absorbed is given by $\alpha \tau$.

The mode of loss— convection, radiation and conduction — is dependent on the difference in the temperature between the solar cell, the environmental temperature, and the geometry of the solar cell. The formula is given in the following equation:

$$Q_{loss} = Q_{conv} + Q_{rad} \tag{4.3}$$

Q_{conv} is the heat convection to the external environment. The convective exchange losses depend on the linear wind speed function and the environment temperature. These losses are proportional to the solar cell temperature and the ambient temperature and it is given by the following equation (Duffie & Beckman, 1991):

$$Q_{conv} = A \times h \times (T_{ext} - T_s) \tag{4.4}$$

where:

T_s is the temperature surface

T_{ext} is the external temperature

h is the heat transfer coefficient

Most of these coefficients a, b and n are in the form of the following equation:

$$h = a + b \times v^n \tag{4.5}$$

Thus, this is proposed as the most commonly used equation to study the relationship between flat solar collectors:

$$h = 5.7 + 3.8 \times v^n \tag{4.6}$$

This transfer mode occurs through the emission and electromagnetic absorption between objects at different temperatures is called thermal radiation. The perfect emitter of blackbody emission power or thermal radiation, given by Stefan-Boltzmann, is proportional to the fourth power of its temperature. This is described by Equation 4.7 below (Kreith et al., 2010; Duffie & Beckman, 1991):

$$Q_{rad} = \sigma \cdot A \cdot T^4 \tag{4.7}$$

The completion of the radiation between the surfaces involve losses from surface radiation and lost into the environment. This is affected by the physical and geometric properties of the surface

and is quantified by the parameters known as the shape factor. To exchange radiation between the two surfaces 1 and 2, the net heat energy of surface 1 can be approximately transferred to surface 2, in the following equation (Kreith et al., 2010; Duffie & Beckman, 1991):

$$q_r^{1\leftrightarrow 2} = -q_r^{1\leftrightarrow 2} = \frac{\sigma \cdot \left(T_1^4 - T_2^4\right)}{\frac{1-\varepsilon_1}{\varepsilon_1 \cdot A_1} + \frac{1}{A_1 \cdot F_{12}} + \frac{(1-\varepsilon_2)}{\varepsilon_2 \cdot A_1}}$$

(4.8)

The general form of the radiation heat transfer coefficient between surfaces is:

$$h^r = \frac{\sigma \cdot \left(T_1^4 - T_2^4\right)\left(T_1 + T_2\right)}{\frac{1-\varepsilon_1}{\varepsilon_1} + \frac{1}{F_{12}} + \frac{(1-\varepsilon_2)A_1}{\varepsilon_2 A_2}}$$

(4.9)

The radiation exchange between two surfaces (convex objects and large shells) is applicable when a sizeable concave surface surrounds a curved object. Under these circumstances, $A_1/A_2 \rightarrow$ 0, and mainly no reflection of the radiation is emitted by the object, $F_{12} \rightarrow 1$. The rate of radiation heat loss is proportional to the emittance of the surface and the difference in temperature to the power of four. The equation is given as the following (Kreith et al., 2010; Duffie & Beckman, 1991):

$$Q_{rad} = \sigma \cdot \varepsilon_1 \cdot A_1 \cdot \left(T_1^4 - T_2^4\right)$$

(4.10)

$$h_r = \sigma \cdot \varepsilon_1 \cdot \left(T_1^2 + T_2^2\right)\left(T_1 + T_2\right)$$

(4.11)

The expression is used in the case of coverage of a solar cell surface at a temperature (T). Therefore, the equation concerning the ambient temperature (T_a) is rewritten in the following:

$$h_{c-s}^r = \sigma \cdot \varepsilon_c \cdot \frac{\left(T_c^4 + T_{sky}^4\right)}{\left(T_c - T_a\right)}$$

(4.12)

The accumulated heat in the solar collector is transmitted to the atmosphere through convection and radiation. The collector heat loss coefficient (U_L) describes how much of the energy is lost to the surroundings through the top with excellent backing insulation. The rate of heat loss depends on the overall heat transfer coefficient of the collector, as in the following equation:

$$Q_{out} = h_{cv} \cdot (T_c - T_a) + \varepsilon \cdot \sigma \cdot (T_c^4 - T_s^4)$$

(4.13)

where:

Q_{out} is the heat loss (W);

U_L is the heat loss coefficient, W/(m²·K);

T_c is the average temperature of the collector (°C); and

T_a is the ambient temperature (°C).

4.2.3.2 Modelling of temperature effects on PV array

The PV array only converts a part of the solar radiation into electrical energy, while the rest is converted into heat. The PV module operating temperature has a significant impact on its performance. However, this depends on many factors such as the semiconductor material used, the manufacturer of the PV module and the installation on site. The effect of temperature on the PV module in this section, including the factors that affect the PV cell operating temperature and their results, is discussed.

(1) Effect of the operating temperature of the solar cell

The solar cell temperature increases while functioning and, adversely affecting its performance. The equations governing the PV cell performance depends on temperature, band gap, diffusion coefficient, integral voltage, intrinsic carrier concentration, a width of the depletion zone and the limitations of models used. The temperature affects V_{oc} as described by Equation 4.14 (Saadah *et al.*, 2017; Singh & Ravindra, 2012).

$$V_{oc} = \frac{n \cdot k \cdot T}{q} \ln(\frac{I_{sc}}{I_0} + 1) = V_t \cdot \ln(\frac{I_{sc}}{I_0} + 1) \qquad \textbf{(4.14)}$$

where:

V_{oc} is thus logarithmically proportional to the short-circuit current (V);

I_0 the inverse of the saturation current (A);

q is electron charge (C); and

k is the Boltzmann constant.

Regarding the temperature effect, the V_{oc} changes linearly and is inversely proportional to the temperature. Under PV cell operating conditions, the short-circuit current is relatively independent of the temperature. When electrons are excited by the thermal effect rather

than the electrical properties of the semiconductor, V_{oc} and FF are reduced. The temperature tends to decrease the performance of a PV cell by decreasing V_{oc}.

However, the saturation current varies with temperature. Also, the band gap energy, E_g, of a semiconductor cell decreases as the temperature increases, and is modelled as follows (Saadah *et al.*, 2017; Singh & Ravindra, 2012):

$$E_g(T) = E_g(0) - \frac{\alpha T^2}{T + \beta}$$ **(4.15)**

where:

$E_g(0)$ refers to the band gap value at zero Kelvin;

$E_g(T)$ is the band gap of a semiconductor at temperature (*T*); and

α and *β* are specific constants of the semiconductors.

Due to the improvement of absorption and photocurrent, the decrease in the band gap causes a slight increase in the short-circuit current, I_{sc}. However, the heating has an undesirable effect on the open-circuit voltage, V_{oc}. From PV materials, it is observed that the linear decrease in V_{OC} and a linear increase in I_{sc}, slightly offset fill factor (FF).

(2) Calculation of temperature of PV cells
Most of the formulas consider the linear character of the PV cell performance to reproduce its temperature dependence and based on its efficiency or its maximum power. The widely used expression which relates the efficiency of a cell to its operating temperature is given in the following formula (Singh & Ravindra, 2012):

$$\eta_c = \eta_{Tref} \cdot \left[1 - \beta_{ref} \cdot \left(T_c - T_{ref} \right) \right]$$ **(4.16)**

where:

η_{Tref} is the efficiency of the cell (or module) at the reference temperature;

T_{ref} is the reference temperature of 1000 W/m²;

T_c represents the operating temperature of the module; and

β_{ref} represents the temperature coefficient.

The coefficients β_{ref} and η_{Tref} are dependent on the properties of the material, representing the linear variation of the yield as a function of the PV cell temperature.

The linear equations equivalent to those proposed equations above can be applied when calculating the power loss of the PV module as a function of its operating temperature. Again, very few models consider elements that aid in cooling the module (power gain) by convection such as wind or fluid that passes to the back of the PV module.

(3) Consideration of temperature in commercial PV models

STCs are used to compare the performance of different cells or modules but are not representative of the real-world operation of a PV module. A high operating temperature is a factor that detracts the PV module performance.

A more complex model, an energy rating model, which considers the effect of the spectral disagreement and the angle of incidence of the light rays, has been developed by the National Renewable Energy Laboratory (NREL). I_{sc} and V_{oc} are defined in Equation 4.17 and (4.18, respectively.

$$I_{sc} = \frac{G}{G_{ref}} \times I_{SC_{ref}} \times \left[1 + \alpha\left(T_c - T_{ref}\right)\right] \tag{4.17}$$

$$V_{oc} = V_{oc,ref} \times \left[1 + \beta.G_{ref}\left(T_c - T_{ref}\right)\right] \times \left[1 + \delta(T_c).\ln\left(\frac{G}{G_{ref}}\right)\right] \tag{4.18}$$

Where α, β and δ are the temperature coefficients for the current, the voltage and the luminous intensity, respectively. Moreover, G is the light intensity (W/m^2) (Ramaprabha & Mathur, 2012; Duffie & Beckman, 1991).

The index refers to STC, Equation 4.18 takes into account the temperature dependence of the module and solar radiation. The models rely on the empirical coefficients such as α, β and δ and, are generally more reliable than models that determine power or efficiency from solar radiation, environmental temperature, and in some cases, wind speed. However, the influence of the solar spectrum distribution, the thermal effects depends on the location and might be responsible for a difference of 10% losses.

The thermal losses are determined by an energy balance between the ambient temperature and the solar cell temperature in the following equation:

$$U(T_c - T_a) = \alpha G(1 - \eta_c)$$ **(4.19)**

where:

α represents the absorption coefficient of the solar radiation of the PV module; this coefficient is usually set at 0.9; and

U represents the thermal exchange by natural convection of the module with its external environment W/(m²·K).

The energy balance per unit area of the PV module, which is cooled by a loss due to the external environment can be expressed as follows:

$$\tau \cdot \alpha \cdot G_T = \eta_c \cdot G_T + U_L \cdot (T_c - T_a)$$ **(4.20)**

where:

τ represents the transmittance of any cover that may be over the cells;

α refers to the fraction of the incident radiation absorbed on the surface of the cell; and

η_c is the efficiency of the module for converting the incident.

Nominal operating cell temperature (NOCT) is determined as a module temperature under the conditions as listed below (Tian *et al.*, 2012):

- solar radiation of 800 W/m^2;
- wind speed 1 m/s;
- ambient temperature of 20⁰C; and
- no-load operation ($\eta_c = 0$).

The solar cell is exploited using the linear radiation or a high circular concentrator to define the loss coefficient. The loss coefficient includes convection and radiation from the top and bottom of the module, mounting frame losses at any ambient temperature, T_a.

To determine the $\dfrac{\tau\alpha}{U_L}$ ratio, the PV cell temperature, ambient temperature, and solar radiation can be used in Equation 4.21, which is expressed as follows (Tian *et al.*, 2012; Duffie & Beckman, 1991):

$$\frac{\tau \cdot \alpha}{U_L} = \frac{\left(T_{c,NOCT} - T_a\right)}{G_{T,NOCT}} \tag{4.21}$$

Assuming that the temperature under any other condition is constant, T_c can be obtained from the following Equation 4.22:

$$T_c = T_a + \left(\frac{G_T \cdot \tau \cdot \alpha}{U_L}\right)\left(\frac{1-\eta_c}{\tau \cdot \alpha}\right) \tag{4.22}$$

The factor $\tau\alpha$ in Equation 4.22 is generally unknown but is estimated to be 0.9, and there are no serious errors in using this value because the term $\frac{\tau\alpha}{U_L}$ is smaller than unity.

4.2.3.3 Choice of Simulation software for the PV model

In this section, the simulation software feature is analysed in Table 3.4 and Table 3.5, MATLAB/Simulink software is chosen to conduct the PV array modelling. A MathWorks Simulink simulation environment provides a physical modelling toolbox in Simscape that can be used to design the PV and PV/T models. The use of Simscape as a modelling tool offers a series of pre-established thermal components and systems such as critical physical properties of electrical and mechanic components, photovoltaic modules, storage tanks, electrical batteries, control systems and power management. See more details in Appendix A.

The thermodynamics of an element model is designed to react accurately to the ambient temperature and material temperature when an element is exposed to solar radiation; these vary the internal temperature of the element model accordingly. It is essential to analyse the effect of the cooling system on temperature changes.

Many models describe exchange radiations with the ground and the sky, and also by convection based on the ambient temperature, sky emissivity, cloudiness and atmospheric pressure. Each parameter is related to a location, a period of the year, and climatic conditions (for example to a given time and place). All these temperature variables have a certain impact on PV cell temperature (T_c). However, in order to avoid the increasing number of the input parameters necessary for the simulation, some parameters such as the heat exchange occurring between the environmental temperature at the front of the PV cell, and environmental temperature at the back of the PV cell with respective symbol T_{env-f} and T_{env-b}, have been left out. The evolution of T_c as a function of ambient temperature (T_a), the thermal behaviour of the photovoltaic cell model, and an analysis of the influence of the PV cell temperature during the operation will be studied.

For this, it is necessary to consider the simple case where the front heat exchange convection, radiation and $T_{a-f} = T_{a-b} = T_a$, where T_{a-f} is the ambient temperature at the front of the cell, T_{a-b} is the ambient temperature at the back of the PV cell, and T_a is ambient temperature. The heat exchange by convection (Q_{conv}), radiation (Q_{rad}) and conduction (Q_{cond}) occurring at the PV module and the evidence of their impact on the temperature of the PV cell, are considered. The resulting thermal equilibrium depends on heat exchange involving Q_{rad}, Q_{conv} and Q_{cond} emitted by the PV cell.

4.3 Simulation results and discussion

The simulation will study several parameters models such as the ambient temperature, solar irradiance, convective heat coefficient and external series resistance and also, predict the thermal behaviour, the power generated and the efficiency of PV cell models. Including, the total power dissipated by the PV cell model composed of a diode (representing the semiconductor material of the PV cell), an internal series resistance (formed of contact resistance, the busbars resistance, grid resistance, and lateral conduction in the emitter) as given by R_{si}, and an internal series resistance (representing the emitter at the edge of the cells, cracks, recombination sites at the cell edge, Schottky-type shunts below grid lines, scratches, and aluminium particles at the surface), as given by $R_{pi.}$

The model is based on solving the thermal balance equations, the equations for the heat loss by conduction, convection and radiation occurring in the PV cell (see Appendix A.1.2), and to determine the energy balance of the PV cell. The equations describe the effect of the thermal capacity of a solar module, more detail on the solar cell are shown in Appendix A.1.3. The model treats the heat conduction through an electrical analogy approach.

4.3.1 Impact of solar radiation on the PV cells performance

This section evaluates the results of PV cells performance based on the influence of varying solar radiation. The PV module output is focused on the maximum electrical energy generated and heat dissipated in a PV module. As well as the heat transfer, and solar radiation intensity changes from 200 to 1000 W/m^2, while the other outside factors are kept constant [that is, ambient temperature at 20°C and a convective heat transfer coefficient of 20 W/(m²·K)]. The outcomes of the study are shown in Figure 4.3 to Figure 4.9 and also in Table B-1.

In Figure 4.3, there is an exponential increase in the total power dissipated (P_d) from 0 to 940 W of the PV cell, composed of the diode, R_{si} and R_{se} as solar radiation increase from 200 to 1000 W/m². The power dissipated by R_{si} (internal series resistance) increased marginally as the solar radiation increases, and the power dissipated by R_{pi} (internal parallel resistance) remained the same. However, the diode representing the semiconductor material property and presents much of the total power dissipation. The semiconductor material property used for the PV cell dissipates power at high solar radiation levels by increasing the temperature and reducing the band gap of a semiconductor, thereby affecting most of the semiconductor material property parameters. Also, the low energy photon will contribute to thermal energy. Comparative outcome trends were found by Islam *et al.* (2014).
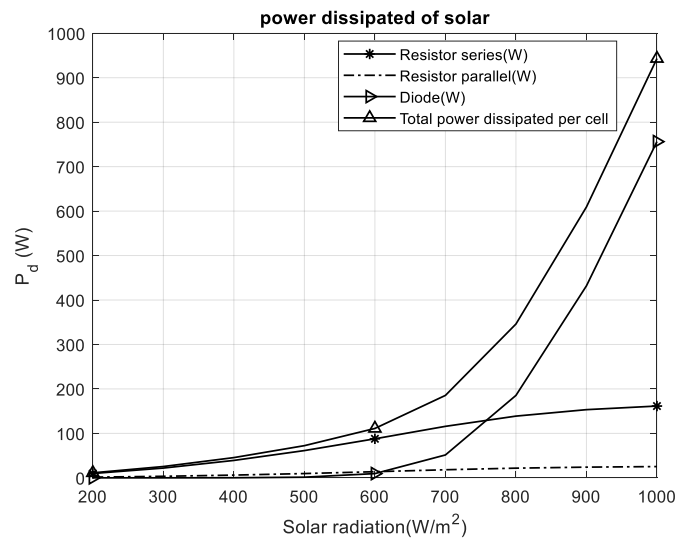
Figure 4.3: Power dissipated within the PV cell

Figure 4.4 exhibits a downward decrease in the heat loss by Q_{cond} of the PV cell, the Q_{cond} increments from 5 to 450 W (in magnitude) as the of solar radiation moves from 200 to 1000 W/m². In this case, the back of the PV panel was assumed to be a perfect conductor. The increase in the rate of heat conduction was attributed to the PV cell semiconductor material property, and the power dissipation was in the form of heat, resulting from the increase in electrical generating at high solar radiation levels.
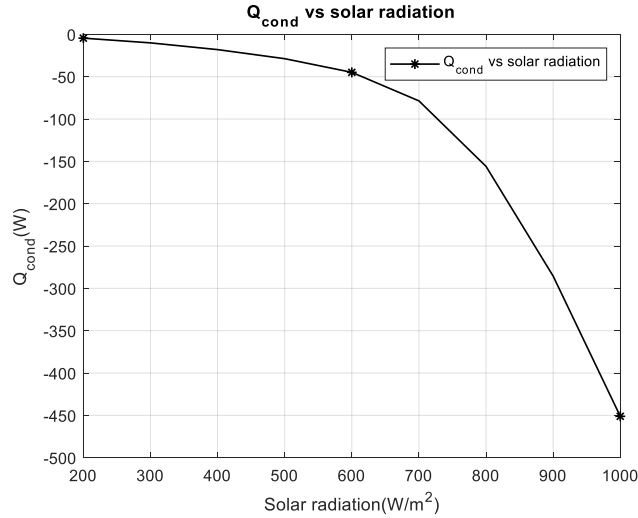
**Figure 4.4: Conduction heat as a function of
solar radiation**

The effect of increasing solar radiation produces a heat loss by convection from a PV cell to the environment, is depicted in Figure 4.5. The figure shows a continuous increase of Q_{conv} from 500 to 3100 W throughout the variation of solar radiation from 200 to 1000 W/m². The heat loss is due to the absorptivity of covering glass (reflection from the top surface of the PV cell), to the loss by conduction and to the power dissipated in the PV cell.
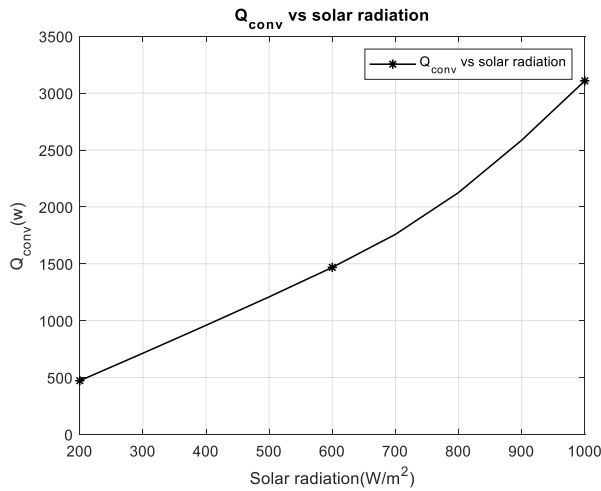
**Figure 4.5: Convection as a function
of solar radiation**
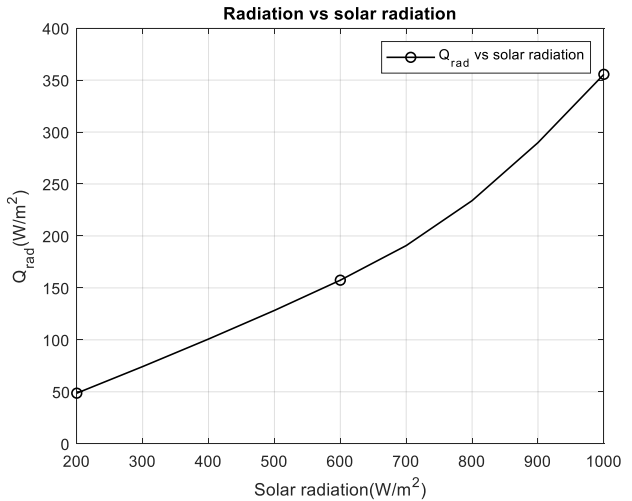
**Figure 4.6: Radiation as a function
of solar radiation**

The relationship is not completely linear between heat by convection and solar radiation because at high solar radiation intensity, the difference between the PV cell temperature and the ambient temperature increases, which in turn increases heat loss by convection.

Figure 4.6 demonstrates the impact of solar radiation on a PV cell in heat loss by radiation. The figure presents a steady increase of Q_{rad} from 50 to 355 W when the solar radiation changes from 200 to 1000 W/m^2. This relationship between the solar radiation and heat loss by radiation is not completely linear because as the intensity of solar radiation increases, the gap between the PV cell temperature and the ambient temperature increases, and which increases the rate at which heat is lost by radiation. The radiation losses depend on the surface emissivity, the surrounding temperature and the temperature of the panel front surfaces.

Looking at the different type of heat transfer occurred in PV cell, Q_{conv} and Q_{rad} were measured positive value, because they are transmitted from the PV cell to the surrounding environment, while Q_{cond} was measured negative because the heat loss was transmitted inside the PV cell. The heat exchange by Q_{conv}, Q_{cond}, and Q_{rad} was 2600 W, 450 W and 300 W respectively.
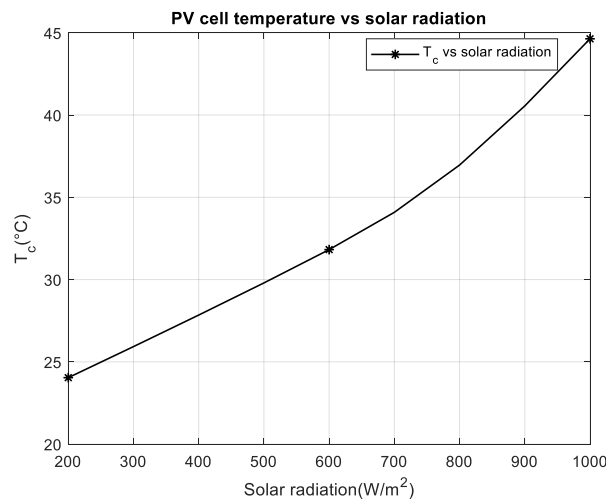
Figure 4.7: The PV cell temperature versus solar radiation

It was also noted in Figure 4.7 that increasing the solar radiation from 200 to 1000 W/m^2 prompted a significant increase in PV cell temperature from 24 to 45°C. It was evident that the higher solar radiation, the higher the PV cell temperature. Similar result trends were reported in detail by Bloem (2008) and Ross and Gonzalez (1980).
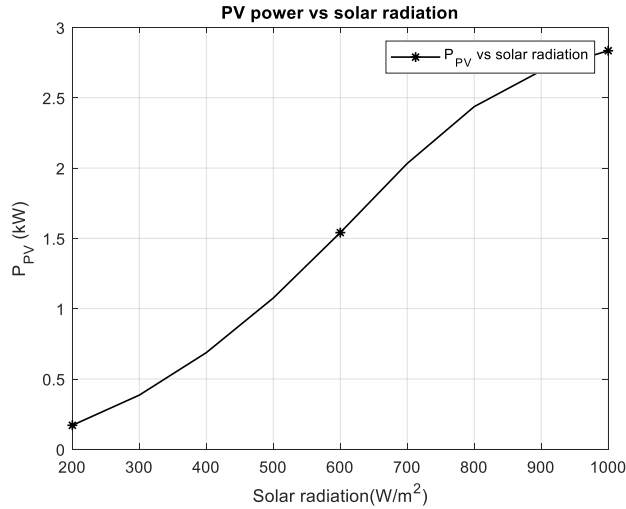
Figure 4.8: PV electrical power versus radiation

Figure 4.8 describes the generated PV power (P_{PV}) as a function of solar radiation, exhibiting an increase in P_{PV} from 0.2 to 2.8 kW when solar radiation increases from 200 to 1000 W/m^2. From this figure, it can be seen that PV power output slows down after 800 W/m^2; this is because of the increased power dissipation occurring in the material at high solar radiation in Figure 4.3, and resulting in a drop in their electrical efficiency. This graph trend is similar to the findings of Islam *et al.* (2014).
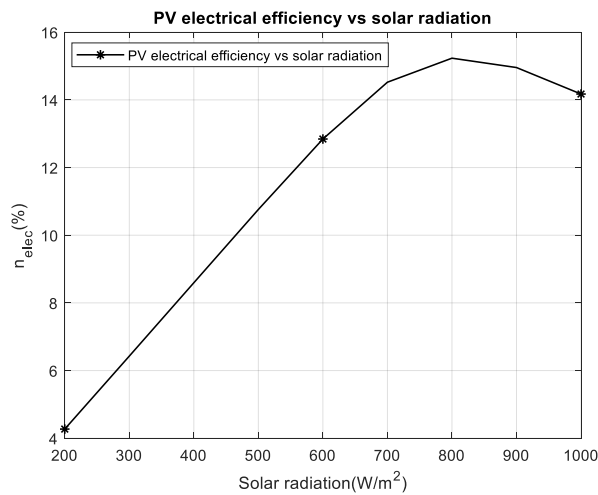
**Figure 4.9: PV cell electrical efficiency
versus solar radiation**

presents the electrical efficiency of the PV cell dependence on solar radiation; two areas of variation are noted: When the irradiance increases up to 800 W/m^2, the electrical efficiency (n_{elec})

135

increases to a maximum of about 15.2%; when the solar radiation exceeds 800 W/m^2, there is a reduction in the electrical efficiency at 1000 W/m^2 and the electrical efficiency was 14.2%. This is because higher solar radiation intensity brings about a more instantaneous heat in the PV cell, as seen in Figure 4.3, raising the PV cell temperature and decreasing its efficiency. The trend of the result obtained is similar to that found by Xiao *et al.* (2014), Islam *et al.* (2014) and Chegaar *et al.* (2013), in terms of the effect of illumination intensity on solar cell parameters.

Summary of solar radiation influence

In studying the impact of solar radiation on the performance behaviour of a PV module, in terms of the operating conditions, this study concludes the following:

- The influence of solar radiation on the PV cell yield, as the increase of radiation causes an increase in the yield.

- Increasing the temperature causes a decrease in the efficiency of this PV module when solar radiation is above 800 W/m^2, so the PV module is sensitive to high solar radiation levels which causes an increase in the heat dissipated.

- The power dissipated is due to intrinsic and extrinsic losses as the solar radiation increases.

It was discovered that the heat transfer by conduction increases exponentially as the solar intensity increases; this depends on the properties of the surface material of the PV cell. The useful energy generated depends on the levels of solar radiation. Also, a significant amount of heat transfer by convection and radiation emanates from the PV cell surface to the environment, due to power dissipation in the PV cell. In Section 4.3.2, the influence of the ambient temperature on PV cell performance will be examined by maintaining other parameters constant.

4.3.2 Influence of ambient temperature on the PV performance

This section analyses the impact of the ambient temperature (T_a) on the energy production of photovoltaic modules. This study focuses on the output energy of a PV module, on the maximum power generated, and on the power dissipated by photovoltaic modules. The PV systems performance under variations of ambient temperature from 15°C and 40°C were examined, while solar radiation was kept at 1000 W/m^2, and convective heat transfer coefficient was kept 20 W/(m²·K). The simulation results were illustrated in Figure 4.10 to Figure 4.16 and also in Table B-2.
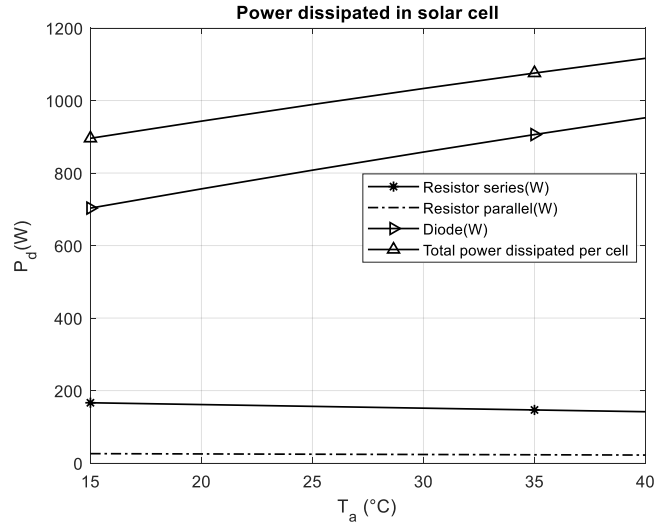
**Figure 4.10: Dissipated power by PV cell versus
ambient temperature**

It was observed in Figure 4.10 that as the ambient temperature increased from 15 to 40°C, the total power dissipated from the PV cell composed of the diode, R_{si} and R_{pi} also increased. It was also observed that the diode dissipates much of the power due to semiconductor material property used for the PV cell, the power dissipated by the R_{si} decreased marginally, while R_{pi} remained almost unchanged, as T_a increased. The increase in the ambient temperature reduces the energy band gap of the PV cell, therefore giving rise to the energy loss in the material. A part of the total power dissipated was transferred by conduction, radiation and convection.
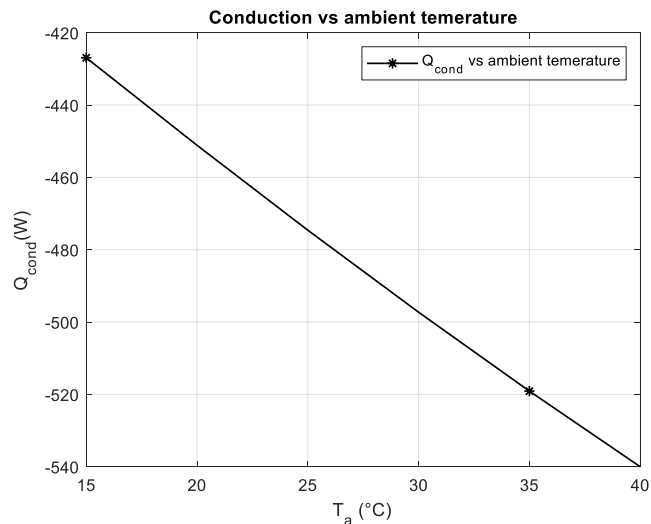
**Figure 4.11: Heat transfer by Q_{cond} within
the PV cell**

Figure 4.11 shows a continuous increase (in magnitude) of heat transfer by Q_{cond} from 425 to 540 W when T_a increases from 15 to 40°C.

As T_a value varies from 15 to 40°C, as illustrated in Figure 4.12, the heat transfer by radiation, Q_{rad} increases from 335 to 450 W. Similarly, the heat transfer by convection, Q_{conv} increases from 3080 to 3195 W over the same ambient temperature range; as shown in Figure 4.13.
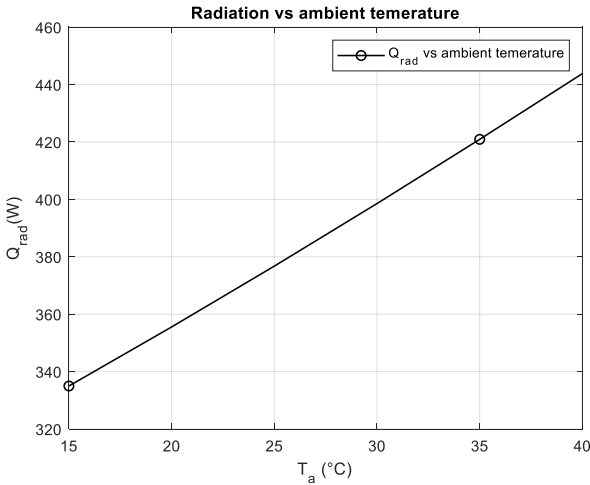
Figure 4.12: Heat transfer by Q_{rad} from the photovoltaic cell to the environment
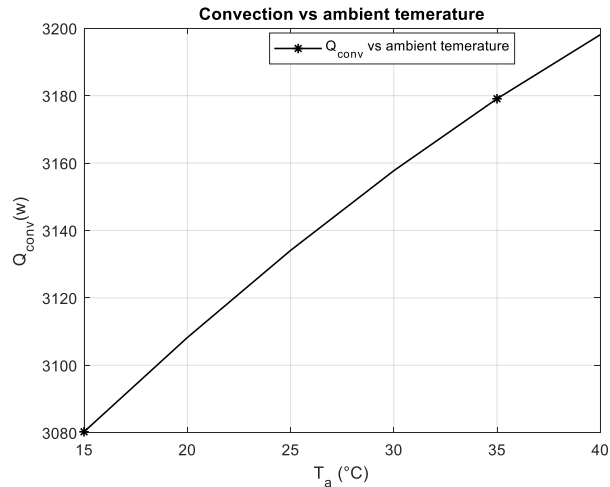
Figure 4.13: Heat transfer by Q_{conv} from the photovoltaic cell to the environment

However, the summary of these results presented in Figure 4.11, Figure 4.12 and Figure 4.13 show that the heat transfer is considerably higher for Q_{conv} than for Q_{rad}, and that both of them was measured as positive because they represent heat transfer out of the PV cell (to the atmosphere). While the Q_{cond}, was considered as negative because heat was transferred into the cell (towards the back of the PV module). Comparing the different types of heat transfer over the selected range of T_a, Q_{conv} as 115 W, Q_{rad} as 100 W and then Q_{cond} as 85 W. These losses are of similar order and not particularly significant when compared to losses due to solar radiation (see Section 4.3.1).

Figure 4.14 shows the elevation of the PV cell temperature as a function of T_a. From the graph, assuming that T_c ranges from 39°C to 66°C, it can be determined that T_a increases by 5°C with a corresponding increase in T_c of 5.4°C. It can be noted that the temperature difference between the photovoltaic cell and the environment at any point is approximately 25°C according to the operating temperature imposed.
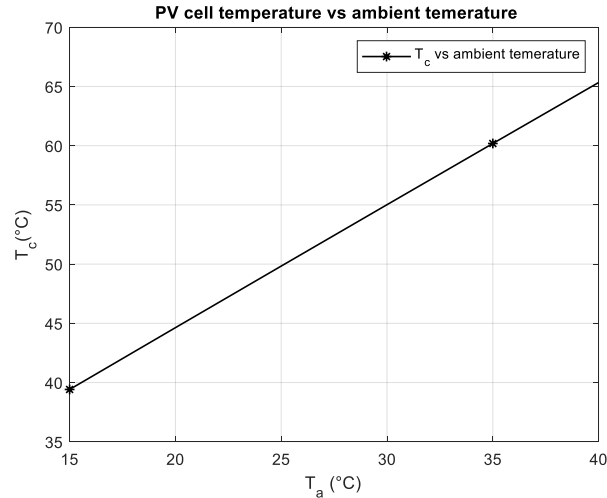
Figure 4.14: T_c **as a function of temperature** T_a

Figure 4.15 presents the PV power as a function of T_a, showing that the PV power drops by 460 W when T_a varies from 15 to 40°C. It can be seen in this figure that the optimum yield was obtained when T_a = 15°C. This occurred due to the fact when T_c was lower, excess heat is drained from the PV cell and when T_a increases, there was a gradual build-up of heat as seen in Figure 4.10, which lowers the output power of the PV cell.
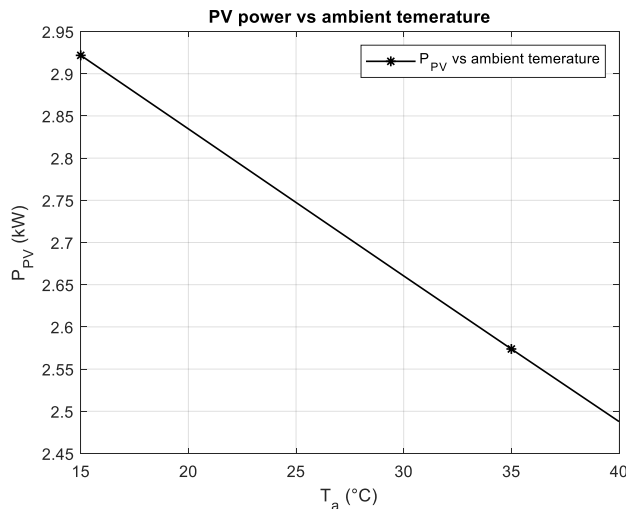
Figure 4.15: PV cells power versus T_a

Figure 4.16 displays the changes in the PV cell electrical efficiency (n_{elec}) as a function of T_a. From the graph, assuming that the PV cell electrical efficiency ranges from 14.7% to 12.4%, It can be seen that the PV cell electrical efficiency decreased by 18.6% from the initial 14.7%, over the selected range of T_a. The efficiency was degraded with the increase T_a because of the rise in T_c.

As the ambient temperature increases, the rate of overall heat transfer decreases from the PV cell to the surrounding environment, resulting in higher solar cell temperatures and lower efficiency. There is a linear relation between ambient temperature and PV cell efficiency. The decrease in temperature enhances the PV cell efficiency.
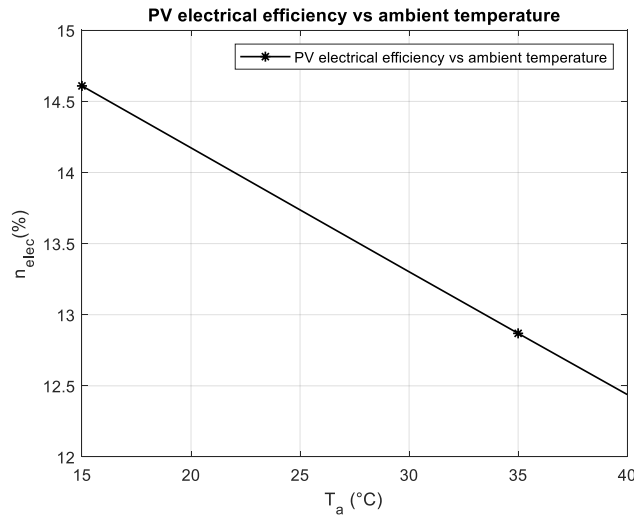
Figure 4.16: PV electrical efficiency versus T_a

Summary of ambient temperature on PV cell

A quick change in atmospheric conditions could have a divergent impact on the PV cell efficiency: lower ambient temperature may drive a considerable heat transfer (through convection and radiation) to the environment, thereby improving PV cell operating temperatures, as well as high electrical efficiencies. Inversely, when the ambient temperature is higher, it causes the PV cells to operate at a lower efficiency. It was observed that the rate of heat loss of a body is directly proportional to the difference in the temperatures between the body and its surroundings provided the temperature difference is small and the nature of radiating surface remains same. The differences in heat transfers are smaller, as compared to the impact of solar radiation (see Section 4.3.1). The lower ambient temperatures lead to enhanced heat losses from the PV cell. The radiative heat loss is enhanced due to the temperature gradient between the PV cell and the ambient temperature. The most significant effect of temperature in the PV cell is due to the intrinsic carrier concentration, causing power dissipation in the form of heat. The influence of the convective heat coefficient on PV cell performance will be examined while other parameters are kept constant. In the next section, a range of simulations of the natural convective heat transfer coefficient h_f was carried, while the other parameters are kept constant.

4.3.3 Influence of the convective heat transfer coefficient on PV cell performance

In this section, the PV cell performance is analysed based on wind speed. It is essential in solving the heat transfer processes between a PV module and the exterior through convective heat flow. The transfer is governed by the Newton law of cooling. A range of natural convective heat transfer coefficient (h_f) simulation was carried out on PV cell, while the other outer parameters were held constant (that is, solar radiation at 1000 W/m^2, ambient temperature at 20°C). The outcomes were presented in Figure 4.17 to Figure 4.24 and also in Table B-3. Note: h$_f$ is the convection coefficient of the front face of the photovoltaic cell that allows the simulation he various heat transfer levels encountered during photovoltaic cell operation.

Figure 4.17 presents the total power dissipation of the PV cell composed of the diode, R_{pi} and R_{si}. From the figure, the power dissipation in R_{pi} is almost constant regardless of changes in h_f, and, it was observed that a slight increase in power dissipation occurs in R_{si} when h_f increases, while the diode presenting much of the total power dissipated in the PV cell. This is due to the cooling effect occurring at the PV cell surface, the total power dissipation and diode power dissipation continuously decrease from 1500 to 900W and 1400 to 750W, respectively. These results reflect the Newton law of cooling between and the body and its surroundings.
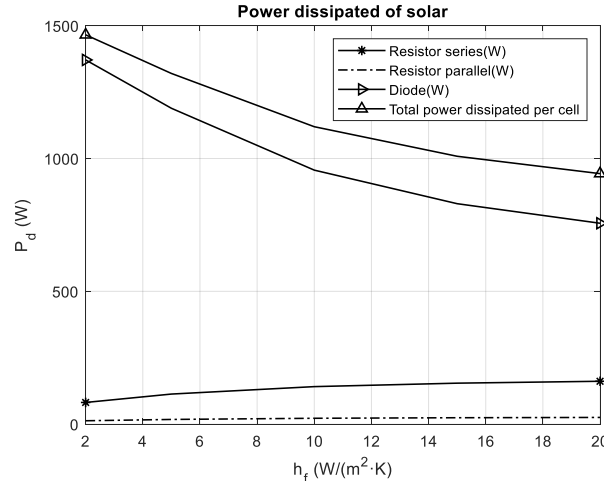
Figure 4.17: PV cell power dissipation versus convective heat transfer coefficient

Figure 4.18 shows a decrease in the heat lost by conduction from 725 to 450 W (in magnitude), while the heat convective coefficient increases from 2 to 20 W/(m²·K). It was evident that as the air velocity increases, the cooling of the PV cell is more effective, resulting in a decrease of power dissipated Figure 4.17 and therefore, decreasing the PV cell temperature.
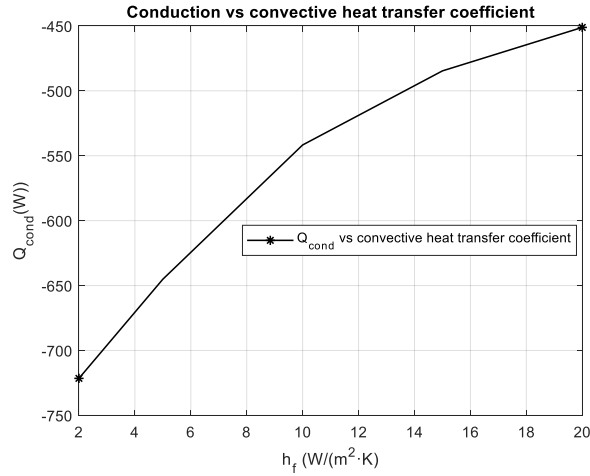
Figure 4.18: Conduction versus convective heat transfer coefficient

Figure 4.19 and Figure 4.20 present a comparison of the convection and the radiative heat transfer. Both convection and the radiation of heat transfer vary following h_f. At $h_f = 2$ W/(m²·K), it was necessary to notice that the heat loss by radiation decreases by 2390 W while heat loss by convection increased by 1425 W. At the high of the h_f range considered, $h_f = 20$ W/(m²·K), the corresponding value for radiation decreased to 400 W, while the corresponding value for convection increased to 3100 W. This is because the temperature of the photovoltaic cell is lower with strong convection, and therefore emits less radiation. When the convection loss is high, more heat is transferred to the environment; lowering the temperature of the PV cell.
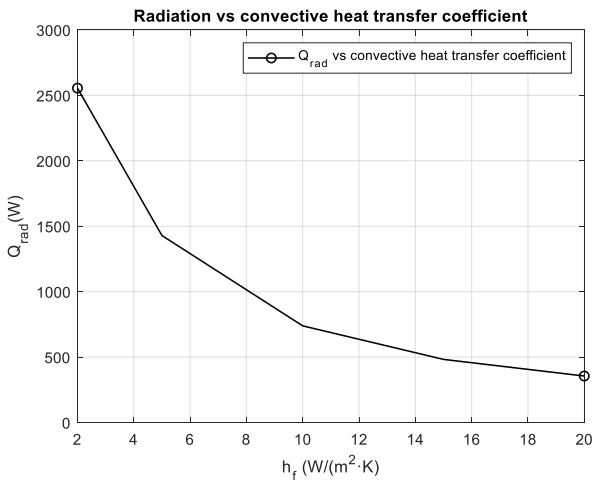
Figure 4.19: Radiation versus convective heat transfer coefficient
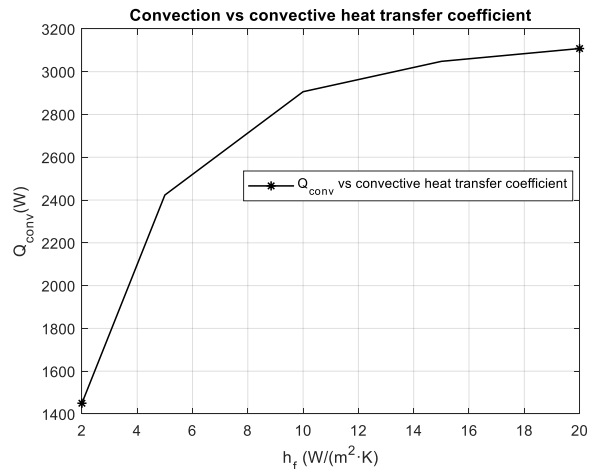
Figure 4.20: Convection versus convective heat transfer coefficient

Looking at different heat loss over the selected range of convective heat transfer coefficient, it is estimated that Q_{conv} was 1150 W, Q_{rad} was 2180 W and after that Q_{cond} was 114 W. These losses due to convective heat transfer coefficient are more significant when compared to losses due to solar radiation, and ambient temperature respectively in Section 4.3.1 and 4.3.2.

Figure 4.21 shows that there is an exponential decrease in the PV cell temperature from 134 to 44°C when h_f increases from 2 to 20 W/(m²·K). It can also be observed that an increase in h_f causes a decrease in PV cell temperature. When h_f is large, the PV cell temperature decreases because the heat is taken into the environment. Similarly, the higher h_f the lower the temperature of the photovoltaic cell for all applied voltages. A close examination of this figure shows that the wind speed is a critical factor in the prediction of PV module temperature as it influences the heat dissipation within the PV module. Relatively at 20 W/(m²·K), the PV cell temperature was 44°C, which is still almost twice as higher as than the optimum PV cell operating temperature of 25°C. The simulation result trend obtained in Figure 4.21 is similar to the findings published by Ali *et al.* (2017), Boudjelthia *et al.* (2016) and Schwingshackl *et al.* (2013).
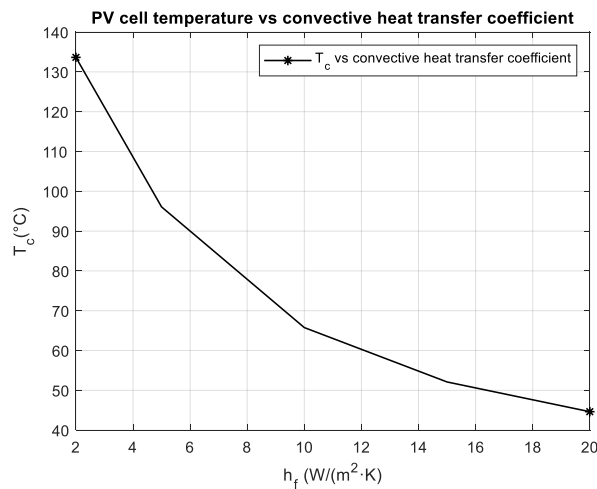
Figure 4.21: PV cell temperature versus convective heat transfer coefficient

Figure 4.22 demonstrates a consistent increase of the generated PV power from 1.4 to 2.8 kW when the convective coefficient is built from 2 to 20 W/(m²·K). When h_f is high the corresponding PV cell power (P_{PV}) is high as well; this because of the increase of convective heat loss at high h_f values, which in turn lowers the PV cell temperature. Inversely, when h_f is low, P_{PV} is low, because the convective heat is low, causing a build-up of heat in the PV cell, hence, increasing its temperature. This result trend is comparable to that found in the report of Du *et al.* (2013).
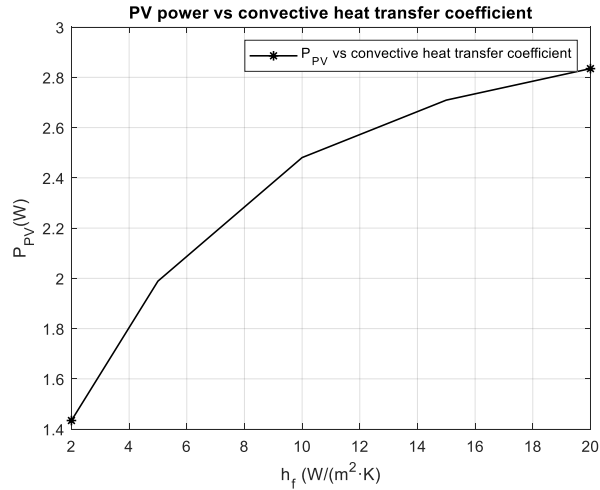
**Figure 4.22: PV power versus convective
heat transfer coefficient**

The electrical power delivered by the photovoltaic cell is maximised at h_f = 20 W/(m²·K) when the thermal power causes the PV cell temperature to be minimised. Figure 4.23 shows the variation of PV cell power as a function of T_c. It should also be noted that when the maximum PV power of 2.85 kW was reached, the PV cell temperature was at 45°C; when the PV cell temperature was at 135°C the corresponding PV cell temperature was 1.43 kW.
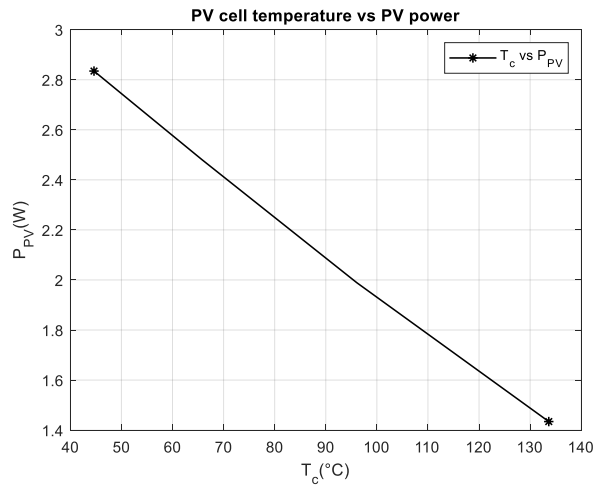
**Figure 4.23: PV power versus PV cell temperature
influenced by h_f**

Figure 4.24 represents an important point of the analysis: the efficiency of PV cell increases to a value of 14.2%, with an increase in convective heat transfer coefficient to 20 W/(m²·K). A high convective heat transfer between the PV cell to the surrounding area occurs, resulting in a

144

decrease in PV cell temperature and then the efficiency was increased. There was a considerable advantage to be gained in the output and lifespan of the PV cell if it is operated in an environment where h_f is in the region of 20 W/(m²·K). A similar result trend is found in the literature; see Ali *et al.* (2017).
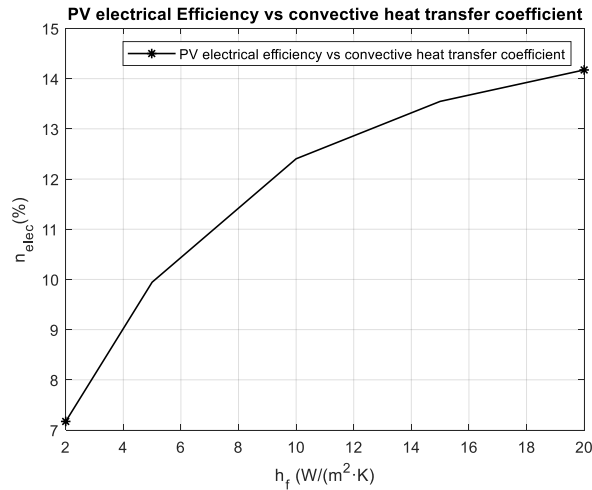
Figure 4.24: PV electrical efficiency versus convective heat transfer coefficient

Summary of convective heat exchange coefficient influence

Studies have shown that heat transfer by conduction and radiation increase as the wind speed increases; also, it depends on the nature of the material encapsulating the photovoltaic cell. The wind speed controls the useful energy generated by the PV cell. The PV cell operating temperature tends to close to the ambient temperature, due to the higher convective heat loss, and therefore increased heat transfer to the surroundings.

A significant amount of heat transfer by convection from the surface of the PV cell to the environment is observed as a result of a decrease in power dissipation in the PV cell. At higher convective heat coefficients, the heat transfer (convection and radiation) from the PV cell to the environment, decreases the thermal efficiency, and additionally, diminishes the PV cell temperatures while increasing its electrical efficiency. As a result, the system has a higher efficiency factor. It was noted that the PV cell is particularly sensitive to convective conditions. The impact of wind cooling plays a principal role and must be considered for a more accurate estimation. The natural convection for the duration of the PV cell also plays a substantial role in

the reduction of PV cell power loss. This is because of the higher heat transfer rate from the panel to the environment is considerable.

In Section 4.3.4, the influence of the external series resistance of a PV cell will be examined by keeping the other parameters constant.

4.3.4 Influence of external series resistance on PV performance

This section explores the impact of external series resistance on PV cell performance. The internal series resistance of the PV cells is an important parameter influencing the maximum power and the FF. Also, it is a parameter demonstrating the quality of the device.
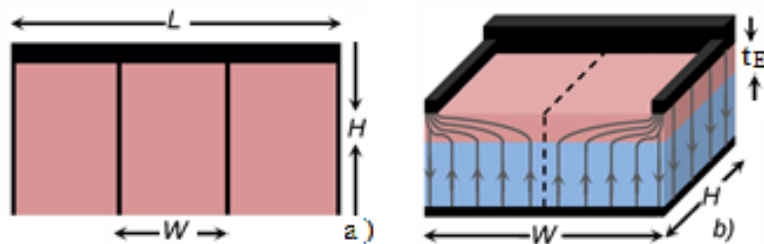
Figure 4.25: Resistive losses in solar cells
(**Wilcox & Gray, 2012**)

There are several resistivity losses in a PV cell (Figure 4.25). The thick black line in Figure 4.25 represents the bus bar electrode, and the thin black lines represent the grid electrodes. The pink colour represents the PV cell emitter, and the base is light blue. The symbols L, H, W and t_E respectively denote the length, the height, the distance between grid electrodes and the emitter thickness. Figure 4.25(*a*) presents the top view of the solar cell, while Figure 4.25(*b*) presents the current flow. The grey lines show the net current flow throughout, while the arrows indicate the direction of the current flow. The dashed line splits a single tile into two half tiles. Current generated in the left half of the PV cell tile flows to the left grid electrode, and similarly, current generated in the right half flows to the right grid electrode.

There are several ways to evaluate the internal series resistance of a PV cell from the I-V characteristic curve. As the temperature of the PV cell increases, the resistance of most materials also increases. Therefore, when optimising the design of a PV cell, it is essential to take into account the loss due to the resistance at the expected operating temperature.

The R_{si} of a PV cell is composed of a variety of internal resistances such as contact resistance (R_c), the resistance of the bus bars (R_b), grid resistance (R_g), and (R_e) lateral conduction in the emitter, (Remitter). This includes back conductor joule loss, the back contact joule loss, the internal joule loss, the bias point loss, the emitter joule loss, the front contact joule loss, the front grid electrode loss and the front busbar joule loss. The total extrinsic series resistance, R_t of the PV cell (Wilcox & Gray, 2012) is as follows:

(4.23)

$$R_{si} = R_e + R_b + R_g + R_c + R_a$$

where:

R_e represents the sum of the emitter series resistance, including accounts for the resistive losses inside of the transparent conducting layers (TCL) and emitter layers;

R_b presents the bus bar resistance, including any resistive loss from the terminal contact pad to the grid electrodes;

R_g presents grid electrode resistance, including the resistive losses caused by the grid electrodes;

R_c represents a contact resistance, including the resistive losses between the grid electrodes and the front lateral conducting layers (LCL); and

R_a is semiconductor resistance, including any resistive losses between the emitter and the back contact.

In this section, a set of values defining external series resistance (R_{se}) values is added to the existed internal series resistance of the PV cell, as shown in Figure 4.26. The performance of the PV cell was evaluated through calibration of the R_{se} value; this, however, dissipates power that is in the form of heat, thus creating useful heat energy.
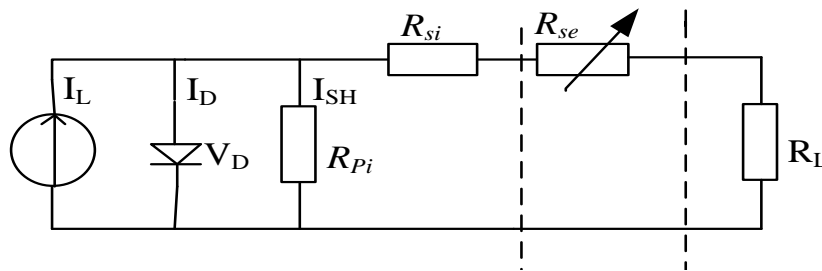
**Figure 4.26: Evaluation of PV performance
under external series resistance**

The primary objective of this section is to assess the distribution of power dissipation caused by R_{se}. The second objective is to highlight the thermal behaviour of photovoltaic cells. For this, the electro-thermo-radiative behaviour of PV for different values of R_{se} has been modelled, keeping the rest of the parameters fixed (For example, solar radiation at 1000 W/m^2, ambient temperature at 20°C and convective heat transfer of 20 W/(m²·K)). Electrical power, heat loss and efficiency and thermal were measured for different external series resistance values from 0 to 100 Ω.

PV cell power dissipation as a function of R_{se}

The performance evaluation of the PV cell composed of the diode, R_{si} and R_{pi} based on the influence of varying R_{se} has been conducted. Figure 4.27 shows a logarithmic growth curve of the total power dissipated (P_d) of the PV cell, which increases from 990 to 3490 W, as R_{se} increases. R_{si} marginally increases, while R_{pi} remains almost the same. Much of the total power dissipated is attributed to the diode (due to recombination current of the semiconductor material property used to make the PV cell) of the model in the PV cell ranges from 750 to 3480 W, R_{pi} and R_{si} resistivity losses reduce as less current flow through them. This power dissipated in the PV cells is due to a large reverse current across the PV cell, there is low current flow in the cell, the overall current becomes limited due to the power dissipated in the PV cell in the form of heat. The power dissipation occurring in a PV cell leads to a local overheating, which in turn results in heat conduction. The thermal resistance of the PV cell depends on the thickness of the material and its thermal resistivity.
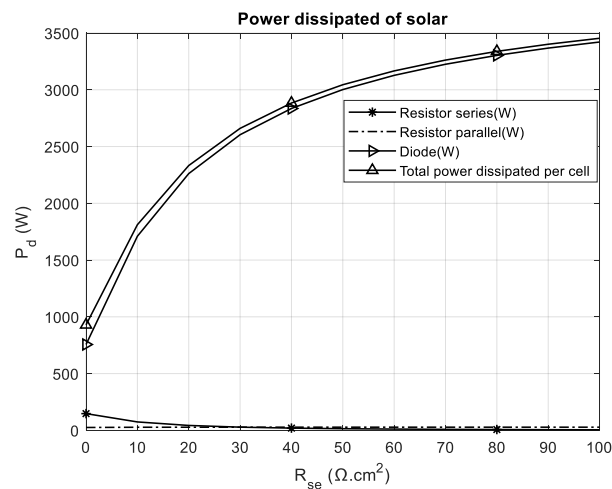
Figure 4.27: Dissipated power by PV cell versus R_{se}

At the point when a photon is absorbed by a PV cell, it produces an electron and a hole pair, with an energy below the band gap and which hypothetically contribute to the current. However, the reverse process occurs when the carriers recombine with no net contribution to cell current and emitting the energy as heat or as a photon. Any energy lost in a PV cell is turned into heat, so any inefficiency in the cell increases the PV cell temperature when it is placed in solar radiation. Relatively a photon contribution to several of the mechanisms that contribute to the total heat dissipation in a solar cell. The rate of recombination loss changes with the variation of R_{se}.

The following phenomenon can be explained: a R_{se} assistant controls the PV self-generated useful heat by partially converting the output of the PV cell into useful thermal energy (dissipating power in the form of useful heat), thereby reducing the output power generated.

This study will focus on the internal heat generation and electrical power generation of the PV cell based on the R_{se} as shown in Table B-4. The method relies on the linear regression equation curve to model the behaviour of different types of power as a function of R_{se} in the PV cell being studied. The subsection below will be presenting the linear regression equation calculation of figures as a function of external series resistance. By means of the linear regression equation, a graphical model can be derived; including the goodness of the fit and the confidence interval of the coefficients for the derived equation.

4.3.4.1 Prediction of heat loss by the PV cell

Figure 4.28 presents the heat loss by Q_{cond} within the PV cell. Q_{cond} increases from 425 to 1715 W (in magnitude) as R_{se} moves from 0 to 100 Ω. This loss was attributed to the electrical power dissipated in the PV cell in Figure 4.27 and part of the power dissipated turns to useful energy within the PV cell. However, the temperature differential is the main impetus behind the conductive flow of heat in a material with a given thermal resistance, and the transfer is governed by the Fourier law. The estimation graph related to useful heat by conduction is described in the following equation:

$$Q_{cond}(R_{se}) = p1 \cdot R_{se}^4 + p2 \cdot R_{se}^3 + p3 \cdot R_{se}^2 + p4 \cdot R_{se} + p5 \qquad \textbf{(4.24)}$$

where:

p1, p2, p3, p4 and p5 are coefficients

Q_{cond} is thermal transfer coefficient by conduction (W)

R_{se} is the external series resistance (Ω)
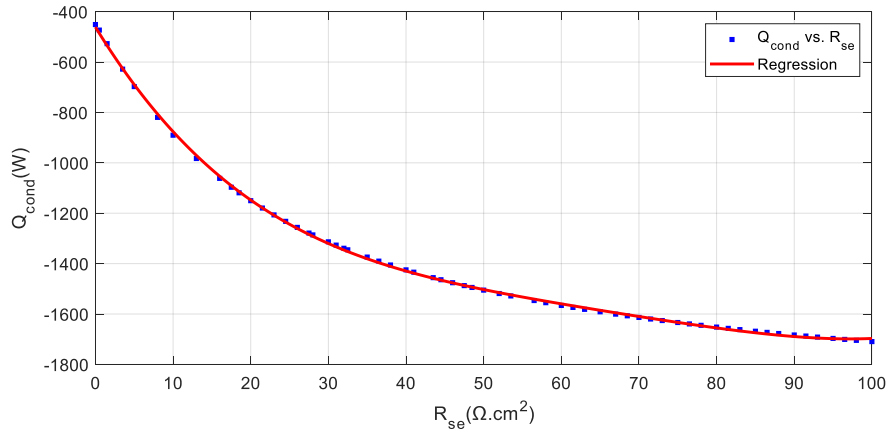
Figure 4.28: Conduction heat transfer versus R_{se}

Table 4.3 introduces a polynomial interpretation of heat loss by conduction simulation results in Figure 4.28; the coefficient of determination (R^2) is 0.9996. R^2 is a marker to pass judgment on the nature of linear regression. Sum of squared errors (SSE) is 2313 and presents the deviations predicted from the actual simulation data. Root Mean Square Error (RMSE) is a good indicator of how accurately the model predicts the response, and it is determined to be 6.37.

Table 4.3: Linear model Poly4 of Figure 4.28

Description of Equation 4.24	Goodness of fit
$Q_{cond}(R_{se}) = p1 \cdot R_{se}^4 + p2 \cdot R_{se}^3 + p3 \cdot R_{se}^2 + p4 \cdot R_{se} + p5$ Coefficients (with 95% confidence bounds): $p1 = 3.547e\text{-}05\,(3.232e\text{-}05, 3.863e\text{-}05)$ $p2 = -0.009531\,(-0.01016, -0.008902)$ $p3 = 0.9784\,(0.9375, 1.019)$ $p4 = -50.36\,(-51.32, -49.41)$ $p5 = -461.2\,(-467.8, -454.6)$	$\text{SSE}: 2313$ $\text{R-square}: 0.9996$ $\text{Adjusted R-square}: 0.9996$ $\text{RMSE}: 6.37$

Figure 4.29 presents a continuous increase of Q_{conv} from 3100 W to 5300 W when the R_{se} goes from 0 to 100 Ω, as the heat is taken away to the environment. The thermal effect on the photovoltaic cell is due to the high generated electrical power dissipation of R_{se}, and also by the heat lost by conduction occurring in the PV cell. The thermal loss by Q_{conv} increases faster when R_{se} varies between 0 and 50 Ω; however, slows down and closes to saturation when R_{se} was above 50 Ω. The approximation curve of the heat loss by convection is expressed in the following equation:

$$Q_{conv}(R_{se}) = p6 \cdot R_{se}^4 + p7 \cdot R_{se}^3 + p8 \cdot R_{se}^2 + p9 \cdot R_{se} + p10 \tag{4.25}$$

where:

p6, p7, p8, p9 and p10 are coefficients

Q_{conv} is thermal transfer coefficient by convection (W)

R_{se} is the external series resistance (Ω)
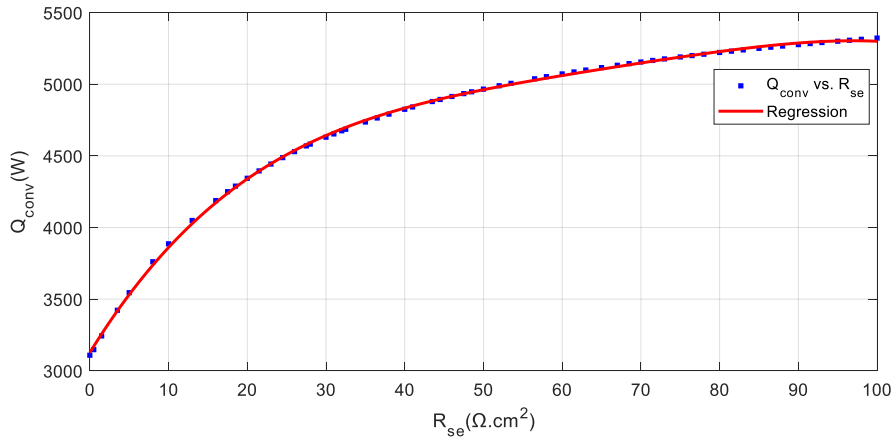
Figure 4.29: Convection heat transfer versus R_{se}

Table 4.4 presents a polynomial interpretation of heat loss by convection in Figure 4.29; the coefficient of determination (R^2) is 0.9996, and it is an indicator of the goodness of the fit. SSE presents deviations predicted from actual simulation data, and it is determined to be 7510. RMSE is 11.48, which is a decent proportion of how precisely the model predicts the response.

Table 4.4: Linear model Poly4 of Figure 4.29

Description of Equation 4.25	Goodness of fit
$Q_{conv}(R_{se}) = p6 \cdot R_{se}^4 + p7 \cdot R_{se}^3 + p8 \cdot R_{se}^2 + p9 \cdot R_{se} + p10$ Coefficients (with 95% confidence bounds): $p1 = -6.334e-05 \ (-6.903e-05, -5.765e-05)$ $p2 = 0.01699 \ (0.01586, 0.01812)$ $p3 = -1.74 \ (-1.813, -1.666)$ $p4 = 89.11 \ (87.39, 90.83)$ $p5 = 3127 \ (3115, 3139)$	SSE : 7510 R - square : 0.9996 Adjusted R - square : 0.9996 RMSE : 11.48

Figure 4.30 presents the incremental change of Q_{rad} from 350 W to 660 W when R_{se} goes from 0 to 100 Ω. This shows a radiative thermal transfer to the high emissivity of the PV cell and the free carriers increase with the R_{se}. The PV cell emits radiation based on its temperature. Also, the losses depend on the absorptivity of the covering glass. The estimation of the curve is stated by the following equation:

$$Q_{rad}(R_{se}) = p11 \cdot R_{se}^4 + p12 \cdot R_{se}^3 + p13 \cdot R_{se}^2 + p14 \cdot R_{se} + p15 \qquad \textbf{(4.26)}$$

where:

p11, p12, p13, p14 and p15 are coefficients

Q_{rad} is the thermal transfer coefficient by radiation (W)

R_{se} is the external series resistance (Ω)
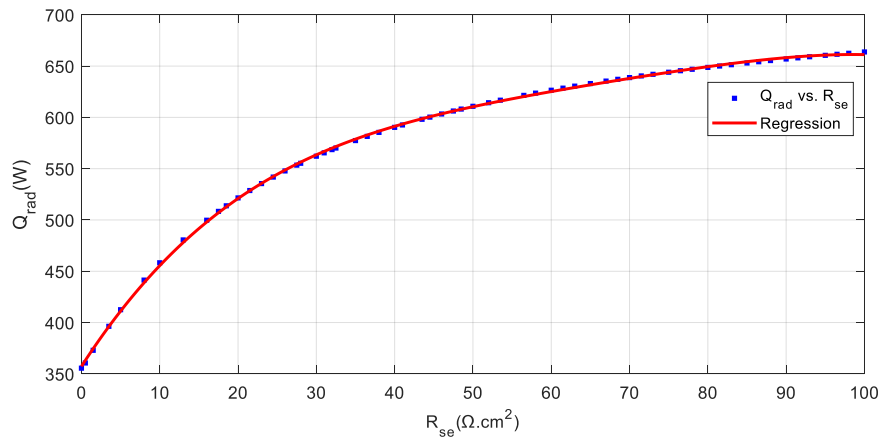
Figure 4.30: Radiation heat transfer versus R_{se}

152

Table 4.5 shows a polynomial interpretation of the simulated heat loss by radiation in Figure 4.30; the coefficient of determination (R^2) is a pointer to pass judgment on the nature of linear regression, and it is 0.9998. SSE is resolved to be 95.27 and represents deviations anticipated from the simulation investigation data. RMSE is a good measure of how conclusively the model predicts the response and defined as 1.293.

Table 4.5: Linear model Poly4 of Figure 4.30

Description of Equation 4.26	Goodness of fit
$Q_{rad}(R_{se}) = p11 \cdot R_{se}^4 + p12 \cdot R_{se}^3 + p13 \cdot R_{se}^2 + p14 \cdot R_{se} + p15$ Coefficients (with 95% confidence bounds): $p1 = -7.765e\text{-}06 \ (-8.406e\text{-}06, -7.125e\text{-}06)$ $p2 = 0.002113 \ (0.001986, 0.002241)$ $p3 = -0.2216 \ (-0.2299, -0.2133)$ $p4 = 11.83 \ (11.63, 12.02)$ $p5 = 357.3 \ (356, 358.6)$	$SSE : 95.27$ $R\text{-}square : 0.9998$ $Adjusted\ R\text{-}square : 0.9997$ $RMSE : 1.293$

Regardless, the outline of these results is presented in Figure 4.28, Figure 4.29 and Figure 4.30 exhibiting that the development of heat loss by Q_{conv} is more noticeable than that in Q_{rad}. Both were measured as a positive value indicating that they are taken away into the surrounding environment, while the Q_{cond} is transferred to the back of the PV cell. Comparing the heat transfer occurring at the PV cell, Q_{conv}, Q_{cond} and Q_{rad}, were respectively 2200 W, 1290 W and 310 W, as a function of R_{se}. The loss attributed to heat conduction due to R_{se}, are more significant when compared to losses due to solar radiation, ambient temperature and convective heat coefficient respectively in Section 4.3.1, 4.3.2 and 4.3.3.

4.3.4.2 Prediction of PV cell temperature as a function of R_{se}

Figure 4.31 shows a logarithmic growth of cell temperature as a function of R_{se}. An increase in the R_{se} from 0 to 50 Ω, Brings about an increase in T_c for temperature from 45 to 59°C. While increasing the R_{se} value from 50 to 100 Ω, Bring about an increase in T_c for temperature from 59 to 62°C. The increase in the temperature is a result of a built-up of electrical power dissipated in the form of heat in Figure 4.27.

To analyse and predict the PV cell temperature as a function of R_{se}, from the graph in Figure 4.31, an equation was derived, relating T_c to R_{se}; Equation 4.27 is approximatively extracted from Figure 4.31.

$$T_c(R_{se}) = p16 \cdot R_{se}^4 + p17 \cdot R_{se}^3 + p18 \cdot R_{se}^2 + p19 \cdot R_{se} + p20 \qquad \textbf{(4.27)}$$

where:

p16, p17, p18, p19 and p20 are coefficients

T_c is the cell temperature

R_{se} is the external series resistance (Ω)
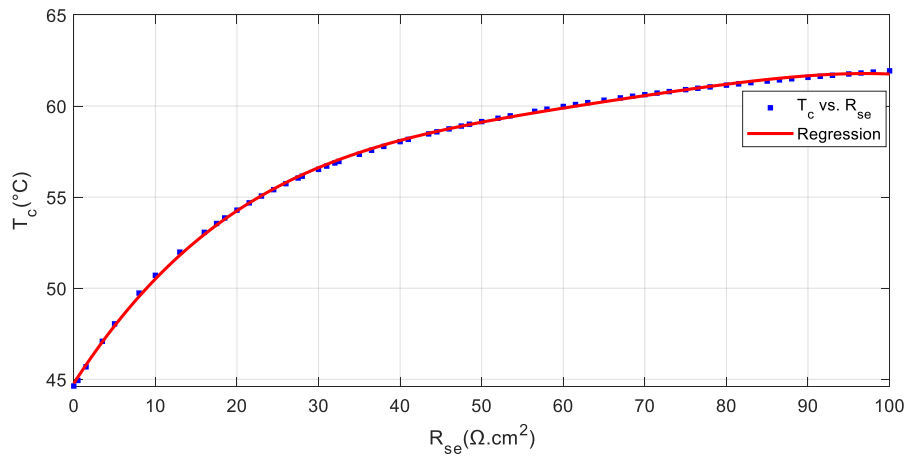
Figure 4.31: PV cell temperature versus R_{se}

Table 4.6: Linear model Poly4 of Figure 4.31

Description Equation 4.27	Goodness of fit
$T_c(R_{se}) = p16 \cdot R_{se}^4 + p17 \cdot R_{se}^3 + p18 \cdot R_{se}^2 + p19 \cdot R_{se} + p20$ Coefficients (with 95% confidence bounds): $p1 = -4.948e\text{-}07$ (-5.393e-07, -4.504e-07) $p2 = 0.0001327$ (0.0001239, 0.0001416) $p3 = -0.01359$ (-0.01417, -0.01301) $p4 = 0.6962$ (0.6828, 0.7096) $p5 = 44.78$ (44.68, 44.87)	SSE : 0.4584 R - square : 0.9996 Adjusted R - square : 0.9996 RMSE : 0.08968

Table 4.6 displays a polynomial interpretation of the PV cell temperature as a function of R_{se}, from the graph in Figure 4.31; the coefficient of determination (R^2) is an indicator of the goodness of linear regression, and it is determined to be 0.9996. SSE is found to be 0.4584 and, it represents the deviations predicted from the simulation of data. RMSE presents a decent proportion of how precisely the model predicts the response and RMSE is found to be 0.08968.

4.3.4.3 Prediction of generated power as a function of R_{se}

It can be seen in Figure 4.32 that the generated PV power decreases as R_{se} increases. The power rapidly falls exponentially from 2800 W to 260 W when R_{se} increases from 0 to 50 Ω, and beyond 50 Ω, the power decreases more slowly from 255 W to 110 W. The power degradation of PV cell is due to recombination accordingly to R_{se} variation, leading to electrical power dissipation in the form of heat by conduction. Thus, the generated electrical power decreasing proportionally to the increase in power dissipated in the PV cell as R_{se} varies in Figure 4.27. The estimation graph is expressed by Equation 4.28

$$P_{PV}(R_{se}) = p21 \cdot R_{se}^4 + p22 \cdot R_{se}^3 + p23 \cdot R_{se}^2 + p24 \cdot R_{se} + p25 \tag{4.28}$$

where:

p21, p22, p23, p24 and p25 are coefficients

P_{PV} is the generated PV power

R_{se} is the external series resistance (Ω)
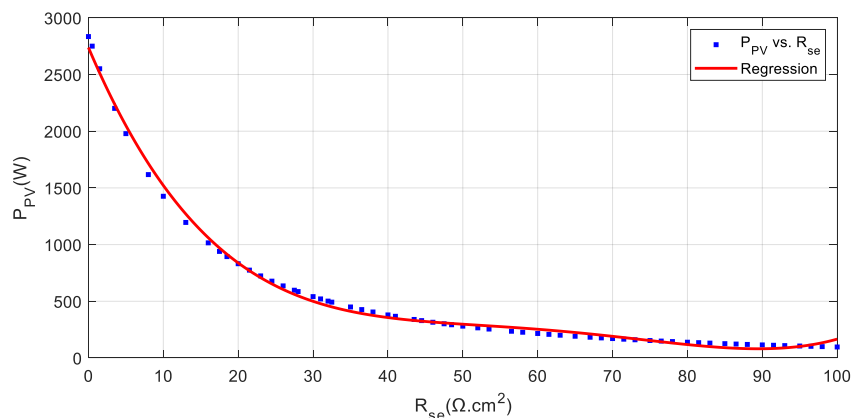
Figure 4.32: PV power versus R_{se}

Table 4.7 presents a polynomial interpretation of generated electrical power as varying R_{se} in Figure 4.32, the computation of the coefficient of determination (R^2) is determined to be 9564; it was a marker to assess the accuracy of the linear regression. SSE is 7510 and represents the deviations anticipated from the simulation exploratory data. RMSE is described as 40.96, and it is a good measure of how correctly the model predicts the response.

Table 4.7: Linear model Poly4 of Figure 4.32

Description of Equation 4.28	Goodness of fit
$P_{PV}(R_{se}) = p21 \cdot R_{se}^4 + p22 \cdot R_{se}^3 + p23 \cdot R_{se}^2 + p24 \cdot R_{se} + p25$ Coefficients (with 95% confidence bounds): $p1 = 0.0001633 \ (0.000143, 0.0001835)$ $p2 = -0.04122 \ (-0.04527, -0.03718)$ $p3 = 3.788 \ (3.525, 4.05)$ $p4 = -155.5 \ (-161.7, -149.4)$ $p5 = 2738 \ (2695, 2780)$	$SSE: 9.564e + 04$ $R\text{-square}: 0.9964$ $Adjusted \ R\text{-square}: 0.9962$ $RMSE: 40.96$

4.3.4.4 Prediction of PV cell electrical efficiency as a function of R_{se}

Figure 4.33 presents the PV cell electrical efficiency dependence on R_{se}. The PV cell electrical efficiency quickly falls exponentially from 14.2% to 2.5% when R_s increases from 0 to 50 Ω, and after 50 Ω the efficiency slowly decreases from 2.5% to 1.5%. This degradation of the electrical efficiency of the PV cell was due to the power dissipation in the form of heat in Figure 4.27. The estimation of the PV cell electrical efficiency graph is expressed by the following equation:

$$\eta_{el}(R_{se}) = p26 \cdot R_{se}^4 + p27 \cdot R_{se}^3 + p28 \cdot R_{se}^2 + p29 \cdot R_{se} + p30 \tag{4.29}$$

where:

p26, p27, p28, p29 and p30 are coefficients

η_{el} is the PV cell electrical efficiency

R_{se} is the external series resistance (Ω)

Table 4.8 shows a polynomial interpretation of electrical efficiency as R_{se} varies from 0 to 100 in Figure 4.33; the computation of the coefficient of determination (R^2) is 0.9996 and R^2 represents

a marker to assess the accuracy of the linear regression. SSE equals to 0.4584 and represents the predicted deviation from the simulation data. RMSE is 0.08968, and it is a good measure of how decisively the model predicts the response.
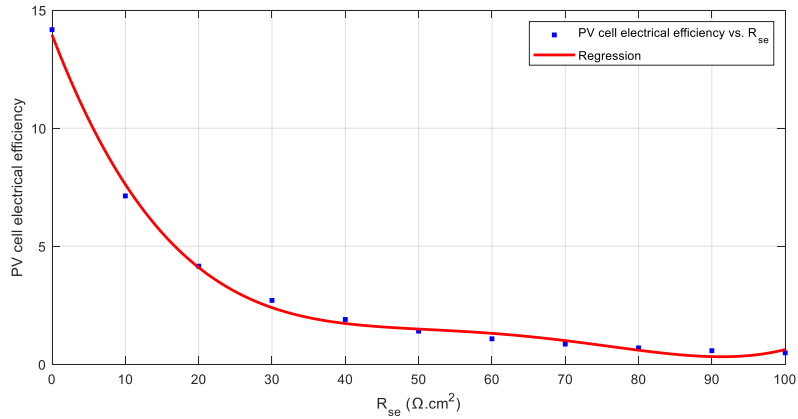
Figure 4.33: PV cell electrical efficiency dependence on *R~se~*

Table 4.8: Linear model Poly4 of Figure 4.33

Description Equation 4.29	Goodness of fit
$\eta_{el}(R_{se}) = p26 \cdot R_{se}^4 + p27 \cdot R_{se}^3 + p28 \cdot R_{se}^2 + p29 \cdot R_{se} + p30$ Coefficients (with 95% confidence bounds): $p1 = \ 8.557e\text{-}07 \ \ (4.796e\text{-}07, 1.232e\text{-}06)$ $p2 = \ \text{-}0.000218 \ (\text{-}0.0002938, \text{-}0.0001421)$ $p3 = \ \ \ 0.02004 \ \ (0.01511, 0.02497)$ $p4 = \ \ \text{-}0.8135 \ \ (\text{-}0.926, \text{-}0.701)$ $p5 = \ \ \ \ 13.96 \ \ (13.23, 14.69)$	$SSE : 0.4584$ $R\text{-}square : 0.9996$ $Adjusted \ R\text{-}square : 0.9996$ $RMSE : 0.08968$

4.3.4.5 Prediction of heat transfer by conduction and generated PV power as a function of *R~se~*

The synthesis of the result is presented in Figure 4.34, by mapping the standardised of the external *R~se~* as a function of the heat transfer by conduction, and the generated PV power. The normalised yields are plotted from simulation results on this map, which incorporates the

polynomial surface of the model. By varying R_{se}, the corresponding values of the electrical power generated and, electrical power dissipated and heat conduction can be determined and as well as the optimal power (electrical or thermal). A suitable fitting polynomial can represent this graphical model to the test results. It can be used to predict the performance result of the PV cell with confidence intervals, by employing the linear regression equation for the graphical model. Figure 4.34 shows the performance and the prediction behaviour of heat conduction and the generated PV power as a function of R_{se}. During the simulation, when R_{se} was set at 100 Ω, it observed that the power reading was 96.97, and the heat conduction was -1709 W.
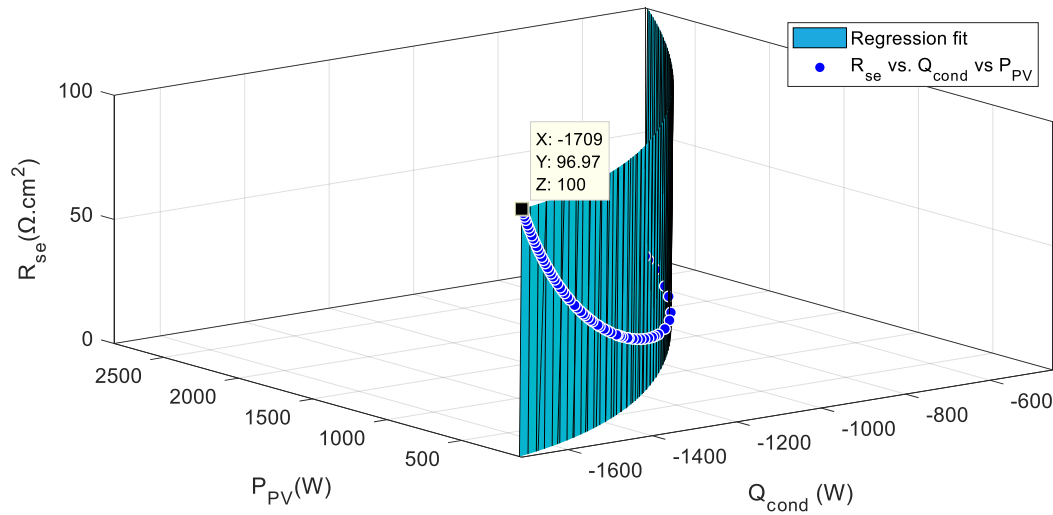
Figure 4.34: *R_{se}* according to the power generated and heat by conduction of the PV module

The estimation graph in Figure 4.34 is expressed by Equation 4.30

$$R_{se}(Q_{cond}, P_{PV}) = p00 + p10 \cdot Q_{cond} + p01 \cdot P_{PV} + p20 \cdot Q_{cond}^2 + p11 \cdot Q_{cond} \cdot P_{PV} + p02 \cdot P_{PV}^2 \qquad \textbf{(4.30)}$$

where:

p00, p10, p01, p20, p11 and p02 are coefficients

Q_{con} is the PV cell electrical efficiency

R_{se} is the external series resistance (Ω)

Table 4.9 describes the polynomial interpretation of the surface plot simulation result of heat conduction and the generated PV power as a function of R_{se} in Figure 4.34; the computation of the coefficient of determination (R^2) is 0.9998, and it assesses the accuracy of the linear

regression. SSE is equivalent to 12.85 and represents the predicted deviation from the simulation data. RMSE is 0.4791, and it is a decent proportion of how conclusively the model predicts the reaction.

Table 4.9: Linear model Poly22 of Figure 4.34

Description of Equation 4.30	Goodness of fit
$$R_{se}(Q_{cond}, P_{PV}) = p00 + p10 \cdot Q_{cond} + p01 \cdot P_{PV} + p20 \cdot Q_{cond}^2$$ $$+ p11 \cdot Q_{cond} \cdot P_{PV} + p02 \cdot P_{PV}^2$$ where x is normalised by mean -1385 and std 328.5 and where y is normalised by mean 561.3 and std 662.5 Coefficients (with 95% confidence bounds): $p00 = -829 \ (-982.3, -675.8)$ $p10 = 3100 \ (2542, 3658)$ $p01 = -4467 \ (-5261, -3673)$ $p20 = 965.3 \ (808.8, 1122)$ $p11 = -223.2 \ (-242.9, -203.5)$ $p02 = 145.4 \ (127.7, 163.1)$	$SSE : 12.85$ $R\text{-}square : 0.9998$ $Adjusted\ R\text{-}square : 0.9997$ $RMSE : 0.4791$

4.4 Conclusion

This chapter studied a comprehensive analysis of the thermal behaviour of the PV cell model under weather conditions. It was observed that the effectiveness of PV array depends on several factors: location, weather conditions, design and the photovoltaic cell material. It was also indispensable to analyse the heat exchanges between the environments, photovoltaic array and losses during the system operation, and the influence of internal and external parameters. The main objective of this work was the development of multi-energy production by partially converting the output of the internal heat generation of the PV cell into useful thermal energy (for domestic hot water).

The mathematical model adapted for design, analysis and the optimisation of the PV cell, based on thermal balance equations, associated with the transmittance, absorptance and reflectance coefficients of the PV cell, as well as the equations for the heat loss by conduction, convection and radiation occurring in the PV cell boundary.

Design and modelling of a PV cell system were developed in MATLAB / Simulink to validate the heat transfer occurring in the PV cell model, which converts the radiation solar into electricity and

as well as, the heat transfer transmitted by the PV cell. A series of simulation has been conducted to quantify the impact of different parameters (solar radiation, ambient temperature and convective heat transfer coefficient, and the series resistance parameter) on the PV cell performance. The simulation results (the electrical power generated, the power dissipated, the heat loss by conduction inside the PV cell, convection, and radiation heat transfer of the PV cell front surfaces to ambient temperature) were compared and analysed to identify the most influential parameters.

The following was noted:

- It was found that the heat transfer by conduction increases exponentially as the solar intensity increases; this depends on the properties of the surface material of the PV cell. The useful energy generated depends on the levels of solar radiation.

- It was observed that the different types of heat transfer are smaller due to T_a, as compared to the impact of solar radiation. T_c and the useful energy were linearly proportional and had little dependency on T_a. PV cell performance is enhanced at lower ambient temperatures.

- It was noted that the PV cell is particularly sensitive to convective conditions. The impact of wind speed (the natural convection) plays a substantial role and must be considered for a more accurate estimation of the design.

- The loss by heat conduction due to R_{se}, was more significant when compared to losses due to solar radiation, ambient temperature and convective heat coefficient respectively in Section 4.3.1, 4.3.2 and 4.3.3.

These results clearly indicate that R_{se} offers an effective way of controlling the increase in the heat of the panel. A variation of R_{se} could be a solution to manage the balance between the amount of thermal and electrical energy. A mathematical expression studying the thermal and electrical power of the PV cell based on the R_{se} was developed. The method depends on linear regression equation curve to model the behaviour of different types of power as a function of $R_{se,}$ including the goodness of the fit and the confidence interval of the coefficients for the derived equation. By varying $R_{se,}$ the corresponding values of the electrical power generated and, electrical power dissipated and heat conduction can be determined.

The optimal electrical and thermal power can be obtained from Equation 4.30, by selecting a value of R_{se} that partially converts the output of the PV cell into useful thermal energy. This method can

be used to optimise combined photovoltaic and thermal efficiency by controlling the heat flow through a working fluid. This method can be used as a balance between the thermal and electrical power, based on the demand and weather conditions, R_{se} can be adjusted to generate more heat while the working fluid transports the generated heat to the load.

These results obtained in this chapter are quite interesting for domestic water heating applications. The next chapter will develop a model that integrates the absorber pipe attached at the back of the PV cell together connected to a hydraulic pump and storage devices, from the PV cell modelled in Section 4.3.4. The validation of cooling the PV cell and heating the working will be conducted, followed by an optimisation study of the thermal and power energy performances using the energy management system.

Chapter 5

Performance evaluation and analysis of the proposed PV/T system

5.1 Introduction

The PV cell performance studied in section 4.3.4 from the previous chapter, characterised by the electrical power and thermal power behaviour under external series resistance variation, are carried over to this chapter. The PV cell is coupled with some components to form a PV/T system. This PV/T model was developed using MATLAB/Simulink to satisfy the transient simulations and boundary conditions. Finally, a series of simulations are carried out to study the impact of R_{se} in the proposed PV/T system. The system operation is divided into three main processes: reducing PV cell temperature, capturing the heat and storing the energy (thermal and electrical).

In the literature, numerous studies were conducted in favour of the development of water-based PV/T system. For such a PV/T system, water flows under the PV cell through a pipe; this could improve the PV cell electrical efficiency through cooling. Likewise, the water temperature would rise as it carries away and the generated heat from the PV cell. The heated water can be used for household applications and solar-assisted heating and cooling technologies.

In this chapter, the self-heating of the PV cells is used to increase the water temperature in the PV/T system for domestic water use. The proposed method includes an absorber pipe attached to the PV cell, forming the PV/T cell. The parameters of the design and system components are simulated and interpreted. This chapter also introduces the energy management of the proposed PV/T system. In this regard, the study is aimed at presenting automated intelligent solutions for energy management using Stateflow.

5.2   Integration absorber pipe loop underneath PV modules

The development of multi-energy production by partially converting the output of the PV cell into useful thermal energy (to increase water temperature for domestic use) is implemented. The energy conversion and heat transfer mechanisms occurring throughout the different processes in a PV/T model were described below:

- Combine a PV cell with an absorber pipe to form the proposed PV/T system to evaluate the influence the PV cell performance and to partially convert the internal heat generation of the PV cell into useful thermal energy for domestic hot water. This assesses the performance of the integrated water-based PV/T system.

- Analyse the heat transfer by conduction capacity from the PV cell, before integrating the absorber pipe into the entire system.

- Address the passive cooling of photovoltaic modules via heat extraction by controlling the working fluid within the absorber pipe to reduce the PV cell temperature and improve PV electrical efficiency.

- The heat energy (useful heat) was carried away by the flowing water in the absorber pipe (useful heat is transferred to increase water temperature by a conductor-convective exchange).

- Develop a control strategy to balance power (thermal and electrical). These tasks are aimed at developing a new PV/T technology system to address gaps in previous studies. The results will add value to the advancement of PV/T technology.

Different formulas are used to calculate the PV/T system operation, such as solar radiation, the environmental temperature, and the flow characteristics of the heat transfer fluid flowing in a closed loop. The thermodynamic properties of the water are used to calculate the water flow, as well as the heat transfer between water and the heat exchanger. The useful heat is considered to be the thermal energy transferred by conduction.

5.2.1 Operating principle and PV/T system component

The proposed PV/T model comprised of an absorber pipe loop at the back of the PV module, a hydraulic pump, a battery to store the energy produced and a water storage system. The absorber pipe is secured beneath the PV cell and joined utilising adaptable coupled connectors. Initially, cold water flows from the storage tank to the absorber pipe and flows back to the storage tank as hot water. Figure 5.1 illustrates the PV/T system.

The system parameters are the total incident solar radiation, ambient temperature and PV/T system output corresponding to the electrical power, and the generated heat. All the parameters are based on the hourly calculation as a function of the area, transmissivity, emissivity and orientation of the PV/T system. These parameters determine the energy efficiency conversion and the loss factor.
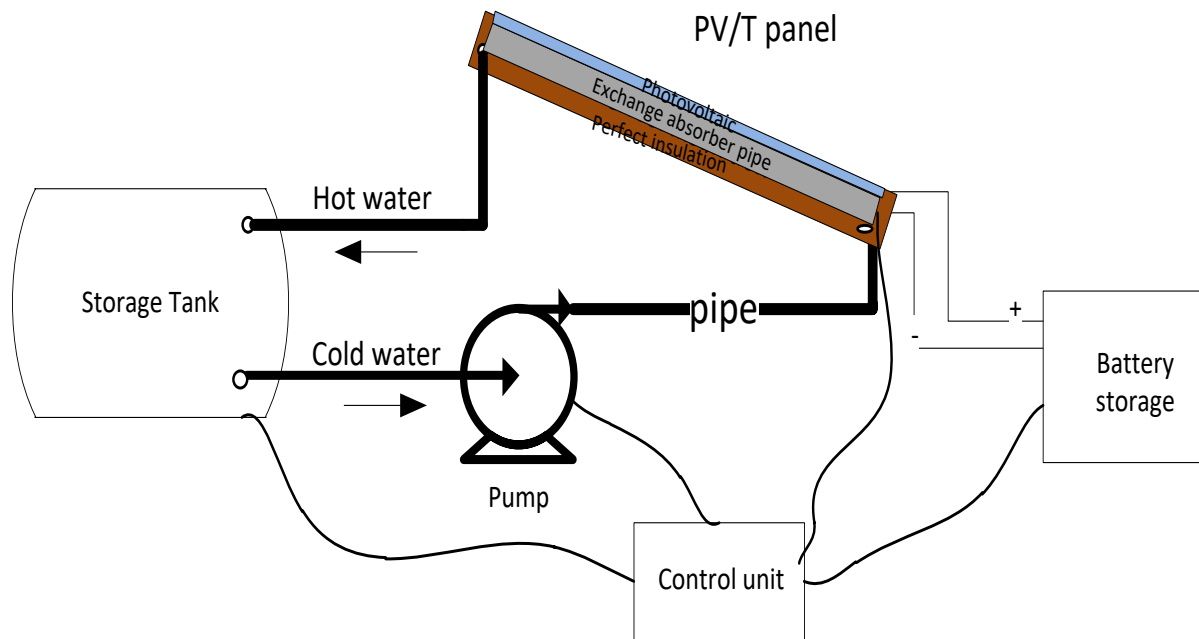
Figure 5.1: Proposed PV/T system model

The PV/T system reduces the heat dissipated in the PV cell while maximising solar radiation absorption. Simultaneously, the PV cell operating temperature reduces and the efficiency conversion increase since the heat flow was transferred from the PV cell to the working fluid.

The pump unit output was governed by the fluid viscosity, the fluid thermal conductivity, the fluid temperature, as well as the energy consumption by the pump. A controller block is associated with the system to control the pump when the water temperature exceeds the safety limit.

A complete mixed storage tank model with uniform water temperature was considered. The solar energy systems require an efficient means to store heat. The temperature of the hot water produced was calculated according to the heat generated, and transferred from the PV/T system and determined by the value selected for R_{se}.

The battery storage unit was used in the PV/T system, associated with a control unit to monitor the state of the charge. The battery storage covers daily demands and typically has enough energy reserve to ensure there is no discontinuous supply in the absence of solar radiation. The estimated state-of-charge (*SOC*) of the battery storage is vital for the performance and safety operation of any battery storage.

5.2.2 Design of PV/T system

The technical parameters of the PV/T system and heat exchangers are shown in Table 5.1 and Table 5.2 below. The pump is compatible with the hydraulic characteristics of the PV/T system and must overcome the head pressure each time the machine is turned on.

Table 5.1: PV/T system parameters detail

Component	Parameter	Value
PV modules	Cell type	mono-crystalline
	Packing factor	0.91
	Conversion efficiency	16%
	Module peak power	3.25 kW
	Maximum voltage, Vm	255 V
	Maximum current, Im	12.4 A
	Open circuit voltage, Voc	310 V
	Short circuit current, Isc	14.64 A
	Internal Series resistance Rsi / cell	0.0042 Ω
	Parallel resistance Rpi /cell	10.1 Ω
	Active total area	12 m²
Absorber pipe	The internal diameters of tubes The external diameters of tubes	Di = 0.0027 m Do = 0.0043 m
	Pipe total length	L = 5 m
	Height	L = 10 m

	Nusselt number for laminar flow heat transfer:	3.66
	Initial liquid temperature:	20 °C
	Heat transfer parameterisation:	Gnielinski correlation
Circulating Pump	Types:	Fixed-discretisation pump
Hot water storage tank	Capacity	200 L
	Initial water temperature	20°C
	Pressurisation specification:	Atmospheric pressure
Li-ion batteries	Nominal voltage	200V
	Battery capacity	42000W*hr
	Initial state-of-charge (*SOC*)	70%

Table 5.2: Initial design parameters

Parameters	Values
Average mass flow rate	0.5 kg/s
C_W	4190 J/kgK
K_c	1.0 W/(mK)
Ambient temperature	20 ºC
Time of simulation	3 hours

5.2.3 A mathematical model of the thermal performance of the PV/T system

The mathematical modelling of the proposed PV/T system is presented in this section. The solar radiation is assumed to be perpendicular to the surface of the PV/T module. The transfer of the generated thermal energy in the system has the following processes: the solar radiation is converted into electrical energy, some of the thermal energy was absorbed and transferred to the absorber pipe, while the rest is released to the environment. The useful heat was removed by the flow of water inside the absorber pipe. Different equations regarding thermal, and electrical energy, the temperatures of the elements and the inlet and outlet fluid temperature as well as PV/T system yields are established.

It is necessary to specify the calculation hypotheses:

- One-dimensional heat transfer through the system layers;
- Uniform mass flow in the collector tubes;
- Heat transfer from the collector edges is negligible;
- No air layer between the PV cell and the heat exchanger;
- All surfaces of layers incorporate uniform temperature;
- Heat dissipation is one-dimensional;
- Forced flow through the heat exchanger tubes exist;
- Wind speed on the face of the collector is assumed to be constant;
- Heat flux received by the collector is a function of time;
- Physical properties of materials are not temperature-dependent;
- Physical properties of the fluid are a function of the temperature;
- Temperatures of the PV/T system components are a function of time; and
- Dust and dirt on the collector are negligible.
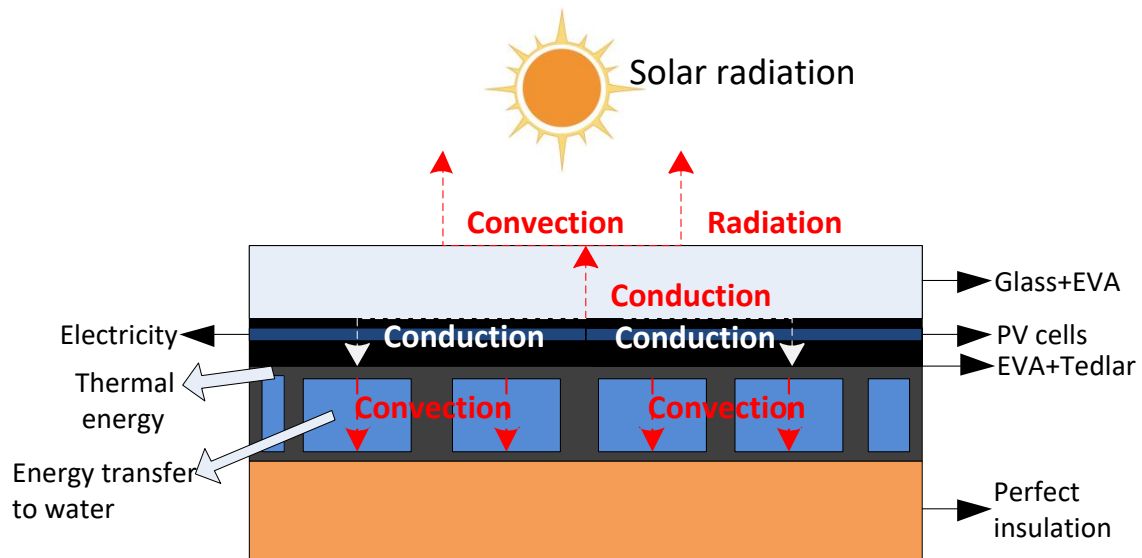
Figure 5.2: Heat transfer characteristics of the PV/T system

Due to the assumptions made in the previous chapter, the mathematical equations of the design, do not need to be optimally determined. Figure 5.2 and Figure 5.3 show the characteristics of heat transfer of the proposed PV/T system.
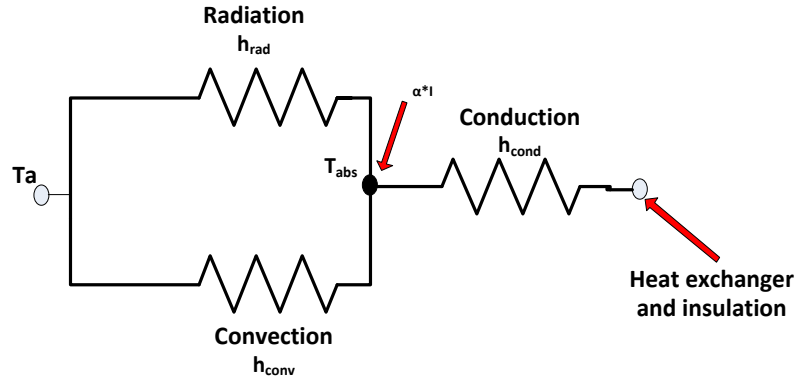
Figure 5.3: PV/T system modelling

5.2.3.1 Choice of simulation software for the proposed PV/T model

MATLAB/Simulink software program is chosen to develop and implement the simulation of the proposed PV/T model, based on simulation software features analysed in Table 3.4 and Table 3.5. MATLAB/Simulink can solve conduction-dominant heat transfer problems involving convection and radiation occurring at boundaries. Also, it can analyse the temperature distributions of components based on material properties, external heat sources, and internal heat generation for steady-state and transient problems which involve thermal management. By appropriately defining the initial and boundary conditions, it was conceivable to compute the temperature between layers and elements, with specific reference to the PV cell and the absorber pipe to form the proposed PV/T model (see Appendix A), hydraulic pump and the storage tank. Thermal fluxes through the distinctive layers were demonstrated. All the heat exchanges were displayed after setting the parameters. Temperatures of the various thermal elements are recognised and shown as perfect temperatures.

This heat transfer is considered transient; because the temperature in the medium and the surroundings vary. Thus, the heat flow will vary within the PV/T model. The outcome provides the thermal and electrical energy of the PV/T model, for both the physical features inside and outside the PV/T model.

This model has a control loop to maintain the temperature inside the PV/T system. The measures used are the ambient temperature, the internal temperature of the PV/T system and the water flow rate, and the fluid temperature in the pipe and the storage tank, as well as the generated and dissipated power.

5.2.3.2 Heat balance in the PV/T system

The PV/T mathematical model was divided into four parts (PV cell, absorber pipe, fluid and storages). The solar energy that is first absorbed by the PV cell can be expressed as:

$$Q_{abs} = A_c \cdot \tau_c \cdot \alpha \cdot G \tag{5.1}$$

A part of the solar radiation is converted into heat by the PV cell, partially via the heat exchanger and while the rest is distributed in the environment due to the temperature difference between the PV cell module and the atmosphere. The loss is defined in the following equation (Zhao et al., 2011).

$$Q_l = h_{cv} \cdot (T_c - T_a) + \varepsilon_c \cdot \sigma \cdot (T_c^4 - T_s^4) + h_{air} \cdot (T_p - T_{heo}) + \varepsilon_{pl} \cdot \sigma \cdot (T_p^4 - T_{heo}^4) \tag{5.2}$$

h_{rd1} is the heat transfer of the radiation through the front of the surface, and it is given as:

$$h_{rd1} = \varepsilon_c \cdot \sigma \cdot (T_c^4 - T_s^4) \tag{5.3}$$

h_{rd2} is heat transfers of the radiation through the backside of the PV cell surface, given by the following equation:

$$h_{rd2} = \varepsilon_{pl} \cdot \sigma \cdot (T_p^4 - T_{heo}^4) \tag{5.4}$$

Assuming that there is a natural convective air layer in the PV cell and heat exchanger, the related convective heat exchange coefficient, h_{air}, can be defined as the following equation (Zhao et al., 2011):

$$h_{air} = \frac{Nu \cdot K_{air}}{\delta_{air}} \tag{5.5}$$

where

K_{air} is the thermal conductivity of air and

δ_{air} is the thickness of the air layer among PV and heat exchanger pipe.

At that point, the Nusselt number can be acquired by the following equation (Zhao et al.,2011):

$$Nu = [0.06 - 0.017 \cdot \left(\frac{\beta_s}{90}\right)] \cdot Gr^{1/3} \tag{5.6}$$

The Grashoff number is assumed as the following equation (Zhao et al., 2011):

$$Gr = \frac{g \cdot \left(T_p - T_{heo}\right) \cdot \delta_{air}^3}{V_{air}^2 \cdot T_{air}}$$

(5.7)

The combination of the above equations allows the expression of useful heat energy (Zhao et al., 2011):

$$Q_u = Q_{abs} - Q_l$$

(5.8)

The heat flowing through the absorber by conduction, which includes the walls of heat exchanger pipe, and is eventually transferred into the flow of water by convection. The rate of extraction of the heat is measured by the amount of heat carried by the fluid passing through it and is expressed by the following equation:

$$Q_u = A_c \cdot U_u \cdot (T_c - T_w)$$

(5.9)

Overall thermal resistance between absorber pipe and coolant is as follows (Zhao et al., 2011):

$$U_L = (U_{in,heo} + U_{heo,hein} + U_{hein,w})^{-1}$$

(5.10)

Heat transfer coefficient (U_{abs}, h_{eo}) from absorber aluminium layer to the outer wall of a heat exchanger is given by the following equation (Zhao et al., 2011):

$$U_{in,heo} = \frac{\lambda_{in}}{\delta_{in}}$$

(5.11)

The temperature of the outer wall of the heat exchanger becomes given as (Zhao et al., 2011):

$$T_{heo} = T_c \frac{Q_u}{A_c \cdot U_{in,heo}}$$

(5.12)

Heat transfer coefficient ($U_{heo,hein}$) from the outer wall to the interior wall of the heat exchanger is defined by the following equation (Zhao et al., 2011):

$$U_{heo,Hein} = \frac{2 \cdot \pi \cdot \lambda_{he}}{In[\frac{D_e}{D_i}]}$$

(5.13)

The average temperature of the inner wall of the heat exchanger is given by the following equation (Zhao et al., 2011):

$$T_{hein} = T_{heo} \frac{Q_u}{A \cdot U_{heo,hein}}$$ (5.14)

Heat transfer coefficient ($U_{hein, r}$) from the interior wall of the heat exchanger to water is this (Zhao et al., 2011):

$$U_{heo,W} = \frac{Nu \cdot \lambda_r}{D_i}$$ (5.15)

$$Re_r = \frac{Q \cdot D_{he}}{V_r \cdot A_p}$$ (5.16)

Stating the expressions used by the following equation (Zhao et al., 2011):

$$m^2 = \frac{U_L}{K\delta}$$ (5.17)

Then, the fin efficiency factor (F) can be found in the following equation (Zhao et al., 2011):

$$F = \frac{\tanh(m\frac{W - D_o}{2})}{m\frac{W - D_o}{2}}$$ (5.18)

The fin efficiency factor of the collector F', it is expressed by the following equation:

$$F^{'} = \frac{1/U_L}{W\{\frac{1}{U_L[D_e + (W - D_e)F]} + \frac{1}{C_b} + \frac{1}{\pi D_i h_w}\}}$$ (5.19)

where:

W is the separating distance between the central axes of the tubes;

D_e and D_i are the external and internal diameters of the tubes, respectively;

C_b is the bond conductance between the tube and the fin; and

h_w is the heat transfer coefficient of water.

The flow rate factor (FR) given by FR is the heat removal factor, defined by the following equation:

$$F_R = \frac{\dot{m}C_f}{A_c U_L F^{'}}\left[1 - \exp\left(-\frac{A_c U_L F^{'}}{\dot{m}C_f}\right)\right]$$ (5.20)

F is the efficiency expressed as:

The thermal efficiency of the PV/T collector is calculated by the following relation:

$$\eta_{th} = \frac{Q_u}{AG} = \frac{\overset{\bullet}{m}c_p \int (T_{fs} - T_{fe})dt}{A_c \int Gdt} \tag{5.21}$$

The electrical efficiency of PV/T collector is equal to this:

$$\eta_{el} = \frac{Q_e}{A_c G} = \frac{A_c G(\eta_{ref}[1 - 0.0054(T_c - 298.15)])}{A_c G} \tag{5.22}$$

the useful heat energy can be expressed in the following equation:

$$Q_u = mc_p(T_0 - T_1) \tag{5.23}$$

It is difficult to determine the mean temperature of the collector compared to the fluid inlet temperature. However, the quantity relates to the actual useful energy gain of a collector surface, which is the quantity known as the collector heat removal factor (F_R) (Zhao et al., 2011).

$$F_R = \frac{mc_p(T_0 - T_1)}{(\alpha\tau)GA - U_L A(T_c - T_a)} \tag{5.24}$$

The efficiency of the PV collector is defined as the ratio of gain of useful energy, Q_u, the solar energy incident (Zhao et al., 2011):

$$\eta = \frac{\int Q_u}{A\int G\partial t} \tag{5.25}$$

$$\eta = \frac{Q_u}{AG} \tag{5.26}$$

$$\eta = \frac{F_R A((\alpha\tau)GA - U_L A(T_c - T_a))}{AG} \tag{5.27}$$

$$\eta = F_R(\alpha\tau) - F_R U_L\left(\frac{T_i - T_a}{G}\right) \tag{5.28}$$

5.2.3.3 Energy balance in the absorber pipe

The fluid temperature in the absorber pipe can be changed by an assortment of procedures. These include advection and conduction through the terminals of the absorber pipe (thermal liquid

172

ports A and B) and convection at the pipe-fluid interface (thermal port H). The energy balance regarding the energy accumulation rate in the pipe is expressed as follows:

(1) **The energy of the fluid in the pipe**

This energy is given by:

$$\dot{E} = \phi_A + \phi_B + \phi_H - \dot{m}\, g\Delta z \tag{5.29}$$

where:

$\dot{E}$ is the energy accumulation rate;

ϕ is the energy flow rate through a port, and the subscript denotes the port at which its value is defined; advection and conduction through the ends of the pipe (thermal liquid ports A and B) and convection at the pipe-fluid interface (thermal port H);

$\dot{m}$ denotes a mass flow rate into the pipe;

Δz is the rise in elevation from ports A to B (m); and

g is the gravitational acceleration (m/s^2).

The total energy of the internal fluid volume is defined in terms of the specific internal energy as follows:

$$E_1 = \rho_1 u_1 V \tag{5.30}$$

where:

u is the specific internal energy of the fluid (kJ/kg);

V is the internal volume of the pipe (m^3); and

ρ is the thermal density inside the pipe volume (kg/m^3).

(2) **Convective heat transfer at the pipe wall**

The heat flow rate between the thermal liquid and the pipe wall is assumed to result from a convective exchange and a purely conductive exchange:

$$\phi_H = Q_{conv} + Q_{cond} \tag{5.31}$$

where:

ϕ_H is the heat flow rate between the thermal liquid and the pipe wall (W);

Q_{conv} is the heat by convection (W) and;

Q_{cond} is the heat by conduction (W).

The heat flow rate due to conduction is computed as follows:

$$Q_{cond} = \frac{ki \cdot S_H}{D}(T_H - T_I)$$

(5.32)

where:

k_i represents the thermal conductivity of the liquid inside the pipe (W·(m·K); and

S_H represents the surface area of the pipe wall (m²) (the product of the internal perimeter and the pipe length).

T_H represents the temperature of the pipe wall (K)

T_i represents the temperature inside the pipe wall (K)

D represents the diameter of the pipe wall

The subscripts H and I denote the pipe wall and the internal fluid volume, respectively.

The heat flow rate due to convection is computed as follows:

$$Q_{conv} = c_{p,avg} \mid \dot{m}_{avg} \mid (T_H - T_{in})\left[1 - \exp\left(\frac{h \cdot S_H}{c_{p,avg} \mid \dot{m}_{avg} \mid}\right)\right]$$

(5.33)

where:

$c_{p,avg}$ denotes the specific heat of the thermal liquid J/(kg K) at the average temperature of the pipe;

h denotes the heat transfer coefficient of the pipe;

$\dot{m}_{Avg}$ denotes a mass flow rate (kg/s) at the average temperature into the pipe;

T_{in} denotes temperature inlet of the pipe;

the subscript *in* denotes the pipe inlet (port A or B depending on flow direction); and

the subscript *avg* is evaluated at the average temperature of the pipe. This expression assumes that temperature varies exponentially between the ends of the pipe.

5.2.3.4 Energy storage system

The main problem of solar energy is its intermittency caused by day and night periods. Also, the intensity of irradiation varies over time (during the day, for example, the solar radiation has a Gaussian shape, and on an annual basis, solar radiation changes with the seasons).

Electrical energy storage offers a solution to the problems of intermittency and overproduction of electrical energy. However, there is a trade-off between installation capacity cost and lifespan of the batteries. The nature of the energy stored can be mechanical, electrical or thermal. Thermal energy storage is an excellent way to optimise the management of thermal energy. Its performance depends on the type of storage materials and their capability.

(1) Storage tank

Three main techniques of heat storage — sensible heat storage, latent heat storage and chemical heat-sensitive storage — in which the temperature of the storage materials varies with the amount of energy stored.

The thermal energy obtained from a PV/T system is transferred and stored in an insulated storage tank. The tank equation model defines the thermal energy balance in the tank.

Tank volume

The tank fluid volume is computed from the total fluid mass at each time step:

$$V = \frac{m}{\rho}$$

(5.34)

where:

V denotes the tank fluid volume (m³);

m represents the tank fluid mass (kg); and

ρ is the tank fluid density (kg/m³).

Mass balance

$$\dot{m} = \dot{m}_A$$

(5.35)

where:

$\dot{m}$ represents the net mass flow rate into the tank (kg/s); and

$\dot{m}_A$ represents the mass flow rate (kg/s) into the tank fluid volume through the inlet port A;

Momentum balance in the tank

The momentum preservation equation in the storage tank fluid volume is defined by the following:

$$p_A + p_{dyn} = p_{ref} + \rho \cdot g \cdot (y - y_A)$$

(5.36)

where:

p_A is the fluid pressure kg/(m·s²) at inlet A;

p_{ref} is the constant tank pressurisation;

p_{dyn} is the dynamic pressure kg/(m·s²):

$$p_{dyn} = \begin{cases} 0, & \dot{m}_A \geq 0 \\[2mm] \dfrac{\dot{m}_A}{2\rho_A S_A^2}, & \dot{m}_A < 0 \end{cases}$$

ρ_A represents the liquid density (kg/m³) at port A;

S_A represents the tank inlet area (m²);

g represents the gravitational constant (m/s²);

y represents the tank level (m), or height, relative to the tank bottom; and

y_A represents the tank inlet elevation relative to the tank bottom (m).

Energy balance in the storage tank

The energy conservation equation in the tank fluid volume is defined by the following:

$$m\left(c_P - h\alpha\right)\dot{T} = \phi_A h + Q \tag{5.37}$$

where:

c_P is the fluid thermal capacity (J/K/kg);

α is the fluid isobaric bulk modulus (psi);

T is the fluid temperature (K);

ϕ_A is the energy flow rate (W), into the tank through port A;

h is the fluid enthalpy(J/kg); and

Q is the thermal energy flow rate (W), into the tank through port H.

Assumptions and limitations

In addition to the above assumptions, the following assumptions apply to the reservoir model:

- The tank is entirely mixed (That is, there is no stratification due to a forced operation mode).

- The amount of heat added to the tank is evaluated by considering heat transfer through the heat exchanger inside the tank.

- The tank pressure is constant and uniform throughout the tank volume. The tank elevation head affects only the inlet pressure calculations.

- Fluid momentum is lost at the tank inlet due to the sudden expansion into the tank volume.

(2) Battery storage

Li-ion batteries play an essential role in RE since the energy produced by a photovoltaic system need to be stored and supply to load permanently without interruption over a predetermined period.

The state-of-charge (*SOC*) of the battery storage depends on several electrical and chemical parameters: charge voltage, open-circuit voltage, temperature, current, internal impedance and specific density of the electrolyte. It is difficult to measure the *SOC* of battery storage directly with a sensor. Several methods for estimating the state-of-charge are available such as:

- the Luenberger observer or the coulomb meter;
- sliding the observer mode; and
- the Kalman filter current integration method.

Battery model

This is a finite battery charge capacity parameter, the voltage a function of charge with the following relationship in Equation 5.38 and 5.38:

$$V = V_0 \left(\frac{SOC}{1 - \beta(1 - SOC)} \right) \tag{5.38}$$

where:

SOC is the ratio of current charge to rate the battery capacity;

V_0 is the voltage (V) when the battery storage is fully charged at no load, as defined by the nominal voltage parameter; and

β is a constant calculated so that the battery voltage is *V1* when the charge is *AH1*.

Specify the voltage, V1 so that the Voltage *V1* < Vnom, and specify ampere-hour *AH1* when the no-load voltage is *V1*.

This equation determines the close correlation between voltage and remaining charge. This estimation simulates the rate of increase of the voltage drop with a low load, making sure that the battery voltage becomes zero, while the charge level is zero.

The parameter of the battery storage used is given in Table 5.1 (Section 5.2).

5.3 PV/T system simulation and discussion

The energy conversion and heat transfer mechanisms occurring throughout the PV/T model are illustrated in this section. The thermal and electrical energy balance occurring in the PV/T model depends on the thermodynamic properties, solar radiation temperature, humidity. Including the geometric parameters and other variables independent of the PV/T system. Various formulas are used to determine the generated power, the power dissipated, the thermal energy recovered from the PV panel, and the heat transfer fluid flowing governed the equations in Section 0 as derived from MATLAB. In the simulation, a water mass flow rate and solar radiation were kept constant at 0.5 kg/s and 1000 W/m^2, respectively; while R_{se} was selected to be 0, 10 and 50 Ω.

5.3.1 Working fluid in the proposed PV/T system

Water was selected as the fluid and is used as a heat transfer medium for this application. Simulink provides the thermal liquid library setting that offers a simple way to define fluid properties. The display shows three-dimension results of the fluid properties such that the thermal conductivity, the kinematic viscosity and density, are represented in Figure 5.4, Figure 5.5 and Figure 5.6, respectively, and provide the trade-offs between input factors and output response.
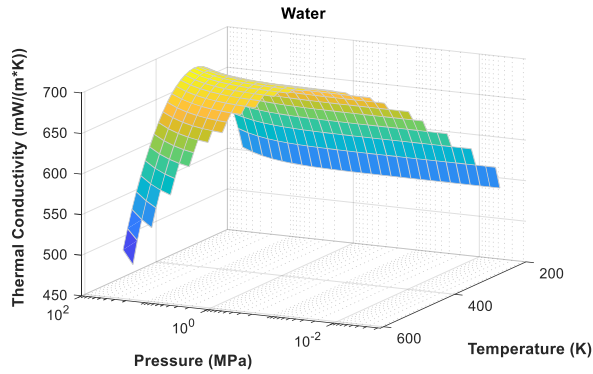
Figure 5.4: Water thermal conductivity in the proposed PV/T system
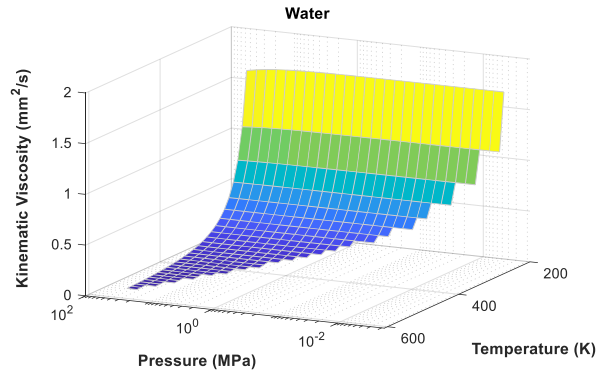
Figure 5.5: Water viscosity in the proposed PV/T system
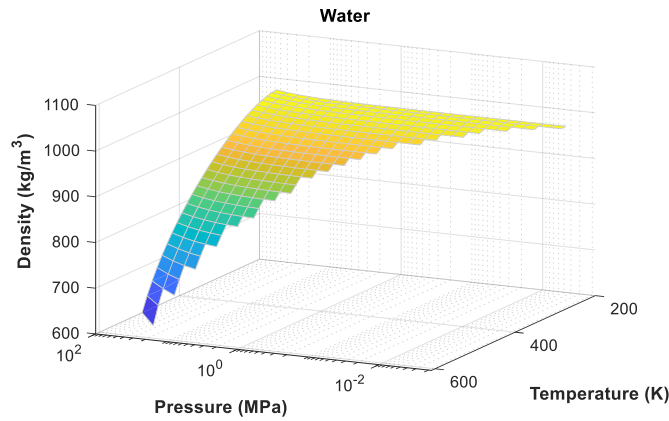
Figure 5.6: Water density in the proposed PV/T system

180

5.3.2 The temperature of the PV/T system under working fluid and R_{se}

The operating temperature of a PV/T system has abundantly been reported in the literature. Since the amount of the power generated by a PV cell in the PV/T system is dependent on temperature, the generated power decreases when the operating temperature of the PV cell increases.
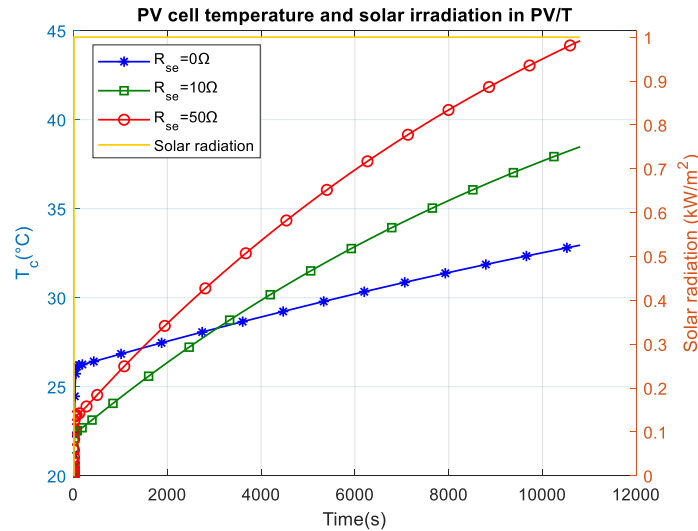
Figure 5.7: PV/T cell temperature and solar irradiation in the PV/T system

Figure 5.7 shows the development of the PV/T cell temperature (T_c) profile ranging from 26.5 to 33 ℃, 22.5 to 37℃ and 23 to 45℃, when R_{se} was set to 0, 10 and 50 Ω, respectively. At a particular flow rate, water absorbs the built-up heat at the back of the PV cell through the attached absorber pipe, enhancing the heat exchange coefficient, which enables a slow increase in the PV cell temperature. This is related to Newton's law of cooling states that the rate of heat loss of a body is directly proportional to the difference in the temperatures between the body and its surroundings. Comparing the temperature cell of PV and PV/T, respectively, for Figure 4.31 and Figure 5.7, it was observed that the average T_c for the PV/T system in Figure 5.7 was 29.75, 30.25 and 35.75℃ when R_{se} was set to 0, 10 and 50 Ω, respectively. While in Figure 4.31, the average T_c of the PV cell was 45, 51 and 59 ℃ for the corresponding values of R_{se}. The PV/T system temperature is substantially lower than the corresponding temperature of the PV cell because the water delays the rise of T_c by absorbing the extra thermal energy of the system. The flow of water within the absorber pipe plays a significant role in reducing the PV cell power loss. The larger the value of was R_{se}, the higher the PV/T cell temperature, which would result in an increase of the

working water temperature due to the heat transfer by conduction and convection within the PV/T system. The lower was the R_{se} value, and then the cooler was the PV/T cell temperature,

5.3.3 Generated power of the PV/T system under working fluid and R_{se}

Following the cooling process of the PV/T system, by allowing the fluid (water) flow at the back of the PV cell. Figure 5.8 shows a slight fall in PV/T cell electrical power (P_{PV}) from 3.26 to 3.05 kW, 1.74 to 1.60 kW and 0.40 to 0.33 kW, when R_{se} was 0, 10 and 50 Ω, respectively. The highest cooling capacity was achieved when the flow rate was maintained at 0.5 kg/s, and the R_{se} was set 0 Ω. This information demonstrated the cooling of the proposed PV/T cell with a working fluid, during the PV/T system operation.

The electrical power generated by the PV cell and PV/T cell, respectively, Figure 4.32 and Figure 5.8, shows that the average electrical power of the PV/T cell in Figure 5.8 was 3.16, 1.67 and 0.36 kW when R_{se} was set to 0, 10, and 50 Ω, respectively. While in Figure 4.32, the average electrical power of the PV cell was 2.84, 1.43 and 0.30 kW when R_{se} was set to 0, 10 and 50 Ω, separately. It is evidently clear that the electrical power production in the PV/T cell is higher than the power produced in PV cell only, and this is so because the water in the PV/T system delayed the rise of T_c by absorbing the extra the heat of the system.
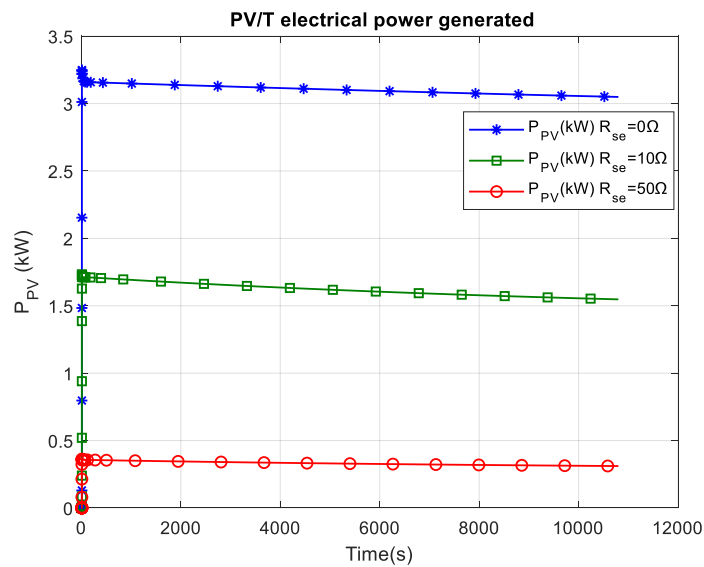

Figure 5.8: PV/T system electrical power generated

The effect of the PV/T cell temperature versus the electrical power generated by the PV/T cell was plotted in Figure 5.9 for different values of R_{se}. This graph shows a clear proof that the heat

transfer fluid used in the cooling process was much more effective than when no cooling was applied. The highest power is achieved when R_{se} was set to 0 Ω.
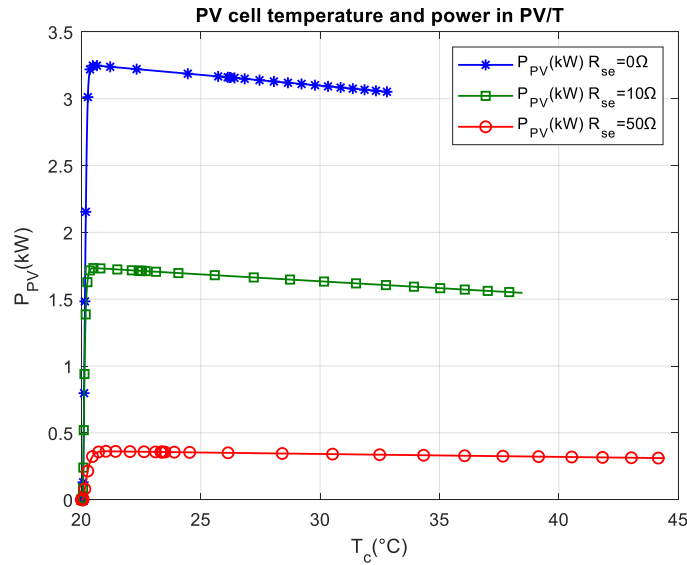
Figure 5.9: PV cell temperature and power in the PV/T system

5.3.4 Power dissipation in the PV/T system under working fluid and R$_{se}$

The internal heat generation known as the dissipated power (P_d) occurring inside the PV/T model under the effect of the working fluid for a selected value of R_{se}, were simulated throughout the simulation time. The total dissipated (P_d) of the PV cell model, comprising R_{si}, R_{pi} and the diode.

The total electrical power dissipated by the PV/T cell due to the variation of R_{se} value throughout the simulation time was presented in Figure 5.10. It was observed that when R$_{se}$ was set to 0, 10 and 50 Ω, the power dissipation varies from 750 to 810 W, from 1650 to 1748 W and from 3150 to 3090 W, respectively. Relating the average total electrical power dissipated in the PV/T system (Figure 5.10) to the average total electrical power dissipated in the PV cell (Figure 4.27). It was found that the total electrical power dissipated of the PV/T system in Figure 5.10 was 700, 1699 and 3120 W for the values of R$_{se}$ was set to 0, 10 and 50 Ω, respectively. While the average of the total electrical power dissipated in the PV cell in Figure 4.27 was 930, 1811 and 3044 W when R$_{se}$ was set to 0, 10 and 50 Ω, respectively. P_d is in similar order and not particularly significant when compared PV/T system to the PV cell.

**Figure 5.10: Total electrical power dissipated
by PV in PV/T system**

Figure 5.11 presents the relationship between the generated power (P_{PV}) and dissipated power P_d during the operation time of the PV/T system; the trade-off in power is noticeable for the selected value of R_{se}.
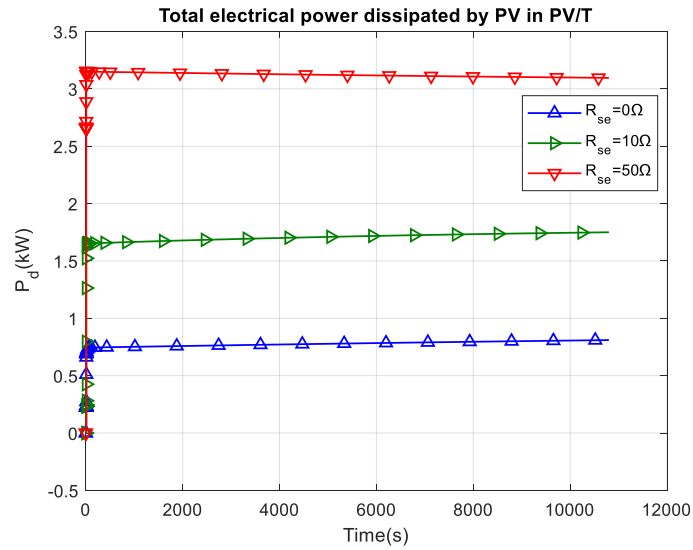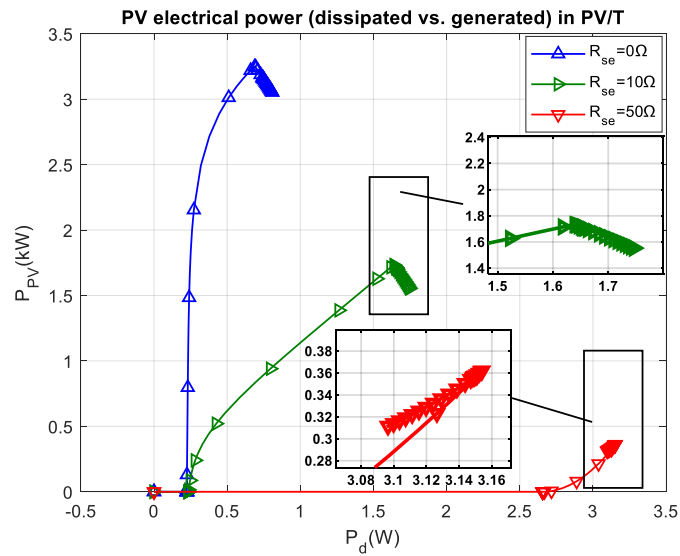

**Figure 5.11: PV electrical power (dissipated versus
generated) in the PV/T system**

5.3.5 Heat transfer occurring in a PV/T system under working fluid (water) and R_{se}

Figure 5.12, Figure 5.13 and Figure 5.14 exhibit the heat transitions occurring in the PV/T system, through heat transfer by radiation, convection and conduction heat transfer.

After the positive peak at the beginning was due to the starting effect, Figure 5.12 presents an almost constant value (in magnitude) of the heat transfer through conduction (Q_{cond}) of 450, 800 and 1600 W, when R_{se} was 0, 10 and 50 Ω, respectively. The heat loss by conduction was measured as negative in the graph due to the fact that the heat was transferred into the PV cell (towards the back of the PV/T cell). The heat conduction is the direct tiny exchange of kinetic energy of particles through the boundary between the two elements and is due to the consequence of the power dissipation of the PV/T cell material in the form of heat, resulting from the selected value of R_{se}. These results in Figure 5.12 are much comparable to results found in Figure 4.28 for the corresponding value of R_{se}. This heat conduction contributes to the heat loss by conduction and radiation.
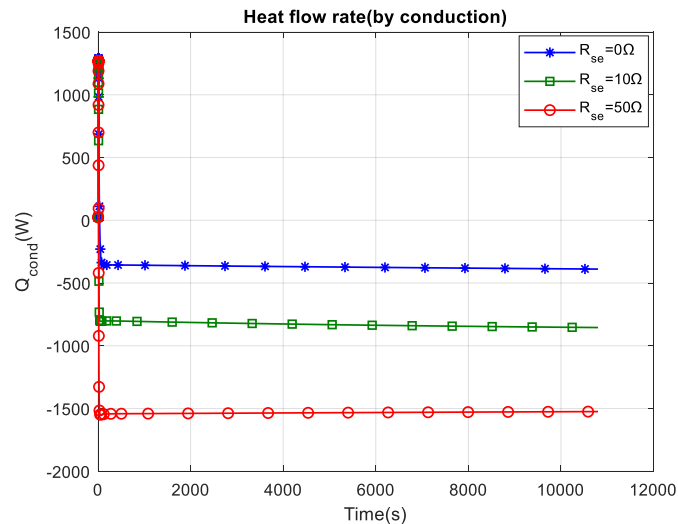
**Figure 5.12: Heat flow rate by conduction within
the PV cell in the PV/T system**

Figure 5.13 shows an increase in heat loss by convection from 750 to 1600 W, from 255 to 2300 W and from 400 to 3100 W, when R_{se} was set to 0, 10 and 50 Ω, respectively. The Q_{conv} was measured as positive in the graph due to the fact that it characterised heat transfer emanating of the PV cell (to the atmosphere). It should be noted that the average heat loss by convection in Figure 5.13 was 1175, 1278 and 1750 W, while the average heat loss by convection in Figure 4.29 was 3200, 3800 and 5000 W when R_{se} was set to 0, 10 and 50 Ω, respectively. The heat

loss by convection to the environment is lesser in the PV/T system than in PV cell because of the working water.
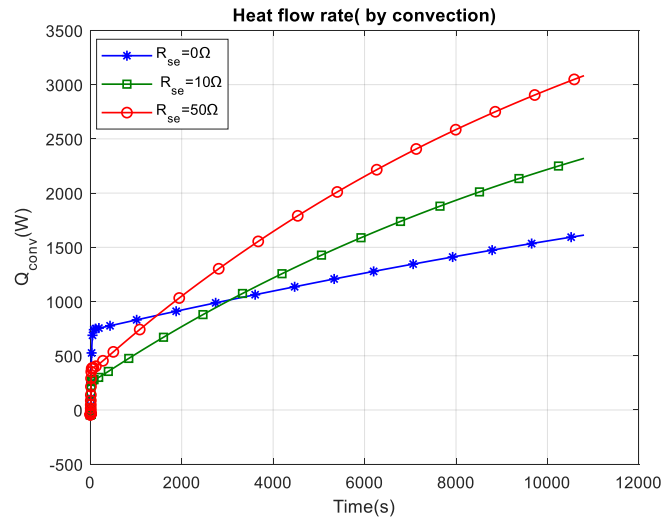
Figure 5.13: Heat flow rate by convection to the environment
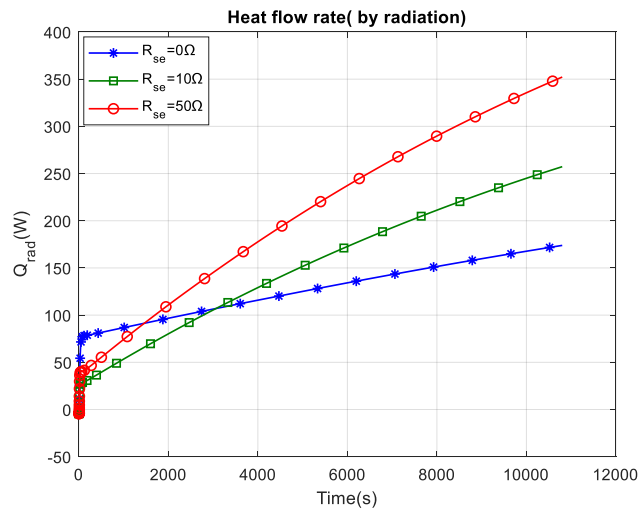
Figure 5.14: Heat flow rate by radiation to the environment

Figure 5.14 shows a gradual increase of heat transfer by radiation (Q_{rad}) from 77 to 174 W, 32 to 257 W and 40 to 352 W when R_{se} was 0, 10 and 50 Ω, respectively. The heat lost by radiation was measured positive in the graph because it represented the heat transfer emanating from the PV cell (to the atmosphere). Relating the heat loss by radiation in the PV/T system (Figure 5.14) to that the PV cell (Figure 4.30), it was found that the average heat loss by radiation to the

186

atmosphere in Figure 5.14 was 126,145 and 196 W for R_{se} at 0, 10 and 50 Ω, respectively, while the average heat loss by radiation to the atmosphere in Figure 4.30 was 352, 450 and 610 W for the corresponding values of R_{se}. The heat loss by radiation to the environment is less in the PV/T system than in PV cell because much of the generated heat was absorbed by the working water.

5.3.6 Energy transfer within the PV/T system under working water and R_{se}

The heat flow rate between water and the absorber pipe wall is assumed to be the outcome from a convective exchange and a purely conductive exchange. The amount of the heat transferred from the PV/T cell to the absorber pipe and then to the heat transfer fluid is presented in Figure 5.15. This figure presents a thermal flow rate ($Q_{thermal}$) which ranges from 5350 to 2150 W, from 3950 to 2700 W and from 2500 to 1550 W for values of R_{se} = 0, 10 and 50 Ω, respectively. This indicated that the thermal exchange between the PV/T cell, the pipe and the fluid decreases over time, due to the heat recovery process (the rate of heat loss of a body is directly proportional to the difference in the temperatures between the body and its surroundings). The accumulated heat diminishes from the back of the PV/T cell because it is taken into the working fluid in the absorber pipe. Thus, it can be seen that there is an improvement of the PV/T cell temperature in Figure 5.7 over the PV cell in Figure 4.31, for the selected value of R_{se}, and as well as the improvement of PV/T cell electrical power in Figure 5.8 over the PV cell in Figure 4.32, for the chosen value of R_{se}. The thermal energy is an important parameter to regulate the amount of heat transmitted by the PV/T cell, to heat the water in the storage tank. This is one of the most significant features of using R_{se} to control the useful heat.
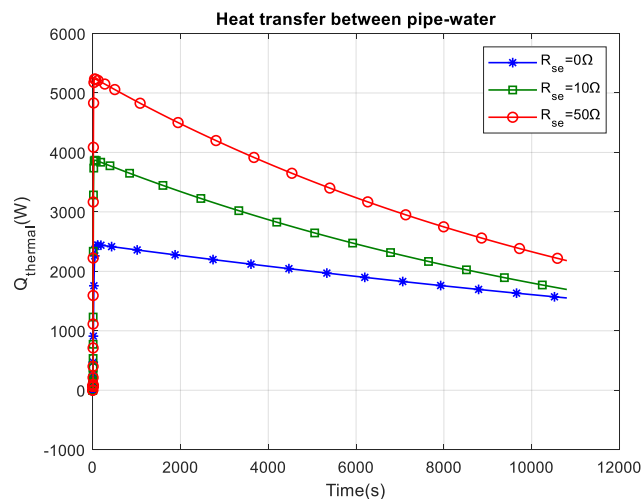

Figure 5.15: Heat flow rate between the thermal water and the pipe wall

The energy of the water within the absorber pipe may vary, depending on the various processes. These include advection, convection and conduction at the pipe-fluid interface and then convection throughout the fluid, as presented in Figure 5.16. The total energy of the internal fluid volume was characterised by the specific internal energy (the specific internal energy of the fluid), and it was acquired as a function of temperature and pressure from thermal liquid properties and the interior volume of the pipe. Figure 5.16 presents the specific internal energy of the volume fluid in the absorber pipe and the thermal storage tank. The thermal conduction in the storage tank ranges from 84 to 123 kJ/kg, 84 to 157 kJ/kg and 84 to 180 kJ/kg for the values of R_{se} = 0, 10 and 50 Ω, respectively. In the same way, the specific internal energy in the absorber pipe ranges from 84 to 125 kJ/kg, 84 to 160 kJ/kg and 84 to 183 kJ/kg for the chosen values of R_{se} = 0, 10 and 50 Ω, respectively.
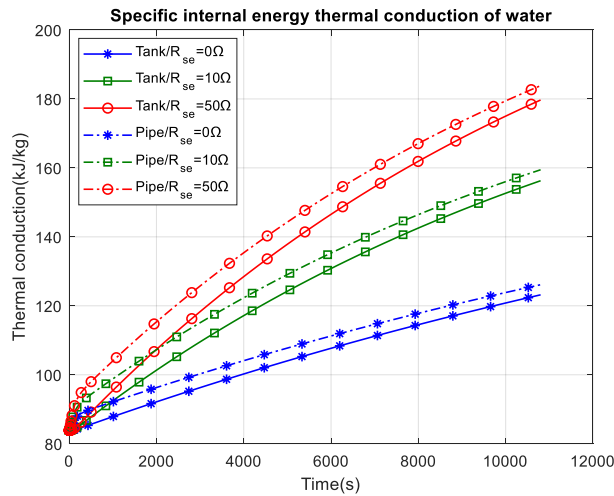
**Figure 5.16: Specific internal energy of the fluid (water)
volume in the pipe and the tank**

5.3.7 Working water temperature in PV/T system under R_{se}

In this section, the dynamic behaviour of the thermal energy absorbed by the working fluid through the absorber pipe attached to the back of the PV cell under a selected value of R_{se}, is discussed. Including, the different process occurring between the internal energy, the thermal fluid and the absorber pipe, which involves the exchange by conduction and convection within the absorber pipe. The outcomes displayed in the figures below demonstrate a significant amount of R_{se} implying higher thermal energy is absorbed. A better explanation of this phenomenon at a startup is that at the beginning of the simulation, the working fluid passes through the thermal absorber pipe attached under the PV/T cell. It was recovered lost heat by conduction at the back of the

PV/T cell was transferred to the working fluid, typically water. This induced an increase in the fluid temperature at the outlet of the PV cell while the working fluid in the channel slowed down the rate at which PV/T cell temperature progressed, thereby improving the heat exchange coefficient. This phenomenon is described by the transport equations for thermal energy (Fourier's law).

Figure 5.17 and Figure 5.18 show the evolution of the water temperature as it repeatedly passed through the absorber pipe and the storage tank, respectively. In Figure 5.17, the working fluid (water) temperature within the absorber pipe (T_{wp}) progressively increases during the simulation time from 20 to 30⁰C, 20 to 37⁰C and 20 to 44⁰C, when R_{se} = 0, 10 and 50 Ω, respectively. In the same way, Figure 5.18 displays accumulated fluid (water) temperatures in the storage tank (T_{wt}). T_{wt} varied considerably from 20⁰C to reach a maximum value of 29⁰C, 32.3⁰C and 42⁰C over simulation time when R_{se} was 0, 10 and 50 Ω, respectively. More significantly, when R_{se} was at 50 Ω, and then higher was the PV/T cell temperature, resulting in an increase in the working water temperature. This is due to the heat transfer by conduction and convection within the PV/T system.
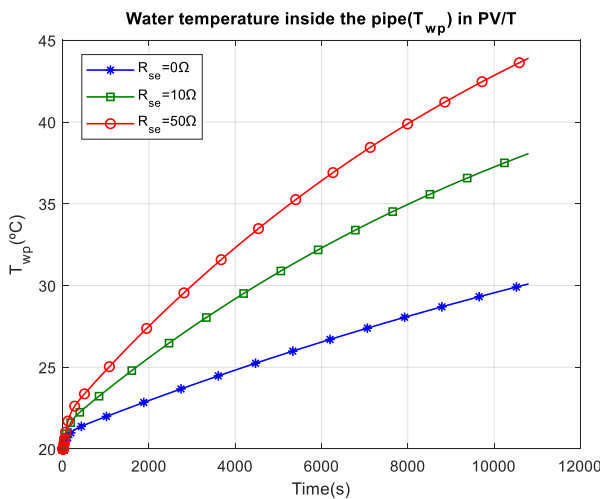
Figure 5.17: Water temperature inside the pipe (T_{wp})
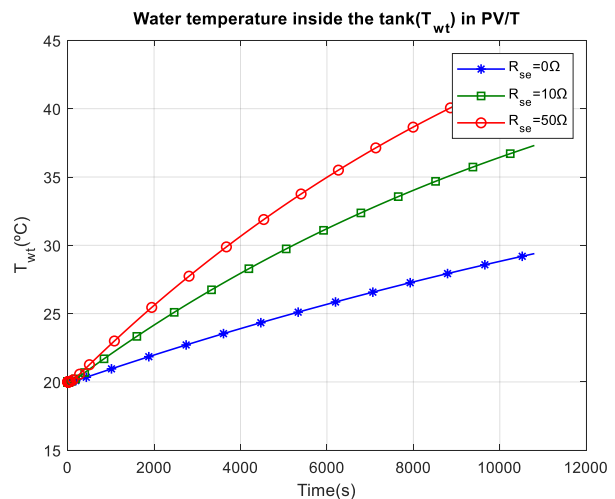
Figure 5.18: Water temperature inside the tank(T_{wt})

The fluid temperature in the storage tank (T_{wt}), within the absorber pipe (T_{wp}), and the PV/T cell (T_c) are all illustrated in Figure 5.19. Over an extended period, the temperature of the PV/T cell, fluid in the pipe and storage tank temperature tend to equalise. The results in these figures clearly show that the larger was the value of R_{se}, the higher the internal heat generation released by PV/T cell, and then the higher was the water temperature. The PV/T cell temperature was reduced by the heat transfer occurring between the working fluid and the absorber pipe.

189
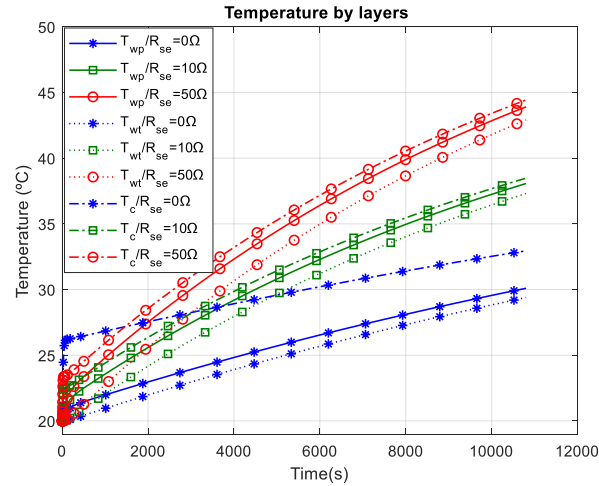
Figure 5.19: Temperature by layers

5.3.8 Energy efficient in PV/T system under working water and selected values of R$_{se}$

The thermal energy conversion efficiency of the PV/T system was illustrated in Figure 5.20. Thermal performance refers to the amount of heat transfer divided by the solar radiation absorbed by the PV/T cell surface area. Figure 5.20 shows the thermal efficiency varies inversely with the above specific values of this quotient (T_w - T_a)/G. Due to the startling effect, the thermal efficiency rises to 20, 33 and 44%, when R_{se} was at 0, 10 and 50 Ω, respectively. As the value of (T_w - T_a)/G increased, the thermal efficiency decreased linearly from 20 to 14%, 33 to 15% and 44 to 19%, when R_{se} was 0, 10 and 50 Ω. It was also discovered that increasing the R_{se} value results in higher power dissipation by the PV/T cell, therefore increasing the thermal efficiency and a decrease in electrical efficiency. As a result, the thermal efficiency of the module and the temperature of the PV cell increased, while the electrical efficiency of the PV cell reduced.
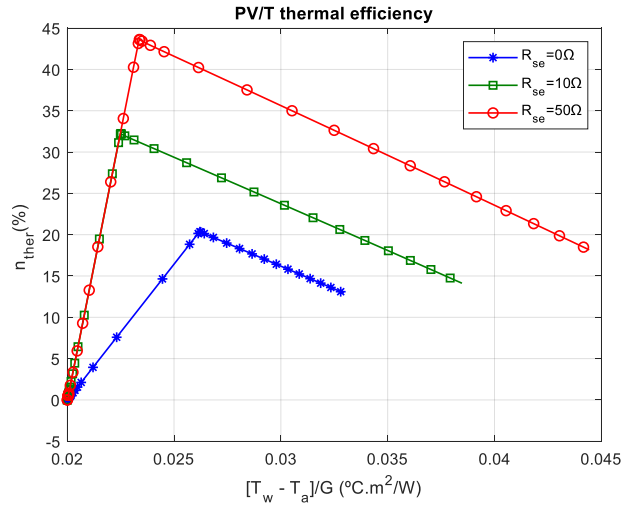
Figure 5.20: PV/T system efficiency versus
[T_w - T_a]/G (ºC.m²/W)

PV/T electrical energy efficiency is presented in Figure 5.21, Over three hours, the average PV/T electrical energy efficiency was determined to be 15.7, 8.15 and 1.7% when R_{se} was 0, 10, 50 Ω, respectively. While the average PV cell electrical energy efficiency in Figure 4.33 was 14.2, 7.1 and 1.5% for the corresponding value of R_{se}. The PV/T cell presents an increase in electrical efficiency of 11.0, 15.5 and 13.0% over the corresponding PV cell efficiency, when R_{se} was at 0, 10, 50 Ω, respectively. Therefore, the PV/T system improved the efficiency of solar energy conversion.
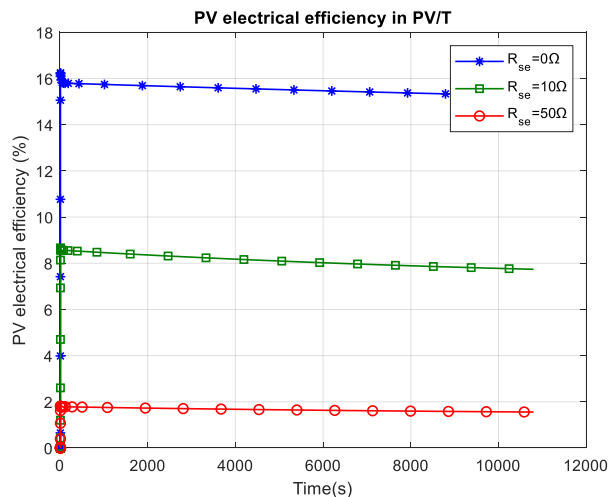
Figure 5.21: PV electrical efficiency in PV/T
system through time

191
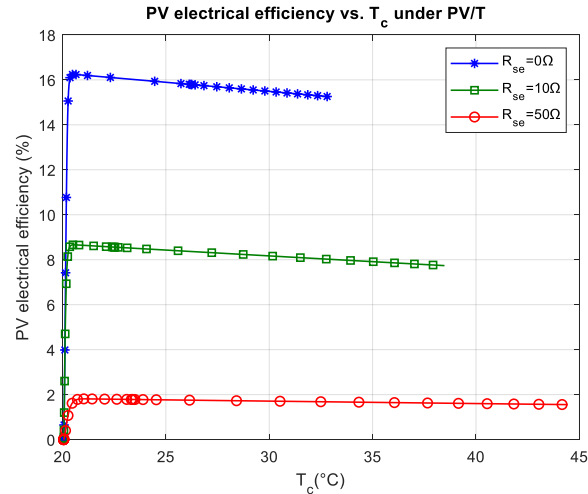
Figure 5.22: PV/T electrical system efficiency versus cell temperature

PV/T system electrical efficiency versus T_c was plotted in Figure 5.22. It was noted that as the PV/T cell temperature increased, the electrical efficiency of the PV/T cell decreased slightly for a selected value of R_{se}. This is because of the high heat transfer rate from the PV/T system to the working fluid (water) and the environment.

5.3.9 Multi-source power management

Stateflow in Simulink is an interactive graphical tool for modelling and simulating state machines of a system that reacts to events called reaction systems. These systems switch from one state to another, based on events and conditions. This tool acts as a supervisory unit, generating the role of instructions. The Stateflow can be configured by defining some behaviour statements that take a form of the *IF-THEN* pair. Specific trigger conditions can be selected that will cause the desired action to be performed.

Stateflow can be used for energy management when considering multiple variables. Moreover, it can be used to develop a discrete event model under the Stateflow to control *ON/OFF* switching between various sources. Example, to manage energy production based on energy demand, the state machine uses the transition conditions to change the state. These conditions can be obtained from the system variable measurements of different input and output flow.

The goal of energy management is to create a control strategy for the power generated by the PV/T system. Combining the PV cell with the absorber pipe to form the proposed PV/T system is simulated as a dynamic source in continuous time. This PV/T system consists of two sources:

electrical and thermal energy. The proposed PV/T systems require the best power management between components to select which energy to prioritise in production, monitoring the PV/T system and controlling the energy balance needed between the thermal and electrical energy.

The strategy is divided into two parts: the first step is to monitor the resource operation, and the second part is the control strategy to balance the thermal and electrical energy, also, taking into account the state-of-charge of the energy stored. When the demand for thermal and electrical energy is high, the component manages the production and stores the energy according to the demand.

As a result, the regulatory module will be responsible for adjusting source-generated energy and storage based on the needs of the consumer. It also incorporates a battery storage management system. The detection algorithm is based on three scenarios:

- If more electrical energy is needed, the proposed PV/T system will increase productivity to meet the demand, based on weather conditions;

- If more thermal energy is required, the proposed PV/T system will increase productivity according to the energy demand, based on weather conditions; and

- The proposed PV/T system can be programmed to equilibrate the productivity of thermal and electrical energy to meet the energy demand, based on weather conditions.

5.3.9.1 Design of the control algorithms using the Stateflow

In the Stateflow, a graph is a tool in which states and transitions are at the base of the construction of a state machine, and it is integrated into Simulink programs. Stateflow is a control logic tool used to model reactive systems, and it is used in energy management systems to control the multi-source system via state machines and flow charts within a Simulink model. The hierarchical custom of the Stateflow library in this study has tools such as graphs and truth tables, and MATLAB functions that can be used, this is shown in Figure 5.23.

This state machine was used under transition conditions: if the transition is valid, it moves from one state to another, such as the transition to set the limit of water temperature in the tank, the electrical energy stored in the battery and the control of the hydraulic pump. The condition to safely switch to different R_{se} values based on energy demand and weather conditions, for the entire system, are presented in Figure 5.24, Figure 5.25 and Figure 5.26, respectively.
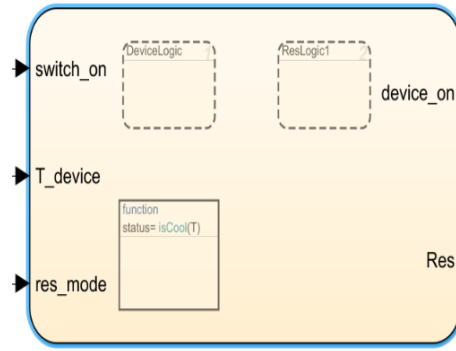
Figure 5.23: State-chart of a PV/T system
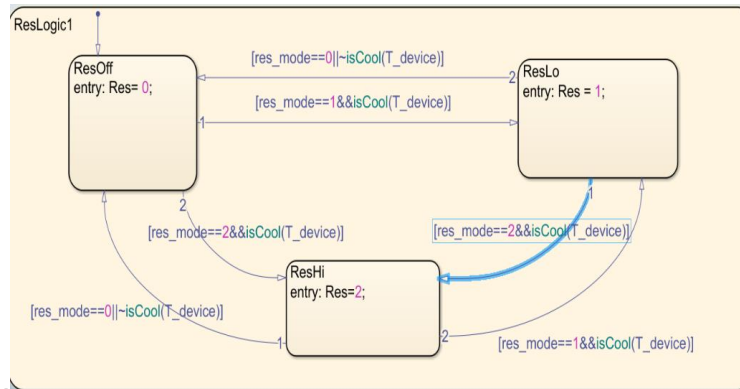
Figure 5.24: Transition condition of PV/T system for R$_{se}$
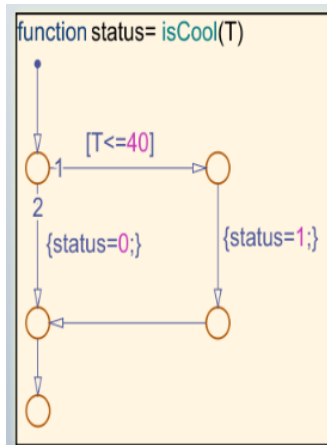
Figure 5.25: Transition of PV/T system of setting water temperature limit
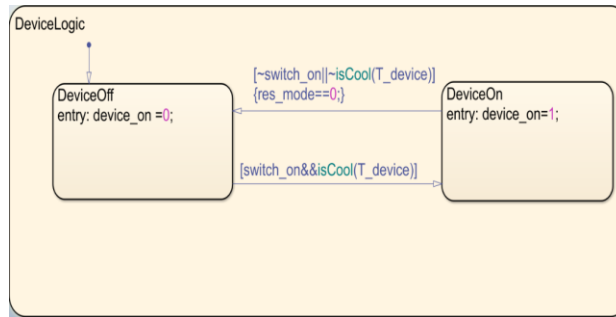
**Figure 5.26: Transition of PV/T system of the pump
and the entire system**

<u>**Stateflow variables**</u>

The inputs of the system:

- Weather conditions

- Available electrical power in the storage battery

- Available thermal power in the storage tank

- Energy demanded by the consumer.

The outputs of the system:

- R_{se}: Value of series resistance;

- P_{pv}: Electrical power provided by photovoltaic panels;

- Q_{thp}: Thermal power provided by photovoltaic panels;

- P_{bat}: Power provided by the battery;

- PV: *On/Off* relay of the PV;

The entire PV/T system consists, PV/T cell, hydraulic pump, battery to store the energy produced, and the water storage system. Different relays or switches activate or deactivate a connection, according to the need of the user, while seeking to maximise comfort and safety.

5.3.9.2 PV/T system energy management simulation results

The simulation ran for three hours with R_{se} set to 0, 50 and 10 Ω for 0 to 3600s, 3600 to 7200s and 7200 to 12000s, respectively. It operates according to the demand for the water temperature of the tank and electrical power.

195

Figure 5.27 illustrates the balance between the dissipated and generated power in the PV/T system based on thermal and electrical power demand, controlled by energy management based on the state machine control algorithms.
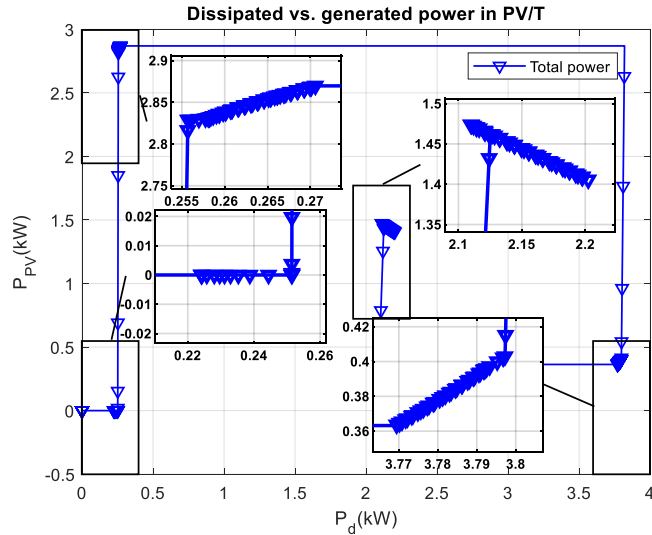
Figure 5.27: Balance between generated and dissipated power

Figure 5.28 shows the heat flow rate by conduction (useful heat) generated within the PV/T system during operation. To meet the energy demand, the energy management system controls a water mass flow rate and the appropriate value of R_{se}. The thermal power value switches to a different value 115, 1860 and 1050 W (in magnitude) corresponding to the chosen R_{se} values of 0, 50 and 10 Ω, respectively.
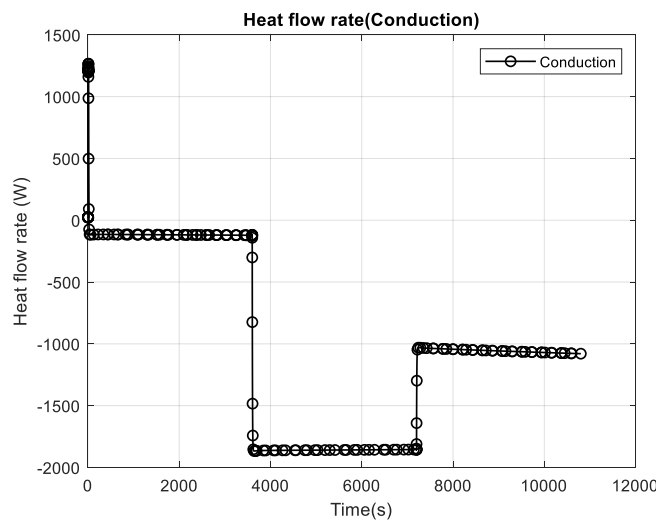
Figure 5.28: Heat flow rate (heat conduction)

196
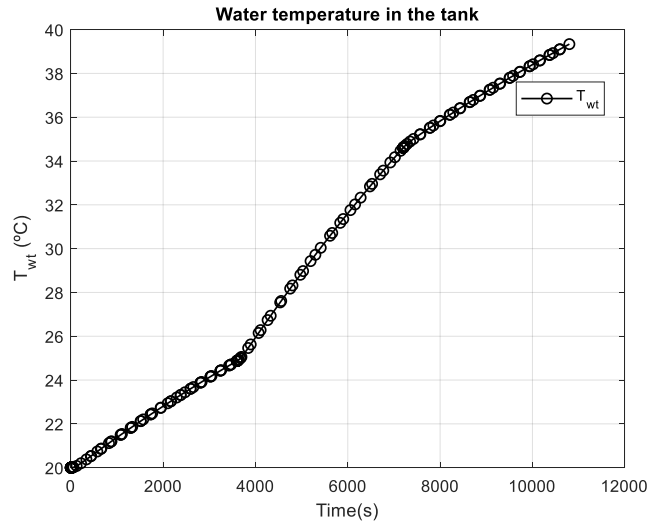
**Figure 5.29: Water temperature in the tank
under the PV/T system**

Figure 5.29 presents the water temperature in the tank; the water temperature increases by 5ºC during the first 60 min, 10ºC during the second 60 mins and 4ºC during the third 60 mins respectively, when R_{se} switches to 0, 50 and 10 Ω. The water temperature gradient was higher when R_{se} was 50 Ω.
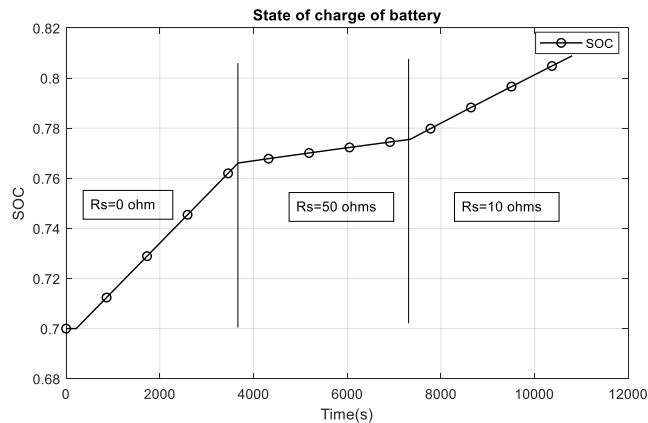
Figure 5.30: State-of-charge of the battery

The energy management monitors the *SOC* of the lithium-ion battery, as defined in Figure 5.30. The *SOC* estimation is imperative for the energy management system; increases the optimisation of electrical storage. As the R_{se} value switches to 0, 50 and 10 Ω, the *SOC* increases from the initial value by 0.064 during the first hour, from 0.764 to 0.7672 during the second hour and by 0.04 on the third hour (Figure 5.30). The power was maximised when R_{se} was 0 Ω.

197

5.4 Conclusion

The PV/T system is not just a product that makes our life easier, nor is it a luxury. For economics reason, the PV/T system will be essential in residential and industrial areas.

In this chapter, a simplified model of the proposed PV/T system for cooling the PV cell and heating the working fluid during the operation was presented and investigated. The mathematical model of the PV/T system has been established based on the global energy balance method and takes into account the different heat transfer such as conduction, radiation and convection occurring in the system.

From the model, a dynamic electrical and thermal simulation of the proposed PV/T model was developed in MATLAB/Simulink using the existing equations. The PV/T system performance based on the material properties and internal heat generation, the fluid temperature inside the absorber pipe, hydraulic pump, the fluid temperature in tank storage, PV/T cell temperature and the *SOC* of the battery storage were analysed and, the description of the thermal and electrical efficiency of each component was presented. Also, the analysis of the energy management system using the Stateflow method and the validation of the developed PV/T model was done. The considered model in Simscape (physical modelling is more accessible and intuitive) allows a more in-depth study of the interaction between various component models and system regulation.

A particular value of R_{se} dictates the amounts of electrical power and useful thermal energy from the proposed PV/T system. The thermal energy is transferred (power dissipated in the form of heat) to the working fluid inside the absorber pipe. The maximum cooling limit was achieved when a water mass flow rate circulating inside an absorber pipe attached at the back of the PV cell was maintained at 0.5 kg/s, and the R_{se} was set to 0 Ω, resulting in the heat transfer by conduction is 0.36 kW and generated electrical power of 3.25 kW. The optimum heat transfer was achieved when the water mass flow rate is maintained at 0.5 kg/s while R_{se} was set to 50 Ω. Then, the heat transfer by conduction was 1500 W, and the generated power was 0.33 kW. This information demonstrates the general useful energy (dissipating power in the form of heat) capacity of a PV cell to transfer heat in the working fluid of the PV/T system.

The simulation results over three hours presented in Figure 5.19, showing the PV cell surface temperature reaching of 35°C, 37°C and 44°C for a selected value of R_{se} = 0,10 and 50 Ω, respectively. Therefore, the initial water temperature at 20°C passing through the absorber pipe will gradually absorb the heat for the PV cell increases up to maximum 30°C, 36°C and 42°C respectively, when R_{se} = 0,10 and 50 Ω. The corresponding water temperature in the storage tank

is 29°C 32.3°C and 43°C when R_{se} = 0,10 and 50 Ω, respectively. Other water flow pattern in the proposed PV/T system are shown in Appendix C.

Over three hours, the average PV/T electrical system efficiency was determined to be 15.7, 8.2 and 1.7% when R_{se} was 0, 10, 50 Ω, respectively. While the corresponding average PV cell electrical efficiency was 14.2, 7.1 and 1.5% for the same selected values of R_{se}. The proposed PV/T system presents an increase in electrical efficiency of 11, 15.5 and 13% over the corresponding PV cell efficiency, when R_{se} was 0, 10, 50 Ω, respectively. Therefore, the PV/T system improved the efficiency of solar energy conversion.

It was shown that by applying energy management algorithms based on the Stateflow to a PV/T system was successfully implemented to save energy (the thermal/electrical energy mix), a priority also was given to the production of thermal/electrical power to meet the demand for energy. The water temperature in the storage tank increases by 5ºC during the first 60 min,10ºC during the second 60 min and 4ºC during the third 60 min respectively, when R_{se} was switched to 0, 50 and 10 Ω. While the *SOC* increases from the initial value by 0.064 on the first hour, from 0.764 to 0.7672 on the second hour and by 0.04 on the third hour for the corresponding value of R_{se}.

The proposed PV/T system provides a straightforward control of thermal and electrical energy. The performance analysis of the PV/T system showed that a substantial amount of thermal and electrical energy could be produced when implementing this novel method. This finding enhances the thermal conversion efficiency of solar energy and contributes to the study of the thermodynamics in the proposed PV/T system.

Chapter 6

General conclusion and recommendations

6.1 Answers to the research questions

This section presents the answers to the research questions stated in chapter one, which emanates from the research work undertaken.

- **Are there any energy gains in coupling the photovoltaic and thermal system?**

The difference between a solar PV and a solar thermal system lies in the ability of the solar PV system to convert the incoming solar radiation into electricity while the solar thermal collector transforms the incoming solar radiation into heat. Coupling the solar PV and solar thermal (PV/T) can simultaneously generate electrical and thermal energy.

Solar energy is exploited at the maximum when using the PV/T system compared to a photovoltaic panel and solar thermal. The photovoltaic panels produce much more heat (85%) than electricity (15%) when exposed to solar radiation. Thus, most of the solar energy captured is converted to wasted heat, causing its degradation and reduction of its energy efficiency. The PV/T system can utilise the wasted heat under the panels for industrial heat applications such as pre-heating water, boiler feedwater, cooking, drying, dyeing, boiler feed water, pasteurisation and sterilisation. The PV/T system offers an opportunity for the end-user to get closer to energy independence and to counteract the foreseeable rise in energy costs from the utility grid. Various types of PV/T systems currently exist, such as — air-based PV/T system, water-based PV/T system, heat pipe-based PV/T system, refrigerant-based PV/T system, BIPVT, SAHP-based PV/T system, nanofluid-based PV/T system and PCM-based PV/T system — were investigated. This study focused on a simple water-based PV/T system architectural design.

The PV/T system has several benefits, such as:

- An energy yield: by 15% over the conventional photovoltaic cells.

- High energy output: a PV/T system generate more electrical and thermal energy compared to the individual systems.

- Space optimisation: save space by combining power generation and thermal on the same surface.

- Non-polluting technology: photovoltaic electricity does not generate pollution. It is an entirely eco-friendly solution that fits into the preservation of the environment.

- Infinite energy source: solar energy is inexhaustible, free and natural.

- A generation of savings: PV/T system saves money for 30 years, either throughout the life of the panel.

- A competitive energy cost: the subsidies needed for solar energy are drastically reduced,

- PV/T system provides broad applications as compared to the independent system.

This PV/T system has some shortcomings. The efficiency varies with the weather conditions.

- Sensitivity as a function of temperature: the performance drop at the higher temperature,

- Limited performance: the stabilisation of the system temperature does not lead to optimal thermal solar production.

- A dependence on solar radiation: no solar energy is produced in the absence of radiation.

- Heat loss by convection and radiation to the environment.

- **What is the potential improvement of the proposed PV/T system?**

This work proposed an efficient way of cooling a PV cell and pre-heating water in the PV/T system. The proposed PV/T system consists of photovoltaic panels, an absorber pipe and a hydraulic pump. The flow of water in the PV/T system increases the energy efficiency conversion of the PV cells; since the heat flow was transferred from the back of the PV panel to the flowing water.

The optimisation of the proposed PV/T system provides flexibility in energy (thermal and electrical) production; depending on the energy demand by the end-user. The PV/T system can offer the cooling of the PV cell, as well as partially convert the photovoltaic electrical output into a useful heat source (to deliver more heat to the water).

It is desirable to potentially improve the water-based PV/T system performance in the following manner:

- o Coupling the photovoltaic panel and solar thermal (PV/T) system that alternates the thermal and electrical energy production based on the user-needs;

- o This proposed PV/T system is designed to balance the thermal and electrical energy based on weather condition and energy (thermal and electrical).

- o Developing subsequent control decisions to improve energy conversion methods within the PV/T system; and

- o Establishing an energy efficiency conversion which will produce and maintain electrical and thermal energy to the optimum efficiency;

- o The major novelty is in the introduction of variable series resistance to manage the thermal output of the system.

- o The energy management monitors of a PV/T system operating mode.

- o This PV/T system is based on the interpretation of the thermal, electrical energy demand and production to achieve the energy balance.

- o Space management and the total energy efficiency (electrical and thermal energy) are higher per square meter as compared to the use of two separate systems.

- o PV/T system prioritises the energy balance, based on the demand and weather conditions.

o A controlled method can adjust the useful heat transfer capacity to working fluid based on energy demand.

o Therefore, the PV/T system can be used as a multifunctional energy device.

- **What are the optimal performances of the proposed PV/T system?**

An investigation into different methods in balancing the PV/T system energy (thermal and electrical) was undertaken. The research focuses on the optimisation of a PV/T system with subsequent decisions to achieve energy efficiency. The implementation of the method is only used to balance and prioritise the hot water and electricity produce.

An algorithm using Stateflow was developed to control the energy productivity in a PV/T system such that it prioritises the thermal or electrical energy based on the energy demand. The algorithm monitored the energy (thermal and electrical energy stored in the storages) and the weather conditions (that is solar radiation intensity, ambient temperature, wind speed). Based on the measurement, the algorithm balances the thermal and electrical energy production to meet the energy demand.

The algorithm was based on three main scenarios:

o If more electrical energy is needed, the PV/T system will increase productivity to meet the demand, based on weather conditions;

o If more thermal energy is required, the PV/T system will increase productivity according to the energy demand, based on weather conditions; and

o The PV/T system can be programmed to equilibrate the productivity of thermal and electrical energy to meet the energy demand, based on weather conditions.

- **What type of energy storage technology is suitable for the proposed PV/T system at the implementation level?**

A promising way of dealing with the intermittency from renewables is energy storage. Different energy storage technologies options have been discussed based on their characteristics, efficiencies, and limitations and the one that is suitable for the proposed PV/T system has been identified.

- o Thermal energy storage (TES) is a technology that stores thermal energy in advance to anticipate future needs for heating and cooling applications. The most common thermal storage used is latent heat storage (LHS) and sensitive heat storage systems. LHS is based on the heat absorption or releases when a storage material undergoes a phase change from solid to liquid or liquid to gas or vice versa, PCM is especially used in RE for heating and cooling of buildings, PV panels, solar water heating systems and heat. The integration of these PCM provides stability and efficiency in renewable energies technology. On another hand, sensitive heat storage (SHS) is technologies that store thermal energy by heating or cooling a liquid or solid storage medium. Different type of SHS such as boreholes, aquifer storage, underground thermal energy storage, water tank storage, cavern storage and pit storage have been investigated. The choice of thermal storage leads toward water tank storage, which is a cost-effective storage option, ideal for low-temperature applications but its efficiency can be further improved by partially converting the photovoltaic electrical output into useful heat source (for hot water).

- o A distinctive type of battery technology has been used in the electrical system as storage devices. They contrast from one another as far as chemical and electrical properties. For technical and economic reasons, the lead-acid and lithium-ion (Li-ion) are the leading storage technologies used in the photovoltaic systems. Parameters such as energy/price and charge stability (ability to hold their charge) disclose a clear trade-off between cost and lifespan of the batteries. The price of a lithium-ion battery is two to three times that of a lead-acid battery of the same capacity. Li-ion batteries are expected to last up to 20 years of activity and widely used in domestic grid-connected solar PV storage systems, in contrast to only five years estimated for the lead-acid types and mostly used for off-grid storage

systems due to their low initial cost. However, an alternative way of expanding the lifespan of lead-acid batteries is to oversize its storage capacity; this would prevent a deep discharge of the batteries yet would increase the expense of the overall installation. The decision for battery technology has shaped towards Li-ion. The fundamental reason for this decision is the longer lifespan offered by these batteries, and it is more economical in the long term. The short lifespan of the lead-acid batteries would require several substitutions of the battery storages during the activity life of the system, thus expanding the overall cost of ownership.

Modelling and simulation of a PV/T system model were developed to evaluate the performance of the system, based on the linear regression and coefficient to predict the outcome. This is a generalised tool used for the analysis of energy production from the PV cell and PV/T system. A variety of parameters — solar radiation, wind speed, ambient temperature and external series resistance — have been studied to analyse the thermodynamic behaviour of the PV/T system based on the heat transfer (conduction, radiation and convection) and power generated within the system. Heat transferred by convection and radiation from the PV cell to the environment observed, as well as heat transfer by conduction and convection to the flowing water within the attached absorber pipe. Special attention was paid to the regulation of the heat transfer by conduction when changing the external series resistance value. It was determined that the external series resistance of the PV cell could be used to control the useful heat (heat by conduction).

Both thermal and electrical storage was developed using Simscape for the more realistic physical model. As the PV/T system produced electrical and thermal energy, storing those energies for later use is essential. In the simulation results, the water temperature increases by 5⁰C during the first 60 mins,10⁰C during the second 60 mins and 4⁰C during the third 60 mins respectively, when R_{se} was switched to 0, 50 and 10 Ω. The water temperature gradient is higher when R_{se} was 50 Ω. Idle, the battery SOC increases from the initial value by 0.064 within the first hour, from 0.764 to 0.7672 within the second hour and by 0.04 within the third hour. Energy management is used to store energy based on demand, weather conditions and creates the most favourable conditions.

- **What is the efficiency analysis of the proposed PV/T model?**

To better understand the dynamics of the PV/T system. Efficiency analysis of a PV/T system performance was studied.

Simulation results of the PV/T system prove to be efficient and cost-effective and successfully extracted heat from the PV/T system. The maximum PV/T thermal efficiency at zero reduction temperature was 40% and varied with an increasing $(T_w - T_a)/G$ to achieve a thermal efficiency for water temperature decrease from 20 to 14%, 33 to 15% and 44 to 19%, when R_{se} was 0 Ω, 10 Ω and 50 Ω.

Also, PV cell electrical energy conversion efficiency has been improved. The PV/T system presented an increase in electrical efficiency of 11%, 15.5% and 13% when R_{se} was 0 Ω, 10 Ω, 50 Ω, respectively, due to the cooling effect in the PV cell operating temperature; this contributed to mitigating the power loss in the PV cell.

6.2 General conclusion

Challenges due to the rise in the cost of oil, its finite quantity, the effect on petroleum derivative products and the ongoing issues of non-renewable resources coal, oil, and natural gas being limited in the gound and which favoured the development of sustainable power sources. The renewable energies, especially in the area of the photovoltaic technology, turns out to be important as it promotes sustainable energy development over non-renewable resources, and it is less harmful to the environment. Due to its low energy conversion efficiency, the photovoltaic cell is combined with the solar thermal (PV/T) system; however, one of the sub-system performance might overtake the other. This study focused on the improvement of the PV/T system efficiency.

The research work undertaken in this thesis contributed to the understanding of the complex phenomena governing heat transfer occurring in the proposed PV/T model. The temperature profiles, the cooling and heating capacity of the PV/T model are presented.

The study started with the introductory chapter, which highlighted the importance and challenges of simultaneous generation of electrical power and heat using PV/T technology. The research gap and the questions developed out of the need for research on PV/T have been highlighted.

Literature survey related to the area of the research is conducted in Chapter 2. Both solar PV and solar thermal systems are reviewed in-depth to understand state-of-the-art. The mechanism of

solar cell conversion and the influence of the various parameters (illumination, temperature, series and parallel parasitic resistances and the ideal factor) are discussed. Including the performance characteristics of various solar thermal with an emphasis on thermal loss and efficiency. Different energy storage technologies are surveyed in the chapter. The integration of various energy storage options have been discussed based on their characteristics, efficiencies, limitations, capacity applications and other factors.

The PV/T technologies are emphasised in Chapter 3. Different heat recovery/cooling of PV/T technologies and their pros and cons, as well as their reasonable applications, are discussed. Various PV/T system typologies found in the literature, such as — air-based PV/T system, water-based PV/T system, heat pipe-based PV/T system, refrigerant-based PV/T system, BIPVT, SAHP-based PV/T system, nanofluid-based PV/T system and PCM-based PV/T were investigated. The outcome of the investigation presented shortcomings in most of these PV/T systems. The philosophy behind the proposed PV/T new model in this thesis is highlighted. The best option in terms of architectural integration and cost-effective water-based PV/T system, where an absorber pipe attached to the back of the PV cell, in which water flow collects the heat and cool down the PV cell temperature.

In this study, modelling, numerical simulation and validation of the performance of combining the PV cell with the absorber pipe to form the proposed PV/T system have been undertaken. The objective of this work was to improve and balance the PV/T system performances which have been accomplished.

Several simulations in Chapter 4 were undertaken to examine and compare the performance characteristics of a PV cell under a variety of environmental conditions and materials. Analytical sensitivities of the heat transfer by conduction convection and radiation occurring at PV cell boundaries were studied in order to identify the most influential parameters of the thermal management. Some of these parameters were subjected to optimisation based on the numerical data to validate the model. The impact of the development of the PV cell model with R_{se} and the prediction of the useful thermal power results were also analysed. The results of the comparison show that the theoretical model is consistent with the results obtained. The study has proven that the PV cell could be partially converted into a useful heat source (for hot water supply) as R_{se} increases.

The PV/T system has been realised in Simscape, through an interfaced process. The useful heat is validated in Chapter 5, where an absorber pipe is attached at the back of the PV cell to form a

PV/T system. The proposed PV/T model was simulated under different operational conditions to evaluate the ability to cool the PV cell and heating the working fluid. The temperature distributions of the proposed PV/T components based on material properties, external heat sources, and internal heat generation of PV/T cell in steady-state and transient conditions have been analysed. The results revealed that the proposed system could meet the cooling of the PV cell and heating of the working fluid.

The model demonstrated that PV/T system could produce useful energy needed, as well as the electrical power optimisation. From the simulation results obtained, the following conclusions were drawn:

- From numerical modelling of the photovoltaic array, it was possible to study some certain aspects of the system, such as performance, temperature, and thermal and electrical power.

- The performance analysis of the PV system was based on ambient temperature, convective heat transfer, solar radiation and R_{se}. Particular attention was given to R_{se}. The result showed a polynomial equation of R_{se} as a function of P_{PV} and Q_{cond}, expressing the approximation graph curve and a calculation of the coefficient of determination (the goodness of the fit R²). R² is an indicator to judge the quality of linear regression.

- The optimal output of a PV/T system was determined during the simulation and expressed by a polynomial approximation, described in Equation 4.30:

$$R_{se}(Q_{cond}, P_{PV}) = -829 + 3100 \cdot Q_{cond} - 4467 \cdot P_{PV} + 965.3 \cdot Q_{cond}^2 + -223.2 \cdot Q_{cond} \cdot P_{PV} + 145.4 \cdot P_{PV}^2$$

- The selected value of R_{se} and the water flow rate dictate the optimal power output (thermal and electrical) to obtain maximum performance of PV/T systems under varying weather conditions (solar radiation, ambient temperature and wind speed). For a numerical calculation of the optimal power output (useful heat and electrical power) obtained by raising and lowering the R_{se} value, the following results were deduced:

  o The maximum water temperature in the storage tank and the electrical battery varies depending on the value of R_{se}. The Stateflow chart varies the R_{se} according to energy demand.

  o Optimum equilibrium operation (balanced energy mix) is when R_{se} was set to 10 Ω and other parameters are fixed.

- The maximum electrical energy is produced when R_{se} was set to 0 Ω, and other parameters are fixed.

- The maximum thermal energy is produced when R_{se} was set to 50 Ω, and other parameters are fixed.

- For cooling purposes, the average temperature of a PV/T cell and the absorber pipe in a PV/T system was 27°C, and the average water temperature was about 25°C When R_{se} was 0 Ω. The PV/T cell and the water reached a maximum temperature of 44 and 42°C, respectively.

  - For the cooling process, the average electrical power of the PV/T system was 0.36 kW higher than the electrical power of the corresponding PV cell, reflecting the effect of the addition of the cooling system. Consequently, a decrease in the temperature of the elements of the PV/T system compares to the photovoltaic cell as well as an increase of 11% of the electrical efficiency of the PV/T system with respect to the photovoltaic module when R_{se} was 0 Ω.

- For water heating purposes, the average temperature of a cell and the absorber pipe in a PV/T system was 32°C for a water mass flow rate equal to 0.5 kg/s and R_{se} equal to 50 Ω, while average water temperature was about 31°C. The cell and the water reached a maximum temperature of 44 and 42°C, respectively.

  - When R_{se} is adjusted to 50 Ω, the average electrical power of the PV/T system was 0.36 kW, and heat transfer through conduction (Q_{cond}) was 1600 W. Most of the power is dissipated in the form of heat while the working fluid transports the generated heat to the load.

- The maximum PV/T thermal efficiency at zero reduction temperature was 40% and varies with (T_w - T_a)/G increasing within three hours and achieved a thermal efficiency for water temperature decreased from 20 to 14%, 33 to 15% and 44 to 19%, when R_{se} was 0 Ω, 10 Ω and 50 Ω. Improvement in thermal performance was noted.

- It was demonstrated that the implementation of energy management algorithms based on the Stateflow was successful to back up the energy (the thermal/electrical energy mix); also, its use can be prioritised for thermal/electrical energy mix production to the meet the energy demand. The following was achieved: 1) the water temperature in the storage tank increases by 5ºC during the first 60 mins, 10ºC during the second 60 mins

and 4ºC during the third 60 mins respectively, when R_{se} was switched to 0 Ω, 50 Ω and 10 Ω. 2) the *SOC* increased from the initial value by 0.064 during the first hour, from 0.764 to 0.7672 during the second hour and by 0.04 during the third hour for the corresponding value of R_{se}.

- This PV/T system, however, is limited by thermal loss through convection and radiation to the environment.

The performance examination of the proposed PV/T system revealed that a considerable amount of energy can be produced when implementing this novel method. This finding improves the electrical and thermal conversion efficiency of the PV/T system and contributes to the study of the thermodynamics of the proposed PV/T system. This method is, however, limited by thermal loss through convection and radiation to the environment.

6.3 Future recommended research work

Even though the description and dynamic evaluation of the PV/T system have been carried out, the system still requires improvements in some aspects. Thus, further points are recommended to enhance the proposed PV/T system performance as follows:

- The developed PV/T models highlighted the important role of radiative and convective exchanges with the environment in the thermal equilibrium of a photovoltaic cell. It was assumed that the heat transfer coefficient at the back surface of the PV/T cell was perfectly insulated. It is recommended to consider the heat loss for both surfaces (front and back) of the PV/T system as these exchanges are considered for their optimisation.

- In this work, a constant water mass flow rate was considered for cooling the PV/T cell temperature; other liquids and flow rate should be considered, as well as the power consumed by the hydraulic pump which depends on them.

- The overall thermal efficiency and electrical efficiency must be optimised to determine the configuration and installation of PV/T system, followed by its optimisation under various climatic conditions and multiple applications.

- The development of the test bench is not yet implemented due to time constraints (under construction), it is recommended to examine the effectiveness of the water-

based PV/T system under climate conditions. Also, long-term plan testing is required to detect unpredictable operational issues in the system.

- Although a test bench is under construction, large scale demonstration projects (seasonal or annual) evaluation remain essential to address the uncertainties of practice in terms of challenges encountered, such as seasonality, dynamic weather, and sustainability of the system in different climatic regions conditions. Thus, a future study must include a feasibility study of the PV/T system applications in various locations.

- It is necessary to evaluate the potential benefits, the PV/T system performance, the reduced electricity costs, and the reduced greenhouse gas emissions.

- An energy management system, using Stateflow has been applied in this PV/T system. Competing methods can also be implemented in these systems such as fuzzy logic and demand management system (DMS) machine learning.

- It will be interesting to develop optimal operational control tools for a PV/T system to predict the production of power, or the demand for energy, based on solar availability, and weather conditions in practical.

- A future study can consider different methods of finding the maximum power point associated with the DC-DC converter. Also, it will be useful to investigate the management methods and improve the robustness, effectiveness and simplicity of implementation. MPPT algorithms can be developed by applying the control methods of an automated system.

References

Ahmed-Dahmane, M., Malek, A. & Zitoun, T. 2018. Design and analysis of a BIPV/T system with two applications controlled by an air handling unit. *Energy Conversion and Management*, 175: 49–66.

Ahuja, D. & Tatsutani, M. 2009. Sustainable energy for developing countries. *S.A.P.I.EN.S. Surveys and Perspectives Integrating Environment and Society*, (2.1). https://sapiens.revues.org/823 8 June 2016.

Aldubyan, M. & Chiasson, A. 2017. Thermal Study of Hybrid Photovoltaic-Thermal (PVT) Solar Collectors Combined with Borehole Thermal Energy Storage Systems. *Energy Procedia*, 141: 102–108.

Alharbi, F.H. & Kais, S. 2015. Theoretical limits of photovoltaics efficiency and possible improvements by intuitive approaches learned from photosynthesis and quantum coherence. *Renewable and Sustainable Energy Reviews*, 43: 1073–1089.

Ali, M., Iqbal, M.H., Sheikh, N.A., Ali, H.M., Shehryar Manzoor, M., Khan, M.M. & Tamrin, K.F. 2017. Performance Investigation of Air Velocity Effects on PV Modules under Controlled Conditions. *International Journal of Photoenergy*. https://www.hindawi.com/journals/ijp/2017/3829671/ 16 January 2019.

Alta, D., Bilgili, E., Ertekin, C. & Yaldiz, O. 2010. Experimental investigation of three different solar air heaters: Energy and exergy analyses. *Applied Energy*, 87(10): 2953–2973.

Al-Waeli, A.H.A., Chaichan, M.T., Kazem, H.A., Sopian, K. & Safaei, J. 2018. Numerical study on the effect of operating nanofluids of photovoltaic thermal system (PV/T) on the convective heat transfer. *Case Studies in Thermal Engineering*, 12: 405–413.

AlZahrani, A.A. & Dincer, I. 2018. Energy and exergy analyses of a parabolic trough solar power plant using carbon dioxide power cycle. *Energy Conversion and Management*, 158: 476–488.

Amiryar, M. & Pullen, K. 2017. A Review of Flywheel Energy Storage System Technologies and Their Applications. *Applied Sciences*, 7(3): 286.

Anderson, T.N., Duke, M., Morrison, G.L. & Carson, J.K. 2009. Performance of a building integrated photovoltaic/thermal (BIPVT) solar collector. *Solar Energy*, 83(4): 445–455.

Arjyadhara, P. 2013. Analysis of Solar PV cell Performance with Changing Irradiance and Temperature. *International Journal Of Engineering And Computer Science*, 2(1): 214–220.

Aydin, D., Casey, S.P. & Riffat, S. 2015. The latest advancements on thermochemical heat storage systems. *Renewable and Sustainable Energy Reviews*, 41: 356–367.

Azmi, B. z., Sulaiman, M. y., Wahab, M.A. & Alghoul, M. a. 2005. Review of materials for solar thermal collectors. *Anti-Corrosion Methods and Materials*, 52(4): 199–206.

Bai, A., Popp, J., Balogh, P., Gabnai, Z., Pályi, B., Farkas, I., Pintér, G. & Zsiborács, H. 2016. Technical and economic effects of cooling of monocrystalline photovoltaic modules under Hungarian conditions. *Renewable and Sustainable Energy Reviews*, 60: 1086–1099.

Bakari, R., Minja, R.J.A. & Njau, K.N. 2014. Effect of Glass Thickness on Performance of Flat Plate Solar Collectors for Fruits Drying. *Journal of Energy*. https://www.hindawi.com/journals/jen/2014/247287/ 24 July 2017.

Banks, D. & Schäffler, J. 2006. *The potential contribution of renewable energy in South Africa*.

Bellos, E. & Tzivanidis, C. 2018. A review of concentrating solar thermal collectors with and without nanofluids. *Journal of Thermal Analysis and Calorimetry*. https://doi.org/10.1007/s10973-018-7183-1 31 October 2018.

Bensalem, S. & Chegaar, M. 2013. Thermal behavior of parasitic resistances. *Revue des Energies Renouvelables*, 16(1): 171–176.

Blaabjerg, F., Chen, Z. & Kjaer, S.B. 2004. Power electronics as efficient interface in dispersed power generation systems. *IEEE Transactions on Power Electronics*, 19(5): 1184–1194.

Bloem, J.J. 2008. Evaluation of a PV-integrated building application in a well-controlled outdoor test environment. *Building and Environment*, 43(2): 205–216.

Bloss, W.H. & Pfisterer, F. 2013. *Advances in Solar Energy Technology: Proceedings of the Biennial Congress of the International Solar Energy Society, Hamburg, Federal Republic of Germany, 13-18 September 1987*. Elsevier.

Bose, B.K. 2010. Global Warming: Energy, Environmental Pollution, and the Impact of Power Electronics. *IEEE Industrial Electronics Magazine*, 4(1): 6–17.

Boudjelthia, E.A.K., Abbas, M.L., Semaoui, S., Kerkouche, K., Zeraïa, H. & Yaïche, R. 2016. Role of the wind speed in the evolution of the temperature. *Revue des Energies Renouvelables*, 19(1): 119–126.

Brett, G. & Rick, B. 2012. TECHNOLOGICAL NICHES: Concentrated Solar Thermal vs. Photovoltaic Solar.

Brittman, S., Adhyaksa, G.W.P. & Garnett, E.C. 2015. The expanding world of hybrid perovskites: materials properties and emerging applications. *Mrs Communications*, 5(1): 7–26.

Budihardjo, I. & Morrison, G.L. 2009. Performance of water-in-glass evacuated tube solar water heaters. *Solar Energy*, 83(1): 49–56.

Cao, X., Yuan, Y., Xiang, B., Sun, L. & Xingxing, Z. 2018. Numerical investigation on optimal number of longitudinal fins in horizontal annular phase change unit at different wall temperatures. *Energy and Buildings*, 158: 384–392.

Chandel, S.S. & Agarwal, T. 2017. Review of cooling techniques using phase change materials for enhancing efficiency of photovoltaic power systems. *Renewable and Sustainable Energy Reviews*, 73: 1342–1351.

Chander, S., Purohit, A., Sharma, A., Arvind, Nehra, S.P. & Dhaka, M.S. 2015. A study on photovoltaic parameters of mono-crystalline silicon solar cell with cell temperature. *Energy Reports*, 1: 104–109.

Chegaar, M., Hamzaoui, A., Namoda, A., Petit, P., Aillerie, M. & Herguth, A. 2013. Effect of Illumination Intensity on Solar Cells Parameters. *Energy Procedia*, 36: 722–729.

Chel, A. & Kaushik, G. 2018. Renewable energy technologies for sustainable development of energy efficient building. *Alexandria Engineering Journal*, 57(2): 655–669.

Chow, T.T., He, W., Ji, J. & Chan, A.L.S. 2007. Performance evaluation of photovoltaic–thermosyphon system for subtropical climate application. *Solar Energy*, 81(1): 123–130.

Chow, T.T., Pei, G., Fong, K.F., Lin, Z., Chan, A.L.S. & Ji, J. 2009. Energy and exergy analysis of photovoltaic–thermal collector with and without glass cover. *Applied Energy*, 86(3): 310–316.

Chu, J. & Cruickshank, C.A. 2014. Solar-Assisted Heat Pump Systems: A Review of Existing Studies and Their Applicability to the Canadian Residential Sector. *Journal of Solar Energy Engineering*, 136(4): 041013-041013–9.

Corbin, C.D. & Zhai, Z.J. 2010. Experimental and numerical investigation on thermal and electrical performance of a building integrated photovoltaic–thermal collector system. *Energy and Buildings*, 42(1): 76–82.

Covary, T. & Kritzinger, K. 2016. Review of South Africa's Solar Water Heating Rebate Programme. *ResearchGate*. https://www.researchgate.net/publication/308168429_Review_of_South_Africa's_Solar_Water_Heating_Rebate_Programme 31 March 2019.

Cristofari, C., Notton, G. & Canaletti, J.L. 2009. Thermal behavior of a copolymer PV/Th solar system in low flow rate conditions. *Solar Energy*, 83(8): 1123–1138.

Dallas, W., Polupan, O. & Ostapenko, S. 2007. Resonance ultrasonic vibrations for crack detection in photovoltaic silicon wafers. *Measurement Science and Technology*, 18(3): 852.

Dash, A., Agrawal, S., Gairola, S. & Singh, S. 2018. Optimization and Performance Characteristics of Building Integrated Photovoltaic Thermal (BIPVT) System in Cold Climatic Conditions. *Asian Journal of Water, Environment and Pollution*, 15: 63–72.

Delucchi, M. 2011. Wind, Water, and Solar Power for the World. *IEEE Spectrum: Technology, Engineering, and Science News*. http://spectrum.ieee.org/energy/renewables/wind-water-and-solar-power-for-the-world 13 June 2016.

Dhass, A.D., Lakshmi, P. & Natarajan, E. 2016. Investigation of Performance Parameters of Different Photovoltaic Cell Materials using the Lambert-W Function. *Energy Procedia*, 90: 566–573.

Dhoke, A. & Mengede, A. 2017. Degradation analysis of PV modules operating in Australian environment. In *2017 Australasian Universities Power Engineering Conference (AUPEC)*. 2017 Australasian Universities Power Engineering Conference (AUPEC). 1–5.

Dong, F., Hou, M., Feng, H., Jin, Z. & Tian, J. 2016. Research on the reconstruction method of PV module based on the door connection. In *2016 IEEE PES Asia-Pacific Power and Energy Engineering Conference (APPEEC)*. 2016 IEEE PES Asia-Pacific Power and Energy Engineering Conference (APPEEC). 337–341.

Du, D., Darkwa, J. & Kokogiannakis, G. 2013. Thermal management systems for Photovoltaics (PV) installations: A critical review. *Solar Energy*, 97: 238–254.

Dubey, S., Sandhu, G.S. & Tiwari, G.N. 2009. Analytical expression for electrical efficiency of PV/T hybrid air collector. *Applied Energy*, 86(5): 697–705.

Dubey, S., Solanki, S.C. & Tiwari, A. 2009. Energy and exergy analysis of PV/T air collectors connected in series. *Energy and Buildings*, 41(8): 863–870.

Duffie, J.A. & Beckman, W.A. 1991. *Solar Engineering of Thermal Processes*. 2 edition. New York: Wiley-Interscience.

Dupré, O., Niesen, B., De Wolf, S. & Ballif, C. 2018. Field Performance versus Standard Test Condition Efficiency of Tandem Solar Cells and the Singular Case of Perovskites/Silicon Devices. *The Journal of Physical Chemistry Letters*, 9(2): 446–458.

Eberhard, A. & Naude, R. 2016. The South African Renewable Energy Independent Power Producer Procurement Programme: A review and lessons learned. *Journal of Energy in Southern Africa*, 27(4): 1–14.

EIA. 2016. *International Energy Outlook 2016*. Washington: statistical and analytical agency within the U.S. https://www.eia.gov/outlooks/ieo/pdf/0484(2016).pdf.

EIA. 2018. U.S. Energy Facts - Energy Explained, Your Guide To Understanding Energy - Energy Information Administration. *Independent statistic and analysis, U.S Energy information Administration*. https://www.eia.gov/energyexplained/?page=us_energy_home 15 May 2019.

EIA. 2019. Use of Energy in United stated. *Energy Information Administration*. https://www.eia.gov/energyexplained/index.php?page=us_energy_homes 4 May 2019.

Elbreki, A.M., Alghoul, M.A., Al-Shamani, A.N., Ammar, A.A., Yegani, B., Aboghrara, A.M., Rusaln, M.H. & Sopian, K. 2016. The role of climatic-design-operational parameters on combined PV/T collector performance: A critical review. *Renewable and Sustainable Energy Reviews*, 57: 602–647.

El-Sebaii, A.A., Aboul-Enein, S., Ramadan, M.R.I., Shalaby, S.M. & Moharram, B.M. 2011. Thermal performance investigation of double pass-finned plate solar air heater. *Applied Energy*, 88(5): 1727–1739.

Gang, P., Huide, F., Tao, Z. & Jie, J. 2011. A numerical and experimental study on a heat pipe PV/T system. *Solar Energy*, 85(5): 911–921.

Garg, H.P. & Adhikari, R.S. 1999. Performance analysis of a hybrid photovoltaic/thermal (PV/T) collector with integrated CPC troughs. *International Journal of Energy Research*, 23(15): 1295–1304.

Großer, S., Lausch, D., Werner, M., Swatek, S., Mergner, M., Naumann, V. & Hagendorf, C. 2012. Shunt Analysis in Solar Cells - Electro-Optical Classification and High Resolution Defect Diagnostics. *Energy Procedia*, 27: 7–12.

Guerrero, J., Muñoz, Y., Ibáñez, F. & Ospino, A. 2014. Analysis of mismatch and shading effects in a photovoltaic array using different technologies. *IOP Conference Series: Materials Science and Engineering*, 59(1): 012007.

Guiqiang, L., Gang, P., Su, Y., Xi, Z. & Jie, J. 2012. Preliminary study based on building-integrated compound parabolic concentrators (CPC) PV/thermal technology. *Energy Procedia*, 14: 343–350.

Hammami, M., Torretti, S., Grimaccia, F. & Grandi, G. 2017. Thermal and Performance Analysis of a Photovoltaic Module with an Integrated Energy Storage System. *Applied Sciences*, 7: 1107.

Han, H., Dong, X., Li, B., Yan, H., Verlinden, P.J., Liu, J., Huang, J., Liang, Z. & Shen, H. 2018. Degradation analysis of crystalline silicon photovoltaic modules exposed over 30 years in hot-humid climate in China. *Solar Energy*, 170: 510–519.

Hasan, A., McCormack, S.J., Huang, M.J., Sarwar, J. & Norton, B. 2015. Increased photovoltaic performance through temperature regulation by phase change materials: Materials comparison in different climates. *Solar Energy*, 115: 264–276.

Hassan, A., Shakeel Laghari, M. & Rashid, Y. 2016. Micro-Encapsulated Phase Change Materials: A Review of Encapsulation, Safety and Thermal Characteristics. *Sustainability*, 8(10): 1046.

Haug, A. 1983. Auger recombination in direct-gap semiconductors: band-structure effects. *Journal of Physics C: Solid State Physics*, 16(21): 4159.

Hegazy, A.A. 2000. Comparative study of the performances of four photovoltaic/thermal solar air collectors. *Energy Conversion and Management*, 41(8): 861–881.

Hendricks, J.H.C. & van Sark, W.G.J.H.M. 2013. Annual performance enhancement of building integrated photovoltaic modules by applying phase change materials. *Progress in Photovoltaics: Research and Applications*, 21(4): 620–630.

Henry, C.H. 1980. Limiting efficiencies of ideal single and multiple energy gap terrestrial solar cells. *Journal of Applied Physics*, 51(8): 4494–4500.

Hermann, W., Wiesner, W. & Vaassen, W. 1998. Hot spot investigations on PV modules -- New concepts for a test standard and consequences for module design with respect to bypass diodes. https://www.osti.gov/biblio/304449 1 June 2018.

Herrmann, W., Wiesner, W. & Vaassen, W. 1997. Hot spot investigations on PV modules-new concepts for a test standard and consequences for module design with respect to bypass diodes. In *Conference Record of the Twenty Sixth IEEE Photovoltaic Specialists Conference - 1997*. Conference Record of the Twenty Sixth IEEE Photovoltaic Specialists Conference - 1997. 1129–1132.

Hsu, H.-J., Hsu, C.-H. & Tsai, C.-C. 2013. The Effect of Bandgap Graded Absorber on the Performance of a-Si1–xGex:H Single-Junction Cells with μc-SiOx:H N-Type Layer. *International Journal of Photoenergy*. https://www.hindawi.com/journals/ijp/2013/364638/ 8 February 2019.

Humada, A.M., Samsuri, F.B., Hojabria, M., Mohamed, M.B., Sulaiman, M.H.B. & Dakheel, T.H. 2014. Modeling of photovoltaic solar array under different levels of partial shadow conditions. In *2014 16th International Power Electronics and Motion Control Conference and Exposition*. 2014 16th International Power Electronics and Motion Control Conference and Exposition. 461–465.

Ibrahim, A., Othman, M.Y., Ruslan, M.H., Mat, S. & Sopian, K. 2011. Recent advances in flat plate photovoltaic/thermal (PV/T) solar collectors. *Renewable and Sustainable Energy Reviews*, 15(1): 352–365.

Infield, D., Mei, L. & Eicker, U. 2004. Thermal performance estimation for ventilated PV facades. *Solar Energy*, 76(1–3): 93–98.

Ion, I.V. & Martins, J.G. 2006. Design, developing and testing of a solar air collector. *The Annals of DUNAREA DE JOS. University of Galati FASCICLE IV Refrigerating Technique, Internal Combustion Engines, Boilers and Turbines*: 1–4.

Islam, M.N., Rahman, M.Z. & Mominuzzaman, S.M. 2014. The effect of irradiation on different parameters of monocrystalline photovoltaic solar cell. In *2014 3rd International Conference on the Developments in Renewable Energy Technology (ICDRET)*. 2014 3rd International Conference on the Developments in Renewable Energy Technology (ICDRET). 1–6.

Jansen, K.W. & Delahoy, A.E. 2003. A laboratory technique for the evaluation of electrochemical transparent conductive oxide delamination from glass substrates. *Thin Solid Films*, 423(2): 153–160.

Jha, A.R. 2009. *Solar Cell Technology and Applications*. Auerbach Publications. https://www.taylorfrancis.com/books/9781420081787 30 December 2018.

Jianfeng, Q., Jili, Z. & Liangdong, M.A. 2010. Analysis of a New Photovoltaic Thermal Building Integration System and Correlative Technology. *Building Energy & Environment*, 29(2): 12-16,66.

Jonas, D., Theis, D., Felgner, F. & Frey, G. 2017. A TRNSYS-based simulation framework for the analysis of solar thermal and heat pump systems. *Applied Solar Energy*, 53(2): 126–137.

Jouhara, H., Chauhan, A., Nannou, T., Almahmoud, S., Delpech, B. & Wrobel, L.C. 2017. Heat pipe based systems - Advances and applications. *Energy*, 128: 729–754.

Kajihara, A. & Harakawa, A.T. 2005. Model of photovoltaic cell circuits under partial shading. In *2005 IEEE International Conference on Industrial Technology*. 2005 IEEE International Conference on Industrial Technology. 866–870.

Kalaiselvam, S. & Parameshwaran, R. 2014. Chapter 6 - Thermochemical Energy Storage. In S. Kalaiselvam & R. Parameshwaran, eds. *Thermal Energy Storage Technologies for Sustainability*. Boston: Academic Press: 127–144. http://www.sciencedirect.com/science/article/pii/B9780124172913000062 29 March 2019.

Kalogirou, S. 2003. The potential of solar industrial process heat applications. *Applied Energy*, 76(4): 337–361.

Kalogirou, S.A. & Tripanagnostopoulos, Y. 2007. Industrial application of PV/T solar energy systems. *Applied Thermal Engineering*, 27(8): 1259–1270.

Kamel, R.S., Fung, A.S. & Dash, P.R.H. 2015. Solar systems and their integration with heat pumps: A review. *Energy and Buildings*, 87: 395–412.

Kapur, J., Proost, K. & Smith, C.A. 2009. Determination of moisture ingress through various encapsulants in glass/glass laminates. In *2009 34th IEEE Photovoltaic Specialists Conference (PVSC)*. 2009 34th IEEE Photovoltaic Specialists Conference (PVSC). 001210–001214.

Karim, M.A. & Hawlader, M.N.A. 2006. Performance investigation of flat plate, v-corrugated and finned air collectors. *Energy*, 31(4): 452–470.

Kempe, M.D. 2005. Control of moisture ingress into photovoltaic modules. In *Conference Record of the Thirty-first IEEE Photovoltaic Specialists Conference, 2005.* Conference Record of the Thirty-first IEEE Photovoltaic Specialists Conference, 2005. 503–506.

Kern, E.C., Jr. & Russell, M.C. 1978. Combined photovoltaic and thermal hybrid collector systems. In 13th Photovoltaic Specialists Conference. 1153–1157. http://adsabs.harvard.edu/abs/1978pvsp.conf.1153K 18 July 2017.

Khan, F., Singh, S.N. & Husain, M. 2010. Effect of illumination intensity on cell parameters of a silicon solar cell. *Solar Energy Materials and Solar Cells*, 94(9): 1473–1476.

Khelifa, A., Touafek, K., Benmoussa, H., Tabet, I. & Adouane, M. 2014. Hot water system based on the hybrid solar collector photovoltaic/thermal PVT. In *2014 15th International Conference on Sciences and Techniques of Automatic Control and Computer Engineering (STA)*. 2014 15th International Conference on Sciences and Techniques of Automatic Control and Computer Engineering (STA). 537–540.

Khelifa, A., Touafek, K., Moussa, H.B., Tabet, I., hocine, H.B. cheikh E. & Haloui, H. 2015. Analysis of a Hybrid Solar Collector Photovoltaic Thermal (PVT). *Energy Procedia*, 74: 835–843.

Khoukhi, M. & Maruyama, S. 2005. Theoretical approach of a flat plate solar collector with clear and low-iron glass covers taking into account the spectral absorption and emission within glass covers layer. *Renewable Energy*, 30(8): 1177–1194.

Kim, J.-H., Kim, J.-T., Kim, J.-H. & Kim, J.-T. 2012. The Experimental Performance of an Unglazed PVT Collector with Two Different Absorber Types, The Experimental Performance of an Unglazed PVT Collector with Two Different Absorber Types. *International Journal of Photoenergy, International Journal of Photoenergy*, 2012, 2012: e312168.

Kim, J.-H., Park, S.-H., Kang, J.-G. & Kim, J.-T. 2014. Experimental Performance of Heating System with Building-integrated PVT (BIPVT) Collector. *Energy Procedia*, 48(Supplement C): 1374–1384.

Kobek, M.L.P., Ugarte, A. & Aguilar, G.C. 2015. Shale Gas in the United States: Transforming Energy Security in the Twenty-first Century. *Norteamérica*, 10(1): 7–38.

Koech, R.K., Ondieki, H.O., Tonui, J.K. & Rotich, S.K. 2012. *A Steady State Thermal Model For Photovoltaic/Thermal (PV/T) System Under Various Conditions*.

Kostic, L.T., Pavlovic, T.M. & Pavlovic, Z.T. 2010. Influence of reflectance from flat aluminum concentrators on energy efficiency of PV/Thermal collector. *Applied Energy*, 87(2): 410–416.

Kostić, L.T., Pavlović, T.M. & Pavlović, Z.T. 2010. Optimal design of orientation of PV/T collector with reflectors. *Applied Energy*, 87(10): 3023–3029.

Kosyachenko, L.A. 2011. Thin-Film Photovoltaics as a Mainstream of Solar Power Engineering. *Solar Cells - Thin-Film Technologies*. http://www.intechopen.com/books/solar-cells-thin-film-technologies/thin-film-photovoltaics-as-a-mainstream-of-solar-power-engineering 21 February 2018.

Kreith, F., Manglik, R.M. & Bohn, M.S. 2010. *Principles of Heat Transfer*. 7 edition. Cengage Learning.

Kribus, A., Kaftori, D., Mittelman, G., Hirshfeld, A., Flitsanov, Y. & Dayan, A. 2006. A miniature concentrating photovoltaic and thermal system. *Energy Conversion and Management*, 47(20): 3582–3590.

Kumar, A., Kumar, S., Nagar, U. & Yadav, A. 2013. Experimental Study of Thermal Performance of One-Ended Evacuated Tubes for Producing Hot Air. *Journal of Solar Energy*. https://www.hindawi.com/journals/jse/2013/524715/ 1 December 2018.

Kumar, R. & Rosen, M.A. 2011. Performance evaluation of a double pass PV/T solar air heater with and without fins. *Applied Thermal Engineering*, 31(8–9): 1402–1410.

Lalwani, M. & Singh, M. 2010. Investigation of Solar Photovoltaic Simulation Softwares. , 1(3): 17.

Lan, Y., Chen, H. & Wei, P. 2012. Performance Investigation of a Hybrid Photovoltaic/Thermal Water Heater in Tibet for Residential Buildings. In *Proceedings of the 2012 Second International Conference on Electric Technology and Civil Engineering*. ICETCE '12. Washington, DC, USA: IEEE Computer Society: 1930–1933. http://dx.doi.org/10.1109/ICETCE.2012.474 5 July 2016.

Leung, P., Li, X., Ponce de León, C., Berlouis, L., Low, C.T.J. & Walsh, F.C. 2012. Progress in redox flow batteries, remaining challenges and their applications in energy storage. *RSC Advances*, 2(27): 10125-.

Li, G., Lu, X., Kim, J.Y., Meinhardt, K.D., Chang, H.J., Canfield, N.L. & Sprenkle, V.L. 2016. Advanced intermediate temperature sodium-nickel chloride batteries with ultra-high energy density. *Nature Communications*, 7: 10683.

Li, K., Liu, C., Chen, Y. & Liu, G.L. 2016. Upgrading both Geothermal and Solar Energy. In *1st Workshop on Geothermal Reservoir Engineering Stanford University*. California: 1–17.

Li, M., Li, G.L., Ji, X., Yin, F. & Xu, L. 2011. The performance analysis of the Trough Concentrating Solar Photovoltaic/Thermal system. *Energy Conversion and Management*, 52(6): 2378–2383.

Lin, W., Gao, W. & Liu, T. 2006. A parametric study on the thermal performance of cross-corrugated solar air collectors. *Applied Thermal Engineering*, 26(10): 1043–1053.

Lindefelt, U. 1994. Heat generation in semiconductor devices. *Journal of Applied Physics*, 75(2): 942–957.

Löper, P., Pysch, D., Richter, A., Hermle, M., Janz, S., Zacharias, M. & Glunz, S.W. 2012. Analysis of the Temperature Dependence of the Open-Circuit Voltage. *Energy Procedia*, 27: 135–142.

Lu, F., Guo, S., Walsh, T.M. & Aberle, A.G. 2013. Improved PV Module Performance under Partial Shading Conditions. *Energy Procedia*, 33: 248–255.

Lu, W.-C. 2017. Greenhouse Gas Emissions, Energy Consumption and Economic Growth: A Panel Cointegration Analysis for 16 Asian Countries. *International Journal of Environmental Research and Public Health*, 14(11). https://www.ncbi.nlm.nih.gov/pmc/articles/PMC5708075/ 21 February 2018.

Luo, W., Sheng Khoo, Y., Hacke, P., Naumann, V., Lausch, D., P. Harvey, S., Prakash Singh, J., Chai, J., Wang, Y., G. Aberle, A. & Ramakrishna, S. 2017. Potential-induced degradation in photovoltaic modules: a critical review. *Energy & Environmental Science*, 10(1): 43–68.

Luo, X., Wang, J., Dooner, M. & Clarke, J. 2015. Overview of current development in electrical energy storage technologies and the application potential in power system operation. *Applied Energy*, 137: 511–536.

Lutyński, M. 2017. An overview of potential benefits and limitations of Compressed Air Energy Storage in abandoned coal mines. *IOP Conference Series: Materials Science and Engineering*, 268: 012006.

Lyu, C., Leong, W.H., Zheng, M., Chen, G., Ye, S. & Liu, Y. 2017. Verification and analysis of a dynamic simulation model of ground-coupled heat pump with solar seasonal heat storage system. *Procedia Engineering*, 205: 3154–3161.

Ma, L., Lu, Z., Zhang, J. & Liang, R. 2010. Thermal performance analysis of the glass evacuated tube solar collector with U-tube. *Building and Environment*, 45(9): 1959–1967.

Maghami, M.R., Hizam, H., Gomes, C., Radzi, M.A., Rezadad, M.I. & Hajighorbani, S. 2016. Power loss due to soiling on solar panel: A review. *Renewable and Sustainable Energy Reviews*, 59: 1307–1316.

Mahmood, N. & Hou, Y. 2014. Electrode Nanostructures in Lithium-Based Batteries. *Advanced Science*, 1(1). https://www.ncbi.nlm.nih.gov/pmc/articles/PMC5115266/ 22 March 2019.

Mangold, D., Schmidt, T. & Müller-Steinhagen, H. 2004. Seasonal Thermal Energy Storage in Germany. *Structural Engineering International*, 14(3): 230–232.

Markvart, T., McEvoy, A. & Castaner, L. 2003. *Practical Handbook of Photovoltaics: Fundamentals and Applications*. Elsevier.

Matsukawa, H. & Kurokawa, K. 2005. Temperature fluctuation analysis of photovoltaic modules at short time interval. In *Conference Record of the Thirty-first IEEE Photovoltaic Specialists Conference, 2005*. Conference Record of the Thirty-first IEEE Photovoltaic Specialists Conference, 2005. 1816–1819.

McKeon, B.B., Furukawa, J. & Fenstermacher, S. 2014. Advanced Lead–Acid Batteries and the Development of Grid-Scale Energy Storage Systems. *Proceedings of the IEEE*, 102(6): 951–963.

Md Kafiul Islam, T.A. 2011. Analysis of Maximum Possible Utilization of Solar Radiation on a Solar Photovoltaic Cell with a Proposed Model. , 1: 66–69.

Mei, L., Infield, D., Eicker, U. & Fux, V. 2003. Thermal modelling of a building with an integrated ventilated PV façade. *Energy and Buildings*, 35(6): 605–617.

Meyer, E.L. & Dyk, E.E. van. 2004. Assessing the reliability and degradation of photovoltaic module performance parameters. *IEEE Transactions on Reliability*, 53(1): 83–92.

Mishra, R. & Saxena, R. 2017. Comprehensive review of control schemes for battery and super-capacitor energy storage system. In *2017 7th International Conference on Power Systems (ICPS)*. 2017 7th International Conference on Power Systems (ICPS). 702–707.

Mohammed, M.F., Rahim, N.A., Hasanuzzaman, M. & Rivai, A. 2013. Effect on insulation of photovoltaic thermal water collector (pvtw). In *2013 IEEE Conference on Clean Energy and Technology (CEAT)*. 2013 IEEE Conference on Clean Energy and Technology (CEAT). 307–311.

Mohammedi, A., Rekioua, D., Rekioua, T. & Bacha, S. 2016. Valve Regulated Lead Acid battery behavior in a renewable energy system under an ideal Mediterranean climate. *International Journal of Hydrogen Energy*, 41(45): 20928–20938.

Molina, M.G. 2012. Distributed energy storage systems for applications in future smart grids. In *2012 Sixth IEEE/PES Transmission and Distribution: Latin America Conference and Exposition (T D-LA)*. 2012 Sixth IEEE/PES Transmission and Distribution: Latin America Conference and Exposition (T D-LA). 1–7.

Monitor, T. & Kurtz, S. 2012. Photovoltaic Module Reliability Workshop 2012: February 28 - March 1, 2012. : 1086.

Moore, A.L. & Shi, L. 2014. Emerging challenges and materials for thermal management of electronics. *Materials Today*, 17(4): 163–174.

Moradi, K., Ali Ebadian, M. & Lin, C.-X. 2013. A review of PV/T technologies: Effects of control parameters. *International Journal of Heat and Mass Transfer*, 64: 483–500.

Moussavou, A.A.A., Adonis, M. & Raji, A. 2016. Design and simulation of solar cell system under different environmental conditions. In *2016 International Conference on the Industrial and Commercial Use of Energy (ICUE)*. 2016 International Conference on the Industrial and Commercial Use of Energy (ICUE). 270–277.

Moussavou, A.A.A., Adonis, M. & Raji, A. 2015. Microgrid energy management system control strategy. In *2015 International Conference on the Industrial and Commercial Use of Energy (ICUE)*. 2015 International Conference on the Industrial and Commercial Use of Energy (ICUE). 147–154.

Munoz, M.A., Alonso-García, M.C., Vela, N. & Chenlo, F. 2011. Early degradation of silicon PV modules and guaranty conditions. *Solar Energy*, 85(9): 2264–2274.

Musallam, A.T., Mohd, Y.O. & MohdHafidz, R. 2014. A Review Paper on PV/T Combination Flat Plate Collector System and Design. *World Essays Journal*, 1(1): 1–5.

Nadeem, F., Hussain, S.M.S., Tiwari, P.K., Goswami, A.K. & Ustun, T.S. 2019. Comparative Review of Energy Storage Systems, Their Roles, and Impacts on Future Power Systems. *IEEE Access*, 7: 4555–4585.

Nagarajan, P.K., Subramani, J., Suyambazhahan, S. & Sathyamurthy, R. 2014. Nanofluids for Solar Collector Applications: A Review. *Energy Procedia*, 61: 2416–2434.

Nayak, J.K., Kedare, S.B., Banerjee, R., Bandyopadhyay, S., Desai, N.B., Paul, S. & Kapila, A. 2015. A1 MW National Solar Thermal Research Cum Demonstration Facility at Gwalpahari, Haryana, India. *Current Science*, 109(8): 1445.

Ndiaye, A., Charki, A., Kobi, A., Kébé, C.M.F., Ndiaye, P.A. & Sambou, V. 2013. Degradations of silicon photovoltaic modules: A literature review. *Solar Energy*, 96: 140–151.

Nilsson, J., Håkansson, H. & Karlsson, B. 2007. Electrical and thermal characterization of a PV-CPC hybrid. *Solar Energy*, 81(7): 917–928.

Norton, B. 2006. A-to-Z Guide to Thermodynamics, Heat and Mass Transfer, and Fluids Engineering: AtoZ. *SOLAR ENERGY*. DOI: 10.1615/AtoZ.s.solar_energy.

Nunes, A.N. 2018. Energy changes in Portugal. An Overview of the Last Century. *Méditerranée. Revue géographique des pays méditerranéens / Journal of Mediterranean geography*, (130). http://journals.openedition.org/mediterranee/10113 6 May 2019.

Odeh, S. 2018. Thermal Performance of Dwellings with Rooftop PV Panels and PV/Thermal Collectors. *Energies*, 11: 1879.

Oman, H. 1998. Battery News From The Intersociety Energy Conversion Engineering Conference. *IEEE Aerospace and Electronic Systems Magazine*, 13(3): 23–31.

Osterwald, C.R., Anderberg, A., Rummel, S. & Ottoson, L. 2002. Degradation analysis of weathered crystalline-silicon PV modules. In *Conference Record of the Twenty-Ninth IEEE Photovoltaic Specialists Conference, 2002.* Conference Record of the Twenty-Ninth IEEE Photovoltaic Specialists Conference, 2002. 1392–1395.

Osterwald, C.R. & McMahon, T.J. 2009. History of accelerated and qualification testing of terrestrial photovoltaic modules: A literature review. *Progress in Photovoltaics: Research and Applications*, 17(1): 11–33.

Othman, M.Y., Yatim, B., Sopian, K. & Abu Bakar, M.N. 2007. Performance studies on a finned double-pass photovoltaic-thermal (PV/T) solar collector. *Desalination*, 209(1): 43–49.

Ould Amrouche, S., Rekioua, D., Rekioua, T. & Bacha, S. 2016. Overview of energy storage in renewable energy systems. *International Journal of Hydrogen Energy*, 41(45): 20914–20927.

Owusu, P.A. & Asumadu-Sarkodie, S. 2016. A review of renewable energy sources, sustainability issues and climate change mitigation S. Dubey, ed. *Cogent Engineering*, 3(1): 1167990.

Oyedepo, S.O. 2012. Energy and sustainable development in Nigeria: the way forward. *Energy, Sustainability and Society*, 2(1): 15.

Pardo, P., Deydier, A., Anxionnaz-Minvielle, Z., Rougé, S., Cabassud, M. & Cognet, P. 2014. A review on high temperature thermochemical heat energy storage. *Renewable and Sustainable Energy Reviews*, 32: 591–610.

pauly, L., Rekha, L., Vazhappilly, C.V. & Melvinraj, C.R. 2016. Numerical Simulation for Solar Hybrid Photovoltaic Thermal Air Collector. *Procedia Technology*, 24: 513–522.

Pavlov, G.K. & Olesen, B.W. 2012. Thermal energy storage—A review of concepts and systems for heating and cooling applications in buildings: Part 1—Seasonal storage in the ground. *HVAC&R Research*, 18(3): 515–538.

Peña-Alzola, R., Sebastián, R., Quesada, J. & Colmenar, A. 2011. Review of flywheel based energy storage systems. In *2011 International Conference on Power Engineering, Energy and Electrical Drives*. 2011 International Conference on Power Engineering, Energy and Electrical Drives. 1–6.

Quintana, M.A., King, D.L., McMahon, T.J. & Osterwald, C.R. 2002. Commonly observed degradation in field-aged photovoltaic modules. In *Conference Record of the Twenty-Ninth IEEE Photovoltaic Specialists Conference, 2002.* Conference Record of the Twenty-Ninth IEEE Photovoltaic Specialists Conference, 2002. 1436–1439.

Rabii, A.B., Jraidi, M. & Bouazzi, A.S. 2003. Investigation of the degradation in field-aged photovoltaic modules. In *Proceedings of 3rd World Conference onPhotovoltaic Energy Conversion, 2003.* Proceedings of 3rd World Conference onPhotovoltaic Energy Conversion, 2003. 2004-2006 Vol.2.

Raman, V. & Tiwari, G.N. 2009. A comparison study of energy and exergy performance of a hybrid photovoltaic double-pass and single-pass air collector. *International Journal of Energy Research*, 33(6): 605–617.

Ramaprabha, R. & Mathur, B.L. 2012. A comprehensive review and analysis of solar photovoltaic array configurations under partial shaded conditions. *International Journal of Photoenergy*, 2012. https://www.hindawi.com/journals/ijp/2012/120214/abs/ 2 August 2017.

Ramos, A., Chatzopoulou, M.A., Guarracino, I., Freeman, J. & Markides, C.N. 2017. Hybrid photovoltaic-thermal solar systems for combined heating, cooling and power provision in the urban environment. *Energy Conversion and Management*, 150: 838–850.

Realini, A. 2003. Mean Time Before Failure of Photovoltaic modules. : 58.

Reyna, J.L. & Chester, M.V. 2017. Energy efficiency to reduce residential electricity and natural gas use under climate change. *Nature Communications*, 8. https://www.ncbi.nlm.nih.gov/pmc/articles/PMC5440627/ 4 May 2019.

Richarz, C. & Schulz, C. 2013. *Energy efficiency refurbishments: Principles, Details, Case studies.* Walter de Gruyter.

Riordan, C. & Hulstron, R. 1990. What is an air mass 1.5 spectrum? (solar cell performance calculations). In *IEEE Conference on Photovoltaic Specialists*. IEEE Conference on Photovoltaic Specialists. 1085–1088 vol.2.

Rosell, J.I., Vallverdú, X., Lechón, M.A. & Ibáñez, M. 2005. Design and simulation of a low concentrating photovoltaic/thermal system. *Energy Conversion and Management*, 46(18–19): 3034–3046.

Ross, R.G. & Gonzalez, C.C. 1980. Reference conditions for reporting terrestrial photovoltaic performance. *Proc. Annu. Meet. - Am. Sect. Int. Sol. Energy Soc.; (United States)*, 3.2. https://www.osti.gov/biblio/6378041-reference-conditions-reporting-terrestrial-photovoltaic-performance 13 January 2019.

Royne, A., Dey, C.J. & Mills, D.R. 2005. Cooling of photovoltaic cells under concentrated illumination: a critical review. *Solar Energy Materials and Solar Cells*, 86(4): 451–483.

Rupnik, B. & Westbrook, O. 2014. Ambient temperature correction of photovoltaic system performance data. In *Photovoltaic Specialist Conference (PVSC), 2014 IEEE 40th*. Photovoltaic Specialist Conference (PVSC), 2014 IEEE 40th. 1973–1977.

Rycroft, M., Editor, F. & Publishers, E.E. 2016. Solar water heater rollout programme gains momentum. *EE Publishers*. https://www.ee.co.za/article/solar-water-heater-rollout-programme-gains-momentum.html 31 March 2019.

Saadah, M., Hernandez, E. & Balandin, A.A. 2017. Thermal Management of Concentrated Multi-Junction Solar Cells with Graphene-Enhanced Thermal Interface Materials. *Applied Sciences*, 7(6): 589.

Saitoh, H., Hamada, Y., Kubota, H., Nakamura, M., Ochifuji, K., Yokoyama, S. & Nagano, K. 2003. Field experiments and analyses on a hybrid solar collector. *Applied Thermal Engineering*, 23(16): 2089–2105.

Salem, F. & Awadallah, M.A. 2016. Detection and assessment of partial shading in photovoltaic arrays. *Journal of Electrical Systems and Information Technology*, 3(1): 23–32.

Samantaray, P. & Sasmita, S. 2016. Performance of solar photovoltaic module under partial shading conditions. In *2016 10th International Conference on Intelligent Systems and Control (ISCO)*. 2016 10th International Conference on Intelligent Systems and Control (ISCO). 1–4.

Sandberg, M. & Moshfegh, B. 2002. Buoyancy-induced air flow in photovoltaic facades: Effect of geometry of the air gap and location of solar cell modules. *Building and Environment*, 37(3): 211–218.

Sandnes, B. & Rekstad, J. 2002. A photovoltaic/thermal (PV/T) collector with a polymer absorber plate. Experimental study and analytical model. *Solar Energy*, 72(1): 63–73.

Sarbu, I. & Calin, S. 2018. A Comprehensive Review of Thermal Energy Storage. *Sustainability*, 10(191): 2–32.

Sarkar, T., Bhattacharjee, A., Mukhopadhyay, K., Bhattacharya, K.D. & Saha, H. 2018. Energy Non-Availability in Distribution Grids with Heavy Penetration of Solar Power: Assessment and Mitigation through Solar Smoother. *Energies*, 11(4): 709.

Sathe, T.M. & Dhoble, A.S. 2017. A review on recent advancements in photovoltaic thermal techniques. *Renewable and Sustainable Energy Reviews*, 76: 645–672.

Saxena, A., Jhamaria, N., Singh, S. & Sahoo, S.S. 2016. Numerical analysis of convective and radiative heat losses from trapezoidal cavity receiver in LFR systems. *Solar Energy*, 137: 308–316.

Schwingshackl, C., Petitta, M., Wagner, J.E., Belluardo, G., Moser, D., Castelli, M., Zebisch, M. & Tetzlaff, A. 2013. Wind Effect on PV Module Temperature: Analysis of Different Techniques for an Accurate Estimation. *Energy Procedia*, 40: 77–86.

SEA. 2010. Mass SWH Implementation in the Western Cape: A strategic analysis for the Provincial Government of the Western Cape. *Climate Technology Centre & Network*. http://www.cityenergy.org.za/uploads/resource_41.pdf 31 March 2019.

Senthil, R. & Sundaram, P. 2018. EFFECTIVE UTILIZATION OF PARABOLIC DISH SOLAR COLLECTORS FOR THE HEATING AND THERMO-ELECTRIC POWER GENERATION. , 9(2): 657–662.

Shamachurn, H. & Betts, T. 2016. Experimental Study of the Degradation of Silicon Photovoltaic Devices under Ultraviolet Radiation Exposure. *Journal of Solar Energy*. https://www.hindawi.com/journals/jse/2016/2473245/ 6 May 2019.

Sharma, D.K., Verma, V. & Singh, A.P. 2014. Review and Analysis of Solar Photovoltaic Softwares. *International Journal of Current Engineering and Technology*, 4(2): 7.

da Silva, R.M. & Fernandes, J.L.M. 2010. Hybrid photovoltaic/thermal (PV/T) solar systems simulation with Simulink/Matlab. *Solar Energy*, 84(12): 1985–1996.

Singh, P. & Ravindra, N.M. 2012. Temperature dependence of solar cell performance—an analysis. *Solar Energy Materials and Solar Cells*, 101: 36–45.

Singh, R., Alapatt, G.F. & Lakhtakia, A. 2013. Making Solar Cells a Reality in Every Home: Opportunities and Challenges for Photovoltaic Device Design. *IEEE Journal of the Electron Devices Society*, 1(6): 129–144.

Sinha, S. & Chandel, S.S. 2014. Review of software tools for hybrid renewable energy systems. *Renewable and Sustainable Energy Reviews*, 32: 192–205.

Skoczek, A., Sample, T., Dunlop, E.D. & Ossenbrink, H.A. 2008. Electrical performance results from physical stress testing of commercial PV modules to the IEC 61215 test sequence. *Solar Energy Materials and Solar Cells*, 92(12): 1593–1604.

Solanki, S.C., Dubey, S. & Tiwari, A. 2009. Indoor simulation and testing of photovoltaic thermal (PV/T) air collectors. *Applied Energy*, 86(11): 2421–2428.

Sopian, K., Yigit, K.S., Liu, H.T., Kakaç, S. & Veziroglu, T.N. 1996. Performance analysis of photovoltaic thermal air heaters. *Energy Conversion and Management*, 37(11): 1657–1670.

Speirs, J., McGlade, C. & Slade, R. 2015. Uncertainty in the availability of natural resources: Fossil fuels, critical metals and biomass. *Energy Policy*, 87: 654–664.

Stocker, A., Großmann, A., Madlener, R. & Wolter, M.I. 2011. Sustainable energy development in Austria until 2020: Insights from applying the integrated model "e3.at". *Energy Policy*, 39(10–2): 6082–6099.

Straube, H., Wagner, J.-M. & Breitenstein, O. 2009. Measurement of the Peltier coefficient of semiconductors by lock-in thermography. *Applied Physics Letters*, 95(5): 052107.

Sun, L. & Chen, H. 2014. Effects of water temperature and fish size on growth and bioenergetics of cobia (Rachycentron canadum). *Aquaculture*, 426–427: 172–180.

Swart, A.J. & Hertzog, P.E. 2016. Varying percentages of full uniform shading of a PV module in a controlled environment yields linear power reduction. *Journal of Energy in Southern Africa*, 27(3): 28–38.

Sze, S.M. & Lee, M.-K. 2012. *Semiconductor Devices: Physics and Technology*. 3 edition. Hoboken, N.J: Wiley.

Tanabe, K. 2009. A Review of Ultrahigh Efficiency III-V Semiconductor Compound Solar Cells: Multijunction Tandem, Lower Dimensional, Photonic Up/Down Conversion and Plasmonic Nanometallic Structures. *Energies*, 2(3): 504–530.

Tang, X., Quan, Z. & Zhao, Y. 2010. Experimental Investigation of Solar Panel Cooling by a Novel Micro Heat Pipe Array. *Energy and Power Engineering*, 02(03): 171.

Teo, J., Tan, R., Mok, V., Ramachandaramurthy, V. & Tan, C. 2018. Impact of Partial Shading on the P-V Characteristics and the Maximum Power of a Photovoltaic String. *Energies*, 11(7): 1860.

Theocharis, T., Niki, F. & Vassilis, G. 2005. Environmental impacts from the solar energy technologies. In Environmental impacts from the solar energy technologies. Energy Policy. http://www.circleofblue.org/wp-content/uploads/2010/08/Tsoutsos_Frantzeskaki_2006_EIA_ST.pdf 13 June 2016.

Tian, H., Mancilla-David, F., Ellis, K., Muljadi, E. & Jenkins, P. 2012. A cell-to-module-to-array detailed model for photovoltaic panels. *Solar Energy*, 86(9): 2695–2706.

Tian, Y. & Zhao, C.Y. 2013. A review of solar collectors and thermal energy storage in solar thermal applications. *Applied Energy*, 104: 538–553.

Tiwari, A., Sodha, M.S., Chandra, A. & Joshi, J.C. 2006. Performance evaluation of photovoltaic thermal solar air collector for composite climate of India. *Solar Energy Materials and Solar Cells*, 90(2): 175–189.

Tiwari, G.N. & Dubey, S. 2010. *Fundamentals of Photovoltaic Modules and Their Applications*. Royal Society of Chemistry.

Tkemaladze, G.S. & Makhashvili, K.A. 2016. Climate changes and photosynthesis. *Annals of Agrarian Science*, 14(2): 119–126.

Tonui, J.K. & Tripanagnostopoulos, Y. 2007. Air-cooled PV/T solar collectors with low cost performance improvements. *Solar Energy*, 81(4): 498–511.

Tripanagnostopoulos, Y., Nousia, T., Souliotis, M. & Yianoulis, P. 2002. Hybrid photovoltaic/thermal solar systems. *Solar Energy*, 72(3): 217–234.

Vázquez, M. & Rey-Stolle, I. 2008. Photovoltaic module reliability model based on field degradation studies. *Progress in Photovoltaics: Research and Applications*, 16(5): 419–433.

Verma, S.K. & Tiwari, A.K. 2015. Progress of nanofluid application in solar collectors: A review. *Energy Conversion and Management*, 100: 324–346.

Vokas, G., Christandonis, N. & Skittides, F. 2006. Hybrid photovoltaic–thermal systems for domestic heating and cooling—A theoretical approach. *Solar Energy*, 80(5): 607–615.

Wang, J.-C., Su, Y.-L., Shieh, J.-C. & Jiang, J.-A. 2011. High-accuracy maximum power point estimation for photovoltaic arrays. *Solar Energy Materials and Solar Cells*, 95(3): 843–851.

Wang, Y., Li, X. & Wang, C. 2017. The Study of Resistance and Relative Mechanism of the Low Efficiency Single Silicon Solar Cell. In 7th International Conference on Management, Education, Information and Control (MEICI 2017). Atlantis Press. https://www.atlantis-press.com/proceedings/meici-17/25886005 13 October 2019.

Warta, W., Schubert, M.C., Rein, S. & Fertig, F. 2011. Impact of Junction Breakdown in Multi-Crystalline Silicon Solar Cells on Hot Spot Formation and Module Performance. *26th European Photovoltaic Solar Energy Conference and Exhibition*: 1168–1178.

Wilcox, J.R. & Gray, J.L. 2012. A distributed emitter model for solar cells: Extracting a temperature dependent lumped series resistance. In *2012 38th IEEE Photovoltaic Specialists Conference*. 2012 38th IEEE Photovoltaic Specialists Conference. 002122–002127.

Wilson, K., Ceuster, D.D. & Sinton, R.A. 2006. Measuring the Effect of Cell Mismatch on Module Output. In *2006 IEEE 4th World Conference on Photovoltaic Energy Conference*. 2006 IEEE 4th World Conference on Photovoltaic Energy Conference. 916–919.

Wohlgemuth, J.H., Cunningham, D.W., Monus, P., Miller, J. & Nguyen, A. 2006. Long Term Reliability of Photovoltaic Modules. In *2006 IEEE 4th World Conference on Photovoltaic Energy Conference*. 2006 IEEE 4th World Conference on Photovoltaic Energy Conference. 2050–2053.

Wohlgemuth, J.H., Cunningham, D.W., Nguyen, A.M. & Miller, J. 2005. Long term reliability of PV modules. In *Proceedings of the 20th European Photovoltaic Solar Energy Conference*.

Wohlgemuth, J.H., Kempe, M.D. & Miller, D.C. 2013. Discoloration of PV encapsulants. In *2013 IEEE 39th Photovoltaic Specialists Conference (PVSC)*. 2013 IEEE 39th Photovoltaic Specialists Conference (PVSC). 3260–3265.

Wohlgemuth, J.H. & Kurtz, S. 2011. Reliability testing beyond Qualification as a key component in photovoltaic's progress toward grid parity. In *2011 International Reliability Physics Symposium*. 2011 International Reliability Physics Symposium. 5E.3.1-5E.3.6.

Wu, J., Zhang, X., Shen, J., Wu, Y., Connelly, K., Yang, T., Tang, L., Xiao, M., Wei, Y., Jiang, K., Chen, C., Xu, P. & Wang, H. 2017. A review of thermal absorbers and their integration

methods for the combined solar photovoltaic/thermal (PV/T) modules. *Renewable and Sustainable Energy Reviews*, 75: 839–854.

Xiao, C., Yu, X., Yang, D. & Que, D. 2014. Impact of solar irradiance intensity and temperature on the performance of compensated crystalline silicon solar cells. *Solar Energy Materials and Solar Cells*, 128: 427–434.

Xu, X., Meyers, M.M., Sammakia, B.G. & Murray, B.T. 2012. Thermal modeling of hybrid concentrating PV/T collectors with tree-shaped channel networks cooling system. In *2012 13th IEEE Intersociety Conference on Thermal and Thermomechanical Phenomena in Electronic Systems (ITherm)*. 2012 13th IEEE Intersociety Conference on Thermal and Thermomechanical Phenomena in Electronic Systems (ITherm). 1131–1138.

Xu, X., Zhou, D., Qin, X., Lin, K., Kang, F., Li, B., Shanmukaraj, D., Rojo, T., Armand, M. & Wang, G. 2018. A room-temperature sodium–sulfur battery with high capacity and stable cycling performance. *Nature Communications*, 9. https://www.ncbi.nlm.nih.gov/pmc/articles/PMC6155237/ 22 March 2019.

Xu, Z. & Kleinstreuer, C. 2014. Concentration photovoltaic–thermal energy co-generation system using nanofluids for cooling and heating. *Energy Conversion and Management*, 87: 504–512.

Y. Tripanagnostopoulos. 2007. Aspects and improvements of hybrid photovoltaic/thermal solar energy systems. *Solar Energy*, 81(9): 1117–1131.

Yang, X., Sun, L., Yuan, Y., Zhao, X. & Cao, X. 2018. Experimental investigation on performance comparison of PV/T-PCM system and PV/T system. *Renewable Energy*, 119: 152–159.

Yin, H.M., Yang, D.J., Kelly, G. & Garant, J. 2013. Design and performance of a novel building integrated PV/thermal system for energy efficiency of buildings. *Solar Energy*, 87(Supplement C): 184–195.

Yinghao, C. & Peter, M. 2011. Mid Term Report - Review-and-Comparison-of-Different-Solar-Technologies. http://www.geni.org/globalenergy/research/review-and-comparison-of-solar-technologies/Review-and-Comparison-of-Different-Solar-Technologies.pdf 28 June 2016.

You, S., Chen, M.-W., Dlott, D.D. & Suslick, K.S. 2015. Ultrasonic hammer produces hot spots in solids. *Nature Communications*, 6: 6581.

Yuan, Y., Gao, X., Wu, H., Zhang, Z., Cao, X., Sun, L. & Yu, N. 2017. Coupled cooling method and application of latent heat thermal energy storage combined with pre-cooling of envelope: Method and model development. *Energy*, 119: 817–833.

Zaraket, J., Khalil, T., Aillerie, M., A. Vokas, G. & Salame, C. 2017. The Effect of Electrical stress under temperature in the characteristics of PV Solar Modules. *Energy Procedia*, 119: 579–601.

Zegaoui, A., Petit, P., Aillerie, M., Sawicki, J.-P. & Charles, J.-P. 2012. Experimental Validation of Photovoltaic Direct and Reverse Mode Model. Influence of Partial Shading. *Energy Procedia*, 18: 1247–1253.

Zhang, X., Zhao, X., Xu, J. & Yu, X. 2013. Characterization of a solar photovoltaic/loop-heat-pipe heat pump water heating system. *Applied Energy*, 102(Supplement C): 1229–1245.

Zhao, H., Wu, Q., Hu, S., Xu, H. & Rasmussen, C.N. 2015. Review of energy storage system for wind power integration support. *Applied Energy*, 137: 545–553.

Zhao, X., Zhang, X., Riffat, S.B. & Su, Y. 2011. Theoretical study of the performance of a novel PV/e roof module for heat pump operation. *Energy Conversion and Management*, 52(1): 603–614.

Zondag, H.A. 2008. Flat-plate PV-Thermal collectors and systems: A review. *Renewable and Sustainable Energy Reviews*, 12(4): 891–959.

Zondag, H.A., de Vries, D.W., van Helden, W.G.J., van Zolingen, R.J.C. & van Steenhoven, A.A. 2003. The yield of different combined PV-thermal collector designs. *Solar Energy*, 74(3): 253–269.

Appendices

Appendix A : MATLAB/Simulink tool

A.1 Modelling in Simscape

The thermodynamics of the proposed PV/T model in Simscape is designed to react accurately when it is exposed to solar radiation, the ambient temperature and material property of the system; which varies the internal temperature of the thermal element model accordingly.

Simscape is a physical modelling of a multi-domain tool based on MATLAB object-oriented language and a toolbox to Simulink. Physical components in Simscape are presented as blocks such as electric motors, bridge rectifiers, battery storage, wind, PV cells, refrigeration systems and hydraulic pump, and they can be assembled to build a system. Simscape can define and create components, nodes (ports), parameters, variables and equations.

A.1.1 Differences between Simulink and Simscape Modelling

There are some distinct differences between Simulink and Simscape, and they are as follows.

- The Simulink model is constructed by defining equations for the system, in contrast, Simscape model is built by blocks representing physical components and physical relationships between them and Simscape analyses and solves the equations that constitute the system;

- The connections in Simulink between blocks are unitless and unidirectional while the connections in Simscape between components have units and are bidirectional

There are interface blocks between Simulink and Simscape

A.1.2 Heat transfer in Simscape

Simscape can solve heat transfer problems with conduction, convection and radiation occurring at boundaries. The heat transfer in Simscape is bidirectional.

A.1.2.1 Conduction in Simscape

The conductive heat transfer block describes a heat transfer by conduction within two layers of the same material (between the ports A and B). Heat transfer by conduction in Simscape is illustrated in Figure A-1. The transfer is dictated by the Fourier law and is represented in Equation A.1.

**Figure A-1: Conductive heat transfer
block in Simscape**

$$Q = k\frac{A}{D}(T_A - T_B)$$
(A.1)

where:

Q is the heat flow;

k is the material thermal conductivity;

A is the area normal to the heat flow direction;

D is the distance between layers (thickness of material); and

T_A, T_B are the temperatures of the layers.

A.1.2.2 Convection in Simscape

The convection block in Simscape is illustrated in Figure A-2. The convective heat transfer block describes a heat transfer by convection between two bodies (between the ports A and B) using fluid motion. The transfer is ruled by the Newton law of cooling and is defined in Equation A.2.

**Figure A-2: Convective heat transfer
block in Simscape**

$$Q = k \cdot A(T_A - T_B)$$ **(A.2)**

where:

Q is the heat flow

k is the convection heat transfer coefficient

A is the surface area

T_A, T_B is the temperatures of the bodies

A.1.2.3 Radiation in Simscape

The radiative heat transfer block represents inFigure A-3, a heat transfer by radiation between two bodies (between the ports A and B). The transfer is dictated by the Stefan-Boltzmann law and is defined in Equation A.3.

Figure A-3: **Radiative heat transfer block in Simscape**

$$Q = k \cdot A(T_A^4 - T_B^4)$$ *(**A.3***)

where:

Q is the heat flow

k is the radiation coefficient

A is the emitting body surface area

T_A, T_B are the temperatures of the bodies

A.1.3 Solar cell in Simscape

The solar cell model in the Simscape is presented in Figure A-4, and it is composed of the solar-induced current, temperature dependence and thermal Port. This study is interesting in the thermal part.

**Figure A-4: The solar cell model
in Simscape**

A.1.3.1 Temperature dependence

Solar cell temperature depends on many parameters such as solar radiations ambient temperature, sky emissivity, cloudiness and atmospheric pressure, solar cell material property.

The relationship between the current I_{ph} generated by solar radiation and the solar cell temperature T is defined in Equation A.4:

$$I_{ph}(t) = I_{ph} \cdot \left(1 + TIPH1 \cdot (T - T_{meas})\right)$$ **(A.4)**

where:

TIPH1 is the First order temperature coefficient for Iph.

T_{meas} is the Measurement temperature parameter value.

I_{ph} is the solar-induced current

The relationship between the saturation current of the first diode I_s as a function of the solar cell temperature T is described in Equation A.5.

$$I_{s1} = I_{s1} \cdot \left(\frac{T}{T_{meas}}\right)^{(TXISI/N)} \cdot e^{\left(EG \cdot \left(\frac{T}{T_{meas}} - 1\right) / (N/V_t)\right)}$$ *(A.5)*

where:

TXIS1 is the Temperature exponent for Is, TXIS1 parameter value.

N is the quality factor (diode emission coefficient) of the first diode.

V_t is the thermal voltage, *kT/q*

I_s is the saturation current of the first diode.

The relationship between the saturation current of the second diode I_{s2} as a function of solar cell temperature T is defined in Equation A.6.

$$I_{s2} = I_{s1} \cdot \left(\frac{T}{T_{meas}} \right)^{(TXISI/N_2)} \cdot e^{\left(EG \cdot \left(\frac{T}{T_{meas}} - 1 \right) / (N_2/V_t) \right)}$$ (A.6)

where:

TXIS2 is the temperature exponent for I_{s2},

N_2 is the quality factor (diode emission coefficient) of the second diode,

I_{s2} is the saturation current of the second diode.

The relationship between the series resistance R_s as a function of the solar cell temperature T in Equation A.7.

$$R_s(T) = R_s \cdot \left(\frac{T}{T_{meas}} \right)^{(TRSI)}$$ (A.7)

where:

TRS1 is the Temperature exponent for R_s

The relationship between the parallel resistance R_p as a function of the solar cell temperature T *in Equation* A.8.

$$R_p(T) = R_p \cdot \left(\frac{T}{T_{meas}} \right)^{(TRPI)}$$ (A.8)

where:

TRP1 is the Temperature exponent for R_p.

A.1.3.2 Thermal element of the solar cell

The solar cell block has an optional thermal port *H* and the thermal element of the solar cell is composed of thermal mass and ideal heat flow source. The thermal mass is directly connected to the component thermal port *H*. An internal ideal heat flow source block supplies a heat flow to the port and thermal mass as shown in Figure A-5. This heat flow represents the internal heat generation. The internal heat generation of the solar cell is the sum of the $I^2 \cdot R$ losses for each of the resistors plus the losses in each of the diodes.
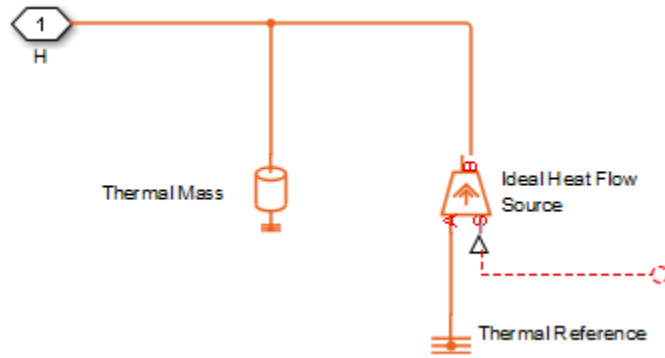
Figure A-5: Solar cell thermal element

A.1.4 Absorber pipe

The absorber Pipe model attached at the back of the PV module is presented in Figure A-6, this transport the thermal liquid components through a closed conduit.

Figure A-6: absorber pipe

The temperature change across the absorber pipe is determined from the energy exchanges between the pipe and the remainder of the model. These exchanges are attributed to advection and conduction of internal energy through the thermal liquid ports (A and B) and to convection of heat through the thermal port H. The differences in elevation and static pressure are established during simulation between the thermal liquid ports.

.

Appendix B : Simulation data of different parameters on the solar panels

Table B-1: Simulation data as a function of solar radiation

Solar radiation (w/m²)	Q_{Rad}(W)	Q_{Cond}(W)	Q_{Conv}(W)	P_{PV} (W)	T_c(ºC)	P_d_R_s (W)	P_d _R_p (W)	P_d_Diode (W)	P_d_Total (W)	n_el (%)
200	48.66435	-4.44351	472.2227	0.170819	24.03924	9.730426	1.525799	2.73E-06	11.25896	4.270478
300	74.27189	-10.0408	713.8097	0.385622	25.92664	21.96633	3.444475	2.54E-05	25.43616	6.427038
400	100.7818	-17.9821	959.1828	0.687638	27.84362	39.17015	6.142154	0.000201	45.51287	8.595474
500	128.3091	-28.7066	1209.107	1.076096	29.79615	61.298	9.611957	0.001448	72.35835	10.76096
600	157.4213	-44.8345	1468.267	1.541237	31.82083	87.79401	13.76672	0.009528	111.089	12.84364
700	190.7167	-78.5444	1758.475	2.033188	34.08809	115.8172	18.16095	0.051446	185.4237	14.52277
800	233.9747	-155.89	2126.176	2.437276	36.96075	138.8353	21.77036	0.185388	345.9939	15.23297
900	289.7974	-285.503	2586.073	2.692177	40.55369	153.3554	24.0472	0.43185	609.2527	14.95654
1000	355.5433	-451.122	3108.214	2.834659	44.63292	161.4716	25.31989	0.756326	943.1179	14.1733

Table B-2: Simulation data as a function of ambient temperature

T_a(ºC)	Q_{Rad}(W)	Q_{Cond}(W)	Q_{Conv}(W)	P_{PV} (W)	T_c(ºC)	$P_d\_R_s$ (W)	$P_d\_R_p$ (W)	P_d_Diode (W)	P_d_Total (W)	n_el (%)
15	334.9788	-426.919	3080.267	2.921776	39.41458	166.4341	26.09803	0.703284	895.8159	14.60888
20	355.5433	-451.122	3108.214	2.834659	44.63292	161.4716	25.31989	0.756326	943.1179	14.1733
25	376.7426	-474.601	3134.075	2.747442	49.83496	156.5035	24.54084	0.807923	988.9671	13.73721
30	398.5446	-497.279	3157.729	2.660414	55.01975	151.5461	23.76349	0.857905	1033.215	13.30207
35	420.9159	-519.094	3179.084	2.573817	60.1866	146.6132	22.98998	0.906136	1075.739	12.86908
40	443.8218	-539.996	3198.075	2.487849	65.33496	141.7162	22.22209	0.952503	1116.442	12.43925

Table B-3 : Simulation data as a function of the convective heat transfer

h_f W/(m².K)	Q_{Rad}(W)	Q_{Cond}(W)	Q_{Conv}(W)	P_{PV} (W)	T_c(ºC)	$P_d\_R_s$ (W)	$P_d\_R_p$ (W)	P_d_Diode (W)	P_d_Total (W)	n_el (%)
2	2555.498	-721.489	-721.489	1.434204	133.6486	81.69704	12.81067	1371.13	1465.638	7.17102
5	1429.235	-645.132	-645.132	1.988977	96.08148	113.2988	17.76604	1189.195	1320.26	9.944887
10	738.9052	-541.692	-541.692	2.480732	65.76236	141.3108	22.15852	956.2734	1119.743	12.40366
15	482.6662	-484.611	-484.611	2.709383	52.10224	154.3355	24.20089	829.9662	1008.503	13.54692
20	355.5433	-451.122	-451.122	2.834659	44.63292	161.4716	25.31989	756.3264	943.1179	14.1733

Table B-4: Simulation data as function of the external series resistance

$R_{se}(\Omega)$	Q_{Rad}(W)	Q_{Cond}(W)	Q_{Conv}(W)	P_{PV} (W)	T_c(ºC)	$P_d\_R_s$ (W)	$P_d\_R_p$ (W)	$P_d\_$Diode (W)	$P_d\_$Total (W)	n_el (%)
0.0001	355.5433	-451.122	3108.214	2.834659	44.63292	147.4306	25.31989	756.3264	929.0769	14.1733
10	458.2629	-890.339	3885.835	1.426256	50.70809	74.17957	27.3031	1709.919	1811.401	7.13128
20	521.4934	-1150.27	4343.572	0.831306	54.28416	43.23621	27.73327	2261.829	2332.799	4.156529
30	562.152	-1313.56	4630.167	0.541227	56.52318	28.1492	27.87449	2604.169	2660.193	2.706133
40	590.2669	-1424.79	4824.98	0.379657	58.04516	19.74598	27.93034	2835.501	2883.177	1.898287
50	610.8131	-1505.24	4965.669	0.280789	59.14429	14.60382	27.95403	3001.878	3044.436	1.403943
60	626.4669	-1566.07	5071.928	0.215991	59.97443	11.23372	27.96377	3127.161	3166.358	1.079957
70	638.7829	-1613.65	5154.974	0.171259	60.62323	8.907174	27.96693	3224.85	3261.724	0.856294
80	648.7226	-1651.88	5221.646	0.139096	61.14411	7.234408	27.96682	3303.134	3338.336	0.695482
90	656.9118	-1683.26	5276.343	0.115205	61.57143	5.991792	27.96506	3367.263	3401.22	0.576023
100	663.7747	-1709.48	5322.02	0.096975	61.92828	5.04366	27.96248	3420.751	3453.757	0.484874

Appendix C : Water flow pattern in the proposed PV/T system

C.1 Open loop water flow in the PV/T system

The performance of the proposed PV/T system was analysed when the water flows from a storage tank to another storage tank through the absorber pipe as an open loop water flow system. The system is described in Figure C-1.
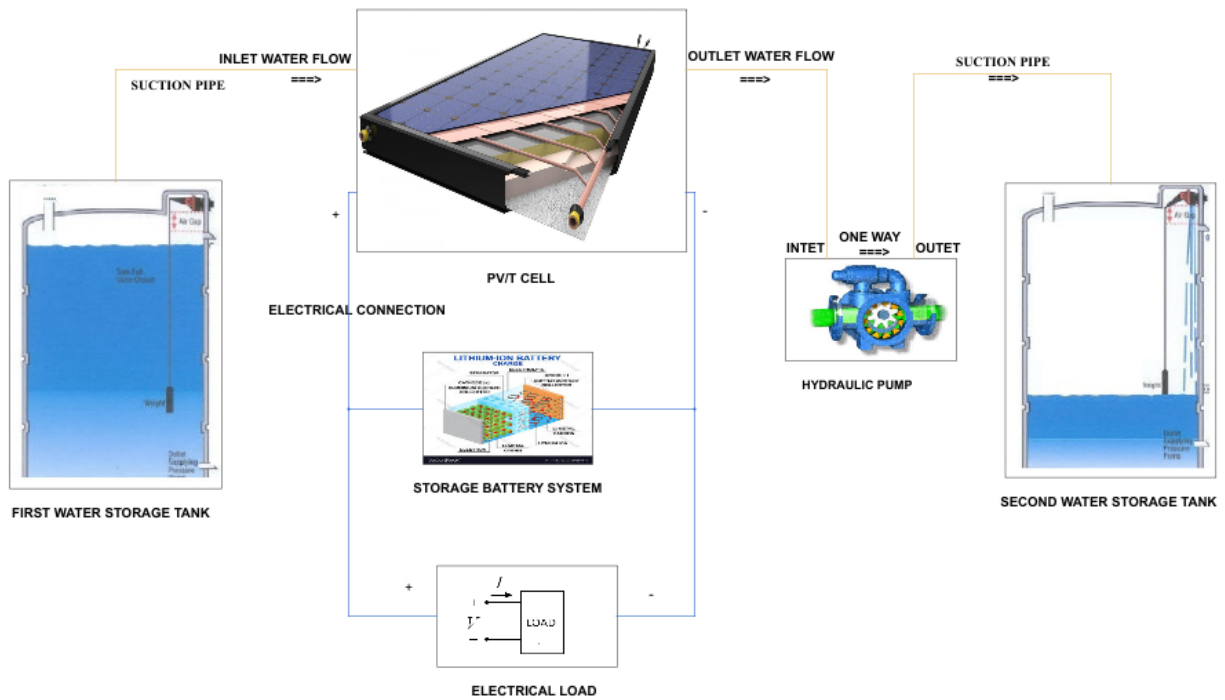
Figure C-1: Open loop water flow in the PV/T system

C.1.1 PV/T cell temperature and power in open loop water flow
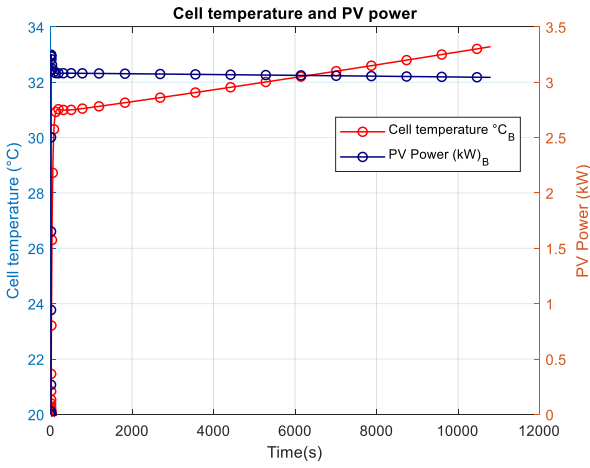
Figure C-2: PV/T cell temperature and power in open loop water flow @ R_{se}= 0 Ω
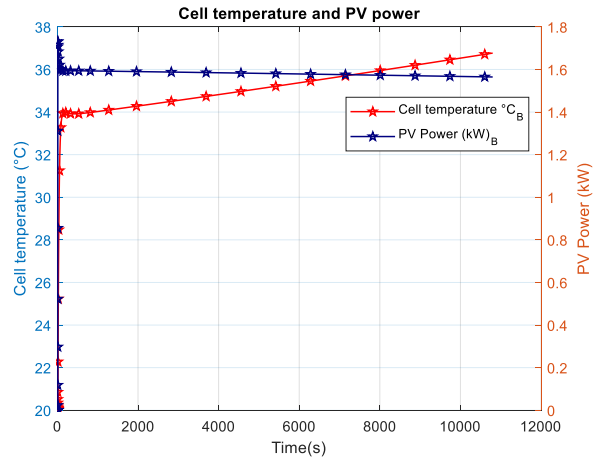
Figure C-3: PV/T cell temperature and power in open loop water flow @ R_{se} = 10 Ω
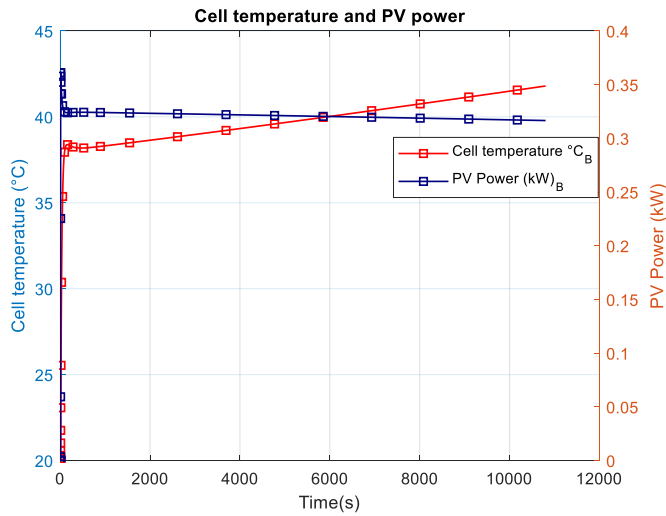
Figure C-4: PV/T cell temperature and power in open loop water flow @ R_{se} = 50 Ω

C.1.2 Heat flow rate of open loop water flow in the PV/T system
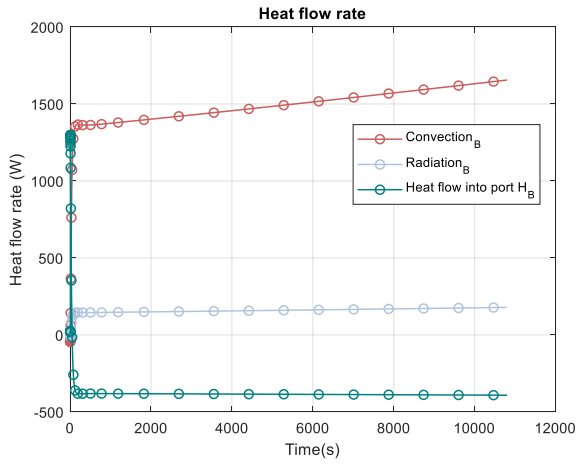
Figure C-5: Heat flow rate of open loop water flow @ R$_{se}$ = 0 Ω
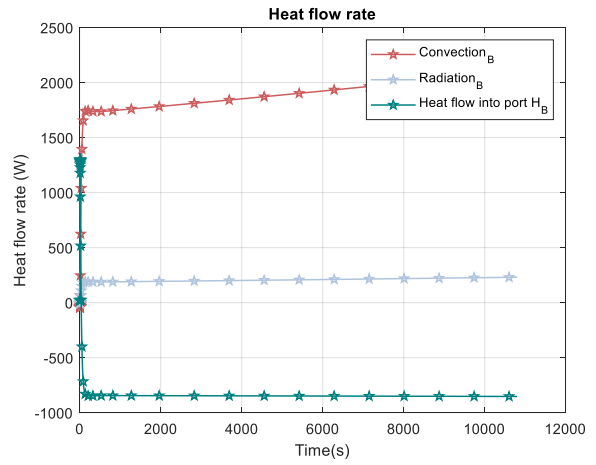
Figure C-6: Heat flow rate of open loop water flow @ R$_{se}$ = 10 Ω
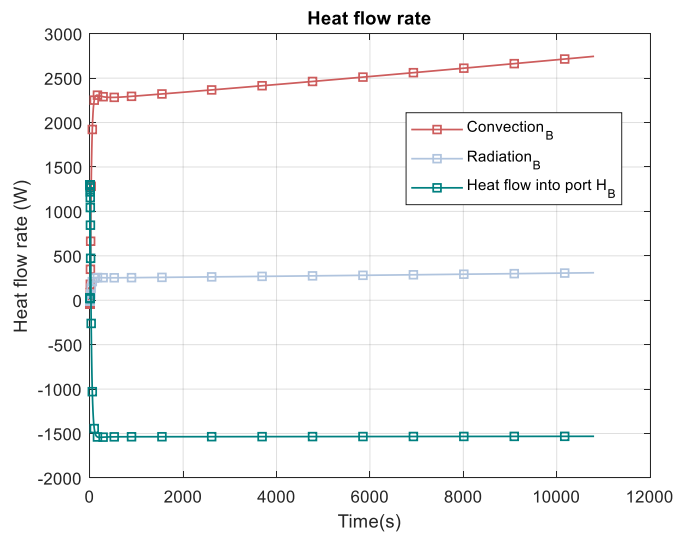
Figure C-7: Heat flow rate of open loop water flow @ R$_{se}$ = 50 Ω

C.1.3 Specific internal energy of open loop water flow in PV/T system
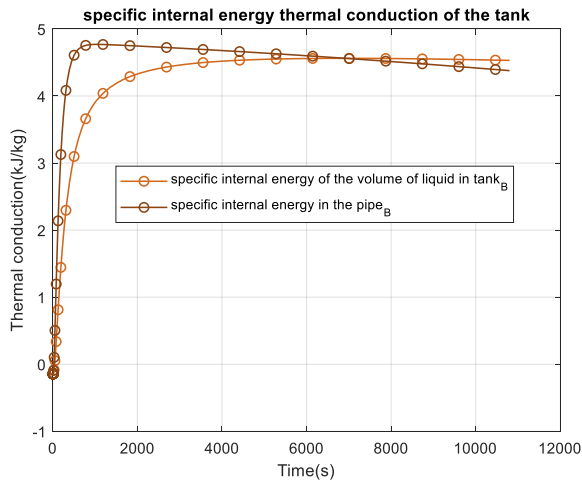
Figure C-8: Specific internal energy in open loop water flow @ R_{se} = 0 Ω
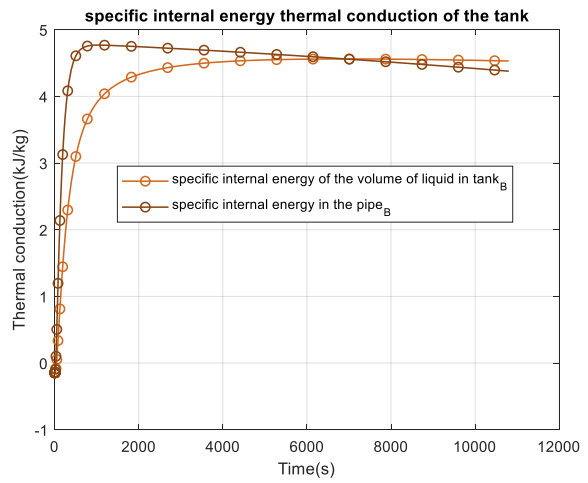
Figure C-9: Specific internal energy in open loop water flow @ R_{se} = 10 Ω
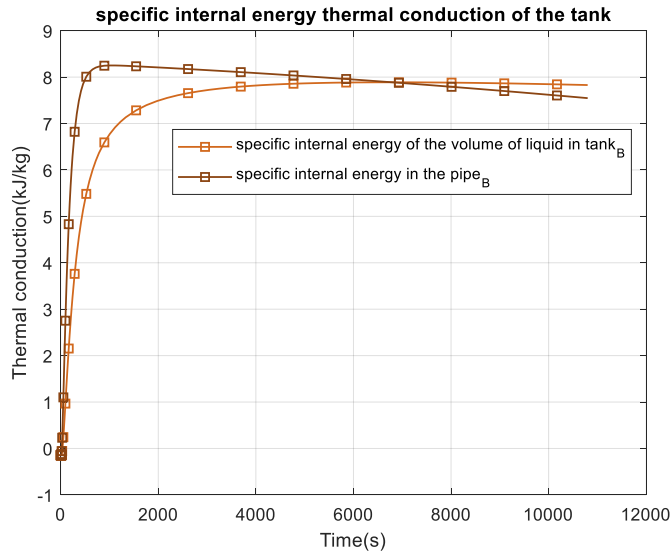
Figure C-10: Specific internal energy in open loop water flow @ R_{se} =50 Ω

C.1.4 Water temperature of open loop water flow in PV/T system
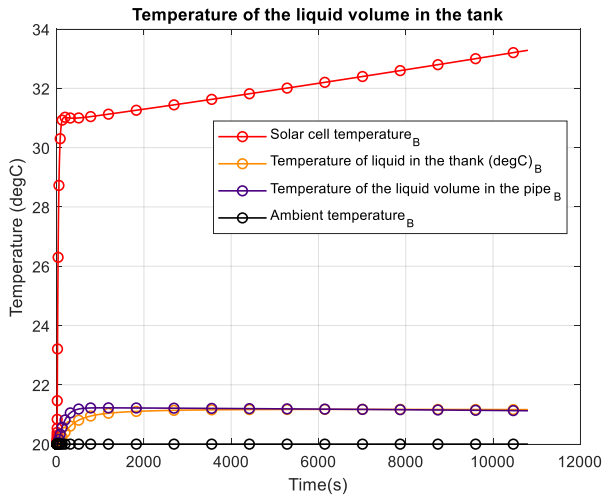
Figure C-11: Water temperature in open loop water flow @ R$_{se}$ = 0 Ω
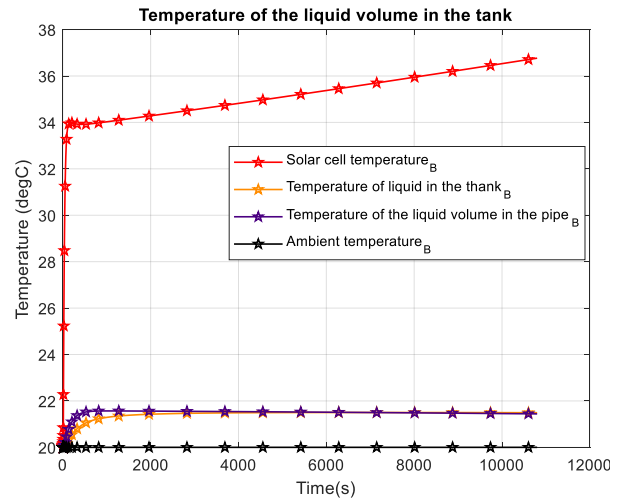
Figure C-12: Water temperature in open loop water flow @ R$_{se}$ = 10 Ω
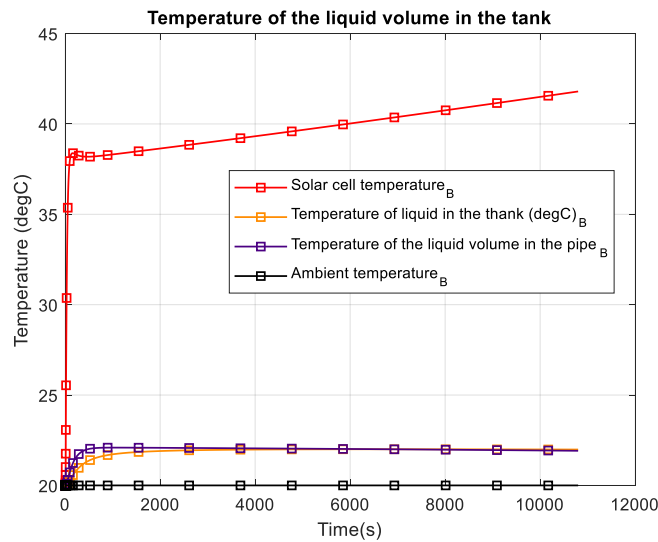
Figure C-13: Water temperature in open loop water flow @ R$_{se}$ = 50 Ω

C.1.5 Hydraulic power delivered in open loop water flow in PV/T system
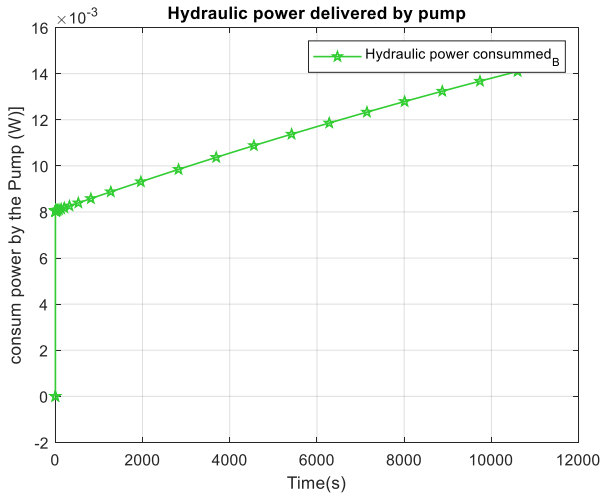
Figure C-14: Hydraulic power consumed in open loop water flow @ R$_{se}$ = 0 Ω
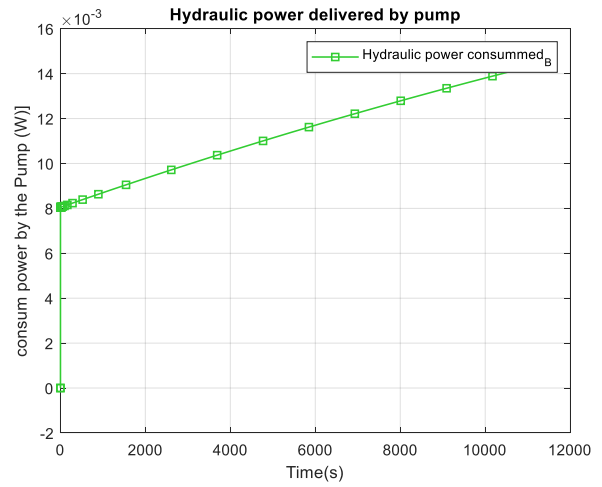
Figure C-15: Hydraulic power consumed in open loop water flow @ R$_{se}$ = 10 Ω
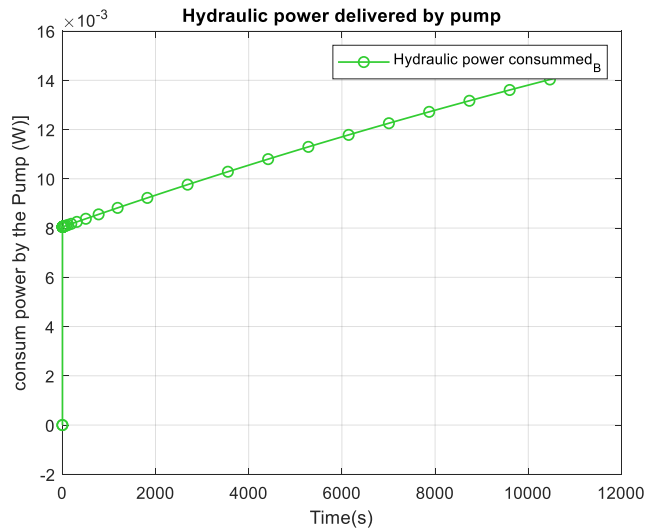
Figure C-16: Hydraulic power consumed in open loop water flow @ R$_{se}$ = 50 Ω

C.1.6 PV/T system efficiency of the in open loop water flow
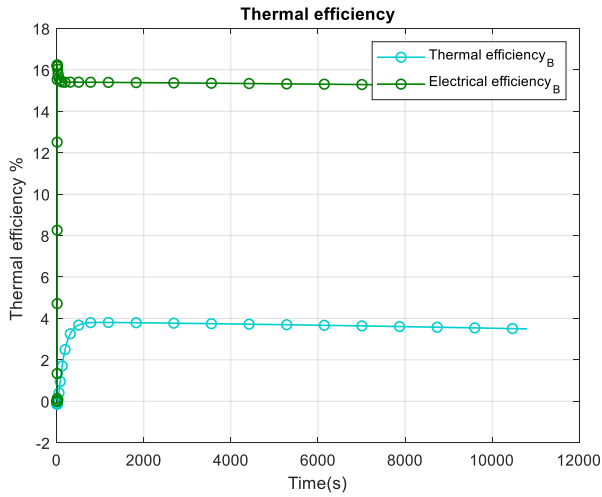
Figure C-17: PV/T system efficiency in open loop water flow @ R_{se} = 0 Ω
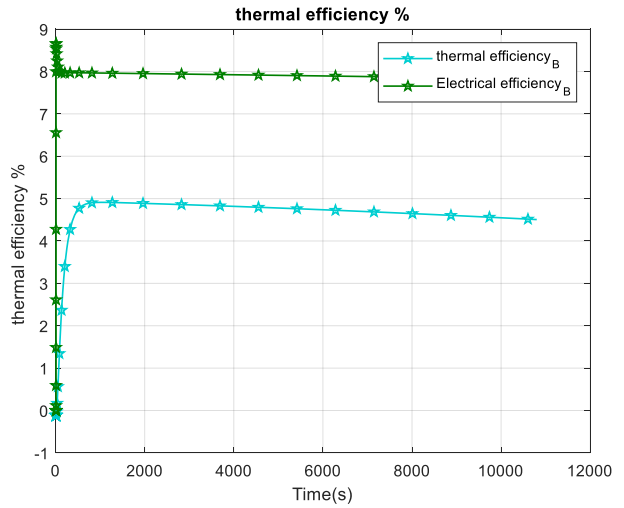
Figure C-18: PV/T system efficiency in open loop water flow @ R_{se} = 10 Ω
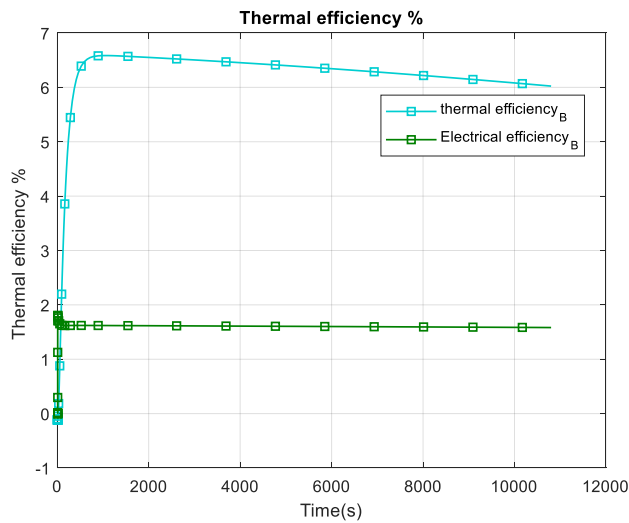
Figure C-19: PV/T system efficiency in open loop water flow @ R_{se} = 50 Ω

C.2 Water flow in between two storage tanks in the PV/T system

The performance of the proposed PV/T system is analysed when the flow of fluid passes through the absorber pipe and moves from tank1 to tank 2 and vice versa. The system is described in Figure C-20.
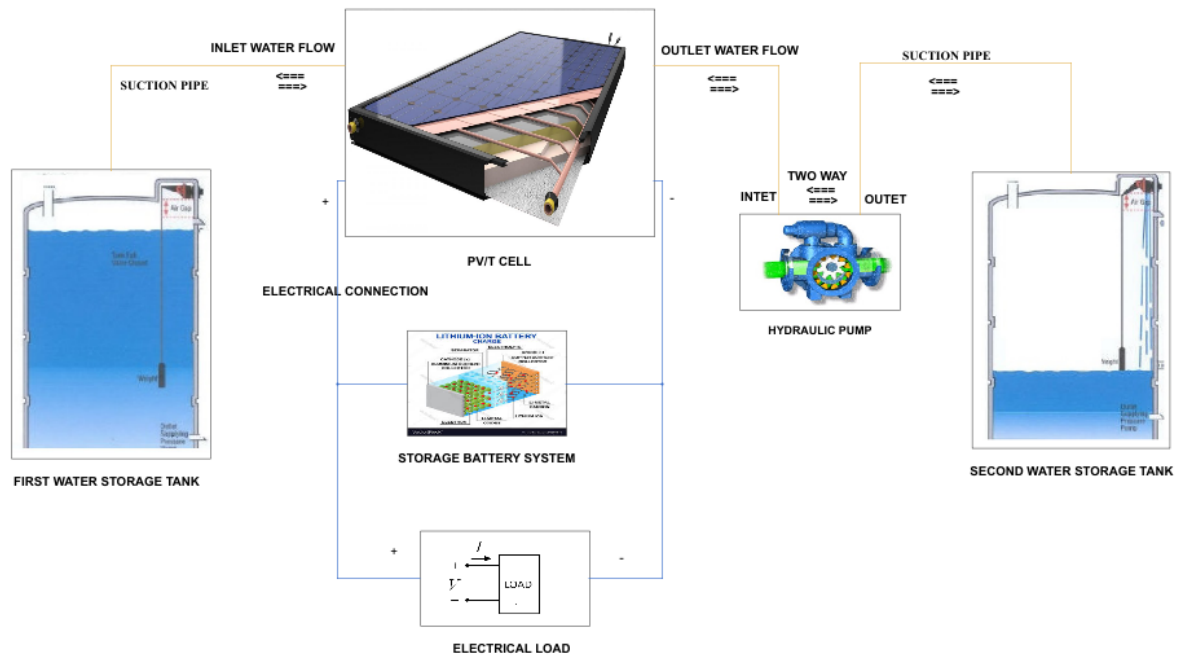
Figure C-20: Water flow in between two storage tanks in the PV/T system

C.2.1 PV/T cell temperature and power when water flow between two tanks
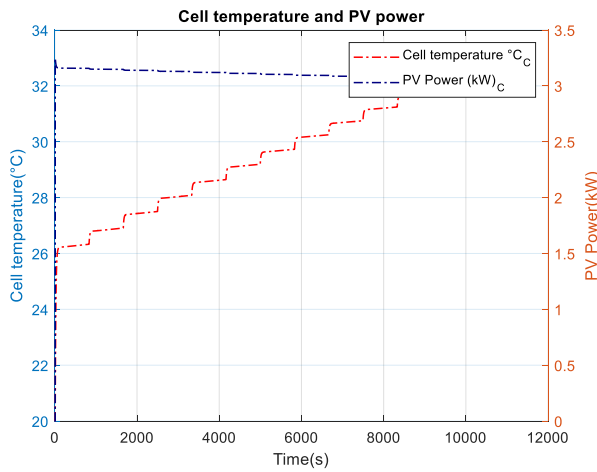
Figure C-21: PV/T cell temperature and power when water flow between two tanks @ R_{se} = 0 Ω
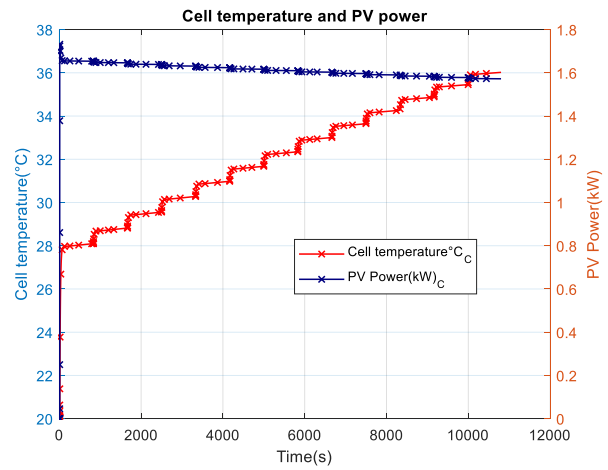
Figure C-22: PV/T cell temperature and power when water flow between two tanks @ R_{se} = 10 Ω
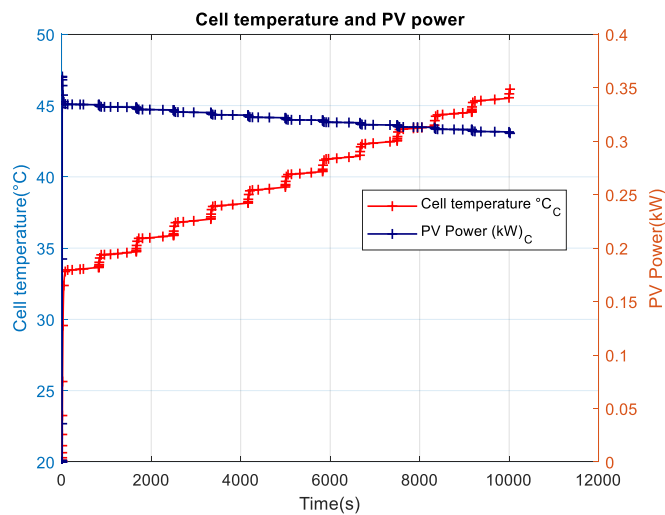
Figure C-23: PV/T cell temperature and power when water flow between two tanks @ R_{se} = 50 Ω

C.2.2 Heat flow rate in PV/T system when water flow between two tanks
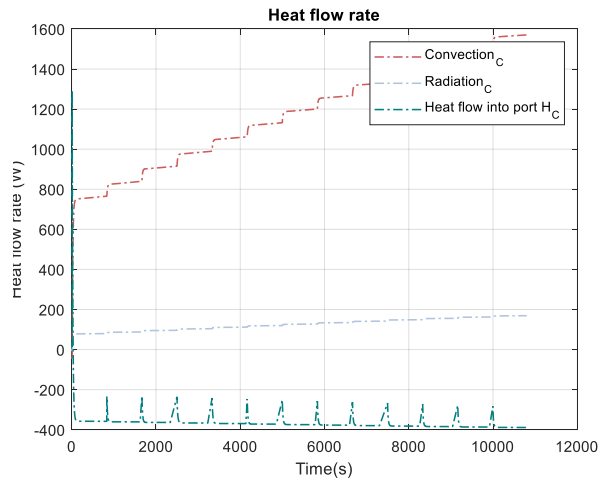
Figure C-24: Heat flow rate when water flow between two tanks @ $R_{se} = 0\ \Omega$
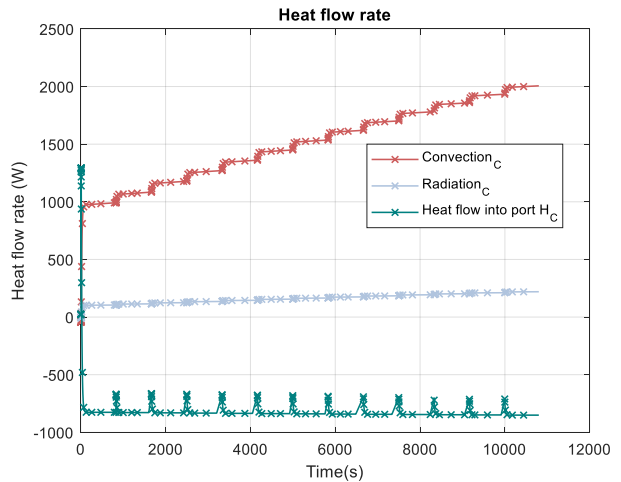
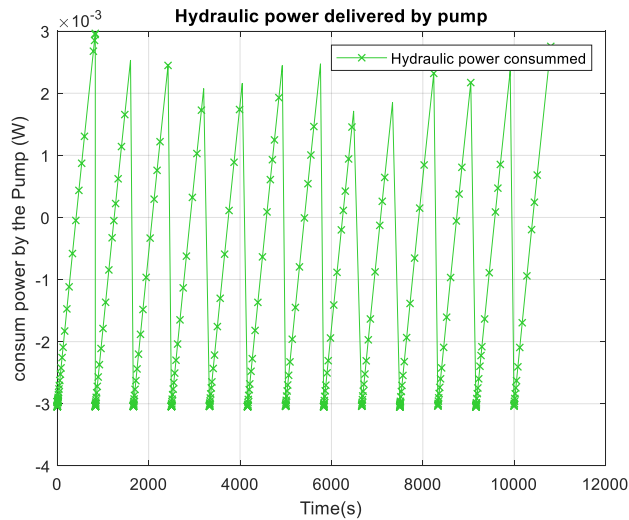**Figure C-25: Heat flow rate when water flow between two tanks@ $R_{se} = 10\ \Omega$**
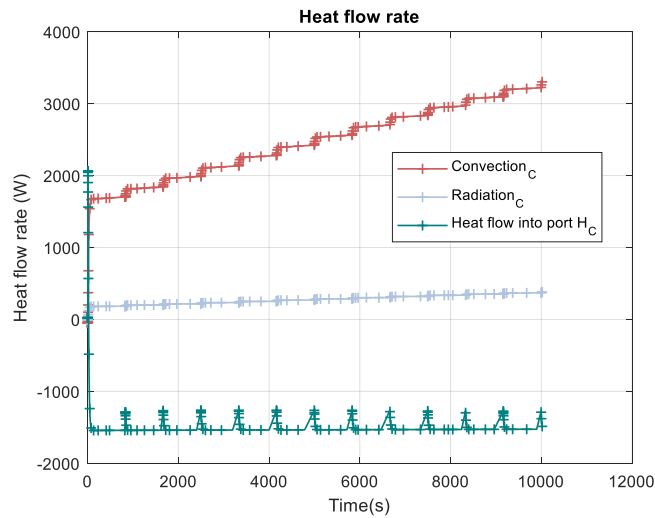
Figure C-26: Heat flow rate when water flow between two tanks@ $R_{se} = 50\ \Omega$

C.2.3 Specific internal in PV/T system when water flow between two tanks
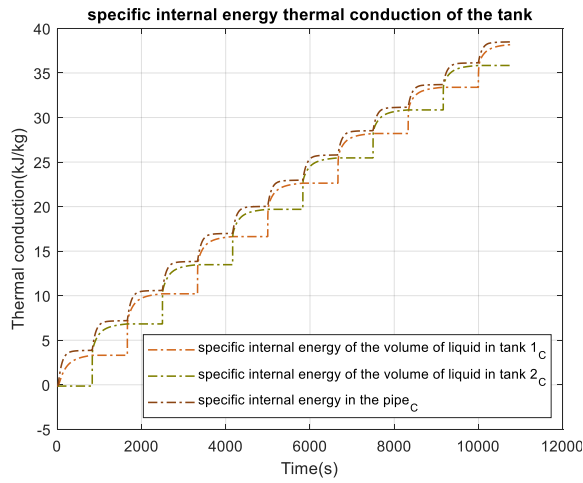
Figure C-27: Specific internal when water flow between two tanks @ R_{se} = 0 Ω
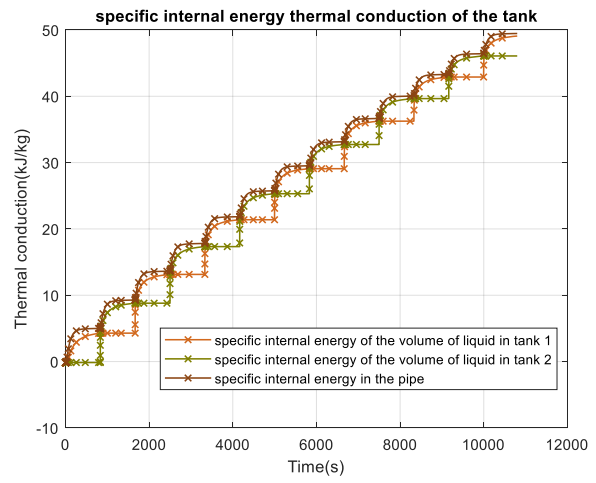
Figure C-28: Specific internal when water flow between two tanks @ R_{se} = 10 Ω
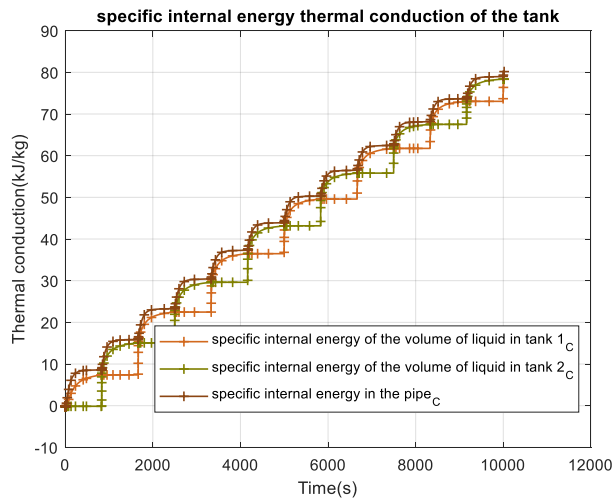
Figure C-29: Specific internal when water flow between two tanks @ R_{se} = 50 Ω

C.2.4 Water temperature in PV/T when water flow between two tanks
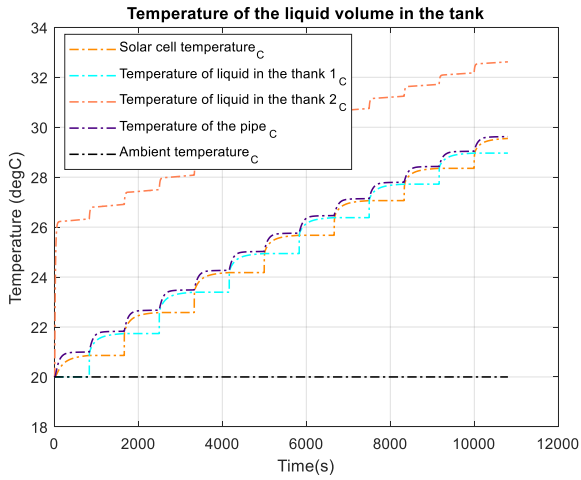
Figure C-30: Specific internal when water flow between two tanks @ R_se = 0 Ω
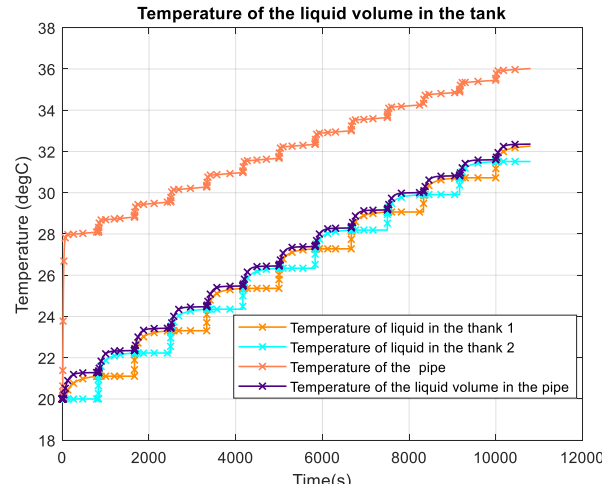
Figure C-31: Specific internal when water flow between two tanks @ R_se = 10 Ω
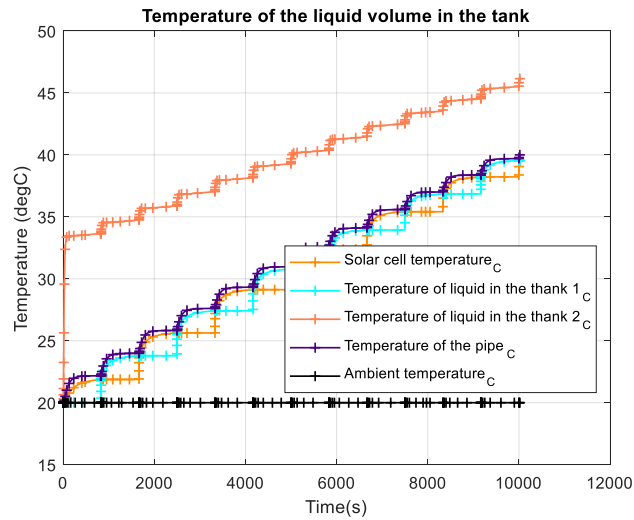
Figure C-32: Specific internal when water flow between two tanks @ R_se = 50 Ω

251

C.2.5 Hydraulic power delivered when water flow between two tanks in PV/T system
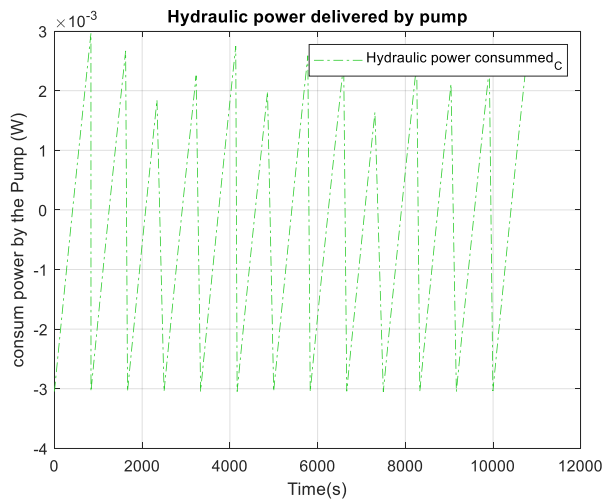
Figure C-33: Hydraulic power consumed when water flow between two tanks @ R_{se} = 0 Ω
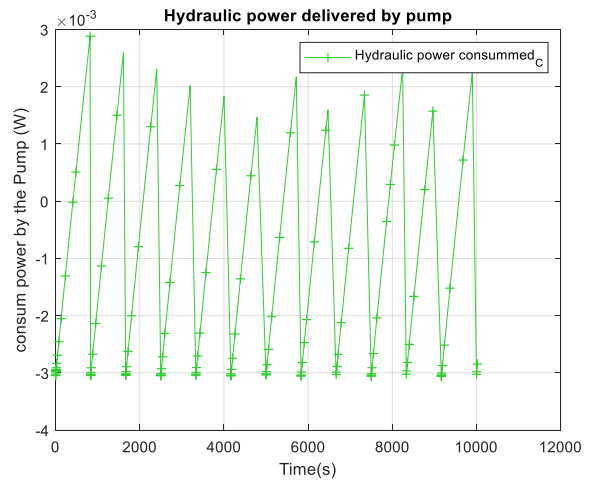
Figure C-34: Hydraulic power consumed when water flow between two tanks @ R_{se} = 10 Ω

Figure C-35: Hydraulic power consumed when water flow between two tanks @ R_{se} = 50 Ω

C.2.6 PV/T system efficiency when water flow between two tanks
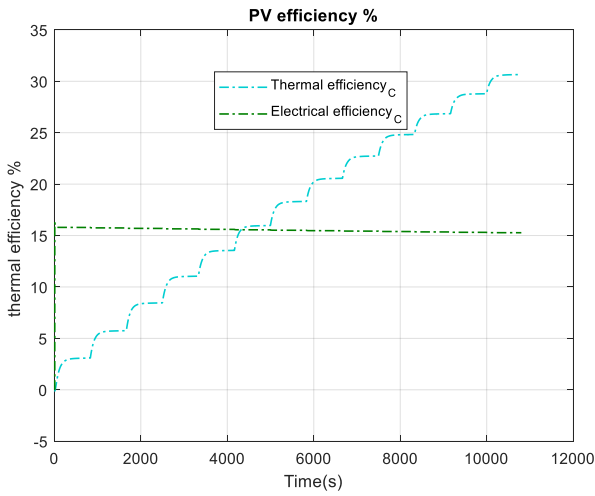
Figure C-36: PV/T system efficiency when water flow between two tanks @ $R_{se} = 0\ \Omega$
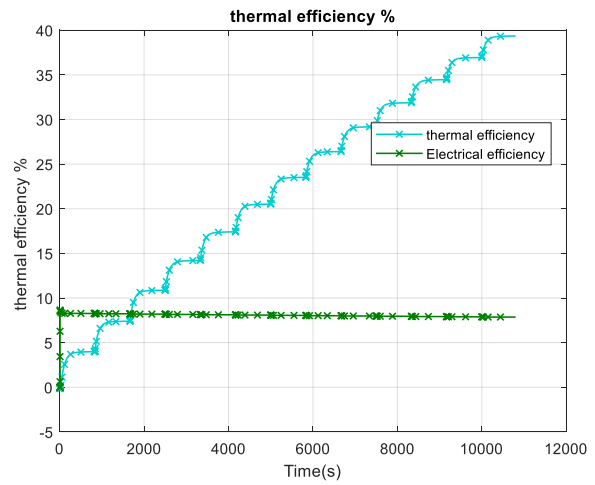
Figure C-37: PV/T system efficiency when water flow between two tanks @ $R_{se} = 10\ \Omega$
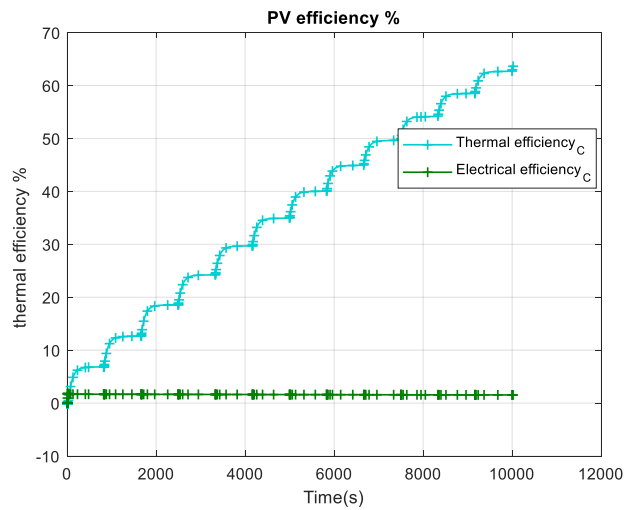
Figure C-38: PV/T system efficiency when water flow between two tanks @ $R_{se} = 50\ \Omega$

C.3 Close loop water flow in PV/T system

The performance of the proposed PV/T system was analysed when the water flows from a storage tank through the absorber pipe and back to the same storage tank as a close loop water flow system. Figure C-39 present the system used in Chapter 5.
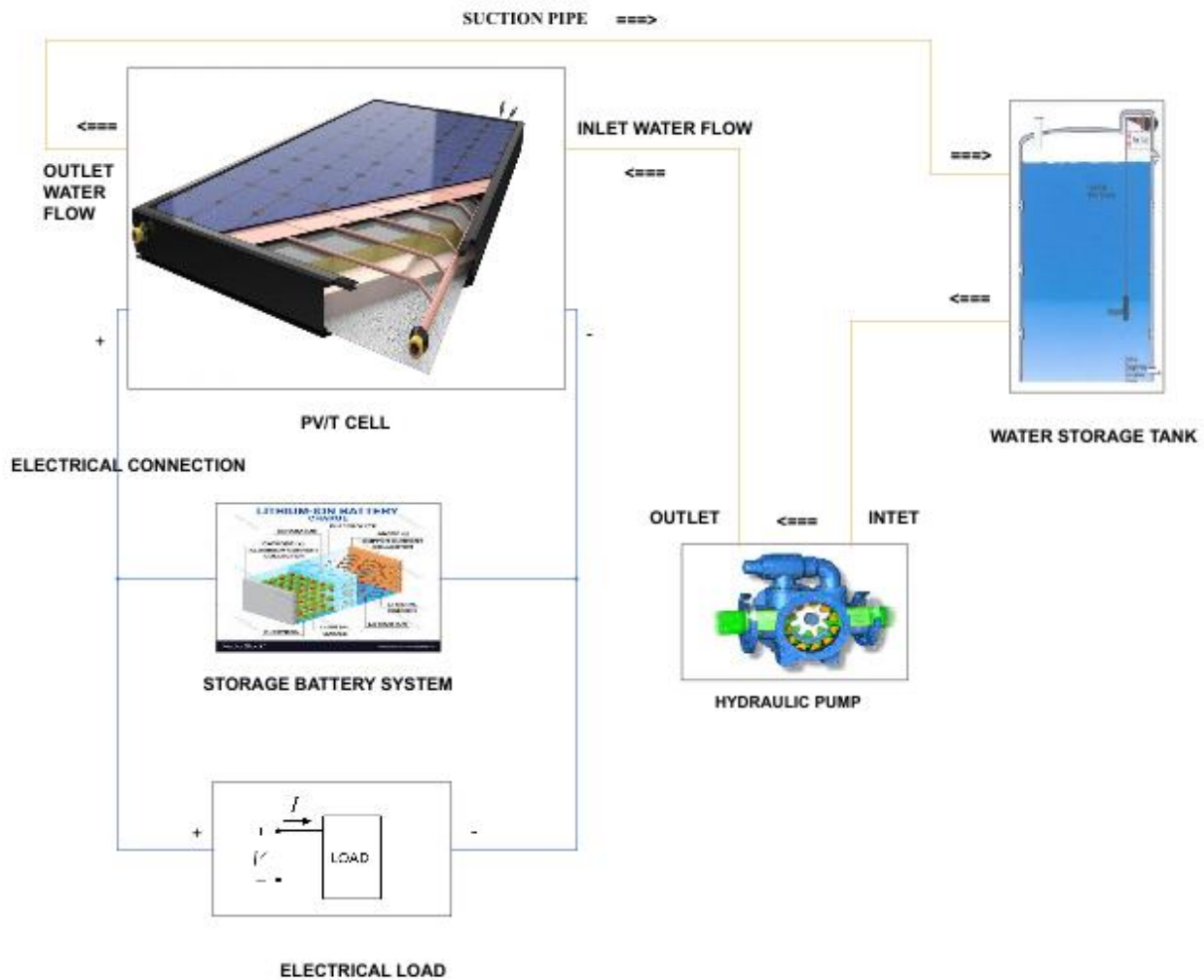
Figure C-39: Close loop water flow in the PV/T system

C.3.1 Heat flow rate of PV/T system in close loop water flow
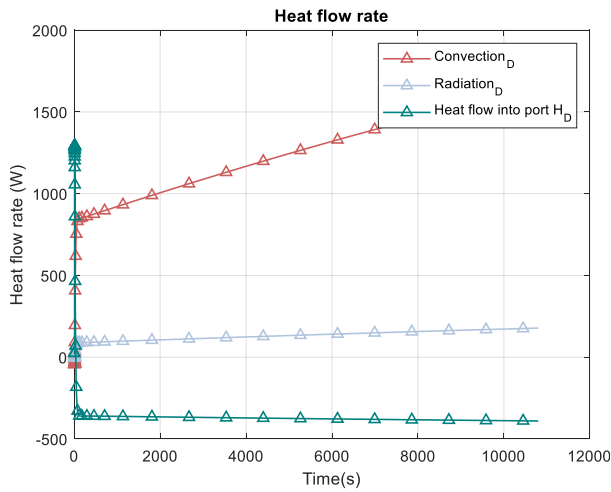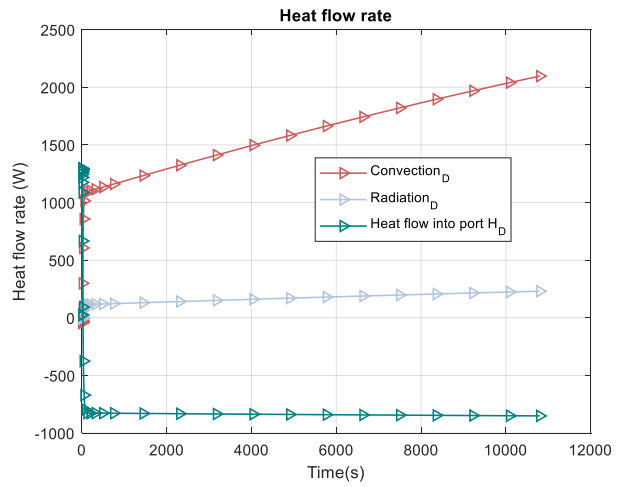

Figure C-40: Heat flow rate in close loop water flow @ R$_{se}$ = 0 Ω

Figure C-41: Heat flow rate in close loop water flow @ R$_{se}$ = 10 Ω
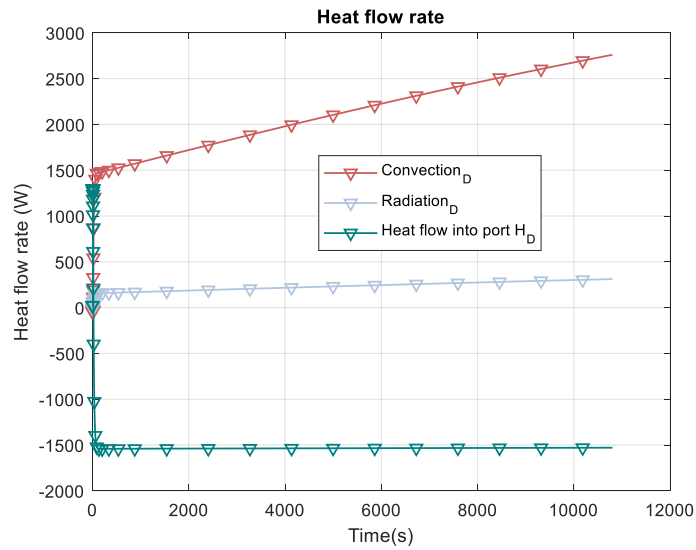
Figure C-42: Heat flow rate in close loop water flow @ R$_{se}$ = 50 Ω
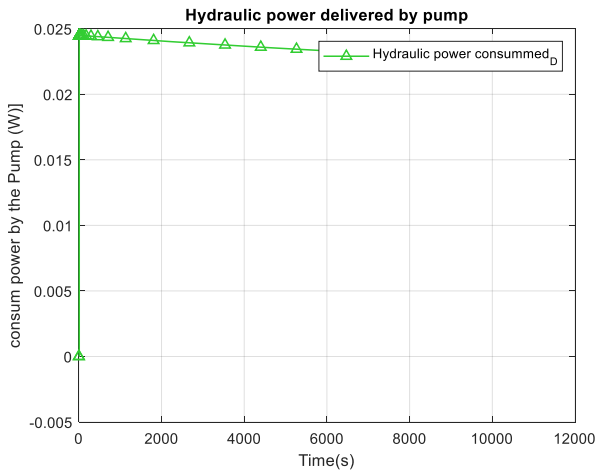
C.3.2 PV/T system efficiency in close loop water flow

Figure C-43: Hydraulic power consumed in close loop water flow @ $R_{se} = 0\ \Omega$
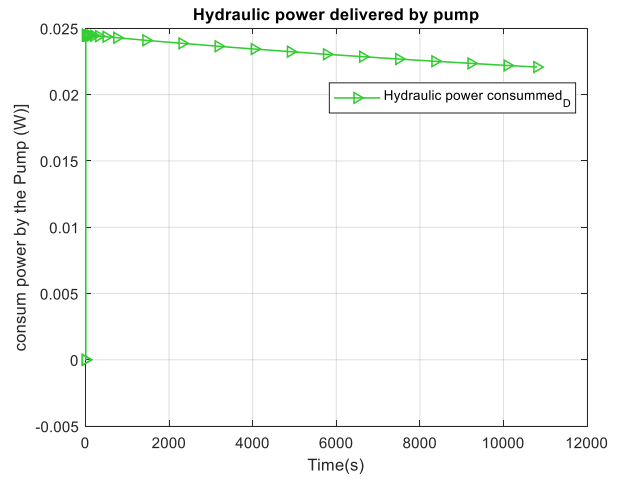

Figure C-44: Hydraulic power consumed in close loop water flow @ $R_{se} = 10\ \Omega$
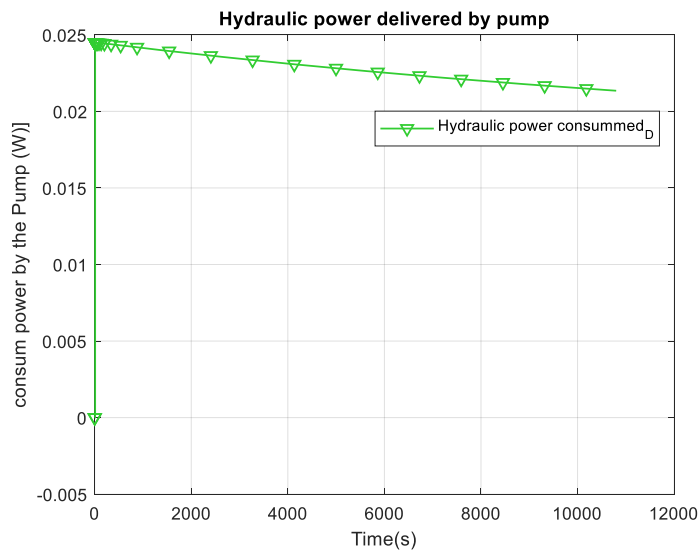

Figure C-45: Hydraulic power consumed in close loop water flow @ $R_{se} = 50\ \Omega$